HARDNESS EFFECTS DUE TO AGING AND DWELL TIME DURING COMPRESSION OF FATTY ALCOHOL COMPACTS AND THEIR EXCIPIENTS

By RUSSELL F. SOMMA

A dissertation submitted to the

Graduate School, New Brunswick

Rutgers, The State University of New Jersey

in partial fulfillment of the requirements

for the degree of

Doctor of Philosophy

Graduate Program in Pharmaceutical Science

Written under the direction of

Professor Nicholas G. Lordi

and approved by

_____

_____

_____

_____

New Brunswick, New Jersey

May 1987

ABSTRACT OF THE DISSERTATION

HARDNESS EFFECTS DUE TO AGING AND DWELL TIME
DURING COMPRESSION OF FATTY ALCOHOL COMPACTS
AND THEIR EXCIPIENTS

By RUSSELL F. SOMMA

Dissertation Director: Professor Nicholas G. Lordi

This study was initiated based on observations made during process optimization trials for a sustained release potassium chloride supplement. It was noted during compression that compact "hardness" varied with time as a function of the rotational speed of the compression equipment.

These changes in compact strength and the subsequent unpredictable effects on the behavior of the sustained release dosage form suggested a need for detailed analysis of the components and their processing. The sustained release system which was studied was of the erosion or matrix type.

Changes in tablet hardness with time are not unique; however, the compacts which have been characterized in this research vary substantially from the more standard tablet formulations. The fatty alcohols used in sustained release dosage forms possess unusual compressional and physicochemical properties which set off the erosion/matrix compact as unique.

The matrix formers (fatty alcohols) were characterized using differential scanning calorimetry, microscopy, as well as being formed into compacts for tensile strength measurements. The potassium chloride was evaluated with respect to moisture content, particle size, compressibility, and tensile strength of resulting compacts. Compression was carried out for all samples and sample mixtures using a universal testing machine, as well as an instrumented single station press.

It was found that the fatty alcohols used in compact formation must have a minimal amount of solid-solid transition as measured by the heat of freezing. Samples with a high solidification energy produce superior tablets.

Potassium chloride, which possesses a fine particle size with an irregular configuration, produces strong compacts. The amount of surface moisture was found to be critical with a high level producing compacts with low tensile strength. Some degree of intracrystalline moisture promotes better compaction properties but also increases aging effects as measured by changes in tensile strength. Potassium chloride with the aforementioned properties was found to be most sensitive to the length of dwell time employed during compression. Fatty alcohol compacts did not exhibit sensitivity to dwell time and reduced the aging properties of potassium chloride when used in mixtures with this material.

Dedicated to my best friend and wife

Mary Louise Somma

Acknowledgements

This work was supported solely by CIBA-GEIGY Corporation, Pharmaceuticals Division. The author would like to thank Dr. LuAnn Ball, Dr. James Clevenger, and Mr. Louis Zagst for their technical assistance, Dr. Nicholas G. Lordi for his advise and technical direction, and Mrs. Jeanne Castaldo for her meticulous typing and preparation of the manuscript.

Contents

Tables

Figures

I. Introduction

The manufacture of dosage forms which modify drug release is a broad area in which many researchers have been involved. The characteristics which are designed into these dosage forms are also broadly based and diverse. One product's release pattern is intended to prevent irritation to the gastric mucosa in the digestive system, while another product's intent is the prolonged or sustained release of a drug entity. These same sustained release products also yield attractive marketing alternatives which include once- or twice-a-day dosing. A large portion of the patient population find 12-hour dosing intervals a distinct advantage over more conventional administration of three or four times a day.

The dosage form intended for sustained release which has received considerable attention is the compressed tablet. The preparation of a sustained release tablet involves many types of manufacturing techniques. These numerous alternatives are also present in the types of raw materials used in preparing sustained release solid dosage forms. For example, a worker may find it feasible to prepare an active constituent which is microencapsulated and then to manufacture a tablet using this modified active ingredient(1). A more commonly used approach is to incorporate various water-insoluble polymeric materials, waxes, fatty acids, or alcohols into the tablet being manufactured. The incorporation of a drug into an insoluble material is

commonly referred to as a matrix or an erosion type sustained release system.

In the insoluble matrix dosage form the active component is suspended in a fused material, such as a fatty alcohol, which is subsequently cooled and then sized into granules suitable for compression. The drug is then released from the finished tablet (matrix) via the following mechanism:

1. Water penetrates the matrix and dissolves the drug.
2. The dissolved drug will then diffuse out to the bulk solution.

This type of release has been dealt with in great detail by Higuchi(2).

It is this erosion insoluble matrix which will be dealt with in this work. The erosion type system which was studied was composed of a combination of fatty alcohols and potassium chloride. Potassium chloride is quite irritating to the gastric mucosa and the use of a slow release dosage form aids in minimizing large quantities of this drug from contacting the gastric mucosa.

During process optimization studies involving this product several interesting observations were made. Compacts which were compressed using standard commercial rotary compression equipment[a] showed an increase in compact hardness with time. The degree with which this increase in hardness occurred appeared to be affected by changes in the rotational speed of the compressing equipment. These changes in machine speed may be directly related to changes in dwell time at the maximum compression point of the equipment. The maximum compres-

---

[a] Manesty Betapress®, Thomas Engineering, Hoffman Estates, Illinois

sion point in a rotary tablet press may be defined as the point where both the lower and upper punches are at their maximum die penetration and the material to be compressed is at its minimum volume.

Changes in compression machine speed have been documented as having various effects on finished compacts. Increases in dwell time are known to increase compact strength measured by a breaking test(3). Machine speed has also been documented as altering compact temperatures as a result of the rate of compressive force application and the magnitude of the force applied(4,5). With these factors in mind, it appears that some physical "modification" occurs in the compact which is related to dwell time and/or temperature.

The phenomenon of changes in tablet hardness (strength) with time is not unique and has been dealt with by several authors(6,7,8). Their investigations centered about conventional tablet components, such as lactose, acacia, and sucrose. Their findings related crystal growth, hygroscopicity, and moisture loss as primary factors in causing increased hardness. The compacts which have been studied in this work vary substantially from these systems. The phenomena which have been observed are intrinsic characteristics related to the unique combination of materials which comprise the matrix controlled dosage form of potassium chloride. The materials' unusual compressional and physicochemical nature and their relationship to changes in compact strength set off the matrix dosage form as unique in comparison to conventional tablets.

The changes in compact strength and the subsequent unpredictable effects on the behavior of the matrix dosage form suggest a need

for a detailed analysis of its components and their processing. This study will concentrate on defining the causative factors responsible for the changes noted in the finished compact. This type of analysis will require raw material characterization and manufacturing process evaluation. The data generated by this work will aid in assuring that a reproducible dosage form is prepared in the manufacturing environment.

II. Background and Literature Survey

The observations presented in the introduction pose an interesting and complex problem. It can be appreciated that changes in compact strength with time may have adverse effects when long-term stability of the finished dosage form is considered. Intuitively, it appears that characteristics of the raw materials and processing of the compacts must have a singular or combined effect in this situation. Therefore, investigation into this area must be based on the concept of more than one causative factor.

An initial literature investigation was designed to determine the extent to which related observations have been reported. A system which exactly duplicates the subject in question was not seen in the documentation, which was reviewed. In light of this, it was decided to search various phenomenologically related systems which have been reported in addition to specific data on the raw materials incorporated in the compacts. The results of this search break the problem down into several areas.

a) Raw Materials/Primary Components

Considerable literature was found which notes the anomalous behavior of fatty alcohols and their mixtures. It was found that this single component yields a wealth of information concerning its manufacture and resulting variant crystalline nature.

Potassium chloride and its counterpart, sodium chloride, have been used in numerous compression studies. Potassium chloride's physicochemical nature possesses several idiosyncrasies which make its characterization vital to this study.

b) Compaction Event and Related Mechanisms

The literature is replete with work performed in this basic area. Various techniques and theories exist to explain observations made during tablet manufacture. In particular, changes in compact strength have been studied as they relate to the compaction process.

c) The Combined Effect of Raw Materials and the Compaction Event on the Final Compact

To clearly understand the data generated by the final product, an analysis of the raw materials and their processing must be undertaken. These combined data will yield possible explanations for the heretofore anomalous compact strength results and how these data relate to the starting materials and their impact on the final product.

A. Raw Materials

A.1 Matrix Forming Components, Processing and Synthesis - The matrix-forming materials are processed into compacted systems by several methods. A general approach used in the pharmaceutical industry is the fusion method(11). In this process the "waxy" component is fused and then the active ingredient is added with constant agitation. An alternative to this procedure would be to mix the active ingredient with the matrix former and then fuse the entire mass with

constant mixing. In either process the fused mass is subsequently cooled below the "melting point" of the mixture. The cooled mass is sized and compressed into matrix tablets. The procedure wherein the active and matrix former are combined and then fused is the method employed in this work.

The blend of potassium chloride and fatty alcohol is fused, cooled, and milled, if necessary. If we consider this process in detail, the various mechanisms become quite involved. This system is further complicated by the inclusion of various particle size fractions of potassium chloride, additional additives (i.e., other fatty alcohols) and the ever present impurity.

To understand the matrix formers used in this study some background with respect to fatty alcohols will be discussed. The component which was used during the initial identification of the hardness problem was cetostearyl alcohol. Cetostearyl alcohol is a common term used in the industry to describe a mixture of long chain primary alcohols, which are predominantly 1-hexadecanol and 1-octadecanol. In addition to these two major components, several other miscellaneous long chain alcohols are present as "impurities." Cetostearyl alcohol is noted in the USP XXI/NF XVI[b] as containing "not less than 40 percent of stearyl alcohol (1-octadecanol), and the sum of stearyl alcohol content and cetyl alcohol (1-hexadecanol) content is not less than 90.0 percent." For the sake of clarity, the single alcohols will be discussed in general using the many commonalities present in this homologous series of compounds. Once these data are presented, the effect

---

b "USP XXI/NF XVI," United States Pharmacopeial Convention, Inc., Rockville, Md., Mack Printing Co., Easton, Pa. (1984).

of mixtures of primary alcohols, such as cetostearyl alcohol will be discussed with their effect on the physicochemical character of these materials.

Alcohols are classified according to the type of carbon atom which bears the hydroxyl group (-OH). In the case of primary (1°) alcohols, the hydroxyl group is linked to a single carbon atom whose configuration is shown in this schematic(9):

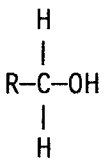

Primary (1°) Alcohol

The primary long chain alcohols used in the pharmaceutical industry as matrix formers have completely saturated carbon chains. This fact is the result of the starting material and synthesis used in their manufacture(10).

Although the fine points in processing of raw materials to produce fatty alcohols may vary depending upon the manufacturer's facilities, the general commerical synthesis scheme may be categorized into several general types.

The sodium reduction process may be used to generate saturated fatty alcohols from a starting material of hydrogenated tallow. Hydrogenated tallow is used to avoid any unsaturation normally seen in crude tallow. The hydrogenated tallow exists predominantly as triglyceride fatty esters. Normally, a solution of the fatty ester, reducing

alcohol, and a solvent is fed into a reaction vessel containing metallic sodium, which is suspended in a solvent (inert to sodium). An exothermic reaction occurs, yielding a solution of sodium alcoholates. This solution of alcoholates is then transferred to a reaction vessel containing water, resulting in hydrolysis of the alcoholates. This results in the formation of a two-phase system, an organic layer (consisting of solvent, reducing alcohol, and fatty alcohol) and an aqueous caustic layer (containing water soluble alcohols or glycerine, depending on the type of fatty ester used in the raw material). These layers are separated and the fatty alcohols are recovered from the organic layer by distillation at reduced pressure.

The reducing alcohol used is a secondary alcohol (cyclohexanol, 4-methyl-2-pentanol) to avoid reaction with the sodium, which produces the by-product hydrogen. The solvents normally used are either xylene or toluene. A general schematic of the process is shown in the following equation:

$$\underset{\text{fatty ester}}{RCOOR'} + 4Na + \underset{\substack{\text{reducing}\\\text{alcohol}}}{2R''OH} \longrightarrow RCH_2ONa + R'ONa + 2R''ONa$$

$$RCH_2ONa + R'ONa + 2R''RONa + 4H_2O \longrightarrow \underset{\substack{\text{product}\\\text{alcohol}}}{RCH_2OH} + R'OH + 2R''OH + 4NaOH$$

These reactions take place at atmospheric pressure and no special manufacturing equipment is required.

The hydrogenolysis process encompasses high pressure hydrogenation of fatty esters to produce the desired primary fatty alcohol.

This process can use a wide variety of starting materials; therefore, the crude tallow is not hydrogenated prior to processing. Normally, the starting material is heated to 300°C then fed with the powdered catalyst (cooper chromite) and preheated hydrogen into the bottom of a heated high pressure reaction vessel. The reaction takes place at 335-338°C and 3,500 PSI. When hydrogen absorption has slowed, the batch is removed and the catalyst is filtered for reuse. The resulting primary alcohols are distilled. Cooper chromite catalysts yield a final alcohol which is completely saturated. A generalized reaction is shown in this equation:

$$\underset{\text{fatty ester}}{RCOOR' + 2H_2} \xrightarrow[\text{catalyst/heat}]{\text{high pressure}} \underset{\substack{\text{product}\\\text{alcohol}}}{RCH_2OH + R'OH}$$

Catalyst selection has a marked effect on the hydrogenation process and the degree of saturation exhibited by the finished product(12,13,14).

A.2 Matrix Forming Components, Physicochemical Properties -

The homologous series of primary alcohols exhibit definite trends in physical properties. For every added CH_2 unit, the normal boiling point increases approximately 20°C, and the specific gravity increases about 0.003 units. Increasing molecular weight decreases water solubility to practically zero above 1-octanol and increases solubility in oil. Below 1-dodecanol, the fatty alcohols are colorless, mobile, oily liquids; 1-dodecanol solidifies at slightly below room temperature. About C_{12} the physical form of the solid alcohols progresses from soft,

crystalline platelets to crystalline waxes(15). Typical physical data for commonly used primary alcohols are summarized in Table I.

The variations in this homologous series are not only isolated to their physical properties. Like most triglyceride type organic compounds, fatty alcohols exhibit a marked degree of polymorphic behavior(16).

Polymorphism is the capacity of any element or compound to crystallize into more than one distinct crystal form. A more generalized concept to consider when attempting to classify a compound as exhibiting polymorphism would be that two polymorphs are different in crystal structure but identical in the liquid and vapor states(17). This concept holds true when we look at the reported data for fatty alcohols. Several workers have studied this group of long chain primary alcohols and have established patterns for crystal behavior throughout the homologous series with emphasis on the chain lengths studied in this work(18,19).

Before discussing specific data, some comments on the types of polymorphic behavior seen with long chain primary alcohols is in order. This work will emphasize the primary alcohols C_{14} to C_{18}. These alcohols make up the majority of fatty alcohols used in pharmaceutical processing. Data relating to other carbon chain lengths will be included only as needed for clarity and completeness of specific points of interest.

Normal primary alcohols have been shown to exhibit very distinct polymorphic behavior. Three forms have been identified for the higher alcohols discussed previously. The three forms have been discussed in the literature using various nomenclature. For our

discussion, the identification scheme used by Tanaka(20) will be adopted.

The α crystal form is observed in a narrow temperature range below the melting point. In this form the molecules are vertical to the layer plane. The layer plane is defined as the segment where the hydroxyl groups of the alochols align themselves. The hydrocarbon section of the molecule remains perpendicular to this hydroxyl layer throughout the α phase temperature range(21). Molecular rotation or twisting along the long axes is noted in this polymorphic form. The β form exhibits the same perpendicular arrangement for the hydrocarbon chain with respect to the layer plan. However, closer chain packing occurs as a result of the translation of the long hydrocarbon axes having been arrested. The γ form is much like the β with respect to packing; however, the long axes are now tilted (approximately 60°) to the layer plane.

The crystal forms have been studied using various techniques, among them are x-ray diffraction, thermal analysis, dielectric measurement, and IR spectroscopy. Tanaka has found reasonable correlation between x-ray and thermal characterization with some minor discrepancies for the C_{16} alcohol. It was Tanaka's opinion that these anomalies were related to the thermal history of the specimens studied. In any event long chain even numbered alcohols were shown to have two low temperature crystal forms. The following schematics represent the crystal behavior for the alcohols studied by the x-ray diffraction technique employed by Tanaka(22).

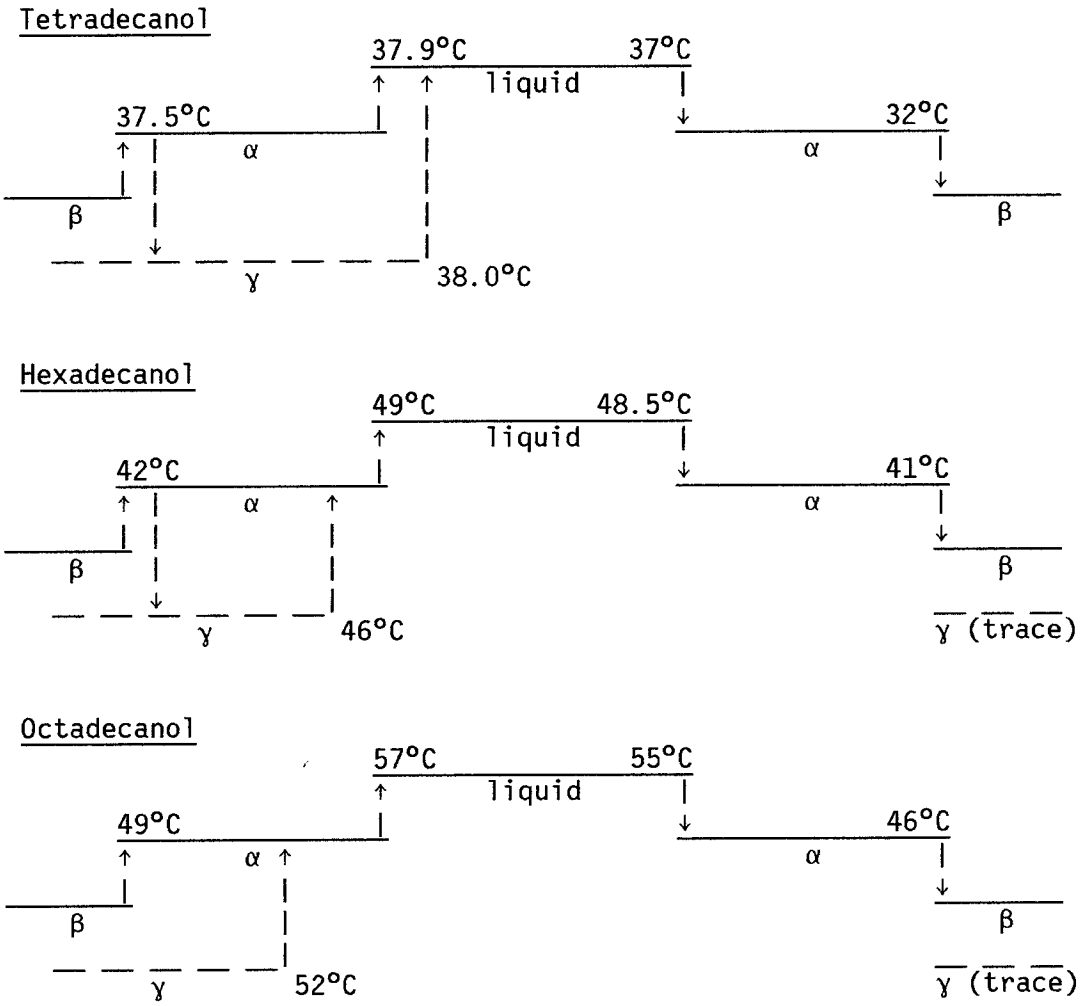

Schematic Profile for Fatty Alcohol Polymorphs

Upon cooling to room temperature, a trace of the γ form was seen for the C_{16} and C_{18} alcohols, while C_{14} exhibited no γ formation after cooling. This observation for octadecanol, wherein the majority of the cooled crystal exhibits mostly the β form has been reported by other workers(18). Tetradecanol was noted, however, to form the γ from the α form gradually during heating above 37.5°C. The existence of a stable γ crystal form was not achieved for C_{14} with incomplete transition to the γ form and subsequent melting of the α and β forms.

Increased chain lengths are attributed with forming stable γ crystal structure because of their slower rates of transformation which

is the governing factor with respect to stability. Longer carbon chains will favor the more stable γ form due to the increased amount of available hydrocarbon chain length lending its effect on van der Waals forces and subsequent packing strength. It is reasonable to expect a retarded rate of transformation with a stable closely packed structure being permitted to crystallize after slow cooling and/or aging at room temperature.

In all the data reviewed, the occurrence of the tilted stable form of the crystal appears with slow cooling, aging, or when the alcohol is recrystallized from volatile solvents, such as toluene or petroleum ether(18,23). These data suggest that of the three forms, the γ must be monotropic or irreversible. This has been shown in the previous x-ray defraction data and has been noted by several other authors(24,25).

In more recent literature it has been noted that the β form for hexadeconal is only seen as a result of impurities contained in the sample. When great care is exercised in sample preparation and storage, the results show only the α and γ forms for hexadecanol. It was also shown that the presence of impurities can stabilize the α form of the crystal, allowing its existence at lower temperatures than had been previously predicted(26). These observations are creditable when it is recalled that earlier workers had noted anomalies when reviewing crystal data for hexadecanol samples(20). These anomalous results have been taken by several authors to assign two low temperature forms to fatty alcohols when sample preparation and inclusion of trace impurities were in fact the causative factors, resulting in α stabilization and/or β formation. Some workers have noted that the

results may suggest that only the low temperature γ form exists because the transitions for hexadecanol occur close together and are quite near to room temperature, making the elucidation of the second low temperature β form non-reproducible. In any event, all workers agree that the γ, tilted form is the most stable configuration at low temperatures for fatty alcohols(19,27). They also agree that either slow cooling, aging, or crystallization from volatile solvents yields the stable γ form(21,23,25,28). One author has suggested that the α form may be isolated by rapid cooling of the sample, permitting its existence at lower temperatures than normally experienced(29,30). Since the purpose of this research is to characterize the effects of fatty alcohols usage in compacted systems employing a combination of various chain length alcohols of commercial purity (~95%) the effects of mixtures and contaminants appeared to be worthy of closer analysis. This becomes more timely in light of some of the conflicting results and observations presented in the literature.

The concept of a stabilized α form at temperatures which approximate room temperature, as discussed previously, has been noted by several authors. The occurrence of this stable form appears to correlate with the composition of the sample under investigation.

It is generally accepted that fatty, long chain alcohols are hygroscopic and readily take up water in their pure form (+99% purity); consequently care must be exercised during exacting thermochemical studies(16). The presence of water in the fatty alcohol has been documented as depressing the α transition temperature and permitting the existence of this hexagonal crystal structure at lower temperatures at the expense of the normally encountered low temperature forms.

The transition temperature for this α form varies as a function of the amount of moisture present in the sample(31,32).

The variations seen in crystal structure are complicated not only by the hygroscopic nature of the fatty alcohols but also by impurities which exist in the samples being characterized. The composition of single, long chain alcohols used commercially in pharmaceutical dosage forms is made up predominantly of an array of C_{12}, C_{14}, C_{16}, and C_{18} alcohols. The complication with respect to the crystal form becomes evident as trace quantities have marked effect on transition temperature of the sample alcohols(31,33,34).

When the matrix forming agent cetostearyl alcohol is studied, all previous factors must be considered in addition to the higher concentrations of hexadecanol and octadecanol and their resulting interrelationship on the crystal structure of the sample. This complex problem has been evaluated by several researchers. Mixtures of C_{16} and C_{18} fatty alcohols have been studied by using analytically pure (+99%) samples of C_{16} and C_{18} and blending them together in various ratios. The resulting crystal structure is studied by x-ray defraction and thermal techniques.

The transition temperature for these combined samples was noted to vary while their fusion temperatures remained reasonably stable. In one case, the combined sample was noted to solidify over a narrow range of temperature. The effect on low temperature solid-solid transitions varied with sample composition. The range of 7.0 to 47.0 mole percent octadecanol with respect to hexadecanol was shown to exhibit the two transition regions when drawn on a phase diagram. The transition temperature depression for C_{16} was more pronounced

than that of C_{18}. Stated another way, hexadecanol appears to be more sensitive to contamination than its counterpart octadecanol. This may be interpreted to mean that a reduced amount of octadecanol is required to cause hexadecanol to form the β crystal structure. Inspection of phase diagram data in Figure 1 confirms the reverse as also being valid. That is, more C_{16} is required to cause C_{18} to form a β crystal region. These studies were conducted with samples having a purity of 99%(35). Similar studies have been conducted to explain this effect on transition points of mixed chain length alcohols. In general, the intermolecular interaction of long carbon groups overwhelms the effect of shorter chain length alcohols. This overwhelming effect thereby requires less of the longer alcohol to effect the shorter chain alcohol(36).

A difference in length of three carbon groups between two mixed alcohols is noted as critical in effecting their crystal behavior. Phase diagrams using hexadecanol and octadecanol clearly show the existence of all three polymorphic forms for these alcohols upon mixing. The more stable γ form is inhibited by these mixtures of alcohol. The inhibition of the stable γ form is made up for by the existence of stabilized α and β forms, which crystallize as a result of mixing the two components.

Since mixtures of C_{16} and C_{18} alcohols in the presence of water can significantly alter the stable range for the α crystal form at the expense of the more stable crystalline configurations, it is logical to assume commercial cetostearyl alcohol will fall within these criteria. Higher concentrations of octadecanol can completely alter the stable

crystalline form of C_{16}, and it may be assumed that simple measurements of temperature transition points will not yield a definitive probe for crystalline variation(37,38). Several workers have resorted to thermodynamic measurements of crystallization energies. These measurements were made using series of single alcohols in an effort to correlate their transition energies with chain length(39). This technique also permits the researcher to gauge the degree of crystallinity which exists within a sample as a result of impurities or mixtures.

The question of how raw materials and their processing impact on the finished fatty alcohol was taken under consideration by one researcher. Fatty alcohols and mixtures of fatty alcohols prepared from starting materials of tallow, coconut, palm kernel, and combinations of coconut and palm kernel oil exhibited similar results when studied using thermal techniques. In addition, no variation between alcohols of equal chain length was noted due to changes in the processing procedure used for their manufacture(24).

A.3 Potassium Chloride Processing and Refining - Potassium chloride is used widely as a source of potassium for patients being treated with non-potassium sparing diuretics. To administer this compound as a potassium supplement, various dosage forms are manufactured by the pharmaceutical industry, the most common of these being a simple solution of the material in a flavored vehicle. Alternative dosage forms include slow release tablets and coated potassium chloride crystals which are encapsulated in hard shell gelatin capsules.

Potassium chloride is obtained through the processing of sylvinite ore. Sylvinite occurs in large underground deposits and is mined

using various techniques. The principle soluble contaminant in this ore is sodium chloride. Depending on the quality of the sylvinite ore, the extraction and refining process used may vary. Approximately 80% of the ore refined in the United States takes advantage of the froth flotation technique. This process lends itself to the medium coarse raw material produced by New Mexico based mining operations.

Sylvinite is a friable ore and gentle crushing must be used during initial sizing operations prior to extraction. The production of excess fines during crushing can cause sodium chloride to be entrained in potassium chloride which is recovered and, thereby, may severely compromise the quality of the finished potassium chloride.

The crushed sylvinite ore contains 1 to 6 weight percent of water insoluble clay. This material must be removed prior to flotation to avoid having the clay inactivate the amine collectors used in the flotation cells. The process media used during hydraulic scrubbing is a saturated brine solution. With constant agitation the clays become dispersed in the process brine. This mixture is then wet screened and the process brine is recycled to a settling lagoon for recovery. The scrubbed ore still contains some clay material and is further refined by mixing with various reagents, such as starch, quar gum, carboxymethylcellulose or polyacrylamides at a concentration of 50-500 grams of reagent to one ton of ore. The selection of the reagent is based on a manufacturers preference or economic considerations.

The material is then prepared for flotation by addition of an extender which imparts a more hydrophobic character to the suspended particles. This extender is usually a heavy oil which may include #5 or #6 fuel oil. The collectors which are added are primary amines. It

has been shown historically that normal amines in beef tallow have an affinity for potassium chloride. More recent workers have found that hydrogenation of the tallow improves the yield. The short chain components of the tallow permit a froth formation. This froth permits flotation of the potassium chloride which is then separated and dried. Trace amines have been shown to minimize the caking normally seen with potassium chloride.

There are other refining methods in use for the processing of potassium chloride. The heavy media technique takes advantage of the specific gravity difference between potassium chloride (1.98 g/ml) and sodium chloride (2.17 g/ml). A heavy solvent media of intermediate specific gravity is prepared (approximately 2.08 g/ml) by mixing saturated brine with pulverized magnetite. This technique permits separation of the ore via settling in this heavy media. This process is limited to coarse grades of ore only.

Fractional crystallization is employed where froth flotation is not applicable. It is also employed when the potassium chloride in the ore exists as the double salt carnallite ($KCl.MgCl_2.6H_2O$). This technique takes advantage of the difference in solubility of potassium chloride and sodium chloride at elevated temperatures in saturated process brine solutions. The ore is heated with the brine to 100°C and potassium chloride becomes saturated while sodium chloride is insoluble. The brine is cooled to 30°C and the potassium chloride recrystallizes and is subsequently separated and dried. This refining process is energy intensive and is seldom used; however, the resulting potassium chloride is of a high quality(40).

A.4 Potassium Chloride and Related Excipients: Physicochemical Properties During Compaction - The physical properties of potassium chloride and the tableting lubricant magnesium stearate are outlined in Table II. Potassium chloride and its properties with respect to tablet formulation have been researched by many authors. The unusual characteristics of potassium chloride may be categorized into several general areas which include particle size/shape, moisture content, and effect of force application during compression. In some of the earlier work reviewed, potassium chloride and sodium chloride were studied using a simple compression process in a single station tablet press with the upper punch force applied and the subsequent force transmitted to the lower punch being recorded via foil strain gauges and a load cell. These studies showed some similarities between the two salts(41). However, no detailed characterization of the materials was made with respect to crystal morphology, moisture content and particle size. It should be noted that the quality of the finished compacted system of potassium chloride should be thought of in terms of the physical characteristics of the potassium chloride with which we start the process of compression.

This concept of the character of starting material was dealt with in Huffine's work(42). He indicates that it is difficult to speak of particles with respect to clearly defined size, distribution and shape but approximations must be made for the bulk of the material being studied. The particles which were rounded and smooth were found to produce poor compacts. The salts (i.e., potassium chloride, sodium chloride) which were used were dissolved and recrystallized to produce

particles with a more irregular configuration. The existence of moisture in the sample was found to "heal" surface flaws on the crystals producing a harder surface with subsequent reduction in compact quality. A reduction in the particle size allows closer packing which then yields compacts of a denser more coherent structure. The pressure of compaction when applied to these fine particles is distributed evenly throughout the powder mass producing numerous junctions or bonds. Sodium chloride was observed to change from a slippage to a plastic flow at higher compaction pressures. This may also be thought of as the material undergoing particle rearrangement followed by an elastic or recoverable region until a yield point is reached. Beyond the yield point, the material begins to experience viscous flow or plastic deformation. This viscous flow of sodium chloride noted by Huffine has been shown to be indicative of the manner in which sodium chloride and potassium chloride form bonds under the force of compression. The term bond in this context is taken to mean the result of intimate contact of crystals during flow past one another which permit localized attraction to occur. These attractive properties may be considered as a function of van der Waals forces, as well as ionic attraction in the case of sodium and potassium chloride.

This question of time related viscous flow was studied by several workers whose aim was to elucidate the time related stress decay of plastically deformed compounds with emphasis on potassium and sodium chloride. Stress decay with time can be directly related to the degree of viscous flow which occurs within a stressed rheological system. That is to say when a constant stress is applied to a sample beyond its yield point, the amount of stress relaxation to a constant level with

time is characteristic of plastically deforming materials. A series of materials were studied by these researchers with respect to their stress relaxation. This work showed that most compressed systems are plastic in nature and can be ranked in a series of increasing viscous or plastic behavior. Sodium chloride was shown to stress decay with time, which lends validity to the accepted theory that sodium chloride and its counterpart, potassium chloride, bond by plastic deformation(43,44). This phenomenon of stress decay and subsequent bond formation must be tempered with the condition of the starting materials. The concept of compression and its related rheological manifestations will be described further in a later section of this paper.

It has been shown by researchers investigating the compressional properties of potassium chloride that irregular crystals yield better tablets as a function of greater contact area and intra-particle entanglement than those compacted using regular rounded crystals. This inhibition of tableting properties was shown to carry over into blends of potassium chloride with other tablet excipients and in particular with magnesium stearate(45).

The moisture content of the potassium chloride was of particular interest in this study. It was shown that there are two critical areas where moisture plays a pivotal role in determining tablet strength. The first area, and the most obvious, is the surface moisture adhering to the crystals. As noted previously in the synthesis section, trace contaminants can cause a marked degree of moisture adsorption onto the surface. This surface moisture may be thought of as a boundary lubricant which inhibits intimate contact and subsequent bond formation. The moisture layer may act by another mechanism wherein it

permits recovery of the compressed system by its lubricant properties thereby breaking the contact areas already formed. The survivability of bonds formed within compacts has been discussed by Hiestand(46). He notes that during removal of a compression force a "peeling" action will occur between particles if sufficient bond structure has not been formed. A rounded crystal with adsorbed surface moisture is a prime candidate for bond degradation during unloading. Compact strength is known to decay as a function of moisture content. Sodium chloride compacts have been shown to be particularly sensitive to moisture having marked effects on the strength of the compacts(47,48).

The second area which was shown to be critical in tablet formation was the internal or occluded moisture within the potassium chloride crystal lattice. This moisture appears to be required to aid in bond strengthening after plastic flow has permitted close inter-particle contact. It has been suggested that the internal moisture aids in secondary crystal growth. It appears that an ideal condition for potassium chloride is a low surface moisture with some degree of internal occluded moisture necessary for bond formation. The particle must be irregular in shape with few rounded surfaces. The need for irregular particles is not unique to compacts of potassium chloride. During sintering of aluminum powder for metal machine parts, irregular aluminum powder yields compressed parts of a higher green strength than those compacted with spherical particles. The green strength is taken as the compact strength of the metal part prior to heat treatment(49).

The size of the particle must be considered if the integrity of the compact is to be understood. In general terms, small particle size

samples yield a much denser compact with little void space available. Small particle sizes allow more surface area contact during the rearrangement segment of the compression process. Large particle fractions usually result in compacts whose final apparent density is less than those resulting from a fine particle size fraction. The apparent density of a tablet is taken to be the actual compact weight divided by the measured volume of the compact in question. The utility of this number will be seen during the discussion of the compression process in a subsequent section of this report(50).

Samples of spray dried lactose and microcrystalline cellulose have been classified into two particle size ranges (0-45 μm and 180-250 μm) by several researchers. These particle size samples were then compacted into tablets. It was shown consistently for both materials that the fine particle size material yielded stronger compacts than the larger particle fraction(51). In that the compressional behavior of microcrystalline cellulose and spray-dried lactose differ, it is noteworthy that the effect of particle size is an area of common ground for both materials. Intuitively, it would follow that, in general, one could anticipate stronger compact strength as a function of reduced particle size. It is interesting to note that the α and β crystal form of anhydrous lactose when compressed yielded two different strengths. The authors used identical particle sizes (0-32 μm) for both crystalline forms(52). It appears that the strength of the resulting compact is quite sensitive to the integrity of the starting materials. This fact is of great importance when considering compacts of potassium chloride.

Considerable literature exists which deals with the use of magnesium stearate as a tableting lubricant. Several workers have characterized lubricant efficiency with respect to the various polymorphic structures of magnesium stearate(53). Within the low concentrations of this lubricant which are used in tablet manufacture, the investigator is not normally concerned with the intrinsic rheological properties of magnesium stearate as a single entity. However, magnesium stearate's secondary effects and how these relate to the behavior of compacts being studied is worthy of note. Previous workers have reported deleterious effects on compacts of potassium chloride when it is blended with magnesium stearate(45). It has been shown that blends of 0.1% by weight of magnesium stearate with sodium chloride can generate substantially weaker interparticulate bonds. This is evident upon microscopic examination of fractured tablets where compact failure is clearly seen to be around the particles. Sodium chloride compacts which do not contain magnesium stearate fracture across the particle which suggests strong interparticulate bond formation. Magnesium stearate produces maximum inhibition effect on excipients that undergo substantial plastic flow, such as sodium chloride and potassium chloride(54,55).

B. Compaction Physics and Related Physical Manifestations

B.1 Theories of Bond Formation in Compacts - The manufacture of sustained release dosage forms was briefly detailed in the introduction. The dosage form most commonly encountered in this area is the compressed tablet. To form a tablet, the required materials are compacted under pressure within the confines of a die and two

punches. The materials are prepared into a uniform "granulation" and fed into a die. The punches are inserted and the volume available to the material is reduced until the desired compaction results or force level is achieved. The manner in which this force of compression is applied and its duration have a marked effect on the quality of the finished tablet.

The change in volume which occurs within the confines of the punches and die may be thought of in a rational manner in sequential terms of the events taking place. Carstensen(56) describes these events as follows:

a. The die is filled by the powder which closely adheres to its cascaded or free flow (untapped) packing.

b. The upper punch enters the die and begins to rearrange the powder bed to a more closely packed matrix.

c. As the punch continues to penetrate the die and reduces volume, an elastic deformation region is achieved. The particles continue to deform in an attempt to fill available void spaces. This region may be thought of as elastic in that the removal of the punch would permit the powder to return to its non-deformed, closely packed state.

d. As compression proceeds, the elastic limit of the powder is reached and the material begins to either plastically flow or fracture, depending on the nature of the powder being studied.

e. The final stage may be referred to as the tablet formation step of powder consolidation. Under plastic flow, the particles permit rearrangement of molecules of one particle with

respect to adjacent molecules. The distance and alignment permits the formation of bonds which yield a coherent compact. Brittle fracture, on the other hand, creates fresh, clean surfaces which are free of contaminants, thereby permitting proper configuration of adjacent particles and subsequent bond formation. As in the case of plastic flow, the compression process permits reduced intermolecular spacing to achieve bond formation. In both situations the compressive force has increased particle contact area, creating the compact system.

The mechanisms of bond formation are grouped into the two aforementioned categories of plastic flow and brittle fracture. In compression the deformation which occurs before the elastic limit is reached is totally recoverable. This is noted to be a region where no bonds are formed. However, as the compression proceeds a point is reached where the deformation is not completely recoverable after the stress of compression is removed. The non-recoverable strain has been dissipated in the viscous or plastic flow and subsequent bonding of the particles. It must be noted that both elastic and plastic deformation occur with the dominant type being predicated by the material being compressed(57). The degree of plastic flow may be approximated by means of measuring the amount of stress relaxation after a selected force level is achieved.

This stress reduction or stress relaxation is a time dependent phenomenon. Reiner(58) explains stress relaxation in the following manner. Once a solid is exposed to a deformation (strain), it is no longer in an equilibrium condition. In our system, the deformation is

supplied by the upper punch deforming the material. As the material is deformed, stress develops within the solid and tends to resist the volume change. If the imposed deformation is held constant, the resulting force (decay) may be measured with time. Real systems are not typically pure elastic solids (Hookian). Therefore, in these real systems, the stress will not be a constant with relation to time. This non-linearity is generally termed visco-elastic.

The stress in visco-elastic systems will decay to some equilibrium level. It is this decay which is considered stress relaxation. This physical property has been used by several researchers to characterize pharmaceutical solids(43).

Brittle fracture is another mechanism for bond formation during compaction(59,60). Higuchi(61) identified this by measurements of surface area of sulfathiazole compacts using nitrogen adsorption as a function of time and compression. This process may be thought of as fragmentation of particles during compaction. Once the yield point of the solid is exceeded, the material undergoes fracture. This fracture produces new "clean" surfaces which act as focal points for bond formation. Huffine(42) noted that new surfaces act as unsatisfied bond locations which come in close contact with an adjoining new surface and a satisfied bond results.

Aspertic melting is a third bond mechanism which is discussed in the published literature. The rationale involved in this theory is not as clearly defined and its validity has been debated on a theoretical basis by many authors. In general terms, aspertic melting or fusion of contact points between crystals accounts for bond formation in several materials, the asperity being the irregular surface of contact

between crystals.

The source of heat to cause fusion at the contact points is supplied via the energy imparted to the system by compression. The majority of the compression energy is taken up in generating new surfaces within the tablet. The remainder is lost to elastic recovery and heat(62).

Workers have attempted to explain this melting theory using thermodynamic and mechanical models. One theory uses an application of the Clapeyron equation to explain how decreases in volume result in lowered fusion points(74). The basis of this concept is taken that only the solid materials are at high pressure with any resulting liquid existing at ambient pressure within the compact matrix. This molten material exists for a very minute period of time and immediately solidifies, forming a bond. This concept is further expanded by Rankell(75), who employs a stressed beam model as crystal structure under compression. This model attempts to explain a situation where point pressure produces a reduced melting point.

On a more basic level, if atomic slippage is accounted for during compaction, sufficient energy is available to yield increased temperatures. The movement of 10 atomic spacings along the crystal slippage plane may produce a localized increase of approximately 10°C, resulting in "hot spots"(65).

In an early experiment Goetzel disproved the fusion bonding hypothesis(66). He used iron particles coated with a low melting alloy. These coated particles were compressed at various rates of loading. Inspection of the finished compacts gave no indication of

fusion. The explanation given was that the heat generated by compression was conducted away from the contact points very rapidly and prevented fusion. These observations are well taken but seem rather unrelated to a pharmaceutical system which for the most part is non-metallic.

More recently Hiestand(67) presented data which was generated using a technique developed in earlier research(68). The data suggests that significant regions of high stress concentration are not present in a compacted matrix, thereby obviating the possibility of fusion at contact points.

These factors are all based on data generated using pharmaceutical excipients whose melting points are quite high (i.e., lactose USP, m.p. 222.8°C[c]). The use of lower melting point materials under compression seems to be a different situation. Freezing points of n-paraffins have been documented as being appreciably affected by moderate changes in pressure. These effects were noted by changing pressures in a dilatometer and the resulting adjustments required in the temperature to establish a new freezing point for the sample being studied(69). In studies of powder cohesion aspertic melting has been attributed to changes in tensile strength of compacted masses when using particles coated with low melting point materials. It was noted that mixtures which contained higher melting point material showed lower tensile strength values for compacted systems. The authors attributed a reduction in point melting in the latter samples as the

---

[c] R. C. Weast (Ed.), "Handbook of Chemistry and Physics," Fifty-First Edition, The Chemical Rubber Company, Cleveland, Ohio, (1970).

causative factor in the retarded strength characteristics(70,71). These data suggest alteration of the bonding mechanism as reflected in changes of tensile strength in powder masses and compacted systems. It would follow that to discount aspertic melting as a possible bonding function when considering compacts made up of heat sensitive materials is not without some question.

B.2 Characterization of Bonding Mechanism - The mechanisms leading to bond formation are quite complex and the methods used to unravel these problems are at times themselves involved. The number of techniques available to the researcher to characterize the actual bonding functions are numerous and care must be exercised in their selection and subsequent implementation. In their review of compaction data treatment, Krycer, Pope, and Hersey broke down the various techniques into several general areas(72). Two of the techniques presented which appeared to yield the most usable information involved the equation developed by Athy and Heckel. The second approach involved the development of cycle plots, which are a measure of radial force (die wall) as a function of normal force (punch force).

It should be noted that the Athy-Heckel equation is most commonly referred to as simply the Heckel equation. However, Carstensen(73) points out that it was first developed by Athy(74) and later a synonymous equation was presented by Heckel(75,76). Data treatment by the Athy-Heckel method provides the researcher with a qualitative description of the bonding mechanism. The cycle plot method employs the use of a single station tablet press equipped with instrumented punches and an instrumented die wall to measure residual forces.

This method permits characterization of plastic flow under compaction.

The Athy-Heckel equation is in the form:

$$\ln E = -(kP + a) \qquad \text{(Eq. 1)}$$

where E is a function of compact porosity:

$$E = 1 - \frac{D'}{D} \qquad \text{(Eq. 2)}$$

As the applied pressure P increases, the apparent density D' (g/cm^3) increases to a certain limit. Therefore, the total porosity E of the tablet is determined by applied pressure P and the true density D of the material being studied.

The most commonly employed form of the Athy-Heckel equation seen in the literature uses a simplified term for relative density where:

$$D_{relative} = \frac{D'}{D} \qquad \text{(Eq. 3)}$$

In which D' (the compact's actual weight divided by its volume) and D are defined as before, and subsequently combined with Eq. 1 to yield the following relationship:

$$\ln(1/1-D_{rel}) = kP + a \qquad \text{(Eq. 4)}$$

P is the applied pressure, and k is a constant equal to the reciprocal of the mean yield pressure Py(72):

$$k = 1/Py \qquad \text{(Eq. 5)}$$

The term a is a function of the original compact volume. The yield pressure may be calculated from the final linear portion of a plot of ln $(1/1-D_{rel})$ versus applied pressure P. The resulting plots for this equation may be broken down into several types. In Figure 2, two typical theoretical plots are shown.

In Type A we see characteristic behavior for a material which undergoes bonding by plastic deformation. The powder in this case is dependent upon its initial particle size and bulk density. As densification proceeds, the particles slip and rearrange with plastic flow occurring past the yield value. The finished compacts retain different degrees of porosity as a function of their initial particle size and bulk density within the die cavity. These materials, in general, are soft materials which deform easily under pressure.

Materials which are typified by Type B behavior are usually harder particles. As compression occurs consolidation is achieved by fragmentation to yield a compact of consistent porosity. This explains the common line established for these materials.

The manner in which the Athy-Heckel equation is applied varies. The general approach agreed upon by many authors is to take all compact measurements at zero pressure. The removal of pressure permits

the compact to recover elastically. Any changes in compact density must then be a function of non-recoverable plastic deformation.

This technique may be further expanded by the use of two contact or dwell times during compaction(77,78). Several researchers have used two dwell times to quantify the amount of plastic deformation occurring during compaction. The material to be studied is filled into the die and compressed. The compact is held at the selected force level for a period of approximately 0.2 seconds, then the force is unloaded. A second sample is then compressed to the same force level and held for approximately 10 seconds. The data from these two contact times are then plotted as ln $(1/1-D_{rel})$ versus pressure (P). The areas under the two dwell time curves are measured. The differences between the areas are a function of the degree of plastic deformation which has taken place in the material being studied.

If the compacts under investigation are measured while they are still subjected to a compressive load they would include an elastic component which increases the value of ln $(1/1-D_{rel})$. The methods described previously permit the researcher to make meaningful comparative measurements for groups of selected materials. This procedure minimizes the variation normally encountered when evaluating the slopes of Athy-Heckel plots. In the present work, this method provided the basis for comparing the plastic deformation for a series of potassium chloride samples.

A question often raised concerning the use of techniques which measure changes in density of compacts is one concerning the initial packing configuration of the sample in the die cavity prior to force application. A detailed knowledge of the initial packing is required

because the bulk density within the die can adversely affect several types of compaction equations. However, the Athy-Heckel equation has proven to be relatively insensitive to this parameter. Several authors have modified bulk densities in the initial packing to confirm this aspect of the Athy-Heckel relationship(79).

The Athy-Heckel equation has found application in the determination of intrinsic properties of materials which are compacted. These studies took advantage of the constant k, which as noted previously is a function of the reciprocal of the mean yield pressure Py. It was shown that lower k values are representative of materials which are hard with less plastic flow at higher pressures, while high k values were seen with softer materials(80). This technique has also been used in the characterization of various forms of starch(81).

The bond mechanism which involves aspertic melting has been studied using the Athy-Heckel equation. Fatty acids were coated on lactose and subsequently compressed. The resulting compacts from the series showed equivalent density. It was noted that as the melting point of the fatty acids in the series increased, the tensile strength of the compacts decreased. The authors attributed this to different amounts of aspertic melting at the contact points between particles. The resulting Athy-Heckel plots were different than those normally seen for lactose alone(70).

The second method commonly used for characterization of bond mechanism is the cycle plot or measurement of die wall pressure as a function of applied force. Substantial literature has been generated concerning the interpretation of these cycle plots. The potential user

of these techniques must exercise caution to assure that the experimental procedure is correct and permits meaningful correlation to existing literature data.

In general terms, the compaction of a sample in the preparation of a cycle plot takes place in a single station tablet press whose upper and lower punches along with the die have been instrumented to measure force. The force applied by the punches is referred to as the axial pressure measured in terms of force per unit area. The die wall measures the radial pressure in terms of force per unit area which is transmitted at right angles from the longitudinal axis of the punch. Materials undergoing this sort of compression analysis may be broken down into several types which include a perfectly elastic body, a body with constant yield stress during shear, and a Mohr body. These interpretations have validity if the die wall is assumed to be perfectly rigid with minimal wall friction being encountered(57). These criteria are referred to as simple compression by Riener(58). The types of behavior encountered will be discussed in detail. A discussion of their usefulness as indicators of the tablet's physical properties will follow.

In the perfectly elastic body, when the axial force is applied, the force sensed by the die wall is of an equal magnitude. The ratio of axial to radial force is equivalent to the relationship commonly noted as the Poisson ratio (υ) where:

$$\frac{\text{axial force}}{\text{radial force}} = \frac{\sigma}{\tau} = \upsilon \qquad \text{(Eq. 6)}$$

A cycle plot for an elastic body is shown in Figure 3. As the axial force is decreased, the radial force decays along the same line with no residual forces being exerted on the die wall. In actual practice, perfect elastic behavior is rarely seen in pharmaceutical compaction processes, since a preponderance of tablets require some degree of force to be ejected from the die after tablet formation.

The compact which shows a constant yield stress during shear more closely approximates conventional systems. This cycle plot's form depends upon the intrinsic properties of the material undergoing compression. A theoretical plot of this behavior is shown in Figure 3. The line O-A represents the elastic region below the yield point of the material. Once the radial force is increased beyond A, deformation begins where the yield stress becomes a function of both the radial and axial force factors. Using the term S to represent yield stress we obtain:

$$\text{axial } (\sigma) - \text{radial } (\tau) = 2S \qquad \text{(Eq. 7)}$$

The yield stress is a constant along the line A-B. At point B axial force is decreased and the yield under shear stops. The die wall experiences force decay along B-C. A test for compressional behavior normally conducted here would be to ascertain if the slopes of O-A and B-C are approximately equivalent. Assuming the force applied axially had sufficient magnitude, point C should be detected where the radial force exceeds the axial force. Some authors take point C and use it to calculate the total yield stress term 2S. This point may also be

taken to be a yield point in response to the radial force. Line C-D should be equivalent to the line A-B, in that it has the same relationship between the axial and radial stress difference. The remaining point D is a function of the yield stress and should be equivalent to the value 2S. This value is the amount of force exerted by the compact against the die wall which must be overcome to permit the tablet to be ejected. Tablets which exhibit this type of cycle plot are considered to form bonds by plastic deformation.

The final model applied to cycle plots is the Mohr body. This term refers to the Mohr-Coulomb yield stress which will occur at the plane of shear for two bodies. The yield stress will be reached when the shear stress on any plane in a compact or particle interface reaches a critical value which varies linearly as a function of the normal stress in that plane. A model of the system may be considered as a block resting on a rough surface. To begin the block moving the normal yield value must be overcome. Once the block is moving along the plane or surface the shear stress required to keep it moving is dependent upon the normal force acting at the block/surface interface. This mechanism may be shown as:

$$\tau = \tau^0 + \mu\ \sigma n \qquad \text{(Eq. 8)}$$

Where shear stress τ is a function of the initial yield stress value τ^0 corrected for friction μ and normal stress σn with respect to the surface. Carstensen(56) assigns a more practical cohesion term C to the classic Mohr-Coulomb relationship such that:

$$\tau n = C + \mu\ \sigma n \qquad \text{(Eq. 9)}$$

Where τn is shear stress on the slippage plane, C is cohesion, μ is a

frictional coefficient and σn is normal stress. Figure 3 shows a theoretical representation of Mohr body behavior. By assigning the yield stress the S term discussed in Eq. 7 we can represent the Mohr body as:

$$\tau n = S + \mu \sigma n \qquad \text{(Eq. 10)}$$

The normal stress on the slippage plane is a function of axial (σ) and radial (τ) forces, such that:

$$\sigma n = \frac{\sigma + \tau}{2} \qquad \text{(Eq. 11)}$$

The shearing stress τn is also a function of these terms which yields:

$$\tau n = \frac{\sigma - \tau}{2} \qquad \text{(Eq. 12)}$$

Combining equations 10, 11, and 12 and simplifying results in:

$$\tau = \frac{(1 - \mu)\ \sigma - 2S}{1 + \mu} \qquad \text{(Eq. 13)}$$

This form defines the functions occurring beyond the yield point A. The slopes OA = BC = υ the Poisson ratio as noted previously. At the yield point C the functions are defined as:

$$\tau = \frac{(1 + \mu)\ \sigma - 2S}{1 - \mu} \qquad \text{(Eq. 14)}$$

These factors take place if the applied axial force was of sufficient magnitude to permit measurement of yield points A and C.

Recall that the C yield point is the result of the radial force exceeding the axial force. The slopes may be defined as:

$$\text{slope AB} = \frac{1 - \mu}{1 + \mu} \qquad \text{(Eq. 15)}$$

$$\text{slope CD} = \frac{1 + \mu}{1 - \mu} \qquad \text{(Eq. 16)}$$

The Mohr body characteristics usually suggest brittle fracture as the primary bonding mechanism taking place during compaction(56,57,59,60,72,82). Several authors have used this concept of slope measurement to assign bonding mechanisms to granulations. If the resulting slopes CD and AB are different, this would suggest a Mohr body. When slopes CD and AB become equal due to a formulation change, the compact is assigned a constant yield stress mechanism. This is indicative of a plastically deforming bond mechanism(83,84).

The researcher who decides to take advantage of the amount of literature and technology available on these subjects should be aware that several conflicts and general assumptions have been encountered. It must be noted that most mathematical models for bond formation assume an ideal solid which is nonporous. Real systems do not exhibit isotropic structure. This is further complicated by the lack of purely elastic behavior for pharmaceutical solids. As an example, several authors(59,60,83) have suggested that sodium chloride behaves as a Mohr body, which is characteristic of brittle fracture. A wealth of physical measurements, which include surface area measurement, microscopic examination, and Athy-Heckel analysis, do not support these observations. Apparently, strict assignment of bond mechanism may not be the desirable function of cycle plots. Perhaps their use as a

tool in ascertaining tablet quality as a function of die wall stress and its impact on capping may be a more practical application. In the end, quantitative interpretation should give way to more practical "ad hoc" usage of the cycle plots as a formulation tool. This would permit the formulator flexibility in defining his requirements with the final result being a physically acceptable tablet. Several researchers have taken force analysis technology normally used in cycle plot elucidation and have assigned their own acceptance criteria(85).

The use of a single station tablet press for measuring compression parameters for materials has been questioned with respect to applicability to rotary equipment. The differences in the density patterns for tablets resulting from both systems have been documented in the literature(86). The primary reason for these different densities are rooted in the manner which the lower punch responds to applied force. In the single station machine, the punch is held rigidly in place by the lower punch plunger. This assembly is not involved in the application of pressure to the compact like the upper punch. In rotary compression equipment, the lower punch is dynamic rather than static, as in the single station machine. The lower punch moves to adjust weight and accommodate upper punch entry and subsequently apply compression force as it rides over the lower compression roller. It is these differences, which dictate the density patterns of tablets prepared on rotary and single station equipment.

These differences between the two types of compression equipment have been studied in detail by Charlton and Newton(87). In their work the punch velocity and subsequent contact time between the punches and the material to be compressed are characterized. In their

study the punch speeds for a Manesty single station F3 and a rotary D3B press were found to be approximately the same at the beginning of the compression cycle. However, because the rotary equipment essentially compresses with the upper and lower punches, the compression times with respect to the compact are different. The authors quote a value of 0.1 seconds contact time for the F press, while the rotary press exhibits a total contact time of 0.083 seconds. The 0.083 second interval comprises the maximum compression under the punch roller, in addition to dwell time imparted by the flat geometry designed into the top of conventional rotary tablet tooling. It is this flat segment that permits maximum force to be exerted for a longer period, which promotes more plastic flow and minimizes the tendency toward tablet capping or lamination. It should be noted that the D press is considered a low speed rotary and is not normally utilized where high speed rotary output is required.

B.3 Die Wall Effects on Compacted Systems - Several discussions in the literature suggest some interesting factors resulting from compression of soft (plastic) materials in a die. One concept which must be considered is the surface area of the die exposed to the compact. This segment during compaction is a source of high shear. If the die under consideration is stationary, as is commonly encountered in pharmaceutical compression operations, this effect can directly impact on tablet quality. Train(88) documented that compression of a plastic material, such as lead shot, resulted in a strong outer layer along the plane of shear within the die. The material inside the compact was not

as tightly bound as was discovered during dissection of the finished compact.

In some later work, which employed scanning electron microscopy for compact characterization, the recrystallization of sodium chloride particles was attributed to the die wall effect(111). Recrystallization occurred at the compact's edges, which had been in direct frictional contact with the die wall. Areas on the compact which had not been exposed to shear did not exhibit a large degree of recrystallization. The authors have associated this recrystallization with an increase in surface energy being stored in the crystal lattice, which ultimately results in increased structure at the die wall interface area upon ejection. Some contribution from atmospheric moisture was also noted as adding to energy release and reduction in lattice disorder yielding recrystallization.

The shear strength of a material will limit the amount of die wall pressure which is generated during compression. For a material to plastically flow, the dynamic shear strength must be exceeded. This results in a coherent tablet formed by plastic deformation. If the plastic flow is inadequate, however, localized, highly stressed regions occur. It is these regions which theoretically generate a laminated or capped tablet upon ejection. The more brittle the compacted material, the more difficult it becomes to relieve these localized regions of stress. This gives rise to the rationale of reducing compression machine speed to remedy tablet capping. This approach permits the compact time to relax prior to ejection. The mouth of the die may be thought of as a focus for stress concentration resulting in capping. This concept of stress localization with respect to die wall effects was

investigated by several workers(102), utilizing an acoustic measuring technique. By analyzing the acoustic emissions of a compact at zero upper punch pressure prior to ejection, the degree of capping was quantified for a particular compact. The authors noted that crack propagation had taken place within the die and not at the die opening as normally expected. The samples used by the authors were known historically to create substantial problems during compression. All materials studied were quite brittle, showing very little plastic flow during compaction.

Recently, several researchers(89) have developed a system which permits a reduction in the residual die wall force prior to ejection. They constructed a rotary compression system which performs a tri-axial compression on the compact. This tri-axial technique involves the upper and lower punches as well as a flexible die wall. As the compression event occurs, a force is applied by all three functions. Once the compact is formed, the equipment is designed to permit the flexible wall of the die to withdraw a minute distance. The withdrawal of the die wall is noted as having marked effects on reducing the capping commonly seen with granulations, which are historically linked with capping problems.

It would appear that monitoring residual die wall force alone would permit the researcher to predict the capping tendency for a given sample. The use of this technique must be tempered in some cases with the elastic behavior of the material being characterized. Several authors(90) have noted that the sole use of residual die wall pressure may be misleading. As noted earlier in this paper, the bonds formed by plastic flow during compression must be capable of

surviving elastic recovery at decompression. This elastic recovery may result in peeling of contact surfaces and subsequent reduction in compact strength. The authors used a measurement of elastic deformation of a compact with time. The percentage of elastic recovery was shown to correlate well with a series of paracetomal granulations. The best granulation showed minimal elastic recovery and, therefore, better utilization of energy during compaction and subsequently better compacts. One must be aware of this concept when making judgments on formulations and temper die wall force analysis with potential elastic recovery artifacts.

B.4 Aspects of Compact Strength - We have mentioned several studies where the finished compact is strong or weak depending on the compression process or raw materials used in sample preparation. Some explanation about the procedure resulting in these assessments of compact strength is required. We must first describe the difference between the commonly used term for tablet evaluation "hardness" and compact strength.

The term "hardness" in the field of solid dosage form technology has been used to define the crushing strength test applied to tablets. This is usually a quality control test to assure suitable physical tablet characteristics. The test is carried out by placing the tablet between two flat plattens. The moving plattens apply a force until the tablet fractures. The force causing the fracture is recorded as kilograms of force or some arbitrary unit, such as Strong-Cobb Units. The difficulty with this system is that the general term "hardness" is not a fundamental property of the compact being tested. Several workers

have established qualitative relationships between "hardness" and various compressional factors, such as density. For our purposes, these techniques yield little useful information as to the integrity of the compact we have formed. Our needs lie more in the area of compact strength as a function of bond formation.

Extensive work has been performed in the area of tablet strength(91,92,93,94,95,96,97). A common method used permits the determination of the actual tensile strength of the compacts tested. The technique takes advantage of a diametral compression procedure. By applying a force to the compact, a molecular rearrangement takes place. The rearrangement manifests itself as several stress components (tensile, compression, and shear). The forces involved are shown diagramatically in Figure 4. The tensile stress component developes in a horizontal plane perpendicular to the axis of applied force. The compact fractures in this manner producing a fissure down its center parallel to the direction of force application. The force required to cause the failure is recorded. This value is then used to calculate tensile strength (σ) with the following:

$$\sigma = \frac{2P}{\pi Dt} \qquad \text{(Eq. 17)}$$

where P is the applied load recorded as force, D is the compact diameter and t is thickness of the compact.

Several precautions must be exercised when using this procedure. The interface between the plattens and the compact may be padded with a soft material. Rudnick(92) has shown that use of a thin, wide pad will yield reproducible results. The padding should be soft enough to permit force distribution to take place over a reasonable

area, minimizing the localization of shear and compression stresses at the contact point. In this manner, the resulting failure will be a function of the tensile strength of the compacted material.

The fractured pieces of the compact must be carefully evaluated by the investigator to determine if normal tensile stress failure has occurred. These observations have been characterized by Fell and Newton(93,94,95). They describe normal tensile failure of the compact when it splits into two halves along the loaded diameter. If the compact fractures into irregular fragments, compressional and/or shear failure has taken place. Fracture which results in a "tongue and groove" or triple cleft fragmentation is considered the result of normal tensile stress failure.

Typical compact fractures are shown in Figures 5. These act as a guide when determining the manner of failure involved in a compact strength test.

Equation 17 has been used by other workers to calculate tensile stress employing modified compression loading apparatus(98). The apparatus described makes use of a fulcrum and anvil system in place of the flat plattens more commonly seen in these studies. The results obtained with the technique were comparable to data reported by researchers using the standard flat platten apparatus. These facts suggest that Equation 17 has a broad range of applicability in tensile strength calculation. One should, however, be aware of variation between testing instruments used in compact evaluation. This variation has been documented by Brook and Marshall(99). Therefore, it is necessary that appropriate calibration procedures be employed prior to experimentation.

III. Experimental

A. Materials

As discussed in the background section, two types of raw material studies will be required to address the questions raised by matrix tablet manufacture. The areas to be characterized involve a detailed study of the raw material's physicochemical properties. This will then be followed by processing experiments. These materials are broken down into two areas. The first group of raw materials is the matrix formers or fatty alcohols used to generate the slow release characteristics of the compacts. The second group is the potassium chloride which is incorporated into the matrix and the other related excipients which are used as required.

The first phase of the experiment involves characterization of the fatty alcohols with respect to their thermal behavior alone and in mixtures. This type of study lends itself to the usage of samples whose purity is high (at least 99%). The second approach takes advantage of the standard levels of purity for samples of fatty alcohols procured for standard pharmaceutical processing procedures (approximately 95%). The more conventional purities will subsequently be used in processing and matrix formation. The population of samples studied and their related purities and origins of supply are summarized in Table III. All fatty alcohols obtained were utilized as supplied by the manufacturer with no further purification being carried out in our laboratory. All

conventional purity materials were stored in double-layered, polyethylene bags which were placed in sealed fiber drums as protection against moisture present in the laboratory environment. Ambient storage conditions were maintained in the range of 23-28°C and 43±5% relative humidity. The high purity fatty alcohol samples were stored in glass vials which were placed in glass desiccators over calcium sulfate mixed with a moisture indicating desiccant[d]. The desiccant was changed as soon as any color variation was noted in the indicator. The desiccators were maintained at ambient room conditions as noted previously.

Fatty alcohols of commercial quality that exhibited chunks or agglomerates were broken down by gentle grinding in a glass mortar and pestle. The resulting material was then passed through a 20-mesh (850 μ opening) screen prior to any experimental procedure.

The potassium chloride used in this work was obtained from standard commercial sources for this material. The samples used and their related lot numbers and specifications are summarized in Table IV. As discussed, the particle size and shape of the potassium chloride is critical to the character of the resulting compacts after compression. In order to adequately address this aspect, all potassium chloride utilized in this study was processed according to the flow diagram in Figure 6. The two particle size ranges resulting from this procedure possess average ranges of 400-420 μ (coarse) and 140-160 μ (fine). These average numbers were obtained from screen analysis data obtained using U.S. standard screens. In addition, the particle

---

[d] Drierite®, W. A. Hammond Drierite Co., Xenia, Ohio.

size was evaluated microscopically to confirm the data obtained from the screen analysis.

Moisture content was determined using a constant weight technique(45). Density measurements were made pycnometrically(100) using n-hexane[e] and toluene[f]. Both liquids were reagent grade quality.

The sized samples were stored in double layered polyethylene bags which were subsequently stored in sealed fiber drums in which a desiccant (calcium sulfate) had been placed. The drums were stored at ambient room conditions. Prior to any experimental procedure, the potassium chloride was passed through a 20-mesh screen to break up any agglomerates which may have formed during storage.

The magnesium stearate[g] used is a standard grade for pharmaceutical manufacturing of solid dosage forms. This material was used to prevent binding of the compacts during compression. It was also used to evaluate the secondary effects this lubricant may have on the wax matrix during compaction. It was stored in tightly closed glass bottles at ambient conditions.

B. Physical Characterization of Potassium Chloride

As previously noted, all potassium chloride used in this study was processed via a milling and screening procedure. The resulting

---

e Fisher Scientific, Springfield, N.J.

f J. T. Baker Chemical Co., Phillipsburg, N.J.

g Mallinckrodt Inc., Drug & Cosmetic Division, St. Louis, Missouri.

material was then evaluated for moisture content, density, and particle size criteria.

B.1 Moisture Content - The measurement of moisture content for all size fractions was patterned after the techniques used by Lazarus and Lachman(45). The samples under consideration were monitored for weight changes using an analytical balance[h]. The measurements were made in glass weighing bottles equipped with ground glass covers. The bottles were previously rinsed with distilled water and dried at 175°C for 24 hours in a laboratory oven[i]. Approximately 20 grams of potassium chloride was then introduced into the bottles and dried at 120°C for 2 hours to ascertain the amount of moisture present on the crystal surfaces of the sample. The hot weighing bottles containing the samples were placed in a desiccator over calcium sulfate and allowed to come to room temperature (approximately 1 hour) prior to making the weighings. All weighings were done in duplicate to assure accuracy of the data obtained from the analytical balance. The samples were then returned to the oven and heated at 175°C with measurements being taken at 24-hour intervals. Each weight measurement was taken as previously described and was repeated until no changes were noted in the sample weight. All sample testing was performed on three replicates for each type of potassium chloride.

---

h Type B-6, Mettler Instruments, Hightstown, N.J.

i Precision Scientific Co., Chicago, Ill.

B.2 Density - All density measurements were made using standard pycnometric methods, employing an intervention fluid of known specific gravity and a Gay-Lussac pycnometer[j]. Later studies confirming these data were made using a helium pycnometer[k].

Standard pycnometric procedures were employed which involved accurate measurement of empty weight for each pycnometer. Then each pycnometer volume was measured using the intended fluid which was filled into the pycnometer. The Gay-Lussac bottles employ a ground glass stopper with a capillary. Once filled, the stoppered is firmly seated and excess fluid is wiped off the capillary tip. The pycnometer is then permitted time to equilibrate in a water batch at 23°C for 1 hour. The weights are made after drying the pycnometer with a paper towel. Care is taken not to draw any liquid out of the capillary. This process permits the worker to accurately calculate volume when using fluids of known specific gravity. The same process is employed when measuring the solid samples; however, the liquid and solid are sonified[l] to remove any entrapped air prior to bringing the pycnometer to final volume. The determinations for density were all run in triplicate. All weighings were made using an analytical balance. The density of the solids under consideration may be calculated using the resulting data in the following equation:

$$\rho \text{ unknown} = \frac{(\rho \text{ liq.})(\text{m samp})}{(\rho \text{ liq.})(\text{V pync})+(W_1 - W_2)} \qquad \text{(Eq. 18)}$$

---

j Fisher Scientific, Springfield, N.J.

k Model #130/20000, Micromeritics, Norcross, Georgia.

l Branson, Model #D-50, Cole Palmer, Chicago, Illinois.

where ρ is the known density (g/cc) of the liquid, m (g) is the sample weight, V (cc) pycnometer volume, W_1 (g) combined weight of the sample and pycnometer, W_2 (g) combined weight of the sample, pycnometer, and liquid.

The helium pycnometer used in these experiments took advantage of displaced sample volume measured by the amount of helium required to fill an evacuated sample cell containing the solid to be measured. Calibrations were accomplished by using a polished steel sphere of known volume. These data were then used to calculate density using an accurate weight measurement of the unknown sample. The results were in agreement with data obtained from the previous "wet" method and that found in the published literature.

B.3 Particle Size - The particle size of the respective fractions of potassium chloride were determined using two methods. The first method employed the use of series of U.S. Standard Sieves[m]. This nest of screens was placed on a sieve shaker[n], which is set at an an intensity level of seven for a duration of 20 minutes. Sample size used for these determinations was 200.0 grams total weight. The sieve patterns were run five times for each sample of material using fresh sample for each measurement. The shaker intensity of seven for 20 minutes and the sample size were selected based on past experience

---

[m] U.S.A. Standard Testing Screen, Fisher Scientific, Springfield, N.J.

[n] Cenco-Meinzer Sieve Shaker, Control Scientific Co., Div. of Cenco Instruments Division, Brookview, Illinois.

with potassium chloride. These conditions were noted as being reproducible with minimal screen blinding and occlusion.

The second method for particle size characterization involved the use of dark field microscopy. Several representative samples were withdrawn and placed on a glass slide for examination. Representative fields were viewed, measured, and subsequently photographed for later analysis.

B.4 Microscopy - A compound microscope[o] was used throughout this investigation. The system was set up with a dark field light condenser to augment the contrast necessary for examination of features in the relatively clear crystalline material. The dark field condenser was normally used in the transmitted mode, wherein the light is projected from beneath the sample. If the circumstances require, the light source may be redirected to an incident configuration by use of a special objective lense system[p]. In this situation the light path, which is projected from above, is parallel to the objective lense. Via a set of mirrors the light is directed onto the sample from the sides, which effectively renders dark field illumination. In both situations, the microscope is calibrated using a standard target[q] of known dimensions (0.1, 0.01mm). This target slide permits the obser-

---

o Panphot, Ernst Leitz, New York, N.Y.

p Ultropak, Ernst Leitz, New York, N.Y.

q Bausch & Lomb Inc., Union, N.J.

ver to accurately calibrate either the reticle located in the eye piece or the image taken using the film back[r].

The accurate determination of field magnification may be obtained by either of two methods depending on whether the observer utilizes the film back or the standard eye piece. The following equation is used for determining the magnification at the eye piece:

$$M = M_{eye} \times M_{obj} \times 1.25 \qquad \text{(Eq. 19)}$$

The factor 1.25 is a correction for the tube factor of the microscope utilized. Tube factor is the additional magnification imparted by the optics contained in the body tube of the microscope.

When using the film back, a correction factor for the distance between the film plane and the objective must be used:

$$M = M_{obj} \times M_{eye} \times 1.25 \times \frac{\text{bellows length (cm)}}{25 \text{ cm}} \qquad \text{(Eq. 20)}$$

Where to calculate the image on the film, the magnification is multiplied by the length of the bellows extension in centimeters and divided by the standard length of 25 cm.

When using the film back, it was found that a high speed[s] black and white film yields the most detailed results. To add further contrast, the use of a #22 Wratten gelatin filter[t] was found to enhance the quality of the resulting photomicrograph. It was noted that particle measurement is somewhat easier when using photographs which have

---

r Polaroid 4x5 Film Holder, Polaroid, Cambridge, Mass.

s Polaroid Type 57/High Speed, Cambridge, Mass.

t Eastman Kodak, Rochester, N.Y.

been properly calibrated using the target slide (calibrator). Three representative samples were withdrawn from each subject lot of material, placed on slides, and observed at the required magnification.

When more detailed analysis became necessary, a scanning electron microscope[u] was employed. This technique permits the investigator to observe crystal interfaces and boundaries normally encountered in compacted systems. The sample to be studied is mounted onto a sample holder and placed in a chamber which is evacuated then charged with argon gas. Also contained in the chamber is an aluminum block coated with gold. A current is applied to the block causing the gold to "vaporize" in the chamber affecting a gold foil to be deposited onto the sample. The resulting foil on the sample is approximately 100-150A° in thickness. Gold is used primarily as it is a good conductor of electricity and an excellent emitter of secondary electrons. The sample is observed under a evacuated atmosphere at approximately 10^{-6} Torr, while a current is being passed through the sample. It is this emission of electrons which is monitored by the SEM detector and subsequently constructed as a video display. The video display is photographed for analysis at a later date. The only disadvantage this technique was noted as having was related to the opaque character imparted to the samples as a result of the gold foil coating.

C. Thermal Analysis

C.1 Instrumentation - The technique of differential scanning calorimetry has been widely used by researchers in the study of long

---

[u] Cambridge S180, Monsey, N.Y.

chain fatty alcohols. The technique of differential scanning calorimetry (DSC) may be thought of as the measurement of differences in energy inputs into a sample and a reference material as a function of temperature. The sample and reference are usually exposed to a time based temperature program (heating rate, °C/min). The measurement of the resulting difference in energy input to the sample and reference varies with the type of instrumentation being used. In the research presented here a DuPont 990 Thermal Analyzer[V] in conjunction with a DuPont 910 Differential Scanning Calorimeter[W] were employed. The DuPont system takes advantage of heat flow or flux differences between the reference and sample containers(103). A schematic representation of the DSC cell is shown in Figure 7.

C.2 Sample Treatment - All samples tested were accurately weighed into aluminum pans specifically designed for use in the Dupont 910 DSC system. The aluminum pans used were nonhermetic sealing and consisted of a pan into which the sample was weighed. The cover was aligned in the pan with the hollow side facing up to minimize open space within the sample pan. This assemblage of pan, sample, and cover was then crimped using the encapsulating press supplied with the DSC system. To assure optimal contact between the sample pan and the constantan disc in the DSC cell, each sample was inspected to assure flatness. A flat sample area prevents thermal gradients within

---

[V] DuPont Company, Analytical Instrument Division, Wilmington, Del.

[W] Dupont Company, Analytical Instrument Division, Wilmington, Del.

the sample and between the pan and the constantan disc. The sample pans (lids and pans) to be used in this study were cleaned in reagent grade methylene chloride[x] and subsequently air dried to eliminate any possible interference with the measurements due to traces of lubricant used during the pan/cover manufacturing process. The weight of each sample was determined by difference.

All thermal scans were carried out using a metal cooling can in place over the cell. This method permitted DSC measurements below ambient temperature (approximately 25°C). The cooling can was separated from the cell by a Teflon® disc, which acts as a thermal insulator to avoid erratic baseline disturbance during charging of the coolant. The coolant used was "dry ice", solid carbon dioxide in a slurry with acetone. This ice slurry resulted in a constant cold sink, which allowed accurate scans down to -10.0°C at atmospheric pressure. Additional "ice" was added during a scan to account for sublimation. The cooling can was enclosed in an open top bell jar, which was purged with a constant flow of dry nitrogen[y] to prevent atmospheric moisture from condensing near the cell. This was accomplished by allowing the nitrogen source to flow through a bed of moisture indicating desiccant[z]. This dry gas stream was then connected to the vacuum inlet port on the 910 DSC cell base. The sample chamber was purged with dried nitrogen[aa] (high purity) at a flow rate of

---

x Fisher Scientific, Springfield, N.J.

y Matheson Gas Products, East Rutherford, N.J.

z Drierite®, W. A. Hammond Drierite Co., Xenia, Ohio.

aa Matheson Gas Products, East Rutherford, N.J.

10 cm^3/min. The gas is heated by the silver block prior to entering the sample chamber. It then circulates through the disc area and exits through a hole in the silver lid(134). The use of an inert atmosphere prevents oxidative reactions during investigation. The nitrogen flow was controlled by a flow meter[ab], which was placed in line to assure 10 cm^3/min at standard temperature and pressure (14 lb/in^2). The flow of nitrogen was directed through the cell purge inlet on the 910 DSC cell base.

C.3 Calibration - Prior to using the calorimeter, several system checks were made. Two empty aluminum crimped pans were put into the system and a temperature scan was run through the desired temperature range. The slope of the resulting line was adjusted via a baseline control to achieve a horizontal line with respect to the grid on the recording paper being used. This baseline correction simplified subsequent temperature determinations and energy calculations. Once a flat baseline was established, the system was corrected and calibrated to standard temperature points. Room temperature calibration was carried out using a standardized thermometer[ac]. The instrument was allowed to come into equilibrium with the room for approximately 1 hour. The output on the chart recorder was then compared to the thermometer and corrections were made, if required. This check was run prior to all testing carried out during each work session.

---

ab Lab-Crest Scientific, Warminster, Pa.

ac Kessler, Westbury, N.Y.

The chart paper used in high temperature calibration has been corrected to account for heat flux encountered when using chromel/ alumel thermocouples. With the corrected paper in place on the recorder, a scan was run using one of several melting point standards commonly used in thermal techniques.

The reference sample employed in the study was indium[ad]. This metallic sample has a well defined, reproducible endotherm, which allows simplified temperature determination and correction, if needed. The melting point for indium is listed in the literature as 156.61°C[ae]. The thermal analyzer was corrected to this point to calibrate the high temperature range for the DSC system. The specifications for the DSC cell note an accuracy level of ±1°C. The results achieved with the reference standard suggest that this temperature tolerance can be attained after the corrections are made using the indium sample. Actual calibration temperature attained using corrected recorder paper was $\bar{x}$ = 156.6°C with a relative standard deviation of 1.9% (n = 10). The melting point of the sample was determined by convention as the intersection of tangents drawn to the baseline and leading edge of the melting endotherm(104,105,106).

Low temperature calibration was carried out in a similar manner. However, the corrected paper was replaced with standard grid paper which was printed in graduations of 2.5°C per centimeter on the x axis. Two low temperature calibration samples were used. These

---

ad Ventron, Alfa Products, Beverly Mass., Lot #081773.

ae R. C. Weast, (Ed.), "The Handbook of Chemistry and Physics," Fifty-Third Edition, Chemical Rubber Publishing Co., Cleveland, Ohio (1972-1973).

samples are traceable to the National Bureau of Standards. These commercial calibrators[af] were selected because their melting points correspond quite well with the range normally encountered with fatty alcohols. The composition of these calibrators is proprietary and was not divulged by the manufacturer. One calibrator was rated at 51.1±1.0°C by the supplier. The second calibrator was rated as 66.2±1.0°C. These low temperature samples were scanned using the same heating rate (5°C/min) and sensitivities (10 mV/cm, 5 mV/cm, y axis) to be employed for fatty alcohol characterization. The DuPont 990 used in this work was equipped with a two pen x-y recorder. The two y-axis sensitivities permit the researcher to scan a sample using a low sensitivity to accommodate the entire thermal event while the high sensitivity allows detailed examination of minute changes in the DSC curve. The heating rate of 5°C/min was selected based on experience using slower and faster rates and was found to yield the best resolution and reasonable sample testing rates. It was also felt that this rate of heating is representative of the conditions normally encountered in a production processing environment.

The results found for the low temperature calibrators were well within the accuracy range anticipated for the system being used. The 51.1°C sample yielded an $\bar{x}$ = 51.3°C with a relative standard deviation of 0.6% (n = 10). The 66.2°C sample resulted in an $\bar{x}$ = 66.4°C with a relative standard deviation of 0.5% (n = 10).

Since the energy liberated or absorbed by the sample was to be calculated an additional calibration procedure was required. The pro-

---

[af] Omega Engineering, Stamford, Conn.

cedure resulted in an instrument calibration coefficient E, which relates the energy to be measured to that of a well established reference standard. The reference standard selected for this work was indium for the reasons previously discussed.

In order to determine heats of fusion or recrystallization, the x-y recorder was set using a time base (min/cm) on the x axis with the y axis sensitivity in mV/cm as in standard thermal scans. The heating rate (5°C/min) was kept constant for all analyses. As noted, the cooling fixture was maintained in place over the DSC cell during these studies. The calibration coefficient was essentially a constant over the pressure (1 atm, ambient) and the temperature range being used in the fatty alcohol studies. In addition, the use of nitrogen as a purge gas further assures the constancy of the instrument factor. Indium has a heat of fusion of 28.4 J/g (6.8 mcal/mg)[ag] as listed in the published literature. A time base scan was run at a sensitivity of 10 mV/cm and 5 mV/cm, respectively.

The resulting fusion peak areas (cm^2) are then measured using a planimeter[ah]. A baseline was drawn tangent to the recorder baseline and boundaries of the peak are defined as the beginning of deviation from the horizontal. Each peak was carefully examined to assure proper peak outline definition.

Each area measurement is made as the difference between two determinations. This is accomplished by first circumscribing the

---

ag R. C. Weast, (Ed.), "The Handbook of Chemistry and Physics," Fifty-Third Edition, Chemical Rubber Publishing Co., Cleveland, Ohio (1972-1973).

ah Keuffel and Esser Co., Teterboro, N.J.

figure recording the output, and without zeroing the planimeter, a second measurement is made. The difference is taken as the true peak area. Five such measurements are then made and averaged.

Using five samples of encapsulated indium with the DSC system run at two different sensitivity levels, several calibration coefficients were calculated using the following working equation(107) given by the instrument manufacturer:

$$E = \frac{\Delta Hm}{60\ \text{sec/min}\ A\ B\ \Delta qs} \qquad \text{(Eq. 21)}$$

where E is the calibration coefficient in μW/mV, A is the peak area in cm^2, B is the time base in min/cm, m is mass of the sample in mg, Δqs is y-axis sensitivity in mV/cm. The E values obtained from both sensitivity levels were unchanged. A sensitivity level of 10 mV/cm was selected to assure that the entire peak area would be contained on the recorder chart. High sensitivity levels were noted as having the tendency of negating studies due to chart run out and were deemed unnecessary. The E-value obtained from this calibration was $\bar{x}$ = 109.5 μW/mV (n = 5) with a relative standard deviation of 2.5%. The value of 109.5 μW/mV was used in all subsequent ΔH calculations.

To confirm this value of E, three measurements were made using fresh indium samples. The resulting ΔH values calculated using E = 109.5 mW/mV in Eq. 21 yielded $\bar{x}$ = 27.6 J/g (n = 3) with a relative standard deviation of 1.0%. These results were considered acceptable in that the manufacturer rates the instrument for calormetric precision as ±1.0% based on metallic samples. These results are also within 2.8% of the literature value of 28.4 J/g and were considered reproducible in

light of technique and instrumental variation due to experimental error.

C.4 Procedure - All determinations either for transition peak or energy measurement were carried out using the cooling device previously described. The starting temperature was set at -5°C and the cell and sample were permitted to isothermally equilibrate at this set point. Once thermal equilibrium was achieved, the uncontrolled temperature indicator light on the DSC program controller went out. At this point, after approximately 2 minutes, the scan (either time or temperature based) was begun. The upper limit temperature for the scan was selected based on the material in question and was set 5° higher than the expected melting point to permit adequate return to baseline after the desired thermal event. In all cases five samples were tested (either transition point or energy measurement) and reported as an average of these data.

C.5 Data Analysis - The data which were generated in this work took two forms. The first, as noted, was measurement of the transition points for samples of fatty alcohol. The second was measurement of the energy either liberated (exothermic) or absorbed (endothermic) by the samples.

In the case of transition point determination, five samples of the subject lot of material were scanned as described (2 cycles, each consisting of heating/cooling). The resulting DSC curves were analyzed for transition points. The points were determined by convention as the intersection of tangents drawn to the baseline and leading edge

of the melting endotherm or the trailing edge of the freezing exotherm(134,135,136).

Energies or fusion of freezing were measured on five samples of the subject material. The desired peak area was measured (planimeter) with the resulting area (cm^2) being used to calculate the energy using Equation 21. The peak to be measured was selected and carefully defined prior to area measurement. The E-value was the calibration constant previously determined.

D. Sample Preparation and Processing

This section refers to the manufacture of the granulation of matrix former and potassium chloride used in subsequent experiments. As noted in the background section, the procedure utilized for granulation manufacture was the fusion method. The potassium chloride and the fatty alcohol are combined, subsequently fused, and then cooled to room temperature. A flow diagram for this process is shown in Figure 7. This processing takes place using materials which have been characterized prior to mixing.

A planetary mixer[ai] with a capacity of 1,000-1,500 grams has been equipped with a liquid filled jacket. The fluid in this jacket may be either heated or cooled via a thermostatic circulator[aj]. The circulating fluid is ethylene glycol[ak]. The heating and cooling cycles of the sample mass are controlled by the rate of circulation and temperature

---

ai Hobart Mixer, Hobart Manufacturing Co., Troy, Ohio.

aj Type FJ, Haake, Saddle Brook, N.J.

ak MCB Manufacturing Chemist, Cincinnati, Ohio.

of the fluid in the system. Fluid temperature as well as mass temperature are monitored throughout the process. Mass temperature was measured at 2-minute intervals by shutting off the mixer and embedding a thermometer[al] in the mass. The intensity of mixing (planetary mixer speed) imparted to the sample was controlled by a variable voltage transformer[am] connected to the mixer motor.

The rate of mixing was monitored via a modified variable speed mixer[an]. The variable speed mixer has been connected to the shaft of the planetary mixer and subsequently rotates during granulation mixing. The rotation of the variable speed mixer was monitored on its mixer control module and calibrated against a hand-held tachometer[ao]. No power was supplied to the variable mixer, with its rotation alone supplying the necessary voltage to register on the RPM meter. This may be thought of as a simple generator arrangement, increasing in voltage output as the speed of the planetary mixer increases.

Once the mass has been fused and cooled, it was removed from the mixing vessel and passed through a 20-mesh screen to remove any large agglomerates. The mass was then placed in double-lined polyethylene bags and stored in sealed fiber drums in which a desiccant had been added.

If lubrication was necessary, the required amount of granulation was introduced into 2.0 kilogram capacity laboratory, V-shaped

---

al Kessler, Westbury, N.Y.

am Staco Energy, Dayton, Ohio.

an Cole Palmer Instrument Co., Chicago, Illinois.

ao O. Zernickow Co., New York, N.Y.

blender[ap]. The blending times used for lubrication were approximately 5 minutes, based on past experience with this type of granulation.

E. Assessment of Compressibility

E.1 Instron Process - A vast majority of the published literature concerning compressibility and compact behavior has been carried out using simple hydraulic/mechanical presses. These systems differ from conventional pharmaceutical compression equipment in that each compact must be prepared individually via a weighing of material and subsequent introduction in the die prior to compression. These instruments permit accurate measurement of force applied and in the case of the Instron Universal Testing Machine, a graphical output of subsequent stress decay after compact formation. It was felt that such a method should be employed to ascertain compression properties of materials to be characterized in this research. This method lends itself to development of volume reduction data, such as the Athy-Heckel or Heckel plots. The compacts prepared would also yield information as to the bond forming ability of the various materials being studied by using the tensile strength test to be discussed later.

E.2 Instrumentation Description - The Instron Universal Testing Machine[aq] employed in this work was capable of a wide range of force (200-5000 kg) application when using a high range load cell (GRM). The strain rate or cross head speed could also be varied widely from

---

[ap] Patterson-Kelley Co., East Stroudsburg, Pa.

[aq] Model #TTDM, Instron Corp., Canton, Mass.

.5 cm/min to a maximum of 20 cm/min. These variations may be employed to ascertain the sensitivity of a particular sample to strain rate. A set of standard F-press[ar] upper and lower punches and their corresponding die was used in a specially designed holding fixture affixed to the testing machine. This holding fixture has been described in the literature(44) and is shown in schematic form in Figure 9. A flat faced punch geometry was used to eliminate concavity effects on the compression results. A punch diameter of 12.7 mm (0.5 in) was selected based on previous data found in the literature(44,50,81).

The function of the Instron involves the use of a load cell within which a bonded wire strain gauge array is located. The crosshead may be set to deliver a preselected level of force automatically or may be controlled manually by observing the force level output on the recorder chart. For the numerous samples processed in this study, the crosshead was used in the automatic mode. This requires several trial compressions in order to determine the correct settings for the level controls contained in the recorder system. This process involved the use of an upper travel limit switch and cam, which are interfaced to the synchronous crosshead drive. Via trial and error, the cam is rotated manually until it disengages the drive at the desired force level. This method eliminates overtravel and variation on the force data printed on the recorder. In that a constant strain is controlled by sample weight and stress levels are determined by the automatic recorder, variations due to minor flexure in the holding fixture were

---

[ar] Elizabeth Carbide Die Co., Inc., McKeesport, Pa.

considered as having no direct impact on the data treatment and results.

E.3 Calibration: Instron - Calibration of the testing machine involves the use of an internal calibration circuit, which shorted the strain gauge to a known resistance equivalent to a 200 kg force level. By adjusting the recorder to a setting of 200 kg full scale deflection, the resulting measurements at all force levels are then calibrated. To assure the internal calibration was correct, four 5.0 kg calibration weights[as] were placed on the load cell and the resulting 20 kg force level was checked on the chart recorder and compared to the 200 kg calibration signal. Excellent agreement for the 20 kg load was found with the recorder set on 200 kg full scale, thus attesting to the accuracy of the calibrator circuit. Calibration using the internal system was checked prior to each work session and each change in force level used in compression.

E.4 Procedure: Instron - Samples to be compressed were accurately weighed using a digital balance[at] capable of resolving 0.1 mg quantities. A 55 mm x 25 mm micro weighing funnel[au] was used during the weighing to assure complete transfer of material into the die cavity on the Instron assembly. Application of several sharp taps to the die holding fixture were made to assure the granules were

---

as Instron Corp., Canton, Mass.

at Scientech 222, Boulder, Colorado.

au Radnote Glass, Arcadia, Ca.

adequately settled in the die cavity. The die wall was dusted lightly with magnesium stearate prior to each sample compression. The crosshead was set in motion at the selected rate and the sample was subsequently compressed. The crosshead continued to deform the sample until the preselected force level was achieved.

Thickness of the compacts was maintained at a constant level by varying the weight of material introduced into the die. This procedure assures a constant basis of strain (dimension) for all samples studied, which may vary due to bulk density and particle configuration(91). A preliminary compaction of each sample was carried out to determine the amount of material required. The rate of strain or cross head speed was selected based on the sample properties desired to be tested. For most samples, wherein the extent of bond formation is the desired result, a rate of 10 cm/min was employed. Strain rates up to 20 cm/min were used in selected cases to assess the compact's dependence on the rate of compaction. It was felt that although published data for strain rates are usually in the range of 1 to 5 cm/min, the use of higher compression rates would yield data which were more predictive of results normally seen under conventional compression rates used in pharmaceutical manufacturing. This was due in part to the nature of this investigation, which in fact was to characterize a phenomenon noted during normal potassium chloride processing.

The dwell time for each sample may be varied at this point by selecting either manual or automatic reversing of the crosshead. A short dwell time may be obtained by having the crosshead reverse immediately when the desired force level is achieved. This function may be preset on the Instron by using the automatic reverse option.

In this manner, dwell times as low as 0.2 seconds with a crosshead speed of 10 cm/min and a chart speed of 50 cm/min can be determined accurately and reproducibly.

The 0.2 second dwell time was somewhat longer than that which has been previously reported by other workers(77,87) for standard compression processes. It was felt, however, that this dwell time would serve as a good basis for comparative analysis between compacts generated using short (0.2 sec) and long (10.0 sec) dwell times. The long dwell times were determined by monitoring the chart recorder until a distance equivalent to 10 seconds had been traversed (approximately 8.3-8.7 cm). Once 10 seconds had elapsed, the crosshead was reversed. As a check on this process, a stop watch was activated as soon as the preset force level was achieved. The crosshead reverse was engaged at the end of 10.0 seconds. The accuracy of these times were confirmed by measuring the length (x axis) of each force curve, with any samples not in the range of 10-10.5 seconds of dwell time being discarded.

Once compression is completed, the compact is ejected from the die using the fixture which allows upward forces to be applied to the lower punch via a lever assembly (Figure 9). This lever permits extrusion of the compact by lifting the bushing which contains the lower punch, thereby pushing the compact up from the bottom and out of the die. Each completed compact was placed in a numbered tray to assure identification of the individual compact and related force curve prior to any further testing.

E.5 Data Analysis, Tensile Strength - The thickness of the finished compacts for tensile strength testing made using either long or short dwell time was measured after ejection. A series of five individual compacts were processed to form each data point. Compacts which were used to establish zero time tensile strength data were tested within approximately 2 minutes after compression. Remaining samples were then placed in appropriate containers, either open or closed, to determine aging effects. Tensile strength was then determined at selected time intervals using Equation 17, which states:

$$\sigma = \frac{2P}{\pi Dt} \qquad \text{(Eq. 17)}$$

E.6 Data Analysis, Heckel Plots - Compacts which were used to generate data to construct Heckel plots were treated in a similar manner. However, in the case of volume reduction analysis, it was considered a better approach to use ten individual compacts per data point to minimize variation. The variability of Heckel plot analysis has been discussed in the theory section. No less than 15 equations exist which attempt to define compression processes(108). The discussion concerning characterization of bonding mechanism gives a detailed account of the Heckel equation and subsequent plots. However, for clarity, the data treatment will be reviewed at this point. The data were treated using Equation 4 which states:

$$\ln (1/1-D_{rel}) = kP + a \qquad \text{(Eq. 4)}$$

The relative density term was calculated by Equation 3:

$$D_{rel} = \frac{D'}{D} \qquad \text{(Eq. 3)}$$

Where D' is the apparent density which is the compact's actual weight divided by its volume. The compact was considered a simple cylinder whose height was the tablet thickness with a diameter of 12.7 mm as determined by the tooling utilized. This was confirmed by periodic measurement of the compact diameter and was found to vary minimally.

The true denisty of the sample material D is determined as previously noted in the particle characterization section. The resulting relative density data was normalized as shown in Equation 4 and then plotted as a function of applied pressure P. The yield pressure for samples were calculated from the final linear portion of a plot of ln(1/1 - D_{rel}) versus applied pressure. Recall from Equation 5:

$$k = 1/Py \qquad \text{(Eq. 5)}$$

Where K is a constant equal to the reciprocal of the mean yield pressure Py(72).

The use of two dwell times was an attempt to quantify the amount of plastic deformation occurring during compaction. The data from these two contact times were plotted as noted. The areas under the curves were measured for the two dwell times. The differences between the areas are a function of the extent of plastic flow which has taken place in the samples. All compact measurements were made at zero pressure to exclude any elastic component which would be present under pressure. The inclusion of an elastic component would lead to

increased values of ln $(1/1-D_{rel})$. Following this procedure provides a tool for meaningful comparative analysis within groups of similar materials.

E.7.a Instrumented Tablet Press Process - The use of standard pharmaceutical compression equipment is a necessary component of any investigation into problems arising during standard manufacturing processes. The use of an instrumented single station press satisfies this requirement and permits the investigator to collect data not normally obtained during more exacting compression studies as noted in the Instron section. For the purposes of this research, a single station F-press[av] was selected for instrumentation with respect to force analysis. Instrumentation applied to measurement of forces involved in tablet formation has been an analytical tool available to the physical pharmacist for many years with some of the published literature dating back 30 years(109). More recently, strain gauge technology in force analysis has been joined by the piezoelectric transducer. The growing popularity of piezoelectric force transducers can be attested to by increased reference to their use in the published literature(85,102,110,111).

E.7.b Instrumentation - The instrumentation applied in the present research involves the use of piezoelectric force transducers. This decision was made based on the nature and strength of the signals generated by these type of force transducers. It was intended

---

[av] Stokes Compacting Equipment Division, Pennwalt Corp., Warminster, PA 18974.

to characterize the diametral force generated using the F-press. The installation technique for the piezoelectric transducer appeared to be preferable when compared to that of strain gauges applied for measurement of die wall force. Another factor which contributed to the selection of a piezoelectric system resides in the fact that the events to be monitored are quite short (approximately 0.5 sec). This obviates the need for the long term signal stability imparted by a strain gauge circuit.

The ICP (integrated circuit piezoelectric) system[aw] selected involves the combining of a miniature voltage amplifier into the same enclosure with the piezoelectric or quartz element. The quartz element is the basis of force measurement.

The ICP transducer (Figure 10) is powered by a well regulated voltage source (approximately 24V). This resulted in a simple 2-wire transducer system, which possessed a fixed voltage sensitivity, independent of cable length or capacitance. The low output impedance (100 ohm) allowed use in dusty environments. The resulting signal was quite large (-10 to +10V) with low noise, which could be directly interfaced into common types of readout instrumentation. In order to maintain a zero level or no signal baseline, the power supply[ax] output was configured as a clamped circuit. By using this type of power supply, all voltage outputs are maintained as positive, obviating the normal tendency of AC coupled signals to move to a stable condition of swinging from a negative position below the no signal level to a posi-

---

[aw] PCB Piezotronics, Depew, N.Y.

[ax] PCB Piezotronics, Depew, N.Y.

tive signal level. Repetitive compression signals slowly move to a stable condition, where the average level corresponds to the zero position. In this position the area above the zero level equals the area below this level(112). This is a common observation when operating an oscilloscope in the AC mode. The clamped circuit option on the commercial power supply eliminated this problem. This permited simplified data measurement and comparison between events.

The use of this sophisticated transducer and power supply arrangement requires the researcher to be aware of two areas which may cause intrinsic system errors. The first is an artifact of the clamped circuit. Although the averaging problem is removed during repetitive events, the power supplies build up a positive charge, which causes the baseline to deviate in a positive direction with each subsequent event. To eliminate this problem, the power supplies must be grounded via a built in control circuit in between each event. The grounding system is accomplished by using an external ground switch which was affixed to the compression machine. By installing the limit switch[ay] in a position where it could be actuated at an appropriate point between compression events, an excellent baseline set point for subsequent data analysis was maintained.

The second point which one must be cognizant of is the time constant for the transducers being used. The time constant of a specific transducer is a product of the bias resistor value (ohms) and total shunt capacitance (pF), the product of which is represented in units of seconds of time(113). Caution must be exercised to maintain the

---

[ay] Micro Switch, Division of Minneapolis-Honeywell Regulator Co., Freeport, Ill.

event within 1.0% of the time constant for the transducer being used. The transducers which were used in this work have a time constant of 500 seconds. This means that one is assured of accurate voltage readings when the duration of the event is 5 seconds or less. The force events seen in single station compression are substantially less than 5 seconds and are not considered to have sufficient duration to influence the resulting data. The accuracy of the output under these conditions is ±2.0% of the measured voltage assuming the recording instrumentation is calibrated.

The components which were instrumented include the upper punch, die wall, and lower punch. The transducer which was used for lower punch instrumentation was capable of high sensitivity in order to characterize ejection forces required after tablet formation. The components which were instrumented are illustrated in Figure 11 with respect to their location and configuration on the F-press.

The upper punch holder was replaced with one which was specifically designed to accommodate the upper force transducer[az]. This provided an adequate fixture to assure proper placement of the force cell assembly. This also permitted the cell to be pre-loaded in the punch holder to assure a zero baseline without a force applied. A drawing showing the upper punch holder construction and the transducer location is presented in Figure 12. The transducer cell was placed in the cavity then the punch holder was aligned and fastened by two 0.5 in. machine bolts to the upper punch yoke on the F-press (see Figure 11). The pressure exerted by the two bolts holds the

---

[az] PCB Piezotronics, Depew, N.Y.

transducer in place while the cavity spacing prevented any spurious force readings during zero force conditions.

The lower punch force transducer was installed as an integral part of the lower punch plunger[ba]. The lower punch holder was cut into two parts. A load stud was then installed in the lower segment. This stud acted as a central connection which passes through the transducer and permits the upper punch holding segment to be threaded in place. The overall length of the punch plunger was corrected to its original overall length (Figure 13). The transducer was pre-loaded in this case to assure a zero baseline. This was accomplished prior to installation in the F-press lower punch assembly (Figure 11).

The die wall instrumentation involves modifications to the standard die and the die table. The die dimensions follow standard specifications given in the IPT tooling handbook[bb]. The die[bc] was fabricated and heat treated to assure a constant elastic modulus prior to installation of the force transducer (Figure 14). The transducer was subsequently installed and pre-loaded to assure a zero baseline at zero pressure input. To install the instrumented die into the die table of the F-press required a channel to be milled into the die table, thereby permitting the transducer connection to extend out from the die socket (Figure 15). To maintain a flat die table, the channel was fitted with

---

ba PCB Piezotronics, Depew, N.Y.

bb "Tableting Specification Manual, IPT Standard Specifications for Tools," IPT Section of Academy of Pharm. Sci., APhA, 1981.

bc PCB Piezotronics, Depew, N.Y.

a plate to cover the channel during press operation. The die used in this work possessed a 12.7 mm (0.5 in) bore diameter. The die was held in place using the standard die screws contained in the F-press.

E.7.c Calibration: Instrumented F-Press - All fabricated components were calibrated by the manufacturer prior to delivery. To confirm these data, all transducers were checked using the Instron prior to installation on the F-press. In this manner the force exerted on the transducer was recorded by the Instron strip chart and simultaneously the voltage output from the transducer was read using a digital voltmeter[bd] (accurate to 1.0 millivolt). The resulting force versus voltage data were compared to that supplied by the manufacturer.

The procedure used to calibrate the transducers involved affixing the various components to the load cell (GRM or CDM as required for sensitivity range) of the Instron. This was accomplished by using rods which were threaded into the chasis of the Instron. These rods were then equipped with three prong laboratory clamps[be], which held the various components in place during force application. The upper and lower punch holders were calibrated with 12.7 mm (0.5 in) flat punches in place. The die wall was calibrated by setting the die on top of the lower punch holder via the previously described clamp arrangement. A rubber plug has been documented by various workers(89,114,115) as approximating a hydraulic fluid. This suggests quite simply that any applied force in one direction will transmit an

---

bd Keithley, Los Angeles, Ca.

be Fisher Scientific, Springfield, N.J.

equivalent hydrostatic pressure in all directions. In this manner a known calibration force applied to the rubber plug surface will generate an equivalent force diametrially within the die. Riener(58) confirmed this observation when soft materials are contained within a die during simple compression. A neoprene[bf] rubber plug was made with a 12.7 mm diameter and a height of 6.76 mm thickness using a cork borer[bg]. The thickness was confirmed using a vernier caliper[bh].

The upper punch holder was set in place on the GRM load cell using the clamping fixture. The chart recorder on the Instron was subsequently zeroed to account for the mass of the punch holder. The 200 kg calibration signal was used to ascertain the accuracy of the load cell as described in a previous section. The crosshead of the Instron was equipped with a 12.7 mm punch which was subsequently aligned with the punch contained in the upper punch holder. The crosshead was set at a strain rate of 10 cm/min. This speed was determined by trial and error to achieve a minimal voltage decay during the test interval in light of the time constant constraints for the transducer. The chart recorder on the Instron was maintained at 50 cm/min for all tests. The automatic reverse was employed to assure minimal dwell time during calibration. Each calibration point represented an average of 10 determinations. All data generated was converted into pounds of force to simplify comparison to calibration data supplied by the manufacturer. All voltage measurements were

---

bf Goodyear Rubber Co., Newark, N.J.

bg Fisher Scientific, Springfield, N.J.

bh L. S. Starrett, Athal, Mass.

subsequently divided by the force (pounds) readings from the Instron and are reported as average sensitivities for comparison to documentation data.

The lower punch was calibrated in a similar manner. However, the high sensitivity range (100 to 200 pounds) was measured using the CDM load cell. The results from these calibrations of the upper and lower transducers are summarized in Table V and graphically depicted in Figures 16 and 17. The resulting sensitivities measured in our laboratory were in good agreement (approximately 3.0%) with the data given by the manufacturer based on system and technique variation. The data appeared to follow a trend somewhat lower than the provided data which might suggest some voltage decrease during the calibration procedure. However, the results are considered to be within reasonable experiemntal error and provide confirmation of the validity of the provided calibration data.

The die wall calibration involved another variable which must be monitored during calibration. The data provided by the manufacturer is given in units of PSI. Since diametral force is a function of area presented to the die wall for measurement, correction must be made for the plug due to deformation under pressure. This deformation constitutes variation in the cylinder height and, therefore, the related surface area of the rubber plug. The calipers provided with the Instron permit accurate measurement of crosshead movement. Therefore, by suitably adjusting the crosshead/punch assembly within the die, plug height may be determined accurately at all force levels. The resulting data from the Instron have been corrected to reflect the pressure in units of PSI with respect to cylinder height.

The instrumented die was affixed using the clamping fixutre over the lower punch holder in the Instron. The die was aligned with the lower punch land area to assure reproducible positioning for all testing. The plug was then inserted in the die and a zero pressure measurement of plug height was taken with the Instron caliper. The resulting plug height of 6.80 mm was in good agreement with the 6.76 mm measurement made with the vernier calipers.

The resulting die calibration data are summarized in Table VI as a function of force readings and plug height using the Instron. The data are shown graphically in Figure 18. The results suggest a somewhat lower trend than that of the manufacturer. However, the resulting line adhered closely to the standard results. This deviation may be attributed to the difference in test techniques used in our laboratory and serve to confirm the established calibration data. As noted, voltage decay is most likely the factor involved in this case and the results suggest good confirmation within expected experimental error.

Since the supplier routinely calibrates such pressure/force instrumentation and our results adhere resonably well, the provided vendor's calibration was used in all subsequent data analyses. Discussions with the transducer manufacturer[bi] confirm the difference as being at a reasonable level for calibration of such force measuring instrumentation. Following calibration, all instrumented components were installed in the F-press as described previously.

[bi] L. Zagst, PCB Piezotronics, Depew, N.Y.

E.7.d Procedure: Instrumented F-Press - For samples of granular material which do not flow readily (i.e. non-lubricated), the samples to be compressed were weighed out[bj] on an individual basis and then introduced into the die. The F-press was rotated by use of the hand wheel to allow the lower punch assembly to be seated solidly with the weight adjustment ring resting on the lower punch holder housing. This point corresponded to the normal die filling position during powered operation.

The recording instrument used in this work was a high speed oscilligraphic recorder[bk]. The recorder has five separate channels which provide ample flexibility for recording all resulting force data. The oscilligraphic recorder was selected over other instrumentation (i.e. digitalized or analog to digital computer interface) due to the limitations imposed by the flow of the subject materials. The recording device was capable of linear speeds to a maximum of 500 mm/sec. This recording rate was found to permit accurate detailed analysis of all force data, including the more intricate data generated by the ejection (lower punch) and die wall transducers. The recorder's y-axis offered a wide range of sensitivities, allowing characterization of low voltage signals. Trial and error has shown that y-axis sensitivities between 100-200 mV/cm yield adequate resolution for data interpretation of low voltage output for all subject samples.

Prior to collecting force data, the individual transducers were zeroed using a digital voltmeter. The power supplies were equipped

---

bj Scien-Tech, Boulder, Colorado.

bk Western Graphtec, Irvine, CA.

with a potentiometer which allowed accurate zero correction. The recorder was also adjusted to a zero point. Following this procedure, the transducers were calibrated via an internal calibration circuit contained in the transducer power supply. The calibration circuit produces a 1.000V output which was checked on the digital voltmeter and the recorder. This procedure was carried out with the clamped circuit disabled to permit accurate correction of the recording device. Once complete, the clamp circuit was engaged to hold the corrected zero level as described elsewhere in this work. The sample material (previously accurately weighed) was charged into the die and the F-press energized to permit compaction under normal running conditions.

E.7.e Data Analysis - The force results were recorded as a function of voltage and were subsequently converted to force using the calibration curve provided by the manufacturer. The data treatment has been detailed in the background section and will be critiqued for selected sample analysis in the results section.

F. Compact Strength Measurement

F.1 Instrumentation - We have previously discussed the need for accurate assessment of the strength of compacts or tablets generated by the compaction process. The techniques described by Fell and Newton have been employed in this research(93,94,95). Previous experience with compacts whose composition is similar to the samples in question has shown these procedures to be reproducible and predictable with respect to tablet quality.

For this research, a conventional tablet hardness tester was employed. The Heberlein[bl] unit used was equipped with flat plattens, which may be padded as noted by Rudnick(92). The padding material was standard blotter paper (approximately 0.03 cm thickness). Most compact samples tested in this work did not require padding to achieve tensile failure. Samples tested with padding are be noted in the results section. All force measurements were recorded as kiloponds of force[bm].

F.2 Calibration - Variation of hardness testing instruments has been documented by Brook and Marshall(99). To account for variation encountered in this work a calibration procedure was established using mechanical tablets[bn], which are designed to "fracture" at selected force levels (5, 10, 15 kp). The mechanical tablets as supplied by the manufacturer were tested using an Instron[bo] Universal Testing Machine equipped with a high sensitivity load cell (CDM cell) to establish a known force value for the fracture limit assigned by the manufacturer. The Instron cross head was set at a strain rate of 1 cm/min for all tests conducted on the mechanical tablets. The weight (approximately 175 gm) of each mechanical tablet was accounted for by zeroing the Instron recorder prior to each determination. Recorder speed was maintained at 10 cm/min for all tests. The calibrators were also tested

---

bl Model #2E/106, Cherry Burrel Corp., Cedar Rapids, Iowa.

bm Kilopond = 1 kilogram of force.

bn Schluiniger, Vector Corp., Marion, Iowa.

bo Model #TTDM, Instron Corp., Canton, Mass.

using the tablet hardness tester to ascertain the extent of correlation between the standardized force analysis system (Instron) and the hardness tester. The results from this calibration procedure are listed in Table VII. All determinations are an average of 10 separate measurements. A plot of these data (Figure 19) suggest reasonable correlation between the manufacturer's ratings and those seen with the Instron. However, the data generated using the hardness tester appears to follow a trend somewhat higher than expected. These results could possibly be attributed to prolonged use of the testing instrument at force levels in excess of 10 kp with resulting fatigue leading to anomalously high readings at the upper end of the linear force scale.

In light of these data, it was felt that a conversion chart should be established to correct the readings obtained from the hardness tester. This approach is creditable when one considers that the marjority of the distortion occurs at the higher force levels, while the low readings adhere closely to rated values. The chart was put in the form of a plot of Instron versus Heberlein hardness tester values. To accommodate points in between the actual readings, additional x and y points were calculated. This approach was considered reasonable for construction of the finished conversion plot (Figure 20), since the actual data points form a straight line with a correlation coefficient (R) of 0.999. Subsequently, all data obtained from the hardness tester were corrected by reading off the corresponding Instron point from the plot.

F.3 Data Analysis - The corrected force taken from the plot (Figure 20) was used to calculate the tensile strength with Equation 17, as noted previously:

$$\sigma = \frac{2P}{\pi D t}$$

The thickness (t) is measured using a dial indicating caliber[bp] with two measurements per compact being made to account for any variation. The diameter of all compacts (either from the Instron or instrumented tablet press) processed in this study was 12.7 mm (0.5 in), which was determined by the tooling employed. Flat faced punches were used in order to eliminate any potential stress localization in the compacts being tested(45). In this manner it was felt the tensile strength data derived would be indicative of the bonding mechanism for the compacted material.

To assure accurate tabulation of data, all compacts tested were placed in a numbered compartment tray for identification prior to actual tensile strength testing. Compacts for storage and aging tests were handled in a similar manner after compression. Unless otherwise noted, all tensile strength values are an average of a minimum of 5 separate measurements on five individual compacts.

The fractured compacts were inspected to assure conformance to the criteria noted by Fell and Newton(93,94,95) as shown in Figure 5. Any compacts not conforming to tensile failure fragmentation were discarded from the sample population for the data point in question.

[bp] B. C. Ames, Waltham, Mass.

Fractured samples were subsequently retained in labeled glass vials and sealed. In this manner samples which were to be subjected to further analysis (i.e. microscopy) were readily available. The sealed vials were then stored in glass desiccators as described elsewhere in this work.

IV. Results and Discussion

The data generated in this work will be discussed in related sections as outlined in the background. This will include the results obtained during the fatty alcohol or matrix former and potassium chloride characterizations and finally combinations of these materials and their related behavior.

A. Matrix Forming Components, Fatty Alcohol Behavior

A.1 Cetostearyl Alcohol - As noted in the introduction, the initial observations made with slow release potassium chloride compacts involved the use of cetostearyl alcohol. This material is actually a mixture of various chain lengths of fatty alcohols. Cetostearyl alcohol is primarily composed of C_{16} and C_{18} chain lengths. Two lots of commercial cetostearyl alcohol were selected for characterization. The composition of these two lots was determined by capillary gas chromatography and is shown in Table VIII. These data present a clear difference between the two lots with Lot #K4991 possessing a higher concentration of low weight tetradecanol which is a lower melting point material. This lot of cetostearyl alcohol also shows a reduced percentage of hexadecanol when compared to #L4593. Lot #L4593 has a total concentration of 31.9% C_{14} and C_{16} as opposed to a total of 29.7%

C_{14} and C_{16} in Lot #K4991. Both of these samples would meet USP XXI/NF XVI[bq] specifications for cetostearyl alcohol.

The two samples were scanned using the DSC system described in the experimental section. In each case five samples were scanned using two cycles each. The second cycle was run immediately upon reaching the low temperature set point (-5°C) after cooling the first thermal cycle. The temperature data in Figures 21 and 22 are for Lots #K4991 and #L4593, respectively, and are averages of all transition points measured. The thermal profiles shown are representative of the samples analyzed.

It is apparent that although Lot #K4991 has a substantially higher concentration of tetradecanol, the extent of low temperature (approximately 29-39°C) solid-solid transition is markedly increased in Lot #L4593. During the second heating cycle for both samples there is a trace of a nonresolvable transition at approximately 45-46°C. The initial recyrstallization for both samples is quite large; however, the relative peak height ratio for Lot #L4593 is quite different when compared to Lot #K4991. Both samples show similar behavior upon cooling with three distinct transitions. The first is taken as the melt (liquid) going to the high temperature α form. The α form may then follow transition patterns to the β form as a result of the mixtures of various chain lengths with some subsequent γ transformation. The fact that three resolvable transition points are seen has been documented as being the result of mixing C_{16} and C_{18} alcohols(34). These researchers have also stated that fatty alcohols in the C_{14} to C_{16} range

---

bq "USP XXI/NF XVI," United States Pharmacopeial Convention, Inc., Rockville, Md., Mack Printing Co., Easton, Pa.

have three forms, while C_{18} has only two. This assignment of polymorphic behavior has been investigated by other researchers. In an exacting analysis of these fatty alcohols Mosselman(16,26) found no supporting evidence of three forms for hexadecanol and attributes variations among reported data to variations in thermal history and sample purity.

Freezing data is taken as the most reproducible representation for fatty alcohols(116). This is reasonable when one considers that the thermal history imparted to a sample is a function of the test conditions and is under the control of the researchers characterizing the sample in question.

If one inspects Figures 21 and 22 for the second heating cycle, the extent of thermal equilibrium can be qualitatively judged. In the case of Lot #L4593, the sample retains a considerable amount of heat energy and suggests a complex series of transformations, while Lot #K4991 more closely approximates a stable system permitting each transition to occur with subsequent relaxation. This is judged by the relative displacement of the thermal profile compared to the baseline. This is an emperical test at best but can aid in an understanding of comparative differences between the two samples. Another aspect of the heating profiles which may be used for comparative purposes resides in the depression of the initial transition temperature between the two cycles. Lot #K4991, when tested under identical thermal conditions as Lot #L4593, shows a reduction of 4.8°C compared to a 6.9°C reduction for Lot #L4593. The use of transition points for evaluating fatty alcohols has been suggested by several authors(36,38).

One aspect of the thermal profile for Lot #L4593 which distinguishes its behavior from Lot #K4991 is the unusual shape of the third cooling peak. This property is present in all profiles except the original sample. This would suggest that the recrystallization behavior is a function of the test conditions used and is most likely dependent upon sample age and storage. Various polymorphic structures seen with fatty alcohols are capable of reasonable stability at ambient conditions. It is quite likely that the test interval used is not sufficiently long enough to permit return of the sample to a stable state. In addition, the potential for supercooling of particular crystal forms has been documented for various alcohols(16,26). In that mixtures of both the γ and β polymorphs are known to exist for combinations of C_{16} and C_{18}, it may be that the particular composition for Lot #L4593 permits stabilization of both forms with subsequent conversion to a single stable form upon aging(25). The cooling/heating rates employed, although reflective of the process being studied, contribute to the complexity of the low temperature structure(39). Combined with the fact that the samples being studied are mixtures, a strict assignment of crystal structure is not advisable; however, comparative analysis using these data are credible.

By inspection of the temperature data contained in Figures 21 and 22, it may be said that the two samples are quite similar in behavior. However, if the thermal profiles are compared, the differences between samples become apparent. Similar results using cetostearyl alcohol have been reported(116). In his work, Junginger tested various samples of cetostearyl alcohol. These materials comprised a high

purity sample, which was prepared using C_{16} and C_{18} alcohols, exclusively. In addition, two commercial cetostearyl alcohol samples were tested. The resulting thermograms (Figure 23) bear a close similarity to those which were shown in Figures 21 and 22. The high purity sample of Figure 23 is noted as having a phase transition at 29°C, which the author notes as corresponding to a β to α transition. The adjacent small peak was not resolvable, but it was suggested as possible γ transformation. The possibility of depression of the α phase transition to room temperature has been documented for mixtures which may acocunt for the small peak noted for the high purity sample(32).

Tanaka(20,22) has shown that some minor α to γ phase transition occurs for C_{16} alcohol. The schematic for polymorphic behavior was presented in the Background, Raw Materials Section. In this example, once the β form has gone to the α form, a trace amount reverts to the γ form with subsequent complete transition to the α form prior to melting. This may account for changes seen with mixtures of alcohols, wherein the resulting α phase may exist at temperatures approximating room temperature (25-28°C).

Batch #K4991 behaves in a similar manner to the commercial material (Lanette O) shown in Figure 23. The cooling curve shows the most detail in all cases. Batch #L4593 behavior suggests similarities to the Lanette N sample. This is due to the broad third cooling peak seen for both samples. In the case of Lanette N, Junginger states that this form of cetostearyl alcohol contains n-alkyl sulfate, which lends itself to crystal lattice disturbence and subsequent changes in the thermal profile. For Batch #L4593, some trace amounts of branched alkane contaminates may be present. This type of trace

impurity is common in synthetic fatty alcohols and would lend itself to disturbance in the crystal structure.

It was apparent from the complex results obtained from these samples that to characterize the mixture, cetostearyl alcohol, it would be necessary to profile representative samples of the primary components tetradecanol, hexadecanol, and octadecanol. These samples should range from high purity (+99%) to a level of purity encountered from commercial sources (approximately 95%).

A.2 Tetradecanol (C_{14}) - The high purity sample (+99%), A1401 was scanned using the parameters previously described. A commercial sample was tested in an identical manner. Both C_{14} thermal profiles are shown in Figures 24 and 25, respectively. The temperature data are averages (n=5) of all transition points measured. The thermal profiles shown are representative of the samples analyzed. Assignment of polymorphic phases will follow the form designated by Tanaka(20) as noted in the Background Section.

Sample A1401 exhibits a melting point which agrees well with the published literature values of 38.0°C(18,118). The cooling curves exhibit a distinct solid-solid transition at 32.5°C and initial freezing at 37.0°C. Similar results have been documented by other researchers(18,118). Upon initial heating, only one peak was noted with a two-peak cooling profile. The second heating cycle showed a minor shoulder which was reproducible but difficult to resolve at approximately 36.0°C. This shoulder may be the result of some trace amount of the α form converting to the γ form prior to melting. Tanaka(22) has discussed this possibility, noting that the β form is the primary

result of cooling a melt of tetradecanol. While heating, the stable β form results in some γ formation at the expense of the α configuration. It should be noted, however, that interpretation of heating profiles is suspect due to the rapid transitions which occur(117). The cooling curve shows two distinct peaks which correspond to freezing of the liquid with α formation, followed by solid-solid transition to the stable β form. Assignment of β configuration may not be strictly correct based on the exacting work published by Mosselman, which notes a mixture of β and γ may exist for this fatty alcohol(16,26). Several other researchers have noted tetradecanol as being a mixture of two low temperature crystal forms β and γ(18,34). The only indication of a possible mixture from our results would be the minor shoulder noted previously at approximately 36.0°C during heating.

The commercial lot of tetradecanol T03360 yielded very similar results when compared to the melting and transition points recorded for Lot #A1401. One point noted for this lot is the relative difference with respect to peak ratios when compared to Lot #A1401.

As noted in the cetostearyl section, the thermal equilibrium for various samples may be approximated based on the relative displacement of the thermal profiles from the baseline. Sample Lot #T03360 seems to retain some degree of heat energy between peaks, which suggests a somewhat more complex and rapid transition pattern when compared to Lot #A1401. Lot #A1401 appears to reach equilibrium between transition peaks, while T03360 is somewhat displaced between events with respect to the baseline. In all samples of T03360 tested, the second cooling peak height was greater than the initial freezing peak height. This suggests a larger degree of solid-solid transition

energy than the more pure sample A1401. As discussed previously, crystal structure can be disrupted by trace amounts of impurities. In that Lot #T03360 represents a sample of commercial purity (95%), it would be expected to behave differently than a sample with a greater degree of purity. This difference would be expected in the area of crystal structure disruption as noted by the relative increase in height of the second peak for this sample.

It is apparent from these data that tetradecanol transforms quickly(117) to a stable form showing a single peak upon recycling the temperature program. This contrasts with the complex patterns seen when recycling samples of cetostearyl alcohol. The mixtures appear to enhance the stabilization of various polymorphic forms which only resort to a simple state upon aging.

After inspection of the DSC curves in Figures 24 and 25, it appears that the presence of tetradecanol alone cannot be the primary factor contributing to the differences noted between Lots #K4991 and #L4593 of cetostearyl alcohol.

A.3 Hexadecanol (C_{16}) - The thermal behavior of hexadecanol is somewhat unusual and exhibits the characteristics normally attributed to fatty alcohols containing some degree of impurities(26). The resulting data produced by the thermal "fingerprints" shown in Figures 26 and 27 follow this trend with both samples yielding a complex endotherm during heating. This form of melting behavior appears similar to that of cetostearyl alcohol. The presence of two polymorphic forms in hexadecanol has been documented by several researchers (26,27, 116,119).

The analytically pure sample #E290H was scanned using five replicates. The thermal treatment was cycled twice with the resulting transition points and DSC curves shown in Figure 26. The melting point for #E290H closely approximates the range of literature values 48.5-49.7 reported(21,34,39,120). The cooling curves exhibit a solid-solid transition at approximately 42.0°C with freezing at a temperature of 48.0°C. Variation due to thermal history and sample purity may contribute to the variation seen between the data reported here and among data noted by other workers. It is reasonable to assign α formation just below the freezing point of the liquid phase. This is then followed by the solid transformation which appears to correspond to β crystal formation according to Tanaka's research. The fact that the β and γ transition points are so close may lead to false conclusions in this situation. Although the β form may be generated upon rapid cooling (5°C/min), sufficient conversion may occur during storage such that subsequent initial heating reveals a solid-solid transformation at approximately 45.0°C, which corresponds quite well with Tanaka's(20) data, which indicates a γ crystal form.

The cooling curve configuration seen for #E290H suggests a rather complete formation of the modifications noted. This may be gleaned from the return to baseline between thermal events seen in the cooling peaks. The peak height ratios are different with each sample group, suggesting a larger liberation of energy with initial freezing followed by subsequent energy evolution during final solid-solid transformation to a stable form.

Quite similar results were obtained for the commercial purity sample of hexadecanol #L2475. Five individual samples were treated as

previously described. The results are shown in Figure 27. The melting point determined for the sample was 49.1°C, which compares favorably with the range of recorded literature values of 48.5-49.7(21,34,39,120). The cooling curves exhibit initial freezing at approximately 48.3°C with subsequent solid-solid transformation occurring at approximately 41.0°C. This transformation takes place at a temperature reasonably close to that seen for the high purity material.

The most pronounced difference between the two samples resides in the shape of the resulting peaks. The commercial quality sample exhibits a shallow trough between freezing and solid-solid transformation, which may be a function of the level of impurity inhibiting complete phase shifts. This type of behavior may also suggest a rapid rate of crystallization between forms.

The assignment of phases for the sample appears to follow that given to the high purity samples, wherein a distinct solid-solid transition occurs at approximately 41.0°C. A slight non-resolvable shoulder was seen on both heating curves during solid-solid transition. This was not seen upon subsequent cooling. This shoulder could conceivably be the result of some minor transformation of the α form to trace levels of γ as proposed by Tanaka(20). However, the existence of three stable forms for hexadecanol has been discounted by Mosselman(26). The existence of β form in hexadecanol is usually the result of impurities contained in the sample. In the case of a low purity sample, strict assignment of polymorphic form must be tempered with the fact that should a segment of β phase exist, its elucidation is non-reproducible due in part to the similar transition points of the γ and β forms for hexadecanol. The heating/cooling rates used in the

study contribute to the non-resolvable nature of this type of cyrstal form.

The appearance of the C_{16} alcohol thermal curves suggests some similarities to that of the cetostearyl alcohol lots previously discussed. It seems credible to expect the presence of hexadecanol to have a reasonable effect on the behavior of mixtures C_{16} and C_{18}. The data also suggest that although a rapid cooling rate produces a solid transition which corresponds to β formation, upon aging the sample shows distinct presence of the stable γ crystal form.

A.4 Octadecanol (C_{18}) - The crystal form for octadecanol has been documented as existing in the γ configuration(18,116). The situation becomes somewhat more complex as impurities are included in the C_{18} alcohol. The results of mixing two long chain alcohols in particular hexadecanol and octadecanol yields the β modification in addition to depression of the α form to temperatures approximating room temperature. As noted in the background section, even number alcohols are capable of existing as either β or γ depending on impurities and thermal history. In particular, the formation of the γ is depressed, resulting in β formation as a consequence of C_{16} alcohol addition(18,37).

In order to adequately characterize the observations noted in the literature, a high purity sample and two commercial purity samples were tested as previously described. A second commercial sample was selected due to the marked difference observed between the high purity sample and the first commercial sample tested. The high purity sample was scanned with the results shown in Figure 28. A single

peak upon heating with a fusion point of approximately 57.0°C was observed. This temperature corresponds quite well with the literature values which range from 57.9-60.0°C(18,34,121). The results of cooling the sample showed a rather simple two-peak exotherm pattern. A freezing point was noted at 56.3°C with a subsequent solid-solid transition taking place at approximately 50.0°C. The solidification point for the cooling cycle was somewhat lower (1-2°C) when compared to literature data. The solid-solid transition took place at a temperature approximating the same depressed level as seen for solidification. This transition point has been assigned the γ conformation by previous workers in this area(116).

The results shown for the commercial samples in Figures 29 and 30, respectively, demonstrate a complex mixture of transitional forms. In both samples the three peak heating curve was only resolvable into two peaks upon cooling. This may be the result of some time-dependent behavior, which only becomes resolvable upon aging. It appears the time between cycles is sufficient for the sample to return to the stable form, resulting in reasonably reproducible heating curves.

The freezing point for both samples was in the range of 56.0-56.5°C with a distinct solid-solid transition taking place at approximately 47.0°C. The heating curves clearly suggest three peaks with the major peak corresponding to fusion at a temperature range of 56-57°C. The transitions upon heating have been assigned various forms by previous researchers. However, the documented transitions upon heating are 49.0°C for the first transition, which is lower than several documented sources(18,34). The transition which occurs at

approximately 53.0°C corresponds well to the β to α transformation level noted at 54.5°C(18). This three-peak heating behavior contrasts to the results seen with the high purity sample L020A and with Junginger's results(116) for high purity C_{18} alcohol.

The peaks seen with heating become more complex as impurities are added to the C_{18} alcohol. The transitions may be differentiated due to suppression of the transition points by the presence of the impurities. As the events become shifted to lower temperatures, the changes may be charted during thermal testing. In particular, as C_{18} is contaminated, the α transition is depressed to a level which may be resolved. Tanaka(20) scanned a sample of octadecanol with results quite similar to those seen in Figures 28 and 29.

It is apparent from these data that purity of the C_{18} sample studied is critical to its crystal structure. The level at which impurities effect C_{18} appear to be quite low, causing major changes in its thermal behavior. The presence of impurities permit resolution of various forms upon heating, which are difficult to resolve upon cooling due to hysteresis. It is apparent that the β form or perhaps a mixture of β and γ exist in a stable form for octadecanol at room temperature as a result of impurities. Pure C_{18} exhibits a single form which may be assigned a γ configuration with resonable certainty. It follows that to understand the results of mixtures of C_{16}/C_{18}, the effect of incremental addition of impurities is critical to characterize the behavior of cetostearyl alcohol, which is predominantly octadecanol.

A.5 Octadecanol/Hexadecanol Mixtures - The construction of a phase diagram using the two high purity samples was undertaken using

a series of 17 sample mixtures. The components were fused then mixed to form a homogeneous mass. The mass was cooled to room temperature and allowed to stand overnight in a glass vial as noted in the experimental section. The samples were withdrawn from these vials, weighed, and subsequently scanned using the two-cycle technique noted to assure a uniform thermal history for all samples. All transition points recorded on the phase diagram represent data obtained from the cooling curves which were found to be reproducible.

The resulting phase diagram is shown in Figure 31. The freezing line for the binary system is not flat but rather has a minor slope which suggests that the freezing points for this mixture are actually a range of temperatures. This confirms in part the variation seen with the samples studied in this research. Recall that most samples studied varied somewhat with respect to their freezing points and level of impurity.

At the mole fractions of C_{16} 0.164/C_{18} 0.836 and C_{16} 0.955/ C_{18} 0.045, we see a distinct transition of behavior from a single solid transition to that of a two-form transition pattern. As the concentration of C_{16} in C_{18} increases beyond 0.164 mole fraction to 0.271, a distinct pattern change takes place. A similar result is seen with increasing concentrations of C_{18} in C_{16}, where a mole fraction of 0.091 C_{18} generates a two-point solid transition pattern. This would suggest that C_{18} is less responsive to impurities when compared to C_{16}. This observation was not expected since the thermal behavior of previously studied samples of C_{16} and C_{18} exhibited much more variation in the C_{18} commercial purity samples. Once the concentration of C_{16} falls below 0.164 mole fraction, the system returns to a single solid

transition region. The fact that higher concentrations of C_{16} result in a transition region at a low range of temperatures would suggest potential processing problems. These process difficulties would involve caking due to retarded recrystallization at normal process temperatures, which range from room temperature to 45°C. Higher concentration of hexadecanol would be undesirable from this aspect. It would also suggest cetostearyl alcohol with higher concentrations of hexadecanol may be undesirable with respect to final tablet release rate testing, which is determined at 37.0°C.

Using the known concentrations of the two subject samples of cetostearyl alcohol, critical areas of the phase diagram can be defined. In the case of cetostearyl alcohol Lot #L4593 with a C_{16} concentration of 31.1%, it becomes apparent that the lower transition form could be favored. This is approximated by the mole fraction $0.313/C_{16}$ with a low transition point of 21.0°C. The cetostearyl Lot #K4991 has a level of 26.0% C_{16} alcohol, which corresponds approximately to the mole fraction $0.271/C_{16}$, whose lowest transition occurs at 30.0°C. As noted previously, the transition points for alcohols are much more predictive of process behavior. It becomes more interesting when one considers the fact that a mole fraction less than the $0.271/C_{16}$ level yields only one solid transition which occurs at approximately 35.0°C. Since this phase diagram is a simple binary mixture, there is no accounting for the third component C_{14} alcohol which is present in commercial cetostearyl alcohol. It is reasonable, however, to state that the level of hexadecanol is a critical factor in the final processing behavior of mixtures such as cetostearyl alcohol. Based on these data, levels of C_{16} in excess of 0.164 mole fraction can be expected to

substantially depress solid-solid transition to temperatures which may pose problems during subsequent matrix tablet processing.

Similar results have been documented by Al Mamun(35), whose research yielded solid transition shifts as a function of mixing long chain alcohols. Other researchers have noted that upon mixing long chain alcohols, the α form becomes resolvable, which accounts for low temperature transition points. These transitions have been assigned β to α, where the γ form is at a much reduced level due to the mixture of impurities(116).

Al Mamun(35) assigns a eutectic composition of 49.2% octadecanol which was obtained by extrapolation of the liquidus line in his phase diagram. The liquid line obtained in the phase diagram constructed in this work was not clearly converging to a selected point as seen in Al Mamun's data. In light of this difference, it was felt that calculation of a eutectic composition based on data from the phase diagram shown in Figure 31 was a better approximation. Using the equation for the liquidus curve(122):

$$T \cong T_A + \frac{R\,T_A^2}{\Delta H_A} \ln (1-X_B) = T_A - \frac{R\,T_A^2}{\Delta H_A}\left(X_B + \frac{X_B^2}{2} + \ldots\right) \qquad \text{(Eq. 22)}$$

$$T \cong T_B + \frac{R\,T_B^2}{\Delta H_B} \ln X_B = T_B - \frac{R\,T_B^2}{\Delta H_B}\left((1-X_B) + \frac{(1-X_B)^2}{2} + \ldots\right) \qquad \text{(Eq. 23)}$$

where starting from the left of the phase diagram T_A, T_B are the freezing points for C_{18} and C_{16} respectively, ΔH_A, ΔH_B are the heats of fusion for C_{18} and C_{16} respectively, R is the gas constant (1.9872 cal/K°mole) and X_A and X_B are the mole fractions for C_{18} and

C_{16} respectively. Equations 22 and 23 may be solved simultaneously in the form:

$$T_A - T_B + \frac{R\,T_B^2}{\Delta H_B} = \frac{R\,T_A^2}{\Delta H_A} X_B + \frac{R\,T_B^2}{\Delta H_B} X_B \qquad \text{(Eq. 24)}$$

Using the freezing temperatures from Figure 31 with the ΔH values of 52.7 mcal/mg and 58.2 mcal/mg(120) for C_{16} and C_{18} respectively an approximate eutectic composition was calculated. The composition calculated was $0.9118/C_{16}$ and $0.0882/C_{18}$ mole fractions for the binary mixture. Inspection of Figure 31 reveals that the point corresponds to the composition just outside the two transition region for the solid mixture. These calculations are a rough approximation and assume ideality with respect to both components as well as constant pressure.

It is interesting that in this situation the commercial cetostearyl alcohol lies in a complex region of the phase diagram as well as being a departure from the approximate eutectic composition. Since the cetostearyl under consideration is in fact a multi-component system care must be exercised in making strict assumptions based on the simple binary system studied here.

A.6 Energy Measurements of Fatty Alcohols - In order to clearly define variation among the fatty alcohol samples tested, it was decided to measure the energy evolved during freezing. As noted, the cooling cycles for fatty alcohols are more reproducible than the corresponding heating results. To assure the procedure was capable of producing reasonable results, a series of high purity fatty alcohols were tested with the resulting energy of fusion data compared to literature values.

The energy values were calculated using Eq. 21 and the procedure described in the experimental section using indium as a standard. The quantities of sample were corrected to represent equivalent molar amounts of each alcohol to permit comparison to the values found in the literature. These data are shown in Table IX. A good correlation of results obtained using the proposed procedure and literature values was seen. As before, variations may exist as a result of thermal history, purity, and exposure to available moisture in the laboratory atmosphere. The results are reasonable in light of the application of the data which is characterization of commercial purity samples which do not lend themselves to exacting thermal analytical measurements.

The first samples to be tested were those used in the preparation of the phase diagram. These blends would act as a guide to ascertain the effect of mixing C_{16} and C_{18} alcohols on their freezing behavior. Four samples were selected which approximate the composition of the commercial samples of cetostearyl alcohol. Each of the freezing exotherms were inspected to assure minimal change in heat capacity after each thermal event. This technique permits the drawing of a representative baseline under the freezing curve. The four samples tested exhibited a two-peak freezing curve with a deep trough between each event. The two peaks were carefully inspected and defined as to a point of departure from and return to baseline. The trailing edge of the initial freezing peak was extrapolated to baseline using the criteria described previously. The area in between the two events was not included in the calculation but was found to be reproducible with respect to area under the curve within a group of five replicate samples. This simplification is reasonable since an exact thermal analytical

assignment of energy is not credible since the samples are mixtures and not pure single entities. The resulting energy results are to be used for comparison between lots of material and their subsequent process behavior.

The results obtained from this study are listed in Table X. The initial freezing peak is assigned ΔH_1. The data shows a trend toward increasing release of initial freezing energy as the concentration of C_{18} increases at the expense of C_{16}. These results are expected in light of the data presented in Table IX for the energy of fusion. It appears that a variation of 6% in fatty alcohol ratio can be mapped with reasonable accuracy using this semi-quantitative technique. The application of this method as a probe during subsequent process evaluation appeared to be a convenient method to assign a value for each sample. A theoretical trend toward increased solid-solid transformation as a function of composition suggests that the ability of the material to return to a stable form increases with a corresponding decrease in the C_{16} component. This corresponds with the observations for the commercial samples of C_{18}, wherein the less pure sample heating curve suggests the presence of a γ formation, which was not seen in the subsequent cooling peaks.

A.7 Process Evaluation: Compaction of Fatty Alcohols - Each of the fatty alcohol samples were compacted using the Instron with the procedure previously described in the experimental section. The tetradecanol sample was not capable of forming a cohesive compact and was not included in the results shown in Table XI. No difference was found between samples which were compacted using short ($\cong$0.2 sec)

and long (≅10 sec) dwell times. All data shown in Table XI represent 10 second dwell times using two force levels. Higher force levels were not included due to a marked increase in lose of material due to extrusion around the lower punch assembly. However, the difference in the two force levels used suggests no variation of the "plastic" material as a function of applied force. Two strain rates (5 cm/min, 10 cm/min) were employed to ascertain the extent of rate of force application. No measurable difference was seen in this case with respect to rate of strain. Samples were compacted directly from the sample container and after processing in the planetary mixer described previously. In all cases the heating rate of 4-5°C/min was maintained in order to assure parallelism with the commercial process. The high purity samples were processed in a smaller container using constant mixing throughout the heating/cooling cycle. This was necessitated due to the amounts and cost of high purity sample available. In all cases the samples were allowed to come to room temperature prior to compaction. Each sample point constitutes an average of 10 samples.

The data shows that the ability of the sample to form a compact is not a function of the treatment imparted by the manufacturing process. However, variation among samples of various purities and between sources of supply was apparent with respect to compact strength. The data suggests that samples of single alcohols having a purity level of less than 99% result in stronger compacts. Under no conditions were cohesive compacts generated using cetostearyl alcohol from Lot #L4593. It was also noted that samples of equivalent commercial purity octadecanol did vary with respect to compact strength.

In order to characterize this variation, five replicates of each of the samples processed were evaluated using the technique described in the previous section on energy measurement. Each sample, which was capable of forming a compact, was characterized with their initial energy of freezing (ΔH_1) being compared to the resulting compact strength. The freezing energy was selected based on the clearly defined exothermic peak generated by these samples.

The results of the measurements are shown in Figure 32. There appears to be a trend of increasing compact strength with increasing energy of freezing for all of the fatty alcohol samples studied. This test appears to be quite predictive with respect to process/compaction behavior for fatty alcohols. A fatty alcohol which releases a large degree of energy upon initial freezing produces a better compact with respect to strength than a fatty alcohol which retains a higher degree of thermal energy.

Samples of the octadecanol compacts were selected for microscopic examination by scanning electron microscopy. The compacts which fractured were scanned along the fractured edge in order to visualize the structure present at the area of tensile failure. Samples, representing the two extreme cases, are shown in Figure 33. Lot #M488 exhibited a tensile strength of 0.06 kp/mm^2, while Lot #L020A did not produce compacts with measurable tensile values. The micrographs clearly show Lot #M488 to be quite crystalline in structure while Lot #L020A is more "waxy" in appearance. It is reasonable to expect Lot #M488 to generate more cohesive compacts if the clearly defined crystalline surfaces are considered as the loci for bond formation. The more amorphous Lot #L020A exhibits very little physical properties

that one would intuitively expect to cause strong bond formation. Recall that crystalline surfaces aid in bond formation as a result of close contact due to van der Waals' forces. Upon consideration of the heat of freezing data, it becomes apparent that Lot #M488 releases the majority of the internal energy upon freezing, while Lot #L020A retains some internal energy which results in a less ordered structure or a solid with a high degree of internal strain within the crystal lattice.

This area of crystalline structure changes as a function of composition and its subsequent effects on thermal properties has been researched by various workers(123,124,125,126,127). In addition, the variation of compact strength as a function of crystal structure has also been investigated for various materials(52,128).

The research carried out by Chow(127) shows that for adipic acid, small amounts of fatty acid impurities generated the most profound effect on the ΔH of fusion. It follows that the additives or impurities generated imperfections in the crystals; thereby, the contaminated adipic acid retained a higher internal strain within the lattice. This increase in crystalline strain was ascertained by measuring decreasing values of ΔH of fusion as a function of increasing impurity. The decrease in ΔH_f suggests a higher internal strain due to "dislocations" as a result of impurities. A similar explanation can be applied to the present research, wherein the sample having the higher values of ΔH of freezing result in superior compacts due to a reduced amount of internal strain or dislocation. It follows that the energy which is released during initial freezing of the sample is highest for samples having the most ordered structure which retains the least amount of internal energy.

This may be envisioned in another fashion where a change in entropy of the crystals directly reflect a change in internal energy. It follows then that a small amount of impurity increases the fatty alcohols internal energy and the overall entropy can be linked to a reduced degree of order within the crystalline structure.

Chow and his coworkers(123,127) noted that the values for ΔH of fusion upon reaching a minimum were then noted to increase as the impurity level was increased. They attributed this phenomenon to a progressive ordering of the impurity defects or dislocations which are associated with the reduction or release of lattice strain as suggested by increased ΔH of fusion values. In their research a plateau value for ΔH_f was achieved.

Although the sample (adipic acid) used in Chow's work(123,127) is not capable of polymorphism several parallelisms are apparent when reviewing the energy of freezing data for the samples of fatty alcohol studied in this work. This fact becomes apparent when the addition of a third impurity is measured as a function of energy of freezing. Of the two samples of commercial cetostearyl alcohol, only Lot #K4991 was capable of forming a cohesive compact. The major difference between the two samples of cetostearyl alcohol was the concentration of C_{14} and C_{16} components. Since changes through a minimum in energy of fusion were noted by Chow, a series of increasing tetradecanol concentration in cetostearyl alcohol was prepared. The C_{14} alcohol was selected since the effect of binary mixtures of C_{16}/C_{18} was previously tested. The results for the ternary mixtures are shown in Table XII. As the tetradecanol level increases, the peak area corresponding to

ΔH_1 of freezing increases while the ability to form a compact is determined as previously discussed. The results suggest that as the tetradecanol to hexadecanol ratio approaches that of Lot #K4991, its ability to form a compact increases, while the ΔH_1 of freezing increases. The ratio of C_{14} to C_{16} of the test sample is 1:6.6, while that of Lot #K4991 is approximately 1:7.0. The trend of these samples shows quite clearly that the presence of tetradecanol is necessary to permit the sample to release the amount of lattice strain or internal energy measured as a function of initial energy of freezing. The internal strain may be thought of as reducing the mixtures ability to form a cohesive compact. The fact that high levels of internal strain generate weak compacts has been discussed previously.

It appears that to determine the applicability of a selected lot of fatty alcohol for a compaction process, it may be more important to know the energy of crystallization rather than its exact polymorphic form. However, one may state that the amount of energy retained by these samples will subsequently be released during solid-solid transition. In the case of mixtures such as those seen with cetostearyl alcohol, this sort of semi-quantitative measurement appears to be more selective than a strict assignment of polymorphic form by transition temperature determination. Intuitively, one may expect a straight chain configuration β to yield reasonable results with respect to compact strength. This, coupled with the fact that mixtures of long chain alcohols can shift the polymorphic behavior, may lead one to consider the β form upon cooling as preferred for compaction processes. This is not strictly adhered to by the results, suggesting that several mixtures theoretically capable of β formation yield different compaction

results. This observation lends further creditibility to a test which measures actual energy released as a probe for subsequent compact formation and differentiation within a group of commercial fatty alcohol "mixtures."

A.8 Aging Effects on Fatty Alcohol Compacts - The fact that the formation of the stable γ form for fatty alcohols is a function of aging, sample compacts were permitted to remain at room temperature for 72 hours. The compacts tested were the same as those shown in Figure 32. Using the tensile strength of the compacts as a probe, no difference was noted in the samples as a result of aging. The compacts were tested at zero time, 30 minutes, 1 hour and then 24-hour intervals through the duration of this test. These data suggest that the strength of a compact does not vary as a function of time and polymorphic conversion to a stable form. This becomes evident when the DSC curves for samples of cetostearyl alcohol are compared.

The cetostearyl alcohol samples shown in Figure 21 and 22 respectively were monitored with time at room temperature. Samples were stored in DSC sample pans as previously described. Inspection of the curves shown in Figures 34 to 37 show that the degree of solid-solid transition varies as a function of age. The samples were scanned once then stored for a selected period. At the end of the test period (120 hours) the samples exhibit a thermal profile which resembles the scan at zero time. At various time points, the presence of different crystal forms is apparent prior to melting. As expected, Lot #L4593 is somewhat more complex in structure than the Lot #K4991 sample. In all cases the cooling curves for respective samples are identical.

Although variation in heating curves has been documented, this stability study shows that the heating curves suggest time-dependent solid modifications in the sample. The variation seen may also be a result of the manner in which the sample solidifies within the sample pan. Recall the crystal strain which may result in this situation is also reflected in the heating curves. These data do not appear to correlate with the effect on the strength of the resulting compacts. The qualities of Lot #K4991 appear to be inherent in its composition. To confirm this, a control stability study was run using a pure sample of a C_{18}/C_{16} mixture with a mole fraction ratio of .687 C_{18}/.313 C_{16}, which closely resembles Lot #L4593. The thermal scans are shown in Figures 38 and 39 for zero time (2 cycles), 24 and 120 hour time intervals. The results adhere very closely to those seen with Lot #L4593 of cetostearyl alcohol confirming that the behavior of this lot of material is dependent upon its unique composition. From these data, it becomes evident that to be capable of forming a usable dosage form from a tensile strength standpoint, composition and the amount of energy released during freezing would provide the most useful information to predict process behavior.

B. Active Ingredient Component, Potassium Chloride Behavior

Prior to the assessment of any compaction process for potassium chloride, a careful examination of its physical structure is necessary. As discussed in the background section, particle size, shape, and moisture content are critical to the preparation of suitable compacts from a tensile strength standpoint. To address this situation, the two lots of potassium chloride used (L7490, 10195) were processed as

shown in Figure 6. This resulted in two size fractions for each lot of material.

B.1 Moisture Content - Using the procedure outlined in the experimental section, each size fraction for both lots of material were tested by drying to a constant weight. The amount of surface moisture retained by the samples was approximated by an initial 2-hour drying period. These results are shown in Table XIII. The data indicate that the amount of surface moisture in Lot #L7490 is at least two to three times the level seen with Lot #10195. In addition, the finer particle size fraction of Lot #L7490 shows a higher degree of weight loss for an equivalent sample size. Since the degree of moisture retention is a function of composition as noted previously, it follows that larger surface areas will hold a larger amount of surface water.

The same samples were subsequently dried to a constant weight using an elevated temperature (170°C) as described by previous workers. The results are shown in Figures 40 and 41 for Lots #10195 and #L7490, respectively. These data indicate that while Lot #L7490 continues to lose residual surface moisture, which is indicated by the spike, the amount of water retained within the crystal lattice is lower than that seen in Lot #10195. In both lots the larger particle size fraction requires a longer period to achieve a constant weight. This is reasonable due to the process of water release from a larger particle which requires the water to traverse a more tortuous path than that encountered in smaller particles. These results were fortuitous since one sample (L7490) possesses a high surface moisture with a low level

of entrapped water, while the remaining sample (10195) is somewhat of a corollary with a low surface moisture and a higher degree of lattice water.

Both of these samples of potassium chloride meet all compendial requirements. However, it is evident that upon careful study both supposedly identical lots of commercial material have differences, which have been documented as producing subsequent effects on tablet/ compact manufacture. From these data alone, the documentation reviewed suggests that Lot #10195 would be preferrable for tablet manufacture, the primary criteria being a low surface moisture with some degree of available lattice moisture to aid bonding during compression and upon subsequent aging.

B.2 Particle Size - Screen analysis of the respective samples was carried out by the method noted previously. The particle size range was intentionally narrowed by the process shown in Figure 6. To define these selected fractions, two series of intermediate screens between 74μ to 180μ and 250μ to 500μ were employed to compare the resulting size fractions. The results for both sample lots are shown in Tables XIV and XV for Lots #10195 and #L7490, respectively. For both size fractions the samples from Lot #7490 appear somewhat coarser than the corresponding size fraction Lot #10195. It is felt that this was a function of the higher degree of surface moisture which caused agglomerates to form in Lot #L7490. In both cases the results suggest that the majority of particles fall within the proposed ranges used to designate the respective size fractions.

Representative samples were withdrawn from a blended sample of each size fraction. These samples were examined using dark field microscopy to confirm the size data obtained from the screen analysis. Representative photomicrographs from Lot #L7490 are shown in Figure 42. The large particles can be easily visualized. The smaller size fraction, using the same magnification level, is more difficult to visualize due to the particles outside the focused area of the field (depth of field) for this magnification level. It is apparent, however, that the majority of particles within the focal plane fall within the size designations assigned to the particle fractions.

The morphology for the respective size fractions reveals several points which must be considered during subsequent compaction. The 400-420μ samples exhibit a clear, rounded configuration. Rounded particles have been documented as producing poor compacts for potassium chloride due to reduced surface interaction during viscous flow(42). Their configuration promotes bond breaking during the subsequent unloading process after compression. This "peeling" of the bonded areas results in weak compacts(46,129). The presence of surface moisture would accelerate this process. Conversely, the irregular particles which are seen for the smaller particle fractions 140-160μ would lend themselves to producing much stronger compacts due to increased surface available for bond formation during viscous flow(44,130,131). When considering both size fractions, the classification process used in their preparation becomes apparent. The larger particles are regular and rounded, as a result of the vibrating sieving operation. The smaller particles show a more fractured and irregular

surface as a consequence of repeated milling to reduce their particle size.

B.3 Assessment of Compressibility and Compact Strength - Both lots of potassium chloride were compressed using the Instron as described in the experimental section. Two dwell times were used in order to characterize the effect of prolonged exposure to compressive force on the compact's tensile strength. These tests were carried out using only potassium chloride in a lightly lubricated die assembly as noted. The use of two strain rates was also employed during these tests.

The coarse particle size from Lot #L7490 did not produce compacts with a tensile strength sufficient to be measured using the Heberlein tester. The other three particle fractions from both lots produced measurable compacts, with the results summarized in Figures 43, 44, and 45. Each data point represents an average of ten determinations. For all three samples the faster strain rate (10 cm/min) produced compacts with a higher tensile strength. Included in this observation was the fact that both short and long dwell times yielded consistantly higher tensile values using a 10 cm/min strain rate. It becomes evident that the longer dwell time combined with the fast strain rate produces the most cohesive compacts. The difference between short and long dwell times is most evident when comparing tensile values at the higher strain rate. Although the long dwell time shows a trend toward stronger compacts, at a 5 cm/min strain rate, the difference in strength is not as well defined as that for the 10 cm/min strain rate. Several workers have noted changes in the compact as a result of

loading rate (strain rate). Nürnberg(4) has shown that the temperature of compacts increase with an increase in the rate of force application. Rees and Rue(132) have shown that plastically deforming materials are susceptible to rates of force application. In their research a microfine cellulose compact is loaded using a modified diametrial test to assess work failure. In their data the plastically deforming cellulose exhibits a greater resistance to failure as a function of loading rate. This variation the authors suggest is possibly a function of a change in the "apparent elastic limit" of the material as a function of the rate of force application diametrially. The fact that higher rates of loading cause particle fracturing as well as plastic flow may contribute to increased toughness of the resulting compact.

In the results presented here, the inflection point of the tensile strength versus force curve occurs at approximately the same force level, irrespective of the loading rate used for compact formation. This would suggest that both 5 and 10 cm/min are rapid enough to be beyond the range of displacement, which would show changes in the "apparent elastic limit." However, the trend of a stronger compact resulting from a more rapid force application is apparent.

The non-isotropic nature of the potassium chloride compacts becomes evident upon close inspection of the data. The fine particle fractions from both lots exhibit quite different behavior. Lot #10195 shows a sharp rise (Figure 45) in tensile strength with an apparent plateau occurring at 0.3 to 0.33 kp/mm^2. The behavior of Lot #L7490 (Figure 43) is quite a different case. The data suggest substantial particle rearrangement with only a moderate rise in tensile strength to a maximum of approximately 0.15 kp/mm^2.

The coarse fraction of Lot #10195 (Figure 44) clearly illustrates non-isotropic behavior caused by large spherical particles. It is apparent a substantial degree of void volume must be reduced for a corresponding increase in tensile strength. The more gradual increase in tensile strength with an apparent plateau at 0.3 kp/mm^2 is similar to the behavior seen with the finer mesh sample of Lot #L7490, the major difference between the two particle size fractions being rate of rise and subsequent maximum strength.

The slight curvature seen in Figure 44 can be attributed to secondary bond breaking as a result of elastic recovery after ejection, while the data seen for Lot #10195 in Figure 45 is indicative of the smaller, more irregular particles' ability to survive elastic recovery. This may be attributed to the larger degree of contact surface and void filling, which are a function of particle size and morphology.

It follows from these data that substantial differences in compact behavior exist for a selected lot of potassium chloride which has been carefully classified into various particle size ranges. This situation may have further influence on compression of potassium chloride, which is not classified into well defined particle size fractions. To address this situation, Lot #10195, which was capable of producing coherent compacts using either coarse or fine particles, was evaluated using a non-classified sample. Commercial processes involve a simple, once-through size reduction step using a hammer mill. Lot #10195 was milled using a standard commercial milling procedure which results in an array of particle sizes for the sample. The distribution of particle sizes is shown in Table XVI. The mill configuration was identical to that shown for milling unprocessed potassium chloride in Figure 6.

The data shown in Table XVI suggest a close approximation of this material to that seen for the 400-420μ classified sample. Despite this similarity, the resulting tensile strength data for the milled sample shown in Figure 46 suggest a more erratic behavior than seen for classified material. The variation in tensile strength as a function of dwell time is quite interesting. The longer dwell time appears to yield more consistant compacts over a range of compressive forces. Short dwell time results in a compact which appears to reach a maximum strength then a lower strength followed by another maximum level. This erratic behavior seems isolated to the milled sample when comparing the short dwell time results for classified samples of Lot #10195.

The milled material exhibits approximately 76% of the particles to be larger than 297μ, while the coarse material possesses 97% larger than 297μ in size. The apparent mixture of predominantly large particles with a higher concentration of fine particles (approximately 24%) seen with the milled material seems to be critical for behavior during compression. The use of correct particle size distribution for tablet granulation to assure good tablet compression is an old reliable method commonly used in industry. Apparently, the combination of fines in the case of coarse potassium chloride compromises compact structure. In other words, the particle size distribution would be incorrect for high speed compression of potassium chloride. It would follow then to correct this situation either less fines should be created by the milling procedure or the mean particle size should be lowered via more strenuous milling.

A detailed exmaination of the cross section of a compact produced using the milled mixture of potassium chloride yields a better insight as to causative factors resulting in erratic compact strength behavior.

The micrograph shown in Figure 47 shows both large particles with considerable void space, while in other locations smaller particles have experienced viscous flow during compression. It is this random structuring of cohesive segments and void spaces which contribute to the erratic behavior seen for a milled spectrum of particle sizes. If one considers the preliminary stages of consolidation during compaction as outlined in the background section, this random tensile strength behavior seems more reasonable. If the milled material introduced into the die is not representative of the entire blend, the subsequent aliquot used for the compact will take on the characteristics of the particle size fraction present in a larger proportion in the sample. One may also speculate that the closely packed, well structured segments may act to inhibit closer contact of the larger particles, thereby contributing to creation of voids which degrade compact strength. This reduced contact area would then permit the compact strength to be a function of the true contact occurring in the smaller particles. The fact that longer dwell times yield a smoother tensile strength curve confirms this concept. During prolonged dwell time, viscous flow is permitted to continue creating better bonding and reduction of void areas and subsequent increased compact strength. Any internal stress generated near voids may be relieved, thereby preventing fracture at the areas of stress localization.

In all the tensile strength data presented, there appears to be an inflection point where a plateau region begins. The pressure level of

11.8 kg/mm^2 appears to be the level in all cases, although in several of the plots the inflection to a plateau region is not as clearly defined. To ascertain the validity of the observation, all the stress decay data was measured from the Instron output. The results are shown (Figure 48) for all the data from Figures 43-46 as a function of the amount of stress decay and tensile strength. The data suggests a decrease in the amount of stress relaxation after a peak value of 11.8 kg/mm^2. These data would indicate the level of 11.8 kg/mm^2 as a yeild point after which the tensile strength remains at a reasonably constant value. The tensile strength values for the milled and large particle fractions, which were not clearly defined, gave results which suggest a slight increase in tensile strength. This is reasonable when the effect of enhanced viscous flow is considered on the improvement of compact strength. In all cases, however, the pressure level of 11.8 kg/mm^2 appears to be applicable to all samples of potassium chloride. The yield level appears to be an intrinsic property for potassium chloride. That is, the actual rheological behavior is a common factor for all sample types regardless of morphology. However, the particle size and morphology must still be considered when evaluating the tensile strength of potassium chloride compacts.

These data suggest to the investigator that a minimum pressure of 11.8 kg/mm^2 must be applied to generate cohesive compacts. To account for poor flow during compression, a prolonged dwell time will assure good compression results.

B.4 Surface Moisture Effects - The difference in moisture content between the two sample lots of potassium chloride is clearly demonstrated in Figures 40 and 41. As noted, the two samples show completely opposite distributions of moisture with Lot #L7490 having the highest surface moisture. Lot #10195 has a minimal surface concentration, but the internal lattice water is higher than Lot #L7490. These data are some of the fundamental factors which permit marked differences in compact strength for the two subject lots. To confirm this, samples from the 140-160μ size fraction for each lot of potassium chloride were dried. The dried materials were subsequently compacted using the Instron. The results of this experiment are contained in Table XVII.

The drying process yields compacts of Lot #L7490, which have a marked increase in tensile strength when compared to undried samples. Increases in tensile strength by prior drying of the potassium chloride have been documented by Carr(133). A slight increase was noted for Lot #10195, but it was not as remarkable as that seen with Lot #L7490. Once the surface moisture effect is eliminated, it is clear that Lot #10195 produced stronger compacts. As was discussed, some degree of available lattice moisture must be present to produce good compacts(47,48). The amount of moisture contained in the lattice structure of Lot #10195 is apparently at a level which permits bridge formation and subsequent bond strengthening.

Micrographs of a fractured compact of Lot #L7490 are shown in Figures 49 and 50. The dried sample shows a structure with "clean" crystalline faces and little evidence of moisture on the surface. The undried sample provides a distorted, less sharp view of the crystals,

which suggests a reasonable level of available surface moisture. It follows then that this surface moisture contributes to a reduced amount of bonding due to an insulation effect between surfaces. Another phenomenon which was touched upon in the physicochemical segment on potassium chloride involves the lubricant nature of surface moisture. The moisture layer may permit recovery of the compressed system during unloading. This recovery may result in bond breaking within contact areas, rendering a weaker compact. This recovery or survivability of bonds formed within compacts has been discussed by Hiestand(46).

Compacts from this experiment were stored at ambient conditions in an open dish for one week. Compacts were tested at periodic intervals for tensile strength (Table XVII). It is apparent that the sample with a high level of surface moisture is invariant with time. This is not unexpected since the structure produced in this case may have weakened during unloading, as previously discussed. It may also suggest that the surface moisture is at an equilibrium concentration at ambient storage conditions with no further uptake possible at ambient humidity conditions. This aspect of invariant tensile strength is not seen after drying. The tensile strength increased by approximately 40%, which suggests substantial bond strengthening and crystal formation. It is possible that the amount of occluded moisture which is available in the sample can now exert some effect. The moisture may migrate toward the now dry surfaces uninhibited by high levels of surface moisture. This effect would take the form of secondary crystal growth. This factor combined with an improved inter-particle

contact structure would account for improved strength for dried potassium chloride from Lot #L7490.

For Lot #10195, the result of drying has minimal effect. This makes sense when it is recalled that the moisture distribution in this lot shows extremely low surface concentrations. It then follows that compact behavior with aging will proceed via a secondary crystal growth pattern either dried or undried. It is interesting to note that upon drying, Lot #L7490 ages to yield a compact with a tensile strength equivalent to that obtained from Lot #10195.

B.5 Aging Effects of Potassium Chloride Compacts - Compacts which were prepared using the Instron were subjected to a 4-week aging study. Both lots of potassium chloride and various particle size fractions were included in this study. Previous experiments have shown that the 10 cm/min strain rate is capable of producing stronger compacts. Since this compression rate is more representative of actual processing conditions, all samples were prepared at 10 cm/min. The finished compacts were stored in open plastic weighing dishes at ambient conditions. The room temperature was in the range of 24-28°C during this test, while the relative humidity remained in a range of 40-50%.

An exacting study of compact tensile strength (hardness) changes with respect to storage conditions has been carried out by Lordi and Shiromani(8). In their research a wide range of controlled humidity levels were employed. Contained in their data was an evaluation of potassium chloride, which encompassed the relative humidity range discussed here. Their data suggest only minor hardness changes for

compacts stored at 20 and 50% relative humidity conditions. They recorded substantial increases in compact strength at levels approaching 80% relative humidity. This factor was not characterized in the present study since the data desired was to address process conditions, which do not approach this environmental moisture level. In addition, several of the particle size ranges contained in the present work were smaller than the 30-40 mesh fraction used in their study.

All of the compacts were prepared from undried potassium chloride with the resulting aging effects shown in Tables XVIII and XIX for Lots #10195 and L7490, respectively. Lot #10195 particle fraction 140-160μ showed the least variant behavior upon aging. Of the two force levels employed, the lowest percentage increase in strength was seen at the higher compressive force. Since Lot #10195 (140-160μ) yields strong compacts at zero time due to the optimal structure produced, subsequent aging effects must be due to occluded moisture which produces secondary crystal growth. Compression to a higher force permits maximum flow and bond formation. Subsequent secondary crystal growth upon aging will, therefore, have a diminished effect when compared to compacts formed at lower pressures. At lower pressures, the structure formed may not completely survive after unloading. If the contact surfaces do not remain completely intact, then subsequent "healing" or crystal growth will produce compacts which will, upon aging, exhibit a larger percent increase in tensile strength. It is clear that all compacts within the 140-160μ range age to an equivalent tensile force level as shown in Table XVIII.

If one considers that 11.83 kg/mm^2 was previously noted as a possible yield point (Figure 48), then intiutively it follows that compacts formed above this level should result in structures which better survive unloading.

This basic pattern is also seen with the larger size fraction of Lot #10195, wherein the lower pressure (11.83 kg/mm^2) produces compacts which exhibit a larger degree of tensile strength increase as a function of time. The larger particle size fraction appears to be more susceptible to aging and secondary bond formation. This is reasonable since the data presented in Figure 40, show that the larger particle fraction exhibits a higher occluded moisture level. It then follows that the subsequent crystal growth will be greater for potassium chloride with this level of occluded moisture. The higher force level results in compacts with an improved structure which survives unloading and diminishes the overall percent strength increase with time.

The milled unclassified potassium chloride provides an interesting comparison in aging effect with the classified particle fractions. As shown in Table XVI, the milled material possesses a spectrum of particle sizes which favor the coarser material. It is this non-uniform structure which accounts for the slightly higher aging effect seen with these compacts. This factor becomes more evident when the 10 second dwell time data is inspected. Although the aging effect is diminished, the overall improvement of structure due to prolonged exposure to compression force is evident. As discussed previously, the non-uniform structure of the compacts is minimized by prolonged dwell time. Some evidence of bond inhibition is apparent due to the lower

tensile values seen after 4 weeks when compared to the 400-420μ samples. Secondary bonding in the larger particles combined with possible structure disruption due to the amount of fines present may be the causative factor for the lower values seen in the unclassified sample. It is reasonable to speculate that the majority of secondary bonding occurrs with the larger particles as seen in the 400-420μ samples. The presence of well structured fine particles may increase void space between large particles, thereby reducing the aging effects seen in the milled sample. The voids, therefore, may act to reduce large particle contact and, therefore, reduce the effect of the available occluded moisture in these particles. These combined factors suggest a credible explanation between the aged (4-week) unclassified and classified 400-420μ size fractions.

This factor must be considered when designing a dosage form where prolonged stability is required to avoid variation in subsequent release rate patterns. Attention to preliminary milling is indicated as a potential source of variation when considering a process for slow or controlled release potassium chloride dosage forms.

The effect of a high level of surface moisture is evident when inspecting the aging results for Lot #L7490, Table XIX. In this situation, the resulting compacts are much weaker than Lot #10195. It is also reasonable to expect that the lower degree of occluded moisture will have only minimal effect on improving bond strength. The ability of bond strengthing is also reduced due to the lubricant or insulating effect of the surface moisture. In addition, if the structure formed at zero time is not suitable to survive recovery after unloading, little secondary effects can be expected. The result of surface moisture is

clearly evident when the dried data shown in Table XVII are compared. In this case the 1-week sample at a lower pressure exhibits a tensile strength comparable to that seen after 4 weeks for Lot #10195.

The erratic behavior exhibited by Lot #L7490 is most evident when comparing the 19.73 kg/mm^2, 10-second dwell time data. These data show a marked departure from the pattern seen in Lot #10195.

It becomes apparent that the formulator must not only be cautious with respect to particle size patterns but must also establish moisture content parameters. If no limits are used, a substantial variation in release patterns can be expected upon aging due to the anomalies demonstrated by these data. One may also speculate that a higher force may be required to overcome the "barrier" effects of the surface moisture.

B.6 Assessment of Densification and Bond Formation: Heckel Plots - A series of compacts were prepared using increasing levels of compression force. The results from these compactions were used to construct Heckel plots for each size fraction of potassium chloride from both lots of material. The true density of each particle size fraction was determined using the procedure outlined in the experimental section. Ten compacts were used to generate individual data points to minimize the variability normally encountered in these types of physical measurements. All measurements were made at zero pressure as noted previously.

The results for Lots #L7490 and 10195 are shown in Figures 51 and 52, respectively. A superficial glance at the two plots reveals

similarities to hypothetical data shown in Figure 2. The three hypothetical size fractions result in a family of three curves, each with its own density profile. In the data presented here, this same phenomenon is suggested. This may be taken as a indication of plastic deformation as the primary bonding mechanism.

Since two dwell times were used, some measure of the degree of plastic flow which occurred was calculated as well as inherent yield values for the respective size fractions. The four curves generated for Lot #L7490 were evaluated with respect to percent difference in area under the curves (%ΔAUC). The 140-160μ size fraction showed an increased difference between the two dwell times when compared to the 400-420μ size fraction, Table XX. All measurements are made at zero pressure; therefore, any differences are directly attributable to an increased amount of non-recoverable plastic deformation.

The 140-160μ (Lot #L7490) %ΔAUC was 2.6, while the 400-420μ size fraction possesses a 0.7%ΔAUC. This indicates that a substantial amount of the viscous flow which occurred for the 140-160μ was not lost due to elastic recovery after unloading. It shows a clear difference between the two size fractions and suggests a causative factor for the poor compacts resulting from Lot L7490, 400-420μ size fraction. The extent of elastic recovery present in this size fraction was apparently sufficient to overcome the poor bond structure produced in this higher surface moisture sample. The morphology of the coarse fraction also contributes to the extent of elastic recovery seen for this sample.

The four curves prepared for Lot #10195 were compared in a similar fashion. In this case the 140-160μ size fraction exhibited a %ΔAUC of 4.3, while the 400-420μ size had a %ΔAUC of 1.2. Both size

fractions produced differences which were higher than that seen for equivalent size fractions of Lot #L7490.

It is clear why the 140-160μ fraction of Lot #10195 produces superior compacts when the extent of viscous flow and subsequent bond formation not lost to elastic recovery is considered. The fact that the coarse fraction of Lot #10195 exhibited only slightly higher degrees of viscous flow than the same size fraction of Lot #L7490, while only Lot #10195 produced suitable compacts, must be attributed to the surface moisture present in Lot #L7490.

Overall the results of %ΔAUC for Lot #10195, both size fractions, are approximately 30% higher than those seen for Lot #L7490. This is not unexpected when it is considered that Lot #10195 yielded compacts of consistently higher tensile strength. However, this fact must be tempered with the morphology, moisture content, and size fraction for the subject samples.

As noted in the background section, Heckel plots also permit the worker to rank materials with respect to yield value. The linear portion of the plots may be used to calculate the constant (k) using the linear form of the Heckel equation (Equation 4). The resulting k value may be used to calculate Py, mean yield value, by using the relationsihp in Equation 5. This was done for all the curves generated in this study. The results are shown in Figure 53, where the maximum tensile strength achieved for a sample is plotted as a function of the mean yield value. The mean yield values were calculated using the 4 terminal points which best fit a straight line in the data shown in Figures 51 and 52. The mean yield values obtained for the two dwell

times were the same in all cases so that an average value of Py is used in each case.

Previous workers in this area(80,81) have shown lower k values are indicative of hard materials with less viscous flow at higher pressures, while high k values are seen with softer materials. Recalling that Py by Equation 5 is a reciprocal of k, several interesting points become apparent. The data suggests that the poorest compacts from Lot #L7490 have a k value of 0.01, while Lot #10195 (140-160μ) possess a value for k of 0.06. In that Lot #L7490 shows minimal viscous flow as a result of measuring %ΔAUC, these data become suggestive of a harder material whose mean yield pressure was not exceeded in this experimentation. However, care must be exercised here since a value of 100 kg/mm^2 exceeds the pressure normally encountered in conventional compression operations. In fact, it exceeds the maximum pressure used in this research by approximately three fold. Since the levels used as maximum in this research are in themselves somewhat higher than conventional compression forces, some secondary factor must contribute to this unusually high Py value.

If the process of densification measurement is considered, the Heckel equation is predictive of values only if flow has occurred plastically or conversely by brittle fracture. If the data for Lot #L7490 is considered, the equation suggests a situation where insufficient pressure has been supplied. This is credible only when the physicochemical criteria for the subject sample is considered. The rounded particles with high surface moisture rearrange; but due to their configuration and the film properties of the moisture, insufficient bonds are formed. Therefore, it follows that the densification profile would

indicate a harder material whose yield value must be substantially higher than that used in the study. It would then follow that the high yield value is a function of the poor survivability of the sample during unloading and not the intrinsic yield value. Recall form Figure 48 that a yield of approximately 11.8 kg/mm^2 was speculated. The only sample which comes close to this value is the 140-160μ sample from Lot #10195. This may be attributed to the successful survival of this sample after unloading. The higher values for the coarser and moisture laiden samples must then be a function of their "peeling" action after unloading and its direct impact on the densification relationship. This effect manifests itself by slope changes yielding lower values of k and subsequently higher values for Py.

C. Mixtures of Matrix Formers and Potassium Chloride

It has been previously shown that both fatty alcohols and potassium chloride vary substantially with respect to tensile strength. The final dosage form is made up of a mixture of these components. In order to evaluate the impact of this combination, several batches of potassium chloride and various fatty alcohols were manufactured. These batches were prepared by the fusion process outlined in Figure 8. The material was processed using the planetary mixer and jacket system previously described. The heating and cooling rates were maintained in the range of 4-6°C/min by means of the jacket circulation system.

The finished granulations were compacted using the Instron. Compact weight was adjusted to yield the same amount of active substance as evaluated previously, allowing additional weight for the

matrix former (fatty alcohol). The pressure levels of 7.89 and 15.78 kg/mm^2 were selected, since pressures above 15.78 kg/mm^2 yielded compacts which exhibited no detectable difference with respect to tensile strength. It was also noted that higher compressive forces caused the fatty alcohol to exude past the lower punch and die assembly. A higher strain rate (20 cm/min) was also evaluated. This increased rate gave no measurable difference from that obtained at 10 cm/min.

C.1 Mixtures of Cetostearyl Alcohol and Potassium Chloride - The initial batches prepared were comprised of the subject lots of cetostearyl alcohol and the two lots of potassium chloride. The ratio of matrix former to active substance was set at approximately 1:7.5. A dwell time of 10 seconds was selected based on previous results with fatty alcohol compression. There was no measurable difference between the short and the extended dwell times. This fact is worthy of comment since the only instance dwell time generated a pronounced effect was for the pure samples of potassium chloride. Recall that previous fatty alcohol data indicated no difference between short and prolonged exposure to maximum compressive force. This initial observation suggests that in a mixture the fatty alcohol component will play a pivotal role in governing resulting compact strength.

The ability of fatty acids to bond strongly to substrates has been documented by several workers(134,135). These results indicate that a discontinuous or deformable coating results in higher tensile strength values for powders. While a continuous elastic film reduces overall tensile strength for the powder mass, it would seem reasonable then

to predict variation due to the concentration of fatty alcohol and the configuration of the substrate (i.e., particle size, morphology) as well as the physicochemical properties of the matrix former.

This becomes apparent upon inspection of the data (Table XXI) for compacts prepared using cetostearyl alcohol, Lot #L4593. This fatty alcohol when combined with potassium chloride failed to yield compacts with measurable tensile strength. The reverse situation exists for cetostearyl alcohol, Lot #K4991. In the case of potassium chloride, Lot #L7490, particle size 400-420μ, no tensile strength was detectable at zero time or upon aging. However, when combined with cetostearyl alcohol, Lot K4991, a minimal tensile strength was recorded after 12 hours of aging at ambient conditions. These data indicate that the compact strength in this situation is a function of the added matrix former. Although the compact strength is higher than the potassium chloride alone, it is only 50% of the recorded value for the fatty alcohol by itself. This difference may be attributed to nonhomogeneous distribution and concentration of the fatty alcohol in the compact, as well as the inability for the larger particle size potassium chloride to survive elastic recovery after unloading.

This demonstrates both conditions described in the literature. The first situation is the inhibition of all bonding by the presence of a coating of fatty alcohol, while the second case provides some measure of tensile strength where none previously existed.

The potassium chloride from Lot #10195 yields results which suggest that its bonding properties are diminished when combined with

cetostearyl alcohol. The 140-160μ fraction still retains the characteristic of being the strongest compact forming configuration, although diminshed by the presence of the matrix former.

It is interesting to note that the result of adding the matrix former to the potasisum chloride (Lot #10195) results in a decrease of 47-50% from the level of equivalent potassium chloride samples compacted at a lower force without the presence of fatty alcohol.

The aging results for Lot #10195 are not as noticeable upon mixing with cetostearyl alcohol. At equivalent time points (24 hours), the pure potassium chloride (Lot #10195, 140-160μ) when compressed at 11.83 kg/mm^2 increased in strength approximately 11%, while the coated material at a higher pressure (15.78 kg/mm^2) showed negligible changes in tensile strength. It becomes apparent that secondary bonding and subsequent tensile strength increase must be inhibited by the presence of the fatty alcohol.

These results also follow the data previously presented which showed that no aging results are seen with respect to tensile strength for fatty alcohol compacts. Although some variation may be seen in Table XXI as a function of age, the amount of change is not as pronounced as that seen with potassium chloride alone.

The question as to which portion of the compact formulation generates the most effect on tensile strength and aging was evaluated by using selected samples of potassium chloride at increased levels of matrix former. Several authors(136) have noted changes in compact tensile strength as a function of increased amounts of coating material.

The data presented in Table XXII demonstrates the result of increasing the amount of available matrix former to the potassium chloride. The compacts were maintained at the same physical size as those in Table XXI to facilitate comparison. As can be seen, all sample combinations except the 140-160μ, Lot #10195, begin to converge on the tensile strength seen for cetostearyl alcohol, Lot #K4991, by itself (0.04 kp/mm^2). This is most apparent in the case of potassium chloride, Lot #L7490. This lot of material exhibited the poorest tensile strength when compared to Lot #10195, without the presence of fatty alcohol.

After tensile failure, a compact consisting of potassium chloride, Lot #L7490, and cetostearyl alcohol, Lot K4991, was inspected along the failure edge. The results are shown in Figure 54. At low power magnification, it is apparent that the matrix structure and strength are a function of the fatty alcohol. The fatty alcohol appears to have built up structure around the potassium chloride. The channels are open areas between the particles of potassium chloride which permit the fatty alcohol to establish a continuous phase to yield the resulting 0.04 kp/mm^2 tensile value.

Upon closer inspection of the impressions left in the matrix, it becomes apparent that during diametrial loading, all tensile failure occurred at these particle boundaries, while no noticeable potassium chloride-potassium chloride failure occurred.

At higher magnification, some minor deformations may be seen in the fatty alcohol coating on the potassium chloride. Most noticeable are the cracks and subsequent exposure of the potassium chloride in various areas. The nature of fatty alcohol, Lot K4991, permits this

type of behavior under pressure. While a softer, more waxy type of fatty alcohol (Lot L4593) will flow and not facture, permitting exposure of the substrate material.

It should be noted that the finer particle sizes appear to retain some influence on tensile strength at this modified ratio. It is reasonable to suggest that the higher surface area of the finer fraction is still not completely encapsulated by the matrix. In addition, the irregular morphology of the potassium chloride is capable of penetrating the coating and exerting potassium chloride-potassium chloride bonding and subsequent aging to a reduced degree.

This supports the previous observation which notes that variation seen with lots of potassium chloride can impact on the overall performance of the finished dosage form. If the consistency in tensile strength seen for Lot #10195 as a function of the change in the fatty alcohol ratio is considered, it would follow that a commercial source of fine potassium chloride possessing Lot #10195's properties would help to minimize variation in the finished dosage form. It may also be expected that potassium chloride similar to Lot #10195 would better tolerate nonhomogeneity of matrix former distribution within the granulation during compression. If the example of Lot #L7490 is taken, it is reasonable to expect some degree of dosage form variation due to nonhomogeneity of fatty alcohol as simulated in this case by a concentration change of the matrix former. Simply stated potassium chloride adhering to Lot #10195 criteria would provide a more reproducible dosage form.

C.2 Hexadecanol/Octadecanol and Potassium Chloride - The previous data demonstrate the differences between lots of cetostearyl alcohol and potassium chloride. It is also apparent that the ratio of fatty alcohol to potassium chloride becomes critical for lots of potassium chloride similar in physical behavior to Lot #L7490 (i.e., surface moisture, morphology). It follows that some critical level must also exist for combinations of fatty alcohols which have been shown to produce strong and weak compacts.

Two lots each of C_{18} and C_{16} fatty alcohol were selected based on their ability to produce good and poor compacts as a function of tensile strength. A series of batches were prepared using these alcohols in various concentrations yielding the results shown in Table XXIII.

Milled potassium chloride was used in order to keep the system similar to that normally encountered in standard processing. C_{18}, Lot #00140, produced strong compacts while Lot #L020A produced poor compacts (Figure 32) for C_{16}, Lot #L2475 was selected for good compacts while Lot #H03100 was considered a poor compact former.

As documented in the previous data for cetostearyl alcohol/ potassium chloride compacts, the aging properties are diminished by the presence of the fatty alcohols. This is apparent when the aging results shown in Table XXIII are inspected. The result of adding poor compact forming fatty alcohols appears to reduce aging effects still further. This corresponds with the data presented for cetostearyl alcohol Lot #L4593, where all potassium chloride samples were inhibited

from forming compacts with measurable tensile strengths. The composition and thermal properties of poor compact forming alcohols appear to preclude the ability of potassium chloride to form a coherent compact.

The two alcohols selected as "contaminates" in this study exhibit similar properties at the 100% concentration level when combined with potassium chloride. The two alcohols selected as good compact formers differ somewhat at the 100% level with respect to compact tensile strength. The C_{16} sample (L2475) exhibits a higher tensile strength value. By using the incremental amounts of the tensile strength reduction at each contaminate level, the graph shown in Figure 55 was constructed. These data suggest that although the C_{16} alcohol produced stronger compacts, the addition of 10% contaminate reduced the strength by 15%. This trend appears to be minimized at the next two data points with the 100% level showing negligible tensile strength for the C_{16} sample.

These data appear to suggest that the C_{18} sample is less sensitive to addition of a contaminate than is the C_{16} sample. A similar observation was made during construction of the phase diagram for C_{16}/C_{18} fatty alcohols. With the phase diagram a level above a mole fraction of .091 C_{18} in C_{16} caused the diagram to take on a twopoint solid transition pattern.

This corresponds to the energy of freezing data, wherein it was shown that alcohols which possess a high initial energy of freezing (ΔH_1) and, therefore, a reduced degree of energy available for solid-solid transition, are better compact formers. It has been shown that waxes which release a large amount of energy at initial freezing are crystalline in appearance while the others are quite amorphous

("waxy"). This soft, waxy characteristic would most likely reduce bond formation due to its fluid-like nature under pressure. Hard crystalline fatty alcohol coatings would lend themselves to cracking and subsequent potassium chloride penetration and bond formation. The soft material on the other hand would yield easily and produce much the same bond inhibition regardless of substrate morphology.

C.3 Thermal Properties of Cetostearyl Alcohol and Potassium Chloride Mixtures - Fatty alcohols have been shown to be sensitive to various contaminates. The thermal properties of these fatty alcohols vary significantly as a function of these additions. Although potassium chloride differs significantly in thermal properties from cetostearyl alcohol, its presence may produce some modification in the thermal behavior of the fatty alcohols. These differences may be the result of particle size or shape of the potassium chloride acting as a nucleus for recrystallization. Mixtures of these components were tested in order to address these questions.

Potassium chloride from Lot #10195 was scanned using the DSC over the temperature range used for fatty alcohol samples. At these temperatures (approximately 0-75°C), the potassium chloride exhibited no changes as indicated by a flat baseline with no deviations. Since the potassium chloride showed no calorimetric variation, blended samples of cetostearyl alochol and potassium chloride were studied. Large samples (approximately 20-30 mg) were used to account for the fatty alcohol concentration and sample heat capacity.

Comparision of a sample of cetostearyl alcohol Lot #K4991 with the blended sample shows minimal differences, Figure 56. The most noticeable change was the peak magnitude as a result of sample size. The

mixture shown in Figure 56 was a physical blend prior to fusion. Figures 57 and 58 show the results of the fusion process using the planetary mixer for samples prepared using cetostearyl alcohol Lots #K4991 and #L4593. The results of aging for 12 hours at room temperature are shown in order to illustrate the time-dependent effects as a result of the presence of potassium chloride. It appears that the previously documented complex nature of Lot #L4593 remains unchanged by processing or the presence of potassium chloride. It also appears that a complex series of intermediate crystal forms exist after processing. The blend containing Lot #K4991 has achieved a reasonably stable form after processing showing only a minor inflection indicating a mixture of low temperature forms. After aging for 12 hours at room temperature, both mixtures exhibit all low temperature forms as one non-resolvable peak upon heating. The cooling curves for both samples are identical to the zero time data generated after processing and to results seen for the alcohols by themselves.

A sample was allowed to remain at 45°C for 24 hours. This temperature was selected as a point, where most of the crystal forms exist prior to melting. The samples were then flash frozen and scanned to determine the extent of crystal forms and potential for solid-solid transformation in the presence of potassium chloride. The results (Figure 59) seen for Lot #L4593 correspond well with data shown previously. The situation for Lot #K4991 shows two well defined forms with only a minimal amount of solid-solid transition. This suggests that under standard processing conditions, which are around 45°C, Lot #L4593 retains a complex structure while Lot #K4991 very quickly resolves to a minimal degree of solid-solid transition. It should be

noted that Lot #K4991 was only resolvable into its constitute crystal forms after annealing at 45°C. Lot #L4593 retains its complex nature showing a marked degree of solid-solid transition. The cooling peaks are identical to those previously presented.

D. Evaluation of Components Using an Instrumented Tablet Press

In order to make credible interpretations of the results obtained in this study, actual processing of materials using standard compression techniques was deemed necessary. As previously discussed, a single station tablet press has been instrumented to yield upper, lower, and die wall forces generated during tableting. Selected components which have been characterized previously were exposed to this form of analysis.

D.1 Potassium Chloride - Both lots of potassium chloride were compressed using the instrumented tablet press. Several force levels were used to assess the result of uniaxial compression of this raw material. These tests were carried out using only potassium chloride in a lubricated and non-lubricated die.

D.1.a Potassium Chloride, Lot #L7490 - Although the coarse particle size from Lot #L7490 has shown previously that it is not capable of producing strong compacts, it has been included in this study as a means of comparative analysis.

All particle size fractions were compressed using similar conditions. The amount of material compressed was adjusted to yield compacts of equivalent thickness. This procedure assures that all mea-

surements are made using similar strain conditions.

The two particle size fractions (140-160μ and 400-420μ) were compressed. A series of three different force levels was employed in order to estimate effect of compression force on these samples. The resulting data indicate that the use of a lubricated or non-lubricated die has little impact on the results since the measured peak ejection forces show little difference within each pressure level for the samples studied. These data are listed in Table XXIV.

It is interesting to note that the ratio of transmitted force approaches unity above a compression level of approximately 10.5-11.5 kg/mm^2. This pressure level was noted previously where compacts of potassium chloride exhibited optimal physical properties. As shown in Figures 43 to 46, a plateau region occurs for tensile strength beyond the 11.8 kg/mm^2 inflection point. Further validity was attributed to this observation by subsequently plotting tensile strength as a function of stress decay (Figure 48). In this case the data suggests a decrease in the amount of stress relaxation after a peak value of 11.8 kg/mm^2. This is credible when the data presented in Table XXIV are considered. As sufficient force is applied, the powder/granule structure approximates an isotropic state, wherein maximum point contact and flow have taken place. It follows that an applied force above this level is necessary to achieve optimal compact properties.

The finished compact must be able to survive ejection. The compacts generated using the coarse fraction of Lot #7490 did not produce compacts with measurable tensile strength. The high surface moisture of Lot #L7490 apparently negates the viscous flow which has

taken place beyond 11.8 kg/mm^2. In the case of compacts generated using the fine fraction of Lot #L7490, we see approach to isotropic behavior at a slightly decreased pressure level. This suggests that a more coherent structure with less particle slippage has occurred. The rationale being that more energy has been expended within the compact as a function of flow and subsequent bond formation. The resulting survivability of these samples must be attributed to particle morphology overcoming the surface moisture with its related lubricant effects.

The force applied during formation of the compacts was recorded using a high speed oscilligraphic recorded; and these data are shown in Figures 60 and 61 for the two size fractions 140-160μ and 400-420μ, respectively. Maximum compressive force data are shown in order to illustrate all of the intrinsic characteristics of the samples. Using a chart speed of 250 mm/sec with an appropriate amount of amplification, the events occurring during force application become apparent. Two lower punch signals were recorded. The second signal was sufficiently amplified to yield a measurable quantity for the ejection force. The die wall signal was also amplified in order to aid in visualizing the compact residual stress prior to ejection.

The most pronounced difference between the two size fractions becomes apparent by inspection of the force transmitted radially. The greater magnitude of radial transmission for the coarse fraction must be attributed to this sample's ability to slip due to the lubricity of the high surface moisture concentration and the spheroid morphology of the potassium chloride. Another way of describing this would be to attribute the granule bed of Lot #L7490 with a very low shear

strength. A low shear strength would indicate an increased die wall force(89). This increased force radially manifests itself in the subsequent peak heights (400-420μ amp. at 1,000 mV versus 140-160μ amp. at 500 mV). This aspect underscores the elastic nature of the coarse sample and its subsequent inability to survive unloading. It should be recalled that the more elastic a material becomes the more it approximates a hydraulic fluid.

Further inspection of the data in Figures 60 and 61 reveals the residual force and stress related, time dependent aspects of the material. If one looks at the interval prior to ejection, a departure from baseline is noted for both the die wall and amplified lower punch signals. These positive deviations indicate residual forces being exerted against the die wall in the radial direction, as well as the lower punch in the axial direction. A decay in the force exerted on the die wall is suggested by the shallow slope noted on the die wall signal.

The shape of the resulting ejection event shows the compact being dislodged and the required force to drive it out of the die. These events may be thought of as (a) overcoming the initial friction (peak value) at the compact die wall interface and (b) the subsequent force required to move it along the wall and out of the die mouth.

The variation seen in the initial slope of the amplified compression peak for the lower punch may be attributed to the rearrangement structuring and collapse occurring within the granules prior to coherent compact formation. These events were discussed in the section on theories of bond formation.

D.1.b Cycle Plot Evaluation of Potassium Chloride, Lot #L7490 -

The compression procedure used to collect the data presented previously was employed to produce the required data for construction of a cycle plot. A series of replicates were compressed in a lightly lubricated die. The upper punch force and the radially transmitted die force were taken from identical time points. An increased chart speed was used (500 mm/sec) to afford more ease in collecting the required data points. The resulting graphic force representations are shown in Figures 62 and 63. In all samples tested, a maximum pressure of approximately 20 kg/mm^2 was used. The length of the compression event for tablet formation was calculated from the strip chart and was found to average 0.26 second (.05). This time interval represents duration from initial slope to the beginning ejection peak.

Figures 62 and 63 illustrate the 400-420μ and 140-160μ particle size fractions, respectively. The two plots differ significantly. Since anomalous behavior has been documented for this lot of potassium chloride, evaluation must be tempered with the known physical properties of the samples. The coarse fraction was shown to have a low shear strength due to the lubricity of the surface moisture known to be present. The dramatic difference in shear strength for the two samples is evidenced by approximately a two-fold increase in radial force transmission for the coarse fraction. The coarse material retains a marked residual die wall force. This is most likely a function of the significant degree of elastic recovery with this sample since little energy has been retained as a result of bond formation. If the particles translate during compaction but do not form substantive bonds during decompression, the resulting elastic recovery will generate

excessively high residual forces. The form of the plot for the 400-420μ is not indicative of the theoretical forms discussed in the background section. It should be noted that both the initial and terminal slopes appear to be equal, which has been taken to indicate plastic deformation as a primary bonding mechanism(72,83).

The 140-160μ fraction yielded results which suggest that the compact acts as a nonporous solid above a pressure of approximately 10.0 kg/mm^2. Within experimental error the plot above 10.0 kg/mm^2 may be thought of as a single line. It is interesting to recall that the level of 11.8 kg/mm^2 was determined as yielding optimal results for this sample of potassium chloride.

The degree of creep recovery which occurs at the upper pressure level of the plot accounts for some of the reduction in residual die wall pressure. The compact may creep in the axial direction and contract radially, which reduces the apparent force transmission seen in this cycle plot. Creep recovery has been carefully characterized for various compacts and has been shown to take place radially as well as axially(137). The terminal slope for this sample differs from the initial slope and suggests deviation from the documented plastic deformation behavior. Since the pressures utilized resulted in an approximation of a nonporous state, it is reasonable to suspect some particle fragmentation. Since this plot is atypical, more detailed assignment of behavior is not credible.

D.1.c Potassium Chloride, Lot #10195 - It should be recalled that all three particle size fractions for Lot #10195 produced compacts having measurable tensile strength values. The moisture concentration

distribution for these samples was substantially different from that seen for Lot #L7490. The amount of surface moisture for Lot #10195 was lower than that measured for Lot #L7490, while Lot #10195 exhibited a much higher intracrystalline moisture concentration (see Figures 40 and 41). These observations must be kept in mind while assessing the instrumented press data presented in this section.

Compression techniques used have been described previously for Lot #L7490. The most apparent difference noted for this series resides in the ejection force measurements from a lubricated and nonlubricated die (Table XXV). The data seen for the 140-160μ fraction exhibit the highest ejection force level. Since compacts from this size fraction have been shown to have the highest tensile strength values, one can assume that these data are complimentary in nature. Since the bond structure established in these compacts survive unloading quite readily, it would follow then that this compact's structure must also strongly resist radial forces exerted by the die wall prior to ejection. It is reasonable to expect a compact with a poor survival rate upon ejection would not resist radially generated forces. Since these compacts would experience a second yield point from the radial force, the subsequent structure would not be intact prior to ejection; and therefore, a lower ejection force would be exerted. If this concept is used when inspecting all the ejection data shown in Table XXV, a trend becomes apparent, wherein the compacts which are known to have lower tensile strength values also exhibit lower ejection forces.

The degree of force transmission appears to follow the pattern previously seen with materials approaching isotropic behavior above a pressure of 11.8 kg/mm^2. The difference in transmitted force for the

coarse fractions of the two lots of potassium chloride may be explained by considering the degree of surface moisture present and corresponding shear strength of Lot #L7490. If departure from unity is taken as a function of energy imparted to the compact during bond formation and particle flow, the difference between the two lots becomes intuitively obvious. Since Lot #L7490 has been shown to exhibit high degrees of surface lubricity and low shear strength, aproach to isotropic behavior must be inhibited due to energy being expended in particle slip and rearrangement. Although this type of intracompact particle translation is normally attributed to bond formation, the layer of surface moisture prevents coherent structure formation. However, the net result in transmitted force is still the same as if a high degree of plastic flow had taken place. The generation of a coherent bond and subsequently a strong compact may be seen for the 140-160μ fraction of Lot #10195. In this case the departure form unity may be attributed to energy being imparted for plastic flow/bond formation. Since for this sample the moisture layer is not present, a strongly bonded structure results. These data for the coarse fraction of Lot #L7490 and fine fraction of Lot #L10195 are similar and could be considered anomalous had the moisture concentrations and distributions not been carefully characterized.

Forces experienced by the samples during compact formation were recorded as described previously. These results are illustrated in Figures 64, 65, and 66 for the 400-420μ, 140-160μ, and IA milled samples, respectively. The ejection force profile for the 140-160μ fraction was recorded at a more sensitive setting to illustrate the difference seen with this sample when compared to other data contained

in this series. It is interesting to note that in all samples tested, the amplified data for initial slope of the lower punch force shows very little deviation when compared to data presented in Figures 60 and 61. This can be taken to represent a reduced degree of rearrangement, intermediate structure formation, and collapse, indicating a more uniform structure(56).

Ratios of upper punch peak height to die wall peak height indicate a rank order for degree of radially transmitted force. The coarse fraction shows the greatest value followed by the milled material and finally the fine fraction exhibiting the lowest value. This behavior was seen for samples prepared in non-lubricated as well as a lubricated die. These increasing radially transmitted forces may be implicated in the creation of a secondary yield for the compacts with commensurate reduction in compact structure and subsequent tensile strength. Unlike Lot #L7490, there is not a marked difference between the radially transmitted force for the 400-420μ and the 140-160μ samples. However, if one considers shear strength, the finer particle fraction obviously has the highest strength which is shown by the lowest die wall effect(89). In all cases a shallow slope is seen in the die wall data, suggesting some degree of stress relaxation prior to the ejection event.

D.1.d Cycle Plot Evaluation of Potassium Chloride, Lot #10195 - Force application plots were constructed for both particle size fractions of Lot #10195 using the procedure noted in the previous section for Lot #L7490. For both samples a maximum pressure of approximately 20 kg/mm^2 was used. The compression time interval is a constant and

was noted previously. The results are illustrated in Figures 67 and 68 for the 400-420μ and 140-160μ particle size fractions, respectively.

At the pressure level used in the compression of these smaples, it is apparent that some degree of hysteresis occurs at approximately 16.0-16.5 kg/mm^2 for both samples. This type of behavior can be expected when the compact begins to approach an isotropic or non-porous state. At this pressure interval, some degree of creep recovery can be expected during unloading. This creep recovery occurs in the axial direction with commensurate contraction in the radial dirction. The documentation of creep during cyclic analysis has been noted by Obiorah(83).

Below the 16.0 kg/mm^2 pressure level, the plot appears to take on characteristics which would be expected during compaction of a plastically deforming material. For both samples there is a distinct linear portion at the initial and terminal segments of the plot. These segments exhibit similar slopes and may be construed as suggestive of a plastic deformation mechanism.

Both samples have demonstrated an ability to produce compacts with reasonable tensile strength (Figures 44 and 45). The residual die wall pressures for the two size fractions may be considered as equivalent (1.0-1.5 kg/mm^2). These levels may be considered as characteristic of potassium chloride which forms good compacts. They contrast markedly with the level seen for Lot #L7490, 400-420μ (Figure 62). Residual die wall force has been noted as characteristic of granulations which exhibit quality compression properties(72). The magnitude of this force must be tempered with the elastic nature of the sample under consideration, as clearly demonstrated in Figure 62. The

finished compact is a result of the bond structure established during plastic deformation being able to survive the resulting unloading and elastic recovery(129).

The differences seen for both lots of potassium chloride must be a function of the moisture content with its related lubricant properties. The absence of this moisture layer appears to be sufficient to allow even the larger, more spherical particles to produce a structure which can survive elastic recovery (see Table XVII). The slightly higher residual force for the finer particle fraction of Lot #10195 may be rationalized if one considers the amount of internal stress localization areas which have been produced as a consequence of compression. In this case the strength of the subsequent structure is sufficient to permit elastic recovery without compromising compact strength.

D.2 Potassium Chloride and Fatty Alcohol Mixtures - The final dosage form for sustained release potassium chloride is composed of a fatty alcohol (cetostearyl alcohol) matrix and potassium chloride. The properties of this mixture have been characterized elsewhere in this report. It was determined that the compact properties are primarily a function of the matrix material with particle size and morphology of potassium chloride acting somewhat as a secondary function. Inspection of the micrograph shown in Figure 54 supports this proposal since particle coverage and the ubiquitous presence of the matrix among these particles is quite evident. This would suggest that compaction of the mixture may approximate the compression of a continuous phase of a viscous fluid. This is credible since the physical structure shown in the micrograph of the matrix suggests a "free flowing" transport of

the unbound fatty alcohol within the compact. This factor would would lead one to expect more isotropic behavior from compacts prepared from these mixtures.

D.2.a Cetostearyl Alcohol, Lot #K4991, and Potassium Chloride, Lot #L7490 - Mixtures representing both particle size fractions of potassium chloride were compressed using the instrumented F-press. All samples were prepared using a lightly lubricated die since the occlusive nature of the fatty alcohol generated a marked degree of sticking to the punch faces and die without lubricant. The results from these compression trials are summarized in Table XXVI. It becomes apparent that little relevant differences exist for the two samples.

The rapid approach to an isotropic structure is suggested from the tabulated force transmission data. Previous data for potassium chloride alone did not show an approximation of unity at the lower compression force levels as seen with these mixtures. The resulting compacts for the two size fractions have been shown to vary with respect to tensile strength. It would appear, however, that these differences are not detectable using the data shown in Table XXVI.

A representative recording of the forces experienced by the compact are shown in Figure 69. Since the outputs from both mixtures exhibited little discernible differences, only the output for the 140-160μ sample is shown. This recording illustrates the similarities between upper and lower punch force data. It appears that the fluid nature of the continuous phase, semi-solid material acts like an elastic body under pressure with equivalent forces being detected uniaxially.

The departure from baseline after ejection for the amplified lower punch signal is due to the extrusion of the fatty alcohol around the lower punch. The amount of material extruded was quite small and could not be detected by weight loss in the finished compact. This artifact may also be visualized in the die wall signal. The punches and die were cleaned subsequent to every test to minimize this effect on the data.

It is interesting to note that the die wall data do not suggest any stress reduction. It is reasonable to assume that areas of high stress localization due to plastic flow within the compact are negated as a result of the continuous phase of fatty alcohol. Although the die wall output is amplified by a factor of ten compared to the upper forces, it is notable that the peak height ratios approximate unity, a factor which was not previously detected for pure potassium chloride. This lends credibility to the concept that the unbound fatty alcohol can freely channel through the compact. This fluid/viscous flow throughout the compact imparts "elastic-like" behavior to the compact, which is illustrated in Figure 69. These data illustrate that under pressure a coated system of particles retaines a rather low shear strength as evidenced by the die wall force effect.

To confirm the fluid-like nature of th coated potassium chloride, a sample representing an increased ratio of fatty alcohol to potassium chloride (1:3.25) was compressed using identical conditions. The results from this trial are summarized in Table XXVII. In this situation we see a result which indicates isotropic behavior at all the force levels used. It is somewhat difficult to state categorically that the material behaves differently than the data shown in Table XXVI.

However, if the lower force levels in Table XXVII are considered, it can be stated that the transmitted force approaches unity much more rapidly and is different within experimental variation than those recorded for the 1:7.5 ratio sample.

The strip chart recording (Figure 70) for the sample supports the previous data since all peak height ratios approach unity. The absence of residual die wall forces is also evident when the die wall signal is inspected. This was discussed in the previous sample where an absence of stress localization was attributed to the continuous phase of semi-solid fatty alcohol. The continuous phase and coatings on the particles appear to overcome the inherent stress factors which are normally established in a compact of pure potassium chloride.

D.2.b Cetostearyl Alcohol, Lots #K4991 and #L4593, and Potassium Chloride, Lot #10195 - Since both prior samples were processed using the same lot of potassium chloride, a third trial was conducted using the 1A milled sample from Lot #10195. This material approximates actual manufacturing conditions and was felt to be predictive for systems being processed in a production environment. The results (Table XXVIII) obtained indicate similar behavior to that presented previously. One difference noted in these data was seen at the lower force level. The lower degree of transmitted force may be a function of the finer more irregular particles of this lot of potassium chloride overcoming the fluid-like nature of the fatty alcohol. It should be recalled that this sample of potassium chloride was attributed with an intermediate shear strength as well as producing reasonably coherent compacts. The transmitted force characteristic is not present at the

increased force level where one can expect increased flow of the fatty alcohol through the interparticle channels available in the compact structure. The force data recorded for the compaction is identical to those shown for mixtures of fatty alcohol and potassium chloride (Figures 69 and 70) and is not repeated here.

It appears that in all cases the presence of the matrix former can overshadow the compression properties of the potassium chloride by itself. The researcher who considers the use of a matrix dosage form must be concerned primarily with the properties of the matrix former as its characteristics will determine the compact's overall properties, particularly at the concentrations studied in this work. This is evident by the data previously presented for cetostearyl alcohol, Lot #L4593, wherein a suitable tablet could not be produced. The compression results for this material are listed in Table XXIX and indicate little variation from data generated for mixtures employing Lot #K4991. This sample was prepared using the 140-160μ particle fraction of potassium chloride, Lot #10195. This size fraction was selected since it produced compacts having the highest tensile strength results (see Figure 45). Despite the morphology of the potassium chloride substrate cetostearyl alcohol, Lot #L4593 overwhelmed its bond forming characteristics.

D.2.c Cycle Plot Evaluation of Mixtures of Potassium Chloride and Cetostearyl Alcohol - A mixture of potassium chloride and cetostearyl alochol was compressed using the procedure previously described. Replicate samples were processed. The resulting average force levels were plotted as a function of upper pressure (axial)

versus die wall pressure (radial). The axial and radial values were collected at identical time points. This graphic representation of the data permits assessment of applied and transmitted pressure during tablet formation and is illustrated in Figure 71.

The results were not unexpected in light of the data discussed previously. The cycle plot exhibits behavior which is similar to that observed for an elastic solid. The plot indicates minimal residual die wall force. If the experimental variation present in the data collection is considered (±3%), it is reasonable to say that the cycle could conceivably be a single line. The characteristics relating to an elastic solid are intuitively obvious. The initial shallow slope for the cycle is indicative of Poission ratio characteristics for an elastic solid with equal magnitudes of force transmission. This factor as well as similarities in the terminal slope appear to support elastic behavior.

These data also suggest that a matrix former to potassium chloride ratio of 1:7.5 results in reheological behavior similar to a non-porous elastic solid. This would indicate that the resulting compact/tablet qualities are a function of the matrix former. To implement a change in finished tablet quality, the worker must consider significant reduction in the ratio of matrix former or the incorporation of an additive to modify the compression properties of the fatty alcohol. The addition of a third component which imparts a more robust, less elastic bond structure would be advisable. The addition of excipients which transform bonding mechanisms have been studied by other researchers(138). Their findings suggest that a material which is somewhat elastic in nature can be modified to a more plastically deforming material. In the case of fatty alcohols, the variation and

resulting influence on the matrix former's crystalline properties must be considered during formulation.

V. Summary and Conclusions

A. Matrix Forming Components

The matrix forming material, cetostearyl alcohol, has been shown to exhibit marked differences during compression. These differences have been correlated with the composition of the selected sample. The composition of the cetostearyl samples characterized indicate that the C_{14} and C_{16} fatty alcohol segments produce the most impact on the quality of the finished compacts.

In general, it was found that mixtures of fatty alcohols produce a more complex thermal fingerprint during DSC studies than those generated by the alcohols by themselves. This was evident when DSC studies on mixtures of high purity hexadeconal and octadecanol were made which approximated commercially available cetostearyl alcohol. It has been shown that a critical ratio of C_{16}/C_{18} exists beyond which a more complex series of solid-solid transitions may occur. The degree to which the amount of solid-solid transition takes place was monitored as a function of transition temperature and heat of freezing. The results for the heat of freezing study clearly show a relationship between the initial heat of freezing (ΔH_1) and the tensile strength of the fatty alcohol compact. Subsequent scanning electron micrographs also yield support to this observation since the more crystalline samples also exhibited higher ΔH_1 values. The ability of irregular crystalline materials has been shown to produce compacts with higher tensile strengths.

The presence of C_{14} (tetradecanol) in mixtures of C_{16} and C_{18} was found to increase the amount of energy liberated during initial freezing and subsequently cause the sample in question to produce compacts having a higher tensile strength. A sample of cetostearyl alcohol with a low concentration of C_{14} was found to produce higher initial heat of freezing results (ΔH_1) when the C_{14} concentration was increased. It is apparent from these data that the heat of freezing (solidification) provides a useful probe in predicting subsequent compact properties.

Conventional fusion processing, compression, and changes in dwell time have been shown to have little effect on the quality of the finished compact as a function of tensile strength. The tensile strength of the compacts is invariant with age.

In all samples studies, the presence of the fatty alcohol dominates the physical properties of the finished compact. As the concentration of the matrix former is increased, the compact's tensile strength approaches that of the matrix former by itself. It is advisable that the formulator who considers the usage of fatty alcohols as matrix formers establish a series of raw material test criteria to assure consistent doage form performance. Since various excipients may be included in tablet formulations, a component which improves the compaction properties of the fusion mass may be included.

B. Potassium Chloride

Several lots of potassium chloride were characterized with respect to physical properties. The resulting compacts from these lots varied significantly in tensile strength. This variation has been linked to

several properties which were inherent in each lot of raw material. The causative factors which were identified were the moisture content (surface and intracrystalline), particle size, and configuration. In general, it was found that potassium chloride with a low level of surface moisture, some degree of entrapped moisture, and a small (140-160μ) particle size with an irregular morphology produced compacts with the highest tensile strength values.

Studies directed at drying to a constant weight were performed on both lots of potassium chloride. One lot possessed a high level of surface moisture with minimal amounts of entrapped moisture. Equivalent particle size fractions from both lots were compressed. In all situations the drier sample produced the strongest compacts. Drying the sample with a high surface moisture prior to compression yielded compacts which did not markedly differ from those of the lot with a lower moisture content with respect to tensile strength. The strength of the compacts was noted to vary upon aging. The presence of some entrapped moisture was noted to increase the magnitude of aging effects on compact strength.

Since potassium chloride bonds during compression by plastic deformation, an increase in the time exposed to maximum compression force (dwell time) was shown to increase tensile strength. Density-pressure analysis suggested differences related to yield pressure for various particle configurations of the two lots of material. A pressure of approximately 11.8 kg/mm^2 was established as a level above which optimal compact formation may be expected.

Mixtures of potassium chloride with fatty alcohol resulted in compacts with a reduced tensile strength. It has been shown that the

matrix former dominates the compacts compression properties. This overwhelming effect was minimized when dealing with a lot of potassium chloride with a low surface moisture and small/irregular particle configuration.

Since all potassium chloride tested conformed to USP requirements, it is evident that more exacting specifications may be needed should the formulator require optimal compaction properties. These specifications should address surface moisture as well as intracrystalline moisture. The subsequent process should be designed to generate particles with a mean of approximately 140-160μ. The milling process should be sufficiently energetic to yield irregular fragmented particles. These criteria will also help to prevent non-homogeneous behavior during compression should the potassium chloride be used in a sustained release matrix.

C. Mixtures

Since the object of the research was to characterize the effect of aging and dwell time on mixtures of potassium chloride and fatty alcohol, it becomes necessary to qualify our objective in light of the results. The initial observation was made under routine manufacturing conditions, where exhaustive characterizations of dosage form components are not normally undertaken. Once each component is studied and understood, the resulting mixture's behavior is reduced to a rationally explainable series of factors.

These factors are nested in the variability documented for potassium chloride and cetostearyl alcohol. Since compact characteristics change when these components are blended, the variation noted in the

objective statement should be tempered with consideration of the quality of the potassium chloride, uniformity of the matrix granulation and thermal properties of the cetostearyl alcohol.

In conclusion, the changes in hardness noted initially are a function of several physicochemical factors and not solely in response to dwell time, as the results indicate a more complex explanation rather than a response to a single variable.

VI. Tables and Figures

Table I - Physical Properties of Pure Alcohols

IUPAC Name[b]	Molecular Formula[a]	Common Names[b]	Molecular Weight[a]	Melting Point °C	Boiling Point °C/mmHg	Freezing Point[c] °C	Density g/ml @ specified conditions
1-decanol	$C_{10}H_{22}O$	n-decyl alcohol	158.28	7.0[f]	232.9/760[a] 236.0/760[b]	6.88	0.8297[a] @20°C/4°C
1-dodecanol	$C_{12}H_{26}O$	n-dodecyl alcohol	186.33	23.8[f]	259/760[a]	23.95	0.8309[a] @24°C/4°C
1-tetradecanol	$C_{14}H_{30}O$	n-tetradecyl alcohol myristyl alcohol	214.38	38.0[f,g] 38.3[b]	167/15[a]	38.26	0.8240[a] @38°C/4°C
1-hexadecanol	$C_{16}H_{34}O$	n-hexadecyl alcohol cetyl alcohol palmityl alcohol	242.43	49.3[f] 49.6[b]	189.5/760[b]	49.62	0.8180[a] @50°C/4°C
1-octadecanol	$C_{18}H_{38}O$	n-octadecyl alcohol stearyl alcohol	270.5	59.0[h] 58.0[b] 60.0[j]	210.5/760[b]	57.98	0.8120[a] @59°C/4°C
1-duodecanol	$C_{20}H_{42}O$	eicosyl alcohol arachidic alcohol eicosanol	299.0	65.0[e,i,b]	369/760[e]	---	0.8410[a] @20°C/4°C
1-hexadecanol/ 1-octadecanol	*[d]	cetyl-stearyl alcohol cetostearyl alcohol tallow alcohol	*[d]	50-54[b] 43-53[k]	316-332/15[b]	*[d]	0.8090-0.8160[b] @25°C/25°C

* Mixtures of cetyl and stearyl alcohol are usually in the ranges of 20-35% and 50-70% respectively. Other physical data vary with actual composition[d].

REFERENCES

a M. Windholz, (Ed.), "The Merck Index," Ninth Edition, Merck and Co., Rahway, N.J. (1976)

b H. F. Mark, J. J. McKetta, D. F. Othmer and A. Standin, (Eds.), "Encyclopedia of Chemical Technology," Second Edition, Vol. 1, K. R. Ericson and H. D. Van Wagenen, John Wiley & Sons, New York, N.Y. (1965) p. 542

c C. W. Hoerr, H. J. Harwood and A. W. Ralston, J. Org. Chem., 9, 267 (1944)

d W. Ainley, (Ed.), "The Extra Pharmacopeia," Twenty-Seventh Edition, The Pharmaceutical Press, London, U.K. (1977)

e R. C. Weast, (Ed.), "The Handbook of Chemistry and Physics," Fifty-Third Edition, Chemical Rubber Publishing Co., Cleveland, Ohio (1972-1973)

f T. Eckert and J. Muller, Arch. Pharm., 311, 31 (1978)

g C. Mosselman, et al, J. Chem. Thermodynamics, 6, 477 (1978)

h K. Tanaka, et al, Bull. Inst. Chem. Res., Kyoto Univ., 37, 281 (1959)

i D. G. Kolp and E. S. Lutton, J. Amer. Chem. Soc., 73, 5593 (1951)

j W. R. Wilcox, Chem. Reviews, 2, 187 (1964)

k "USP XXI/NF XVI," The United States Pharmacopeial Conv. Inc., Rockville, Md., p. 1548 (1985)

Table II - Physical Properties of Potassium Chloride and Magnesium Stearate

Molecular Formula	Common Name	Molecular Weight	Melting Point °C	Density g/ml
KCl	potassium chloride	74.55[a]	773[a]	1.98[a]
$Mg(C_{18}H_{35}O_2)_2$	magnesium stearate	590.0 [b]	145[b]	1.028[b]

[a] M. Windholz, (Ed.), "The Merck Index," Ninth Edition, Merck and Co., Rahway, N.J., (1976).

[b] E. S. Pattison, (Ed.), "Fatty Acids and Their Industrial Applications," Marcel Dekker, New York, N.Y., (1968).

Table III - Fatty Alcohol Samples and Origins of Supply

Alcohol	Lot #	Analytical Purity[a]	Source
High Purity Material			
1-Tetradeconal	A 1401	+ 99.0%	Analabs, Div. of Foxboro North Haven, Conn.
1-Hexadeconal	E 290H	+ 99.0%	Analabs, Div. of Foxboro North Haven, Conn.
1-Octadecanol	L 020A	+ 99.0%	Analabs, Div. of Foxboro North Haven, Conn.
Commercial Material			
1-Tetradecanol	T03360	approx. 95%	Pfaltz & Bauer Inc. Stamford, Conn.
1-Hexadecanol	H03100	approx. 95%	Pfaltz & Bauer Inc. Stamford, Conn.
1-Hexadecanol	L2475	approx. 95%	M. Michel Co. New York, N.Y.
1-Octadecanol	000140	approx. 95%	Pfaltz & Bauer, Inc. Stamford, Conn.
1-Octadecanol	M488	approx. 95%	M. Michel Co. New York, N.Y.
Cetostearyl	K4991	C_{14} alcohol 3.7%[b] C_{16} alcohol 26.0% C_{18} alcohol 61.8%	Procter & Gamble Cincinnati, Ohio
Cetostearyl	L4593	C_{14} alcohol 0.8%[b] C_{16} alcohol 31.1% C_{18} alcohol 62.8%	Conoco Chem. Co. Houston, Texas

[a] Manufacturers label claim.

[b] Remaining materials are primarily long and short chain alcohols and a trace of alkanes CIBA-GEIGY/PAC Data 3/21/82.

Table IV - Potassium Chloride Samples and Origin of Supply

Lot #	Description	Grade	Specifications	Source
L7490	White, granular crystals	Granular	USP	Mallinckrodt Inc.[a]
10195	White, granular crystals	Granular	USP	Mallinckrodt Inc.[a]

[a] Mallinckrodt Inc., Drug & Cosmetic Div., St. Louis, Mo.

Table V - Transducer Calibration Data Using The Instron

	Force(lb)	mV	mV/lb (n=10)	$\bar{X}$ All Force Levels	mV/lb[b]
Upper Punch	1028	1172	1.14 (.04)	1.18 (.02)	1.22 ± 1.0%
	2133	2538	1.19 (.03)		
	3996	4755	1.18 (.02)		
	7730	9210	1.19 (.05)		
Lower Punch	162[a]	188	1.16 (.05)	1.13 (.02)	1.14 ± 1.0%
	319[a]	360	1.13 (.02)		
	567	630	1.11 (.01)		
	2086	2340	1.12 (.03)		
	4304	4830	1.12 (.02)		
	7496	8400	1.12 (.01)		

[a] CDM cell used for measurement on Instron.

[b] PCB Piezotronics data sheet for Model 200M22, SN943 and Model 204M02, SN222.

Table VI - Die Wall Transducer Calibration Data Using The Instron

Pressure PSI	Plug[a] Height(in)	mV	mV/PSI (n=10)	$\bar{X}$ All Levels	mV/PSI[b]
5,473	0.234	1,095	0.20 (.01)		
10,363	0.228	1,969	0.19 (.01)	0.19 (.005)	0.21 ± 1.5%
21,821	0.215	4,250	0.19 (.02)		
39,648	0.195	7,500	0.19 (.01)		

[a] Rubber Plug h_o = 6.760 mm (.268 in).

[b] PCB Piezotronics data sheet for Model 108M11, SN7558.

Table VII - Hardness Tester Calibration Data[a]

Suppliers' Rating	Instron[b]	Heberlein[b]
5.0kp ± 0.2	4.9kp ± 0.1	5.4kp ± 0.1
10.0kp ± 0.3	9.5kp ± 0.2	10.0kp ± 0.1
15.0kp ± 0.4	15.1kp ± 0.5	16.7kp ± 0.2

[a] Mechanical tablet ratings as measured by Instron in kp (kiloponds of force) and the hardness tester in kp units.

[b] Each measurement is an average of 10 determinations (n=10).

Table VIII - Cetostearyl Alcohol Composition[a]

Alcohol	Lot # K4991	Lot # L4593
C_{14} Alcohol	3.7%	0.8%
C_{16} Alcohol	26.0%	31.1%
C_{18} Alcohol	61.8%	62.8%

Remaining materials are primarily long and short chain alcohols and a trace of alkanes.

[a] CIBA-GEIGY, Physical and Analytical Chemistry Section, 3/21/82, Suffern, N.Y.

Heat of Fusion, High Purity Fatty Alcohol Samples

Alcohol	Lot #	Weight[a]	Calc. Δ H[b]	Lit. Value
1-Tetradecanol	A1401	3.94 mg	227.3 J/g (0.1)	213.0[c],224.7[d] J/g
1-Hexadecanol	E290H	4.46 mg	232.7 J/g (1.2)	220.6[c],229.6[d] J/g
1-Octadecanol	L020A	4.98 mg	235.6 J/g (1.8)	236.7[e],243.7[c] J/g

[a] Represents 1.84×10^{-5} moles of each alcohol.

[b] n = 5, (std. dev.).

[c] T. Eckert and J. Müller, Arch. Pharm. (Weinheim), 311, 31 (1978)

[d] C. Mosselman and H. Dekker, J. Chem. Soc. Farraday Trans., 71, 417 (1975)

[e] G. Gioia Lobbia, G. Berchiesi, and M. A. Berchiesi, J. Thermal Anal., 10, 205 (1976)

Energy of Freezing as a Function of C_{16} Concentration[a]

% C_{16}/MOLE FRAC	% C_{18}/MOLE FRAC	ΔH_1 J/g	ΔH_2 J/g
31/.334	69/.666	117.0 (1.3)[b]	44.0 (1.1)[b]
29/.313	71/.687	118.6 (1.3)	50.5 (1.5)
27/.292	73/.708	119.6 (2.2)	53.0 (2.5)
25/.271	75/.729	120.3 (1.5)	57.2 (1.7)

[a] All energy measurements are recorded as Joules/gm (J/g), ΔH represents the first measured peak, ΔH_2 corresponds to the second peak.

[b] n = 5 (std. dev.)

Compact Strength of Fatty Alcohols Recorded as Tensile Strength[a]

ALCOHOL	APPLIED FORCE	UNTREATED[b] 5 cm/min	UNTREATED[b] 10 cm/min[c]	PROCESSED[b] 5 cm/min	PROCESSED[b] 10 cm/min[c]
C_{16}					
E290H (+99%)	3.94 kg/mm^2	0.03 kp/mm^2	0.03 kp/mm^2	0.03 kp/mm^2	0.03 kp/mm^2
	7.89 kg/mm^2	0.03 kp/mm^2	0.03 kp/mm^2	0.03 kp/mm^2	0.03 kp/mm^2
L2475 (95%)	3.94 kg/mm^2	0.11 kp/mm^2	0.11 kp/mm^2	0.11 kp/mm^2	0.11 kp/mm^2
Commercial	7.89 kg/mm^2	0.11 kp/mm^2	0.11 kp/mm^2	0.11 kp/mm^2	0.11 kp/mm^2
C_{18}					
L020A (+99%)	3.94 kg/mm^2	---	---	---	---
	7.89 kg/mm^2	---	---	---	---
000140 (95%)	3.94 kg/mm^2	0.09 kp/mm^2	0.09 kp/mm^2	0.09 kp/mm^2	0.09 kp/mm^2
Commercial	7.89 kg/mm^2	0.09 kp/mm^2	0.09 kp/mm^2	0.09 kp/mm^2	0.09 kp/mm^2
M488 (95%)	3.94 kg/mm^2	0.06 kp/mm^2	0.06 kp/mm^2	0.06 kp/mm^2	0.06 kp/mm^2
Commercial	7.89 kg/mm^2	0.06 kp/mm^2	0.06 kp/mm^2	0.06 kp/mm^2	0.06 kp/mm^2
Cetostearyl Alcohol					
L4593	3.94 kg/mm^2	---	---	---	---
	7.89 kg/mm^2	---	---	---	---
K4991	3.94 kg/mm^2	0.04 kp/mm^2	0.04 kp/mm^2	0.04 kp/mm^2	0.04 kp/mm^2
	7.89 kg/mm^2	0.04 kp/mm^2	0.04 kp/mm^2	0.04 kp/mm^2	0.04 kp/mm^2

[a] All strength data are calculated using Equation , the results are expressed in units of tensile strength, kiloponds/mm^2 (kp/mm^2). All sample points are an average of 10 determinations.

[b] Untreated represents samples taken directly from containers, processed represents after fusion in planetary mixer.

[c] Two strain rates are used, 5 cm/min and 10 cm/min.

Effects of C_{14}[a] on Energy of Freezing for Cetostearyl Alcohol, Lot L4593, and Resulting Increase in Tensile Strength

% C_{14}	ΔH_1	kp/mm^2[c]
0.8%	96.3 (0.5)[b]	--
2.8%	98.5 (1.6)	--
4.8%	99.4 (1.3)	0.02

[a] Tetradecanol Lot #A1401

[b] n = 5 (std. dev.) recorded as Joules/gm.

[c] n = 10 per data point, calculated using Equation for tensile strength. No compacts were able to be formed at the 0.8 and 2.8% C_{14} levels.

Table XIII - Surface Moisture of Potassium Chloride[a]

	400-420μ % WT. LOSS	140-160μ % WT. LOSS
Lot L7490	.011	.014
	.011	.015
	.013	.015
Lot 10195	.005	.005
	.005	.005
	.005	.006

[a] Lots L7490 and 10195 were dried at 120°C for 2 hours to determine amount of surface moisture.

Table XIV - Characterization of Size Fractions for Potassium Chloride, Lot 10195

Fine Particle Fraction (140-160μ)

Screen	Opening	Percent Retained[a]
80 mesh	180μ	0
100 mesh	149μ	82 (4.6)
120 mesh	120μ	8 (0.8)
140 mesh	106μ	5 (1.1)
200 mesh	74μ	3 (0.6)
PAN	—	2 (0.4)

Coarse Particle Fraction (400-420μ)

Screen	Opening	Percent Retained[a]
35 mesh	500μ	3 (1.0)
40 mesh	420μ	25 (3.0)
45 mesh	350μ	62 (3.1)
50 mesh	297μ	7 (1.5)
60 mesh	250μ	2 (0.8)
PAN	--	1 (0.6)

[a] n = 5 (std. dev.) 200g batch at intensity 7 for 20 minutes using Cenco Sieve Shaker

Table XV - Characterization of Size Fractions for Potassium Chloride, Lot L7490

Fine Particle Fraction (140-160μ)

Screen	Opening	Percent Retained[a]
80 mesh	180μ	0
100 mesh	149μ	91 (5.1)
120 mesh	120μ	4 (1.1)
140 mesh	106μ	2 (0.5)
200 mesh	74μ	2 (0.2)
PAN	—	1 (0.5)

Coarse Particle Fraction (400-420μ)

Screen	Opening	Percent Retained[a]
35 mesh	500μ	6 (1.6)
40 mesh	420μ	32 (4.1)
45 mesh	350μ	53 (4.5)
50 mesh	297μ	7 (1.6)
60 mesh	250μ	1 (0.4)
PAN	--	1 (0.3)

[a] n = 5 (std. dev.) 200g batch at intensity 7 for 20 minutes using Cenco Sieve Shaker

TABLE XVI - Particle Size Distribution, Milled Lot 10195[a]

SCREEN	OPENING	PERCENT RETAINED[b]
20	850 μ	1 (0.2)
40	420 μ	27 (2.0)
50	297 μ	48 (3.5)
80	180 μ	15 (1.5)
140	106 μ	5 (0.5)
200	74 μ	2 (0.8)
PAN	-----	2 (0.6)

[a] Samples were not classified subsequent to milling and reflect materials as a result of once-through milling.

[b] n = 5 batches (std. dev.) 200g at intensity 7 for 20 minutes using Cenco Sieve Shaker

Table XVII - Surface Moisture Effects on Tensile Strength of Potassium Chloride Compacts[a]

PRESSURE kg/mm²	0 TIME kp/mm²	1 HR kp/mm²	3 HR kp/mm²	24 HR kp/mm²	1 WEEK kp/mm²	LOT #	CONDITION
11.83	.10	.10	.10	.11	.10	L7490	140-160μ Undried
11.83	.21	.25	.29	.33	.37	L7490	140-160μ Dried
11.83	.32	.34	.34	.36	.40	10195	140-160μ Undried
11.83	.34	.34	.35	.36	.39	10195	140-160μ Dried

[a] Compacts were processed using 10-second dwell time and a 10 cm/min strain rate. Potassium Chloride was dried at 95°C for 24 hours prior to compression. Storage was carried out at room temperature and ambient humidity conditions. Tensile strength is recorded as kp/mm².

Table XVIII - Aging Effects on Tensile Strength of Potassium Chloride, Lot 10195, Compacts[a]

PRESSURE kg/mm²	0 TIME kp/mm²	.5 HR kp/mm²	1 HR kp/mm²	2 HR kp/mm²	3 HR kp/mm²	24 HR kp/mm²	1 WK kp/mm²	4 WK kp/mm²	% Inc. w/Aging	Conditions
11.83	.32	.34	.34	.34	.34	.35	.38	.4	20	140-160μ .2" D.T.
11.83	.32	.33	.34	.34	.34	.36	.4	.4	20	140-160μ 10" D.T.
19.73	.34	.37	.37	.37	.37	.37	.4	.4	15	140-160μ .2" D.T.
19.73	.34	.38	.38	.38	.38	.38	.4	.4	15	140-160μ 10" D.T.
11.83	.23	.28	.28	.28	.30	.30	.33	.34	32	400-420μ .2" D.T.
11.83	.25	.3	.31	.31	.31	.33	.35	.37	32	400-420μ 10" D.T.
19.73	.28	.31	.31	.31	.31	.34	.353	.37	24	400-420μ .2" D.T.
19.73	.30	.34	.34	.34	.35	.35	.37	.38	21	400-420μ 10" D.T.
11.83	.16	.19	.19	.20	.20	.20	.22	.25	36	1A Milled .2" D.T.
11.83	.24	.28	.29	.29	.29	.30	.32	.35	31	1A Milled 10" D.T.
19.73	.21	.23	.25	.26	.26	.27	.30	.32	34	1A Milled .2" D.T.
19.73	.26	.27	.27	.29	.29	.30	.32	.34	24	1A Milled 10" D.T.

[a] n = 10 for each data point, Strain Rate 10 cm/min, stored at room temperature and ambient humidity conditions. Tensile strength is recorded as kp/mm²; D.T. = dwell time; % Inc.w/Aging = percent increase in tensile strength with aging.

Table XIX - Aging Effects of Tensile Strength of Potassium Chloride, Lot L7490, Compacts[a]

PRESSURE kg/mm²	0 TIME kp/mm²	.5 HR kp/mm²	1 HR kp/mm²	2 HR kp/mm²	3 HR kp/mm²	24 HR kp/mm²	1 WK kp/mm²	4 WK kp/mm²	% Inc. w/Aging	Conditions
11.83	.08	.09	.09	.09	.09	.09	.11	.10	20	140-160μ .2" D.T.
11.83	.10	.10	.10	.09	.10	.10	.09	.12	17	140-160μ 10" D.T.
19.73	.10	.10	.10	.10	.10	.10	.10	.12	17	140-160μ .2" D.T.
19.73	.11	.13	.13	.13	.14	.13	.15	.15	27	140-160μ 10" D.T.

[a] n = 10 for each data point, Strain rate 10 cm/min, stored at room temperature and ambient humidity conditions. Tensile strength is recorded as kp/mm²; D.T. = dwell time; % Inc.w/Aging = percent increase in tensile strength with aging.

Table XX - Heckel Plot, %Δ AUC for 0.2 and 10 Second Dwell Time[a]

Size Fraction	Lot #L7490	Lot #10195
140-160μ	2.6	4.3
400-420μ	0.7	1.2

[a] ΔAUC = difference in area under the curve for both dwell times used to construct the Heckel Plots.

Table XXI - Compact Tensile Strength of Cetostearyl Alcohol and Potassium Chloride Mixtures[a]

PRESSURE kg/mm²	LOT #KCl	PARTICLE SIZE	LOT #CSA[b]	0 TIME kp/mm²	1 HR kp/mm²	12 HRS kp/mm²	24 HRS kp/mm²	48 HRS kp/mm²	72 HRS kp/mm²
7.89	L7490	400-420μ	L4593	--	--	--	--	--	--
15.78	L7490	400-420μ	L4593	--	--	--	--	--	--
7.89	L7490	400-420μ	K4991	--	--	--	--	--	--
15.78	L7490	400-420μ	K4991	--	--	0.02	0.02	0.02	0.02
7.89	L7490	140-160μ	L4593	--	--	--	--	--	--
15.78	L7490	140-160μ	L4593	--	--	--	--	--	--
7.89	L7490	140-160μ	K4991	0.05	0.05	0.07	0.07	0.07	0.07
15.78	L7490	140-160μ	K4991	0.05	0.05	0.06	0.06	0.06	0.06
7.89	10195	400-420μ	L4593	--	--	--	--	--	--
15.78	10195	400-420μ	L4593	--	--	--	--	--	--
7.89	10195	400-420μ	K4991	0.12	0.12	0.12	0.14	0.14	0.14
15.78	10195	400-420μ	K4991	0.14	0.14	0.14	0.15	0.15	0.16
7.89	10195	Milled	L4593	--	--	--	--	--	--
15.78	10195	Milled	L4593	--	--	--	--	--	--
7.89	10195	Milled	K4991	0.10	0.11	0.11	0.12	0.12	0.13
15.78	10195	Milled	K4991	0.14	0.12	0.10	0.12	0.13	0.14
7.89	10195	140-160μ	L4593	--	--	--	--	--	--
15.78	10195	140-160μ	L4593	--	--	--	--	--	--
7.89	10195	140-160μ	K4991	0.15	0.15	0.15	0.17	0.18	0.18
15.78	10195	140-160μ	K4991	0.18	0.15	0.18	0.17	0.18	0.18

[a] 1:7.5 ratio of fatty alcohol to potassium chloride, aging/storage at room temperature, ambient conditions, used 10 cm/min strain rate with 10 second dwell time.

[b] cetostearyl alcohol

Table XXII - Compact Tensile Strength of an Increased Level of Cetostearyl Alcohol and Potassium Chloride Mixtures[a]

PRESSURE kg/mm²	LOT #KCl	PARTICLE SIZE	0 TIME kp/mm²	1 HR kp/mm²	12 HRS kp/mm²	24 HRS kp/mm²	48 HRS kp/mm²	72 HRS kp/mm²
7.89	L7490	140-160μ	0.03	0.03	0.04	0.04	0.03	0.04
15.78	L7490	140-160μ	0.03	0.03	0.03	0.04	0.04	0.04
7.89	10195	400-420μ	0.05	0.05	0.05	0.06	0.06	0.07
15.78	10195	400-420μ	0.10	0.05	0.08	0.08	0.08	0.11
7.89	10195	Milled	0.06	0.06	0.05	0.06	0.07	0.07
15.78	10195	Milled	0.08	0.08	0.09	0.08	0.08	0.09
7.89	10195	140-160μ	0.12	0.12	0.12	0.14	0.13	0.13
15.78	10195	140-160μ	0.14	0.14	0.14	0.16	0.17	0.15

[a] 1:3.25 ratio of fatty alcohol to potassium chloride, cetostearyl alcohol, Lot K4991, aging/storage at room temperature, ambient conditions, used 10 cm/min strain rate with 10 second dwell time.

Table XXIII - C_{16}/C_{18} Fatty Alcohol Combinations and Potassium Chloride Mixtures[a]

PRESSURE kg/mm²	C_{18} LOT#	C_{16} LOT#	% C_{18}	% C_{16}	0 TIME kp/mm²	1 HR kp/mm²	12 HRS kp/mm²	24 HRS kp/mm²	0 TIME kp/mm²
7.89	00140	--	100	--	0.11	0.11	0.12	0.12	0.13
15.78	00140	--	100	--	0.12	0.12	0.12	0.13	0.13
7.89	--	L2475	--	100	0.18	0.19	0.18	0.20	0.21
15.78	--	L2475	--	100	0.20	0.19	0.19	0.20	0.22
7.89	00140	H03100	90	10	0.09	0.10	0.10	0.11	0.12
15.78	00140	H03100	90	10	0.12	0.12	0.12	0.11	0.14
7.89	L020A	L2475	10	90	0.15	0.15	0.15	0.16	0.17
15.78	L020A	L2475	10	90	0.17	0.18	0.17	0.18	0.18
7.89	00140	H03100	75	25	0.06	0.06	0.07	0.07	0.06
15.78	00140	H03100	75	25	0.08	0.07	0.08	0.08	0.09
7.89	L020A	L2475	25	75	0.12	0.11	0.11	0.11	0.13
15.78	L020A	L2475	25	75	0.14	0.12	0.13	0.14	0.14
7.89	00140	H03100	70	30	0.05	0.05	0.06	0.06	0.07
15.78	00140	H03100	70	30	0.06	0.05	0.07	0.06	0.07
7.89	L020A	L2475	30	70	0.09	0.09	0.10	0.09	0.11
15.78	L020A	L2475	30	70	0.11	0.10	0.12	0.11	0.13
7.89	00140	H03100	50	50	0.02	0.02	0.03	0.02	0.03
15.78	00140	H03100	50	50	0.03	0.03	0.02	0.02	0.03
7.89	L020A	L2475	50	50	0.04	0.05	0.05	0.04	0.05
15.78	L020A	L2475	50	50	0.05	0.04	0.03	0.05	0.05
7.89	--	H03100	--	100	0.02	0.01	0.01	0.02	0.02
15.78	--	H03100	--	100	0.03	0.01	0.01	0.02	0.03
7.89	L020A	--	100	--	--	--	--	--	--
15.78	L020A	--	100	--	--	--	--	--	--

[a] Milled Potassium Chloride, Lot 10195, 1:7.5 ratio fatty alcohol to Potassium Chloride, aging/storage at room temperature, ambient conditions, 10cm/min strain rate, 10 second dwell time.

Table XXIV - Compression Results, Potassium Chloride, Lot L7490

LOT #L7490 400-420μ

Applied Pressure Level (kg/mm^2)	Ratio of Trans. Force[a] lower/upper	Ejection Force[a] (kg/mm^2)	Lubricated Die
Approx. 8.0	0.82 (.01)	0.09 (.01)	No
	0.83 (.01)	0.09 (.01)	Yes
Approx. 10.5	0.85 (.02)	0.14 (.02)	No
	0.85 (.01)	0.14 (.02)	Yes
Approx. 20.0	0.97 (.04)	0.20 (.04)	No
	0.97 (.03)	0.21 (.03)	Yes

Lot #L7490 140-160μ

Approx. 8.0	0.72 (.01)	0.08 (.02)	No
	0.73 (.01)	0.08 (.02)	Yes
Approx. 10.5	0.93 (.02)	0.15 (.03)	No
	0.93 (.03)	0.15 (.03)	Yes
Approx. 20.0	0.99 (.01)	0.23 (.03)	No
	0.97 (.02)	0.23 (.03)	Yes

[a] n = 5 (std. dev.)

Table XXV - Compression Results, Potassium Chloride, Lot 10195

Applied Pressure Level (kg/mm^2)	Ratio of Trans. Force[a] lower/upper	Ejection Force[a] (kg/mm^2)	Lubricated Die
LOT #10195 400-420μ			
Approx. 10.0	0.84 (.01)	0.18 (.01)	No
	0.84 (.01)	0.15 (.01)	Yes
Approx. 13.0	0.93 (.01)	0.30 (.02)	No
	0.93 (.01)	0.28 (.03)	Yes
Approx. 20.0	0.98 (.02)	0.39 (.02)	No
	0.98 (.01)	0.35 (.01)	Yes
LOT #10195 140-160μ			
Approx. 10.0	0.80 (.01)	0.44 (.04)	No
	0.84 (.01)	0.24 (.01)	Yes
Approx. 13.0	0.83 (.02)	0.67 (.05)	No
	0.88 (.02)	0.31 (.03)	Yes
Approx. 20.0	0.90 (.01)	0.66 (.1)	No
	0.93 (.01)	0.50 (.1)	Yes
LOT #10195 1A MILLED			
Approx. 10.0	0.78 (.02)	0.17 (.02)	No
	0.77 (.01)	0.15 (.03)	Yes
Approx. 13.0	0.89 (.03)	0.36 (.05)	No
	0.91 (.01	0.24 (.02)	Yes
Approx. 20.0	0.95 (.02)	0.43 (.03)	No
	0.97 (.02)	0.37 (.02)	Yes

[a] n = 5 (std. dev.)

Table XXVI - Compression Results, Cetostearyl Alcohol and Potassium Chloride Mixtures[a]

Applied Pressure Level (kg/mm^2)	Ratio of Trans. Force[b] lower/upper	Ejection Force[b] (kg/mm^2)
CETOSTEARYL ALCOHOL, 400-420μ POTASSIUM CHLORIDE		
Approx. 10.0	0.89 (.02)	0.06 (.02)
Approx. 13.0	0.95 (.01)	0.09 (.02)
Approx. 20.0	0.99 (.01)	0.15 (.02)
CETOSTEARYL ALCOHOL, 140-160μ POTASSIUM CHLORIDE		
Approx. 10.0	0.94 (.02)	0.07 (.02)
Approx. 13.0	0.97 (.02)	0.12 (.01)
Approx. 20.0	0.99 (.01)	0.16 (.02)

[a] Cetostearyl Alcohol, Lot K4991, Potassium Chloride, Lot L7490, 1:7.5 ratio

[b] n = 5 (std. dev.)

Table XXVII - Compression Results, Increased Level of Cetostearyl Alcohol and Potassium Chloride Mixture[a]

CETOSTEARYL ALCOHOL, 140-160μ POTASSIUM CHLORIDE

Applied Pressure Level (kg/mm^2)	Ratio of Trans. Force[b] lower/upper	Ejection Force[b] (kg/mm^2)
Approx. 10.0	0.98 (.01)	0.07 (.02)
Approx. 13.0	1.00 (.01)	0.08 (.03)
Approx. 20.0	0.99 (.02)	0.09 (.02)

[a] Cetostearyl Alcohol, Lot K4991, Potassium Chloride, Lot L7490, 1:3.25 ratio

[b] n = 5 (std. dev.)

Table XXVIII - Compression Results, Cetostearyl Alcohol and Milled Potassium Chloride Mixture[a]

CETOSTEARYL ALCOHOL, 1A MILLED POTASSIUM CHLORIDE

Applied Pressure Level (kg/mm^2)	Ratio of Trans. Force[b] lower/upper	Ejection Force[b] (kg/mm^2)
Approx. 10.0	0.92 (.02)	0.12 (.01)
Approx. 13.0	0.98 (.01)	0.15 (.03)
Approx. 20.0	0.97 (.01)	0.15 (.03)

[a] Cetostearyl Alcohol, Lot K4991, Potassium Chloride, Lot 10195, 1:7.5 ratio

[b] n = 5 (std. dev.)

Table XXIX - Compression Results, Cetostearyl Alcohol and Potassium Chloride Mixture[a]

CETOSTEARYL ALCOHOL, 140-160μ POTASSIUM CHLORIDE

Applied Pressure Level (kg/mm^2)	Ratio of Trans. Force[b] lower/upper	Ejection Force[b] (kg/mm^2)
Approx. 10.0	0.98 (.02)	0.04 (.01)
Approx. 13.0	0.99 (.03)	0.05 (.02)
Approx. 20.0	1.00 (.02)	0.04 (.02)

[a] Cetostearyl Alcohol, Lot L4593, Potassium Chloride, Lot 10195, 1:7.5 ratio

[b] n = 5, (std. dev.)

Figure 1 - Phase Diagram[a] of C_{16} and C_{18} Fatty Alcochols, Literature Reference

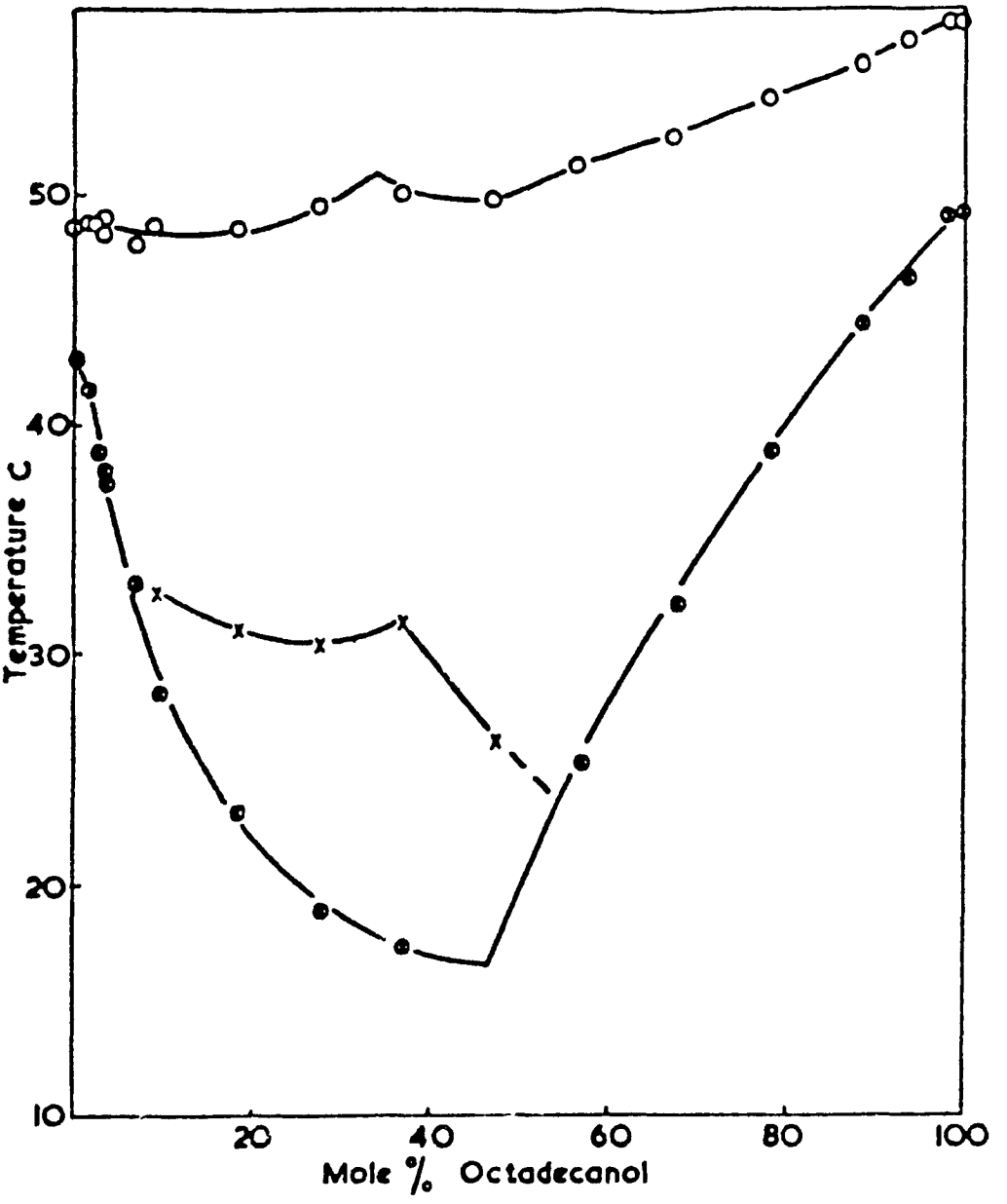

PHASE DIAGRAM OF C_{18} AND C_{16} FATTY ALCOHOLS

[a]Symbol ○ indicates freezing points and x and ⊗ indicate transition points.

J. Am. Oil Chem. Soc., 5, 234 (1974)

Figure 2 - Typical Theoretic Heckel Plots[a]

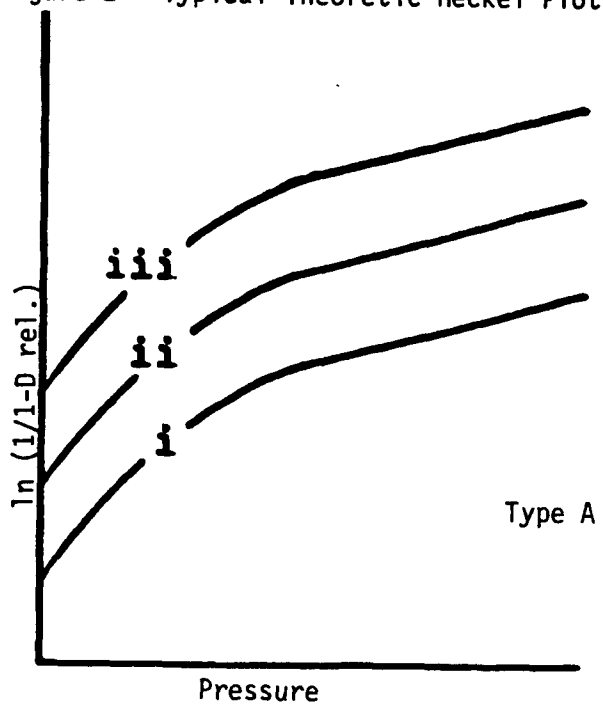

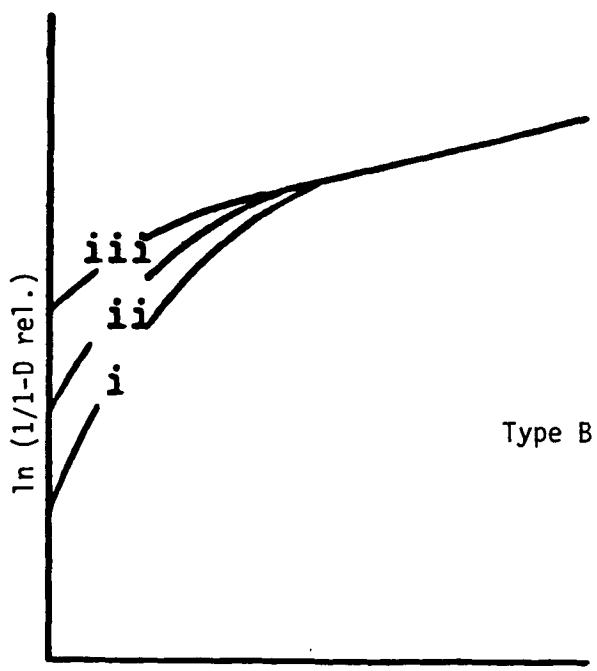

[a] Lines i, ii, iii refer to three different size fractions

Drug Dev. and Ind. Pharm., 8, 307 (1982)

Figure 3 - Cycle Plots, Theoretical Examples[a]

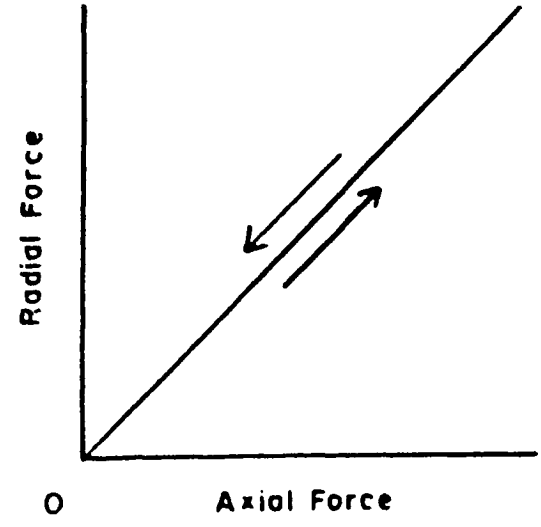

Elastic Body

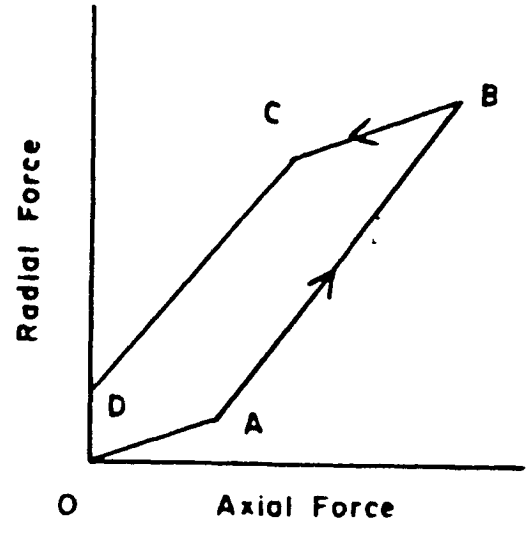

Constant Yield Stress

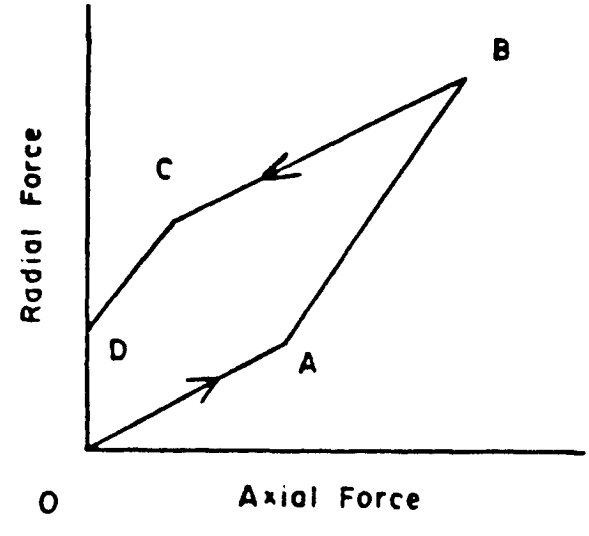

Mohr Body

[a] Points A, B, C, and D are described in detail within the text.

"Pharmaceutical Dosage Forms: Tablets," Vol. 2, Chapter 4, Marcel Dekker, New York, N.Y., 1981

Figure 4 - Tablet Stress Components[a] During Diametral Compression

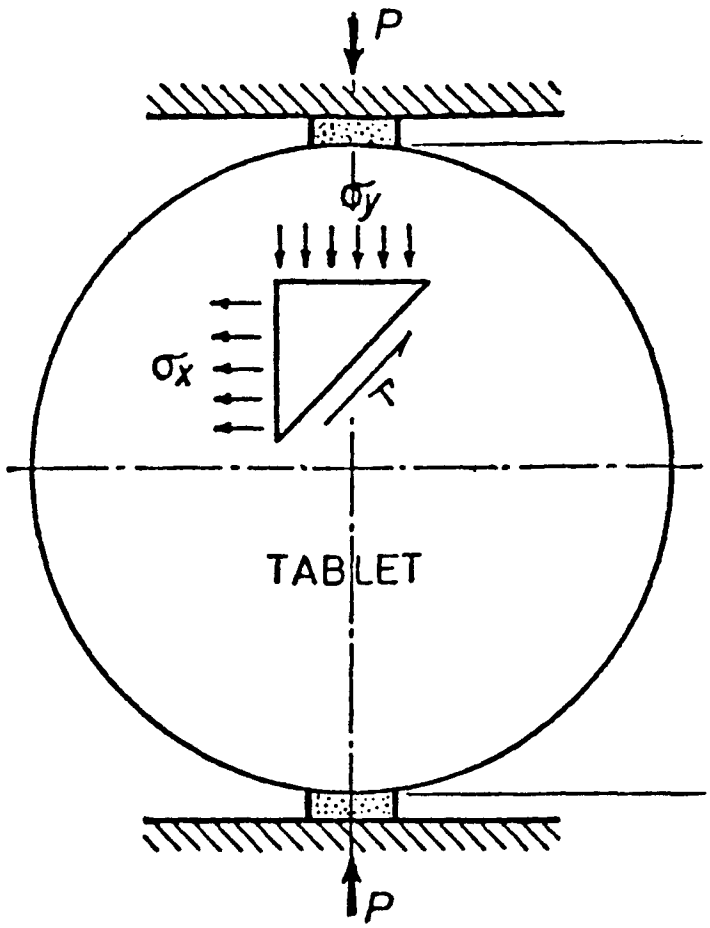

[a] P = force of compression, σy compressive stress, σx tensile strength, τ shear stress.

The Pharm. J., 205, 709 (1970)

Figure 5 - Typical Compact Fracture Patterns

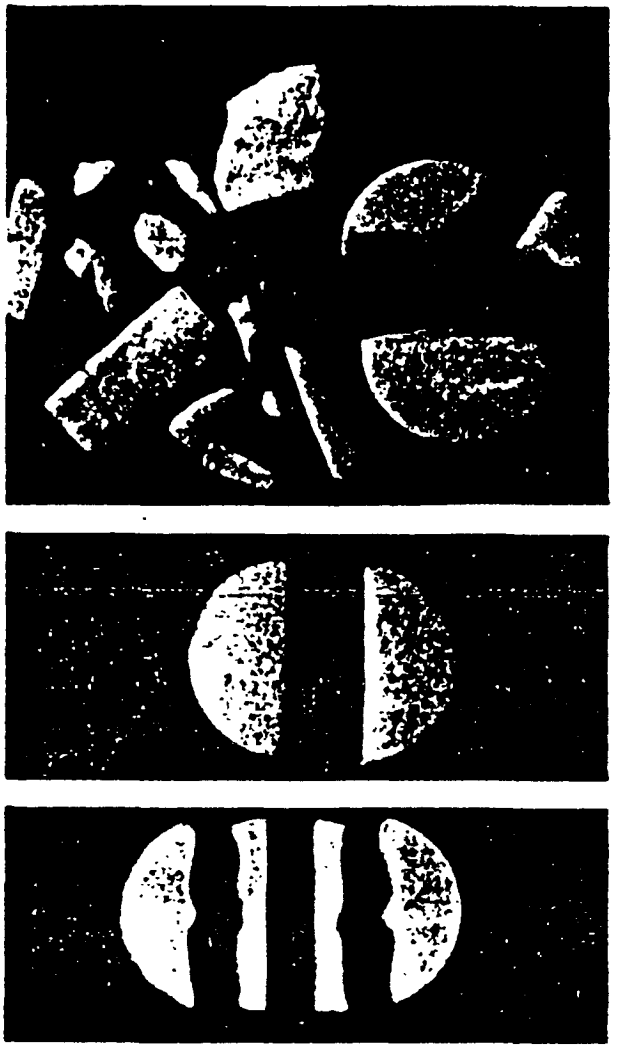

(Top) Shear-type failure
(Middle) Normal tensile failure
(Bottom) "Triple-cleft" failure

Figure 6 - Flow Diagram for Potassium Chloride Sizing

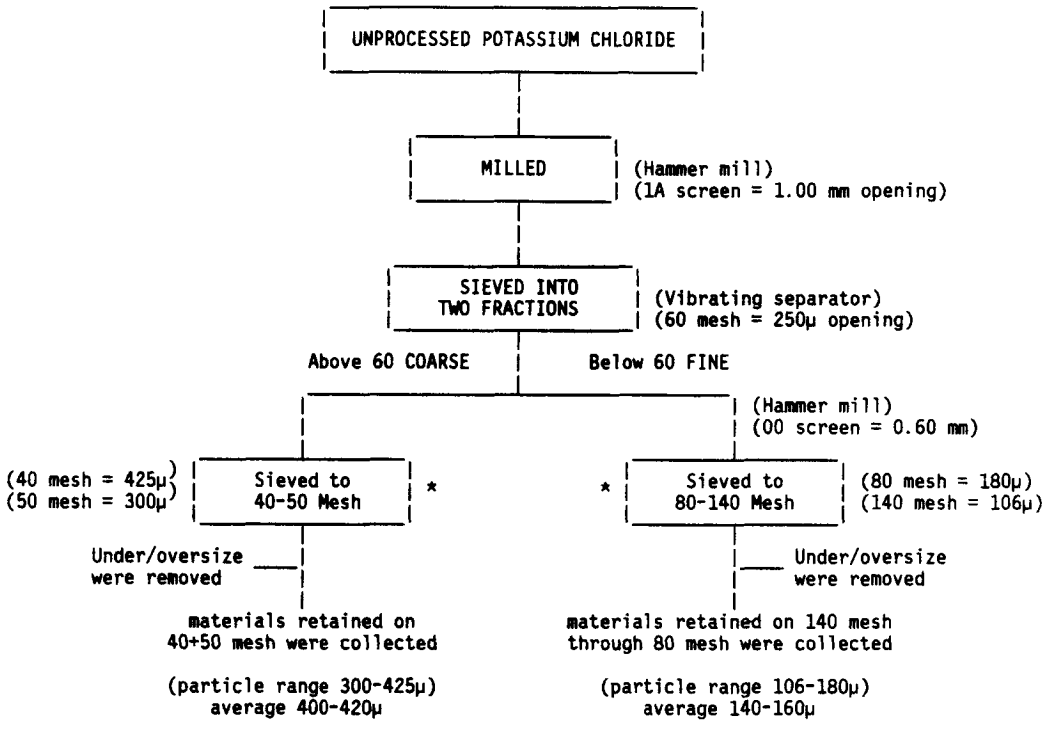

* 500 g of material in U.S. standard screens at intensity 7 for 20 minutes.

Figure 7 - Schematic Representation of the DSC Cell

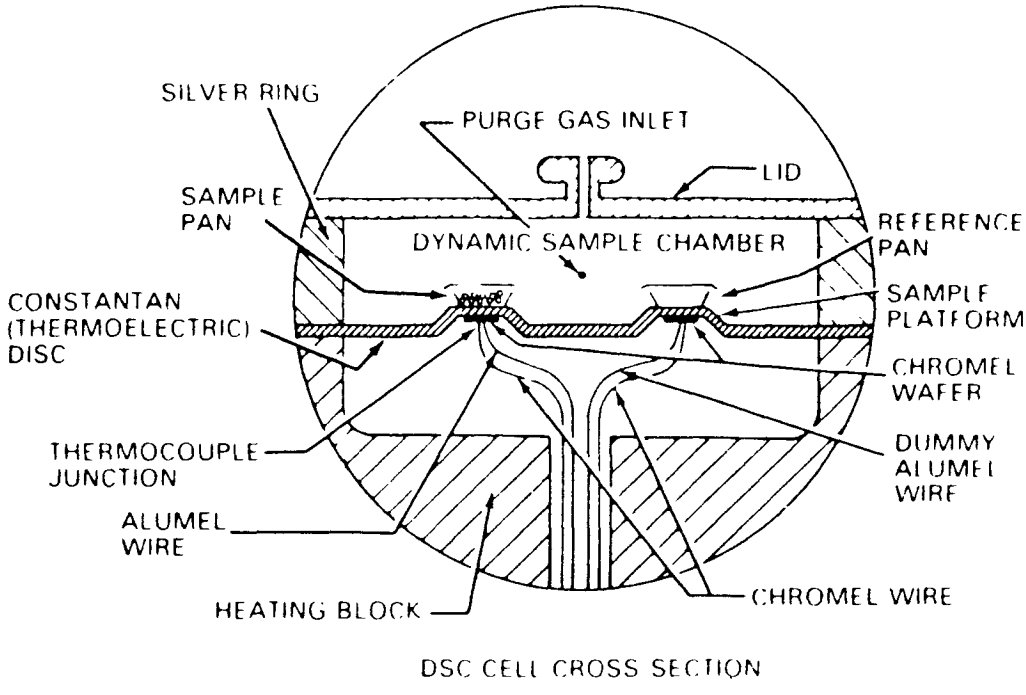

"Instruction Manual 910 DSC System," Revision B, DuPont Company, Anal. Instr. Div., Wilmington, Del., 1980

Figure 8 - Matrix Granulation Fusion Procedure

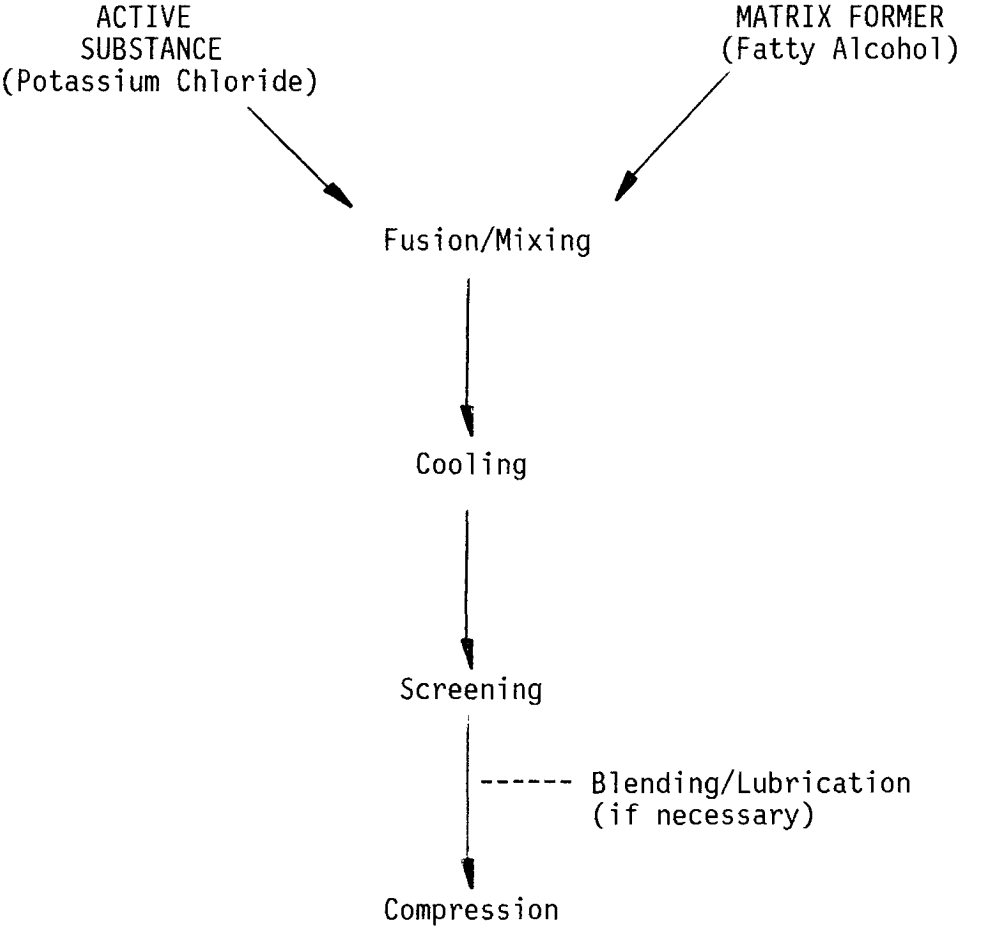

Figure 9 - Instron Punch Holding Fixture

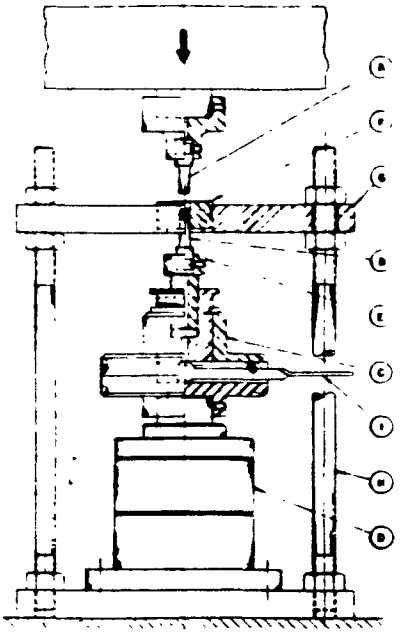

Fixture for compressing particulate solids
Key: A, upper punch; F, die; G, metal plate; B, lower punch, E, threaded bushing; C, flange holding lower punch, I, lifting lever; H, steel rods; D, compression cell.

J. Pharm. Sci., 55, 1128 (1966)

Figure 10 - Integrated Circuit Piezoelectric Transducer

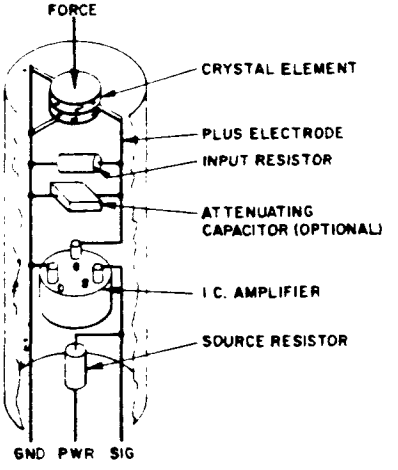

"General Guide to ICP Instrumentation,"
PCB Piezotronics, Depew, N.Y., 1971

Figure 11 - F-Press Configuration Showing Instrumented Components[a]

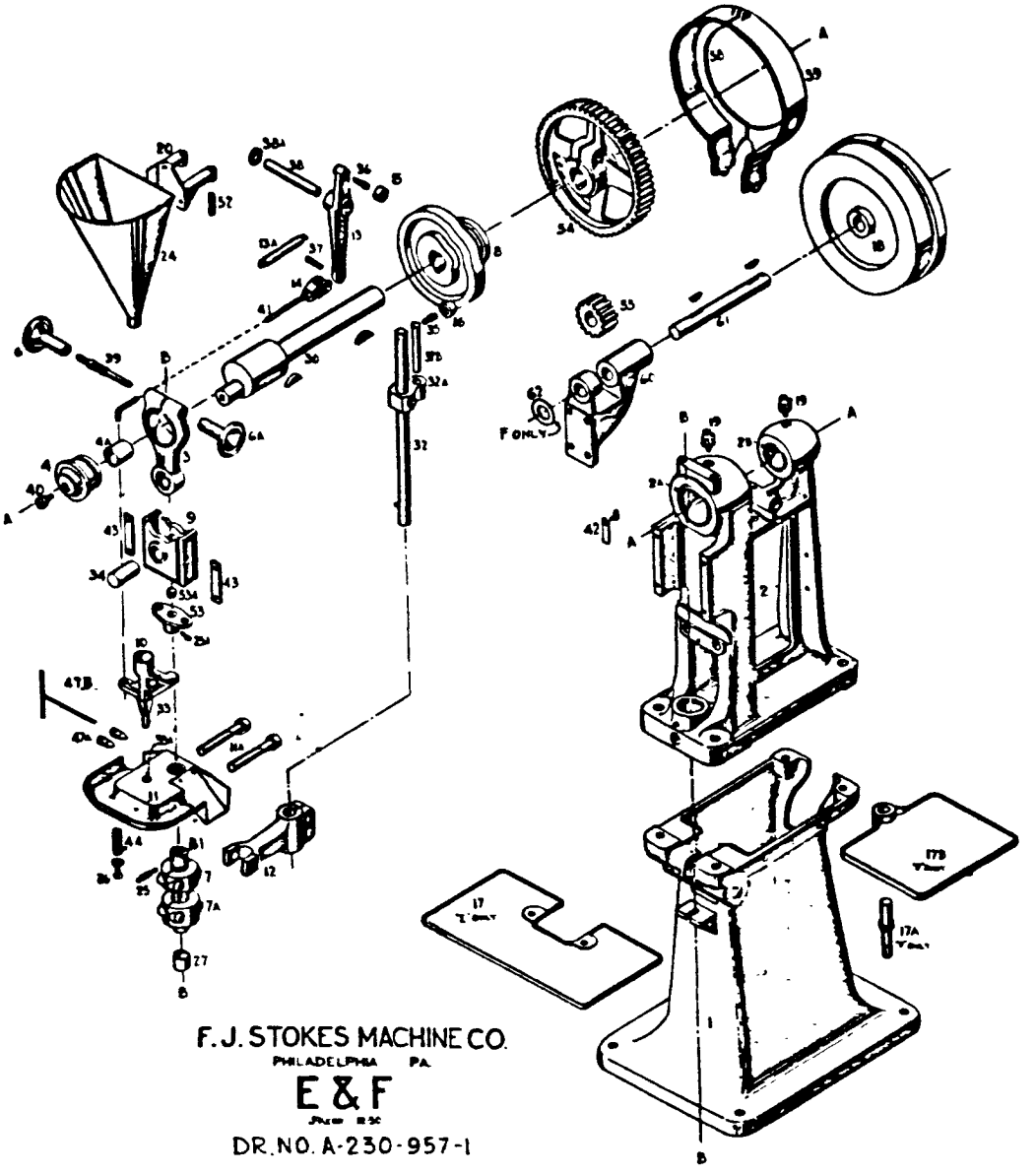

[a] #25A Upper Punch Holder
#31, 7, 7A Lower Punch Holder
#11 Die Table

Figure 12 - Upper Punch Holder, Transducer Location Drawing

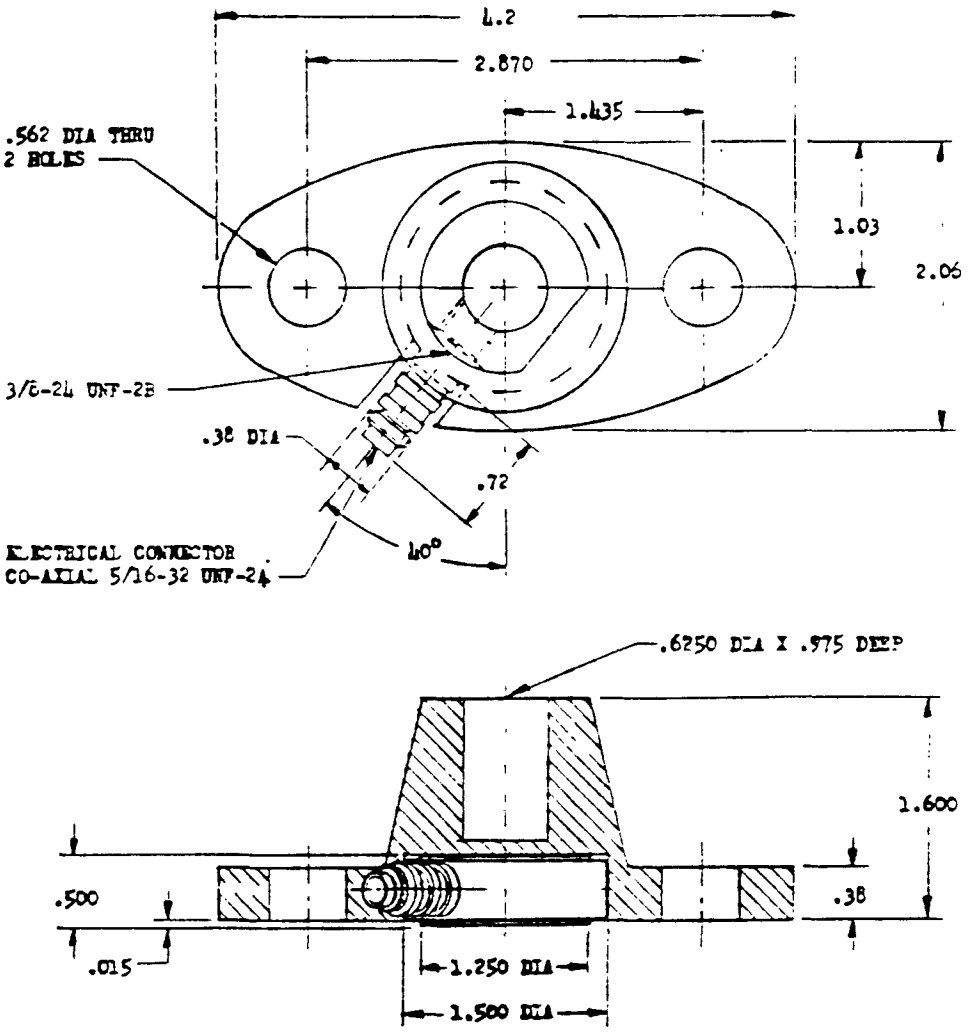

PCB Piezotronics, Depew, N.Y.
Drawing #200-9220-90
Dimensions are in inches.

Figure 13, Lower Punch Holder, Transducer Location Drawing

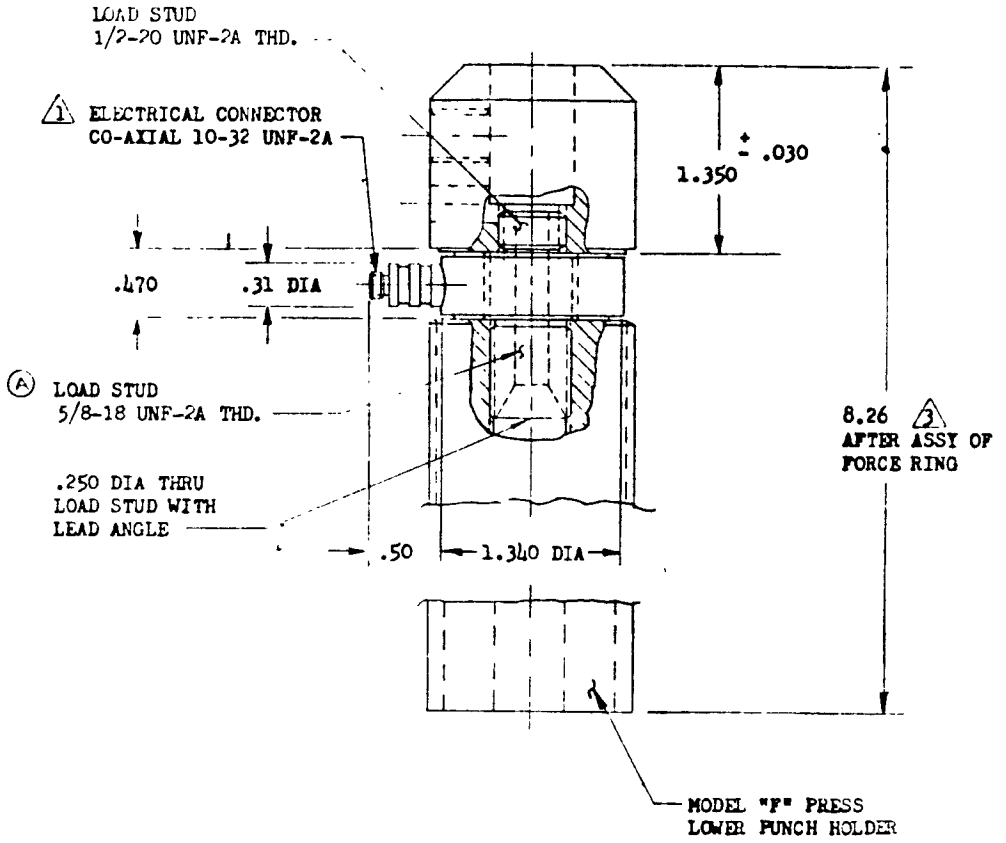

3. LENGTH OF PUNCH HOLDER WITH FORCE RING INSTALLED TO BE ± 0.050 FROM LENGTH AS RECEIVED.
2. LOWER PUNCH HOLDER SUPPLIED BY CUSTOMER AND MODIFIED BY PCB INC.
1. ORIENTATION OF ELECTRICAL CONNECTOR TO HORIZONTAL TAPPED HOLE ± 3°.

PCB Piezotronics, Depew, N.Y.
Drawing #204-9020-90
Dimensions are in inches.

Figure 14 - Instrumented Die, Transducer Location Drawing

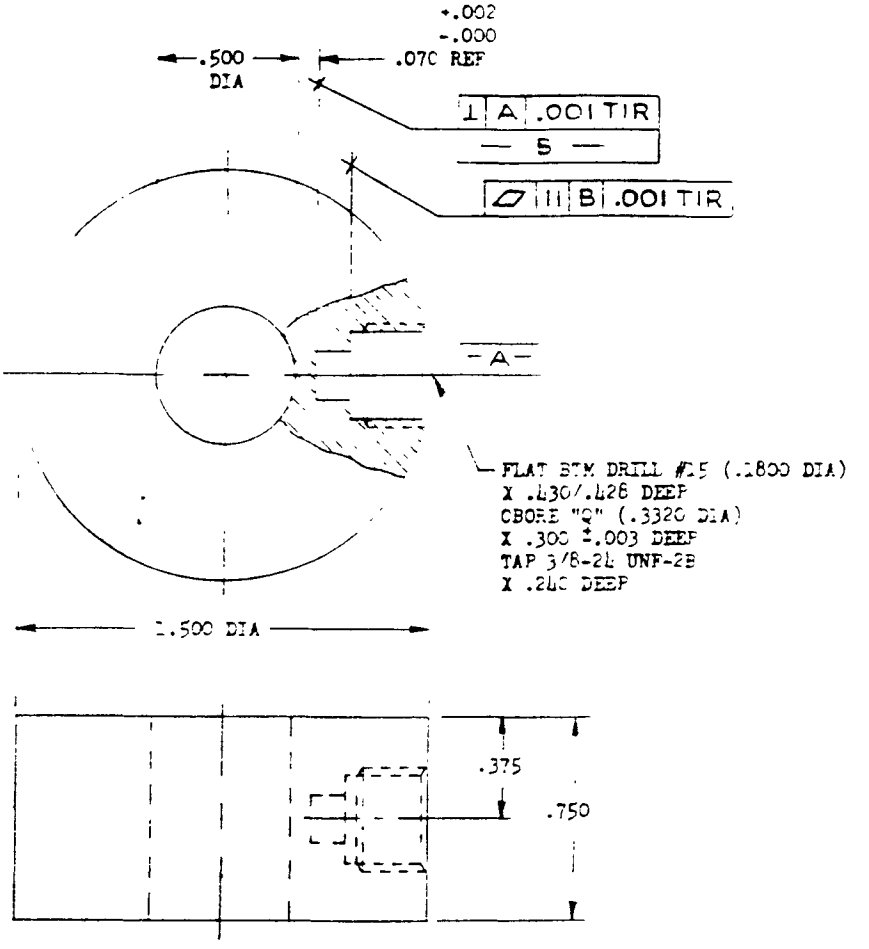

PROPOSED MACHINING OF DIE TO ACCEPT MODEL 108M11 PRESSURE TRANSDUCER.

PCB Piezotronics, Depew, N.Y.
Drawing #108-9110-61
Dimensions are in inches.

Figure 15 - Die Table Modifications

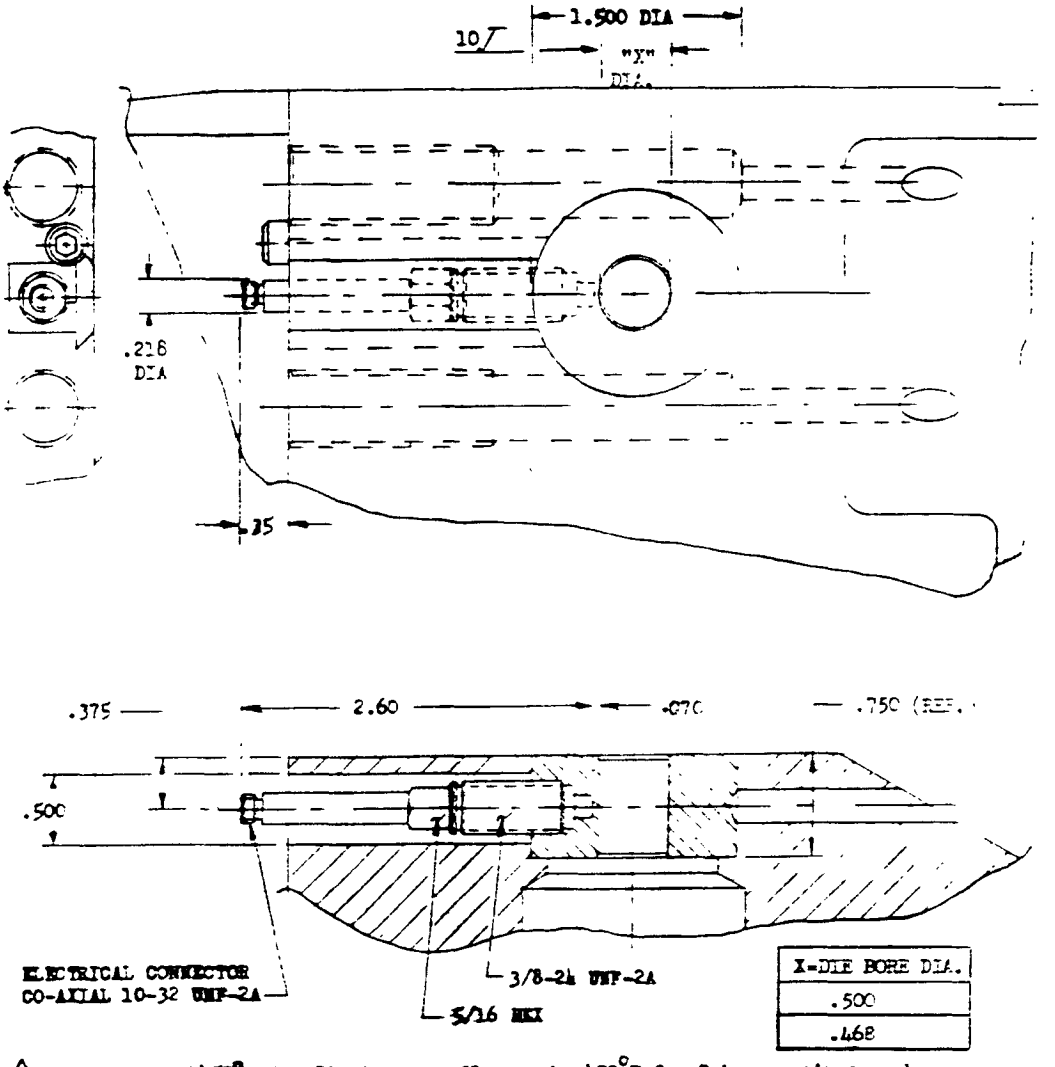

PCB Piezotronics, Depew, N.Y.
Drawing #108-9110-90
Dimensions are in inches.

Figure 16 - Upper Punch Transducer Calibration

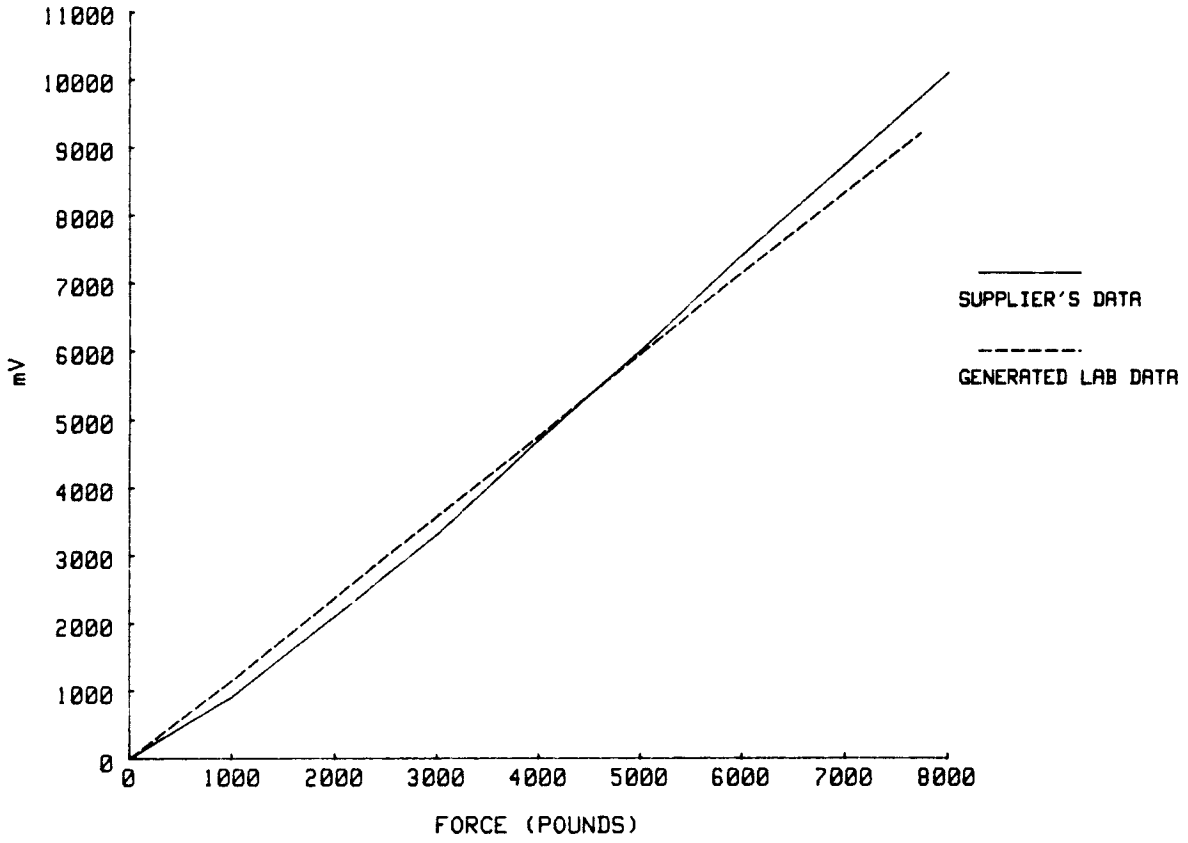

Figure 17 - Lower Punch Transducer Calibration

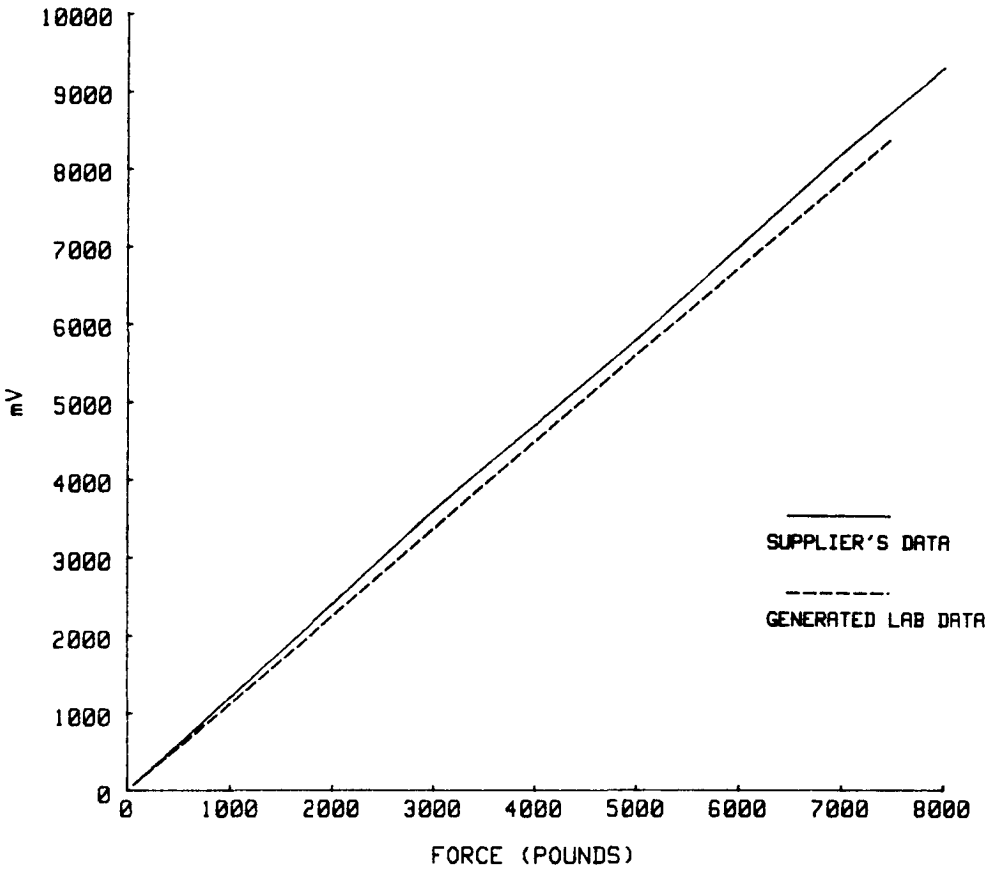

Figure 18 - Die Wall Transducer Calibration

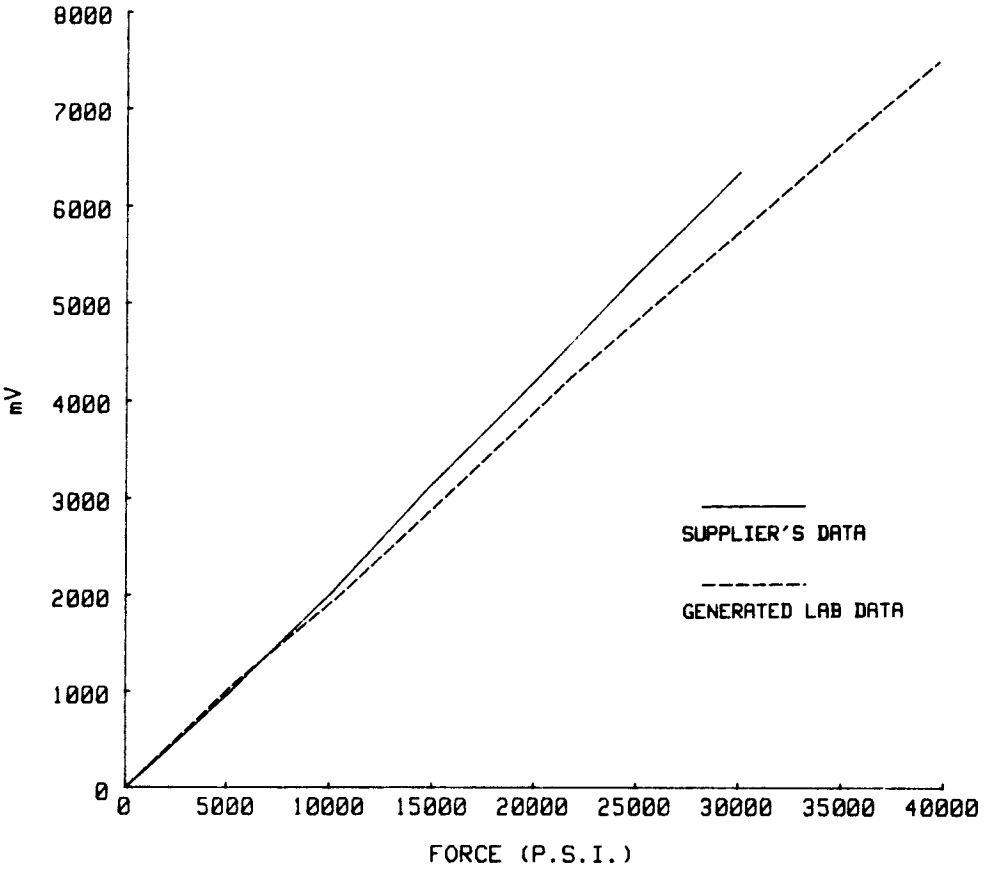

Figure 19 - Mechanical Tablet Ratings as a Function of Instron Results

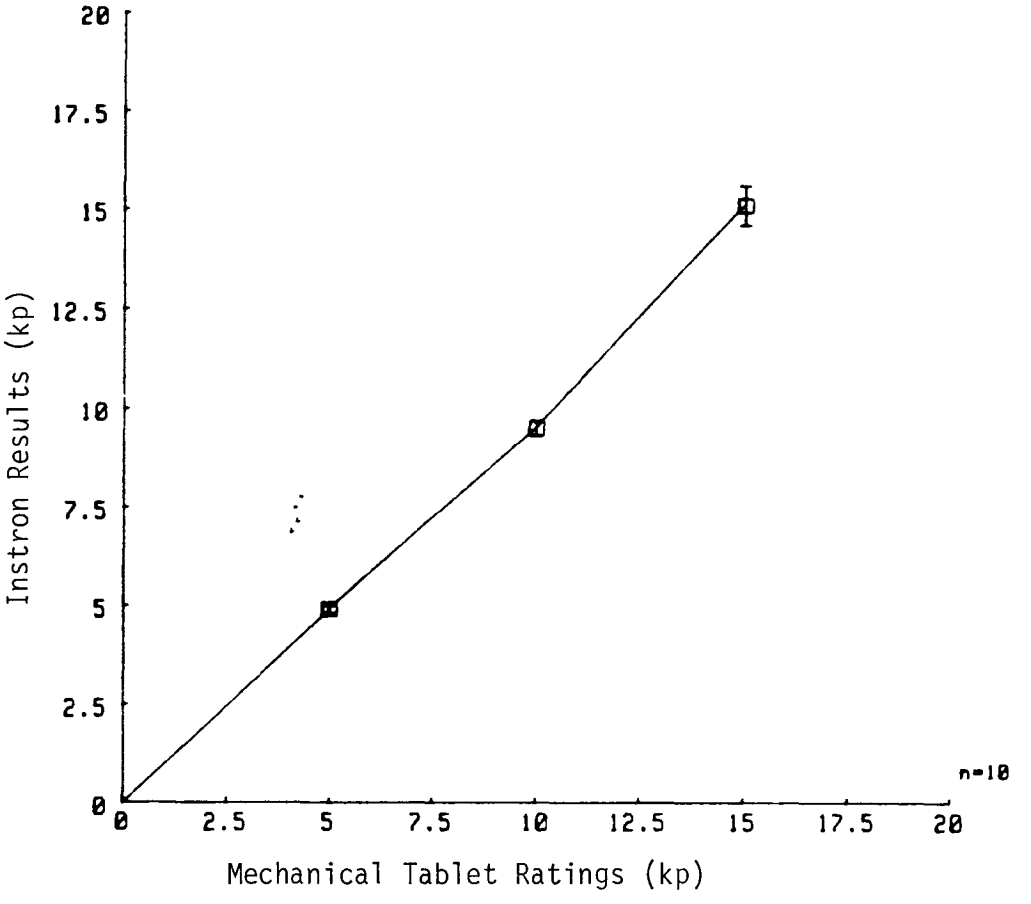

Figure 20 - Hardness Data, Conversion Chart

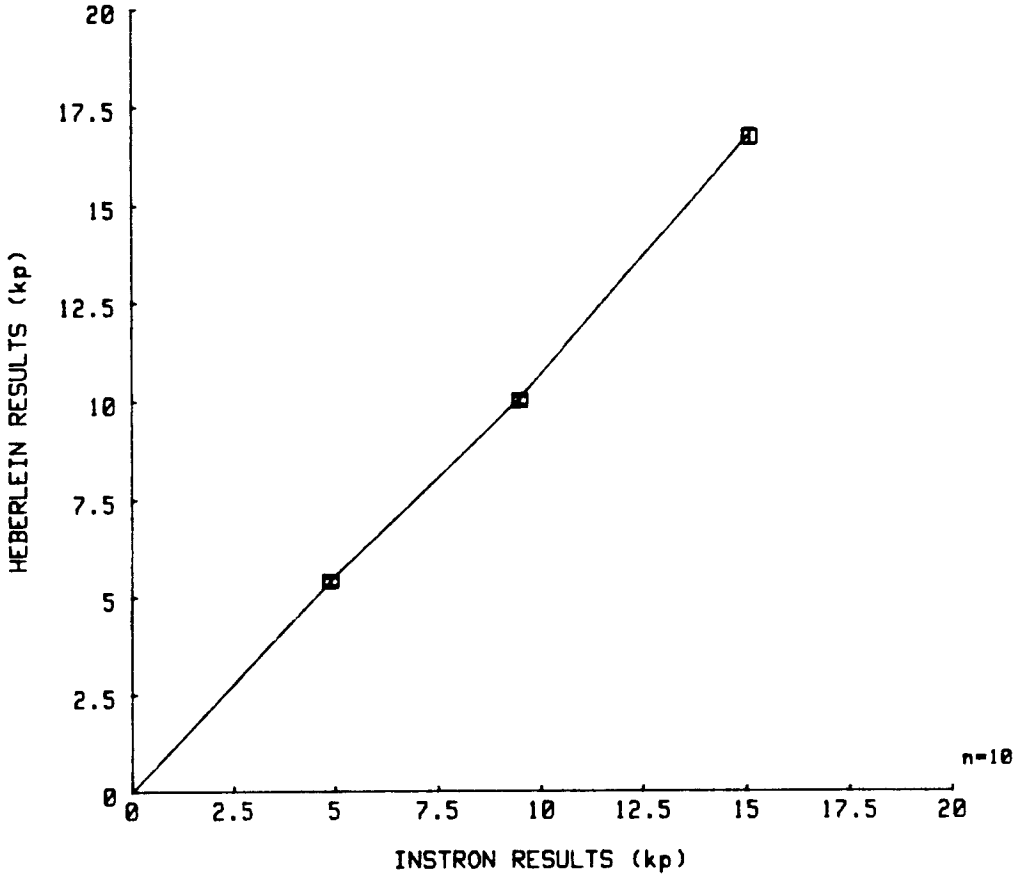

Figure 21 - Thermal Profiles for Cetostearyl Alcohol, Lot K4991

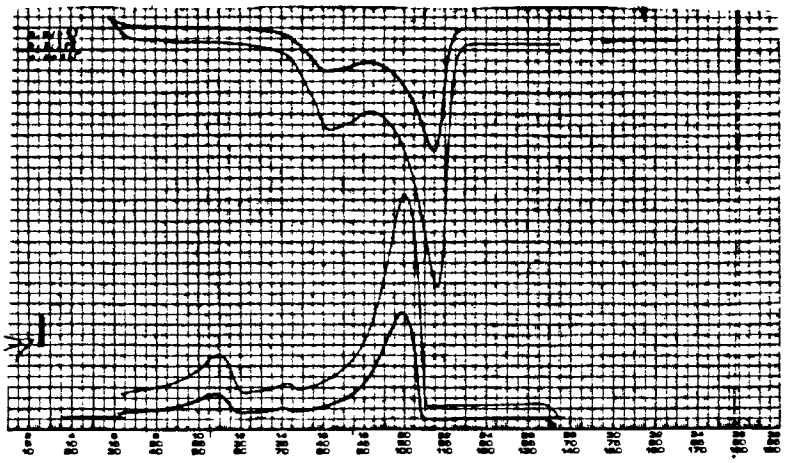

Heating °C
34.0 (0.6)*
46.4 (0.7)

Cooling °C
50.3 (0.9)
37.1 (0.5)
29.0 (0.7)

First Cycle

Sample:	Cetostearyl Alcohol, K4991
Weight:	3.35 mg
Heating Rate:	5°C/min
Range (y):	5, 10 mV/cm X axis: 2.5°C/cm

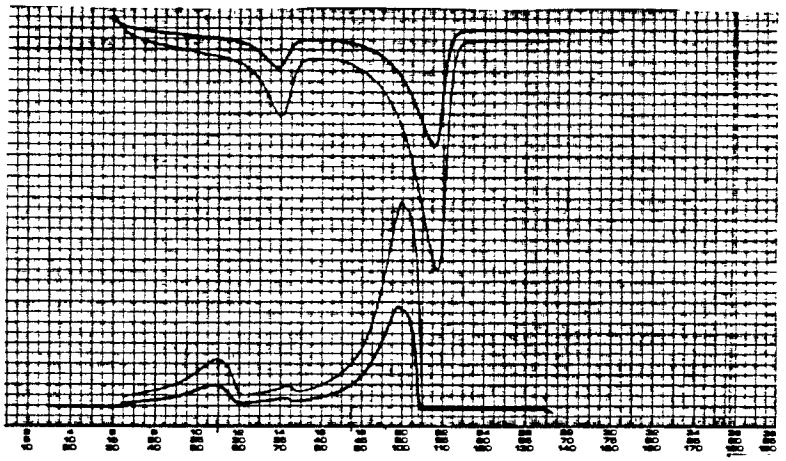

Heating °C
29.2 (0.4)
46.5 (0.8)

Cooling °C
50.3 (0.9)
37.6 (0.7)
29.6 (0.6)

Second Cycle

* n = 5, (std. dev.)

Figure 22 - Thermal Profiles for Cetostearyl Alcohol, Lot L4593

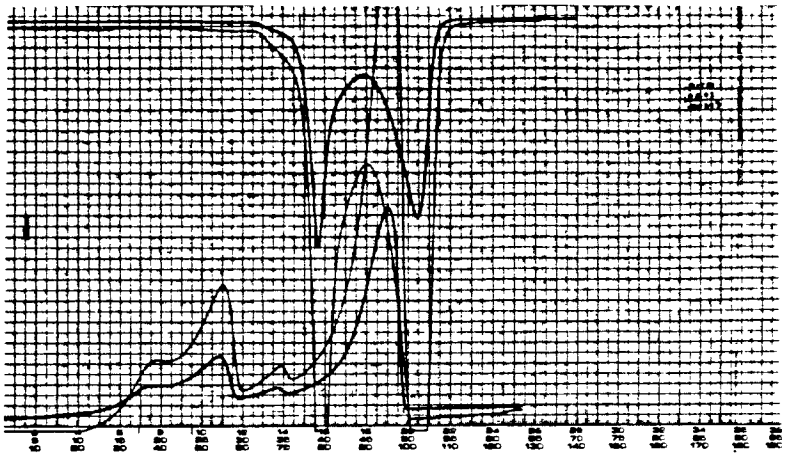

First Cycle

Heating °C
37.4 (0.3)*
45.6 (0.5)

Cooling °C
50.3 (0.5)
38.3 (0.3)
31.6 (0.4)

Sample: Cetostearyl Alcohol, L4593
Weight: 2.97 mg
Heating Rate: 5°C/min
Range (y): 5, 10 mV/cm X axis: 2.5°C/cm

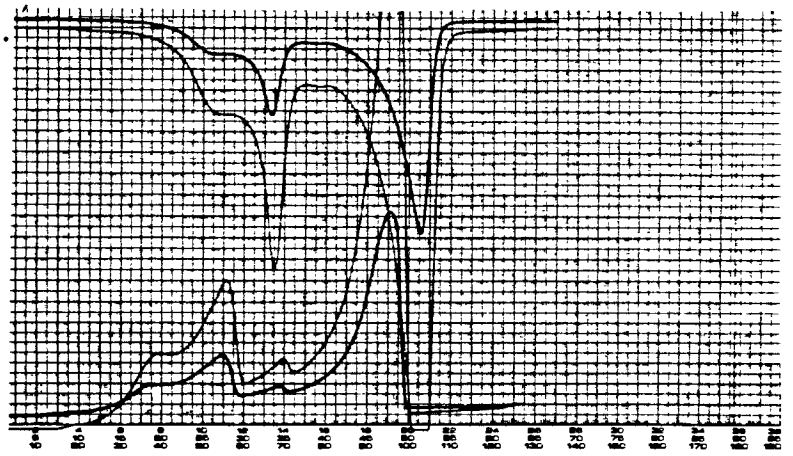

Second Cycle

Heating °C
30.5 (0.6)
46.6 (0.7)

Cooling °C
50.1 (0.6)
37.6 (0.5)
30.4 (0.7)

* n = 5, (std. dev.)

Figure 23 - Thermal Profiles, Cetostearyl Alcohol Literature Data

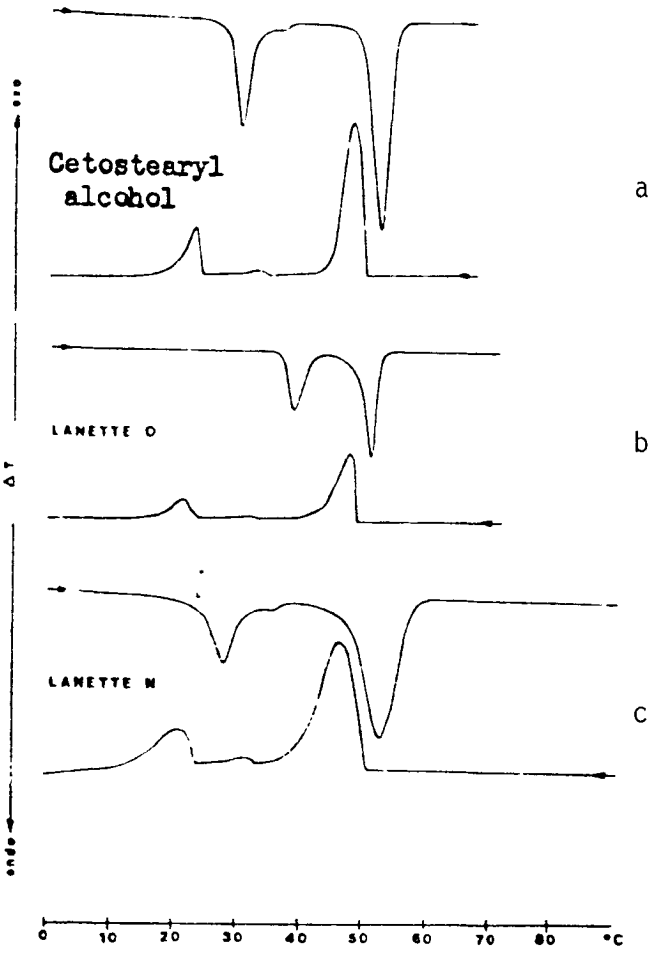

DSC Curves representing the following:

a) High purity cetostearyl alcohol
b) Commercial quality cetostearyl alcohol (Lanette O)
c) Emulsifying cetostearyl alcohol (Lanette N)

Pharm. Ind., 41, 380 (1979)

Figure 24 - Thermal Profiles for Tetradecanol, High Purity

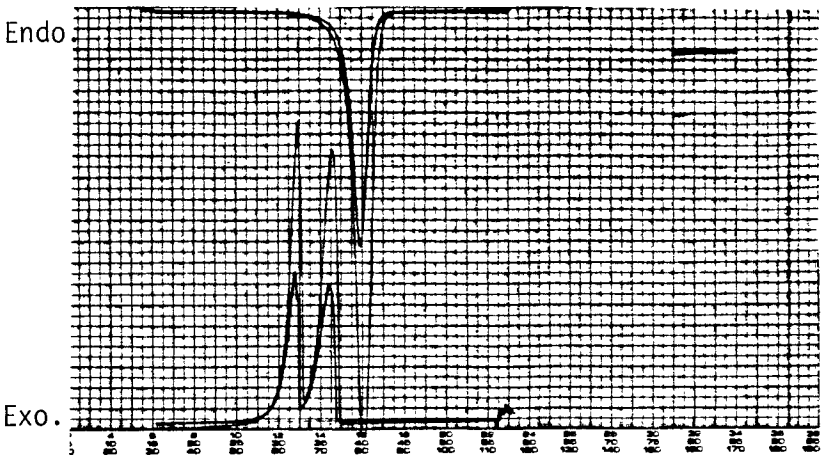

First Cycle

Heating °C
38.0 (0.4)*

Cooling °C
36.8 (0.2)
32.5 (0.3)

Sample: Tetradecanol, A1401
Weight: 2.64 mg
Heating Rate: 5°C/min
Range (y) 5, 10 mV/cm X axis: 2.5°C/cm

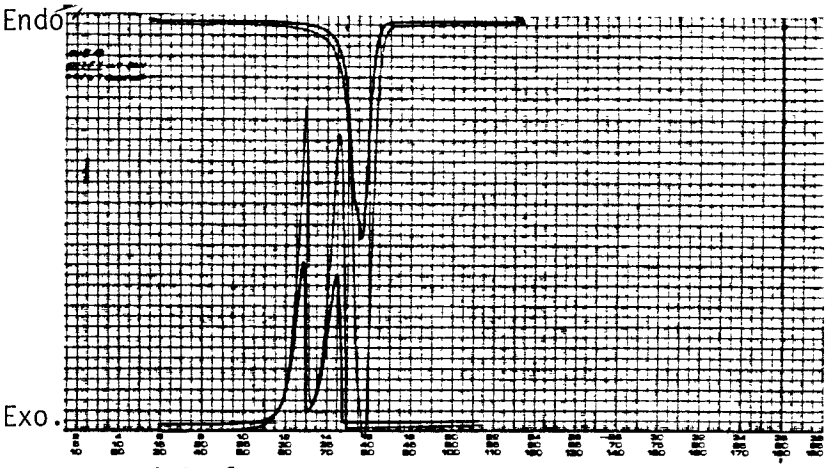

Second Cycle

Heating °C
36.5 (0.3)

Cooling °C
37.0 (0.2)
32.5 (0.3)

* n = 5, (std. dev.)

Figure 25 - Thermal Profiles for Tetradecanol, Commercial Purity

Endo.

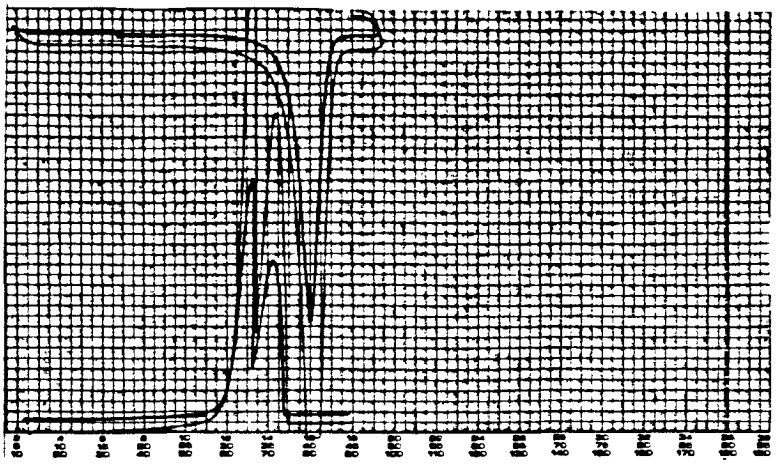

Exo.

First Cycle

Heating °C
37.5 (0.3)*

Cooling °C
36.8 (0.2)
33.0 (0.4)

Sample: Tetradecanol, P&B TO3360
Weight: 2.57 mg
Heating Rate: 5°C/min
Range (y): 5, 10 mV/cm X axis: 2.5°C

Endo.

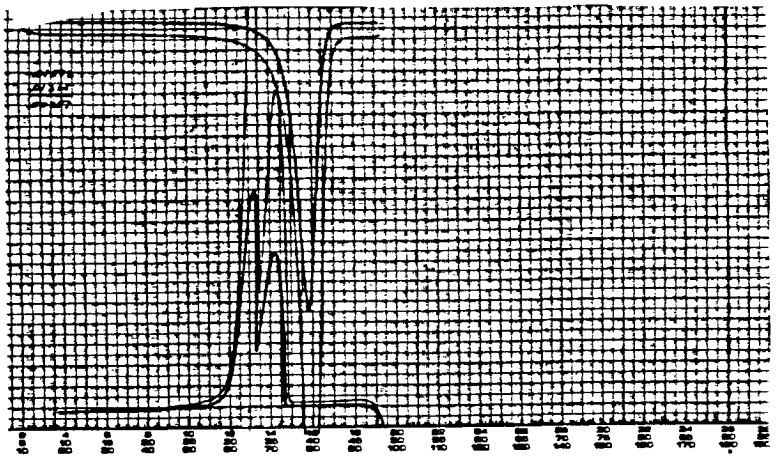

Exo.

Second Cycle

Heating °C
37.0 (0.1)

Cooling °C
36.8 (0.3)
33.3 (0.2)

* n = 5, (std. dev.)

Figure 26 - Thermal Profiles for Hexadecanol, High Purity

Endo.

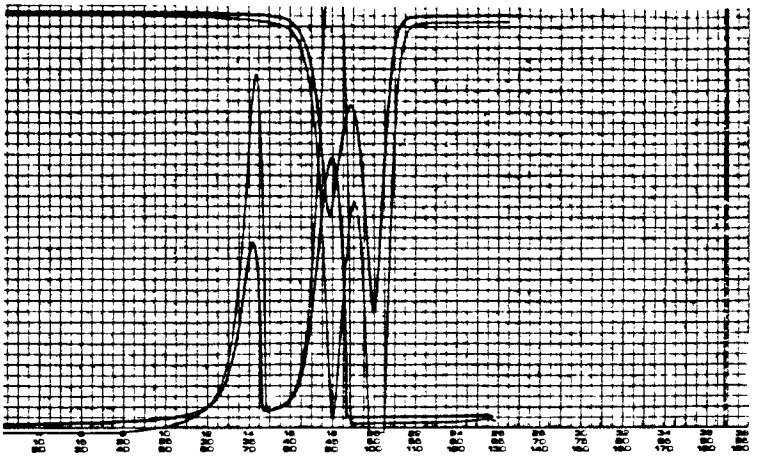

Exo.

First Cycle

Heating °C
44.2 (0.8)*
48.7 (0.8)

Cooling °C
48.4 (0.7)
42.1 (0.8)

Sample: Hexadecanol, E290H
Weight: 4.47 mg
Heating Rate: 5°C/min
Range (y): 5, 10 mV/cm X axis: 2.5°C/cm

Endo.

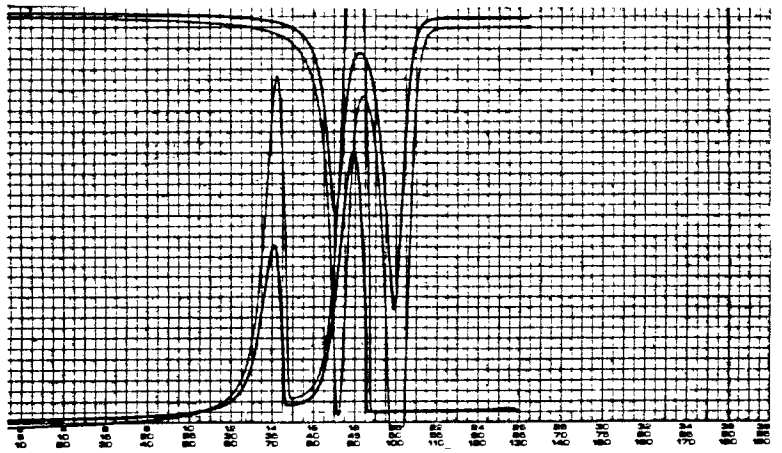

Exo.

Second Cycle

Heating °C
43.8 (0.6)
47.4 (0.7)

Cooling °C
47.6 (0.5)
41.8 (0.7)

* n = 5, (std. dev.)

Figure 27 - Thermal Profiles for Hexadecanol, Commercial Purity

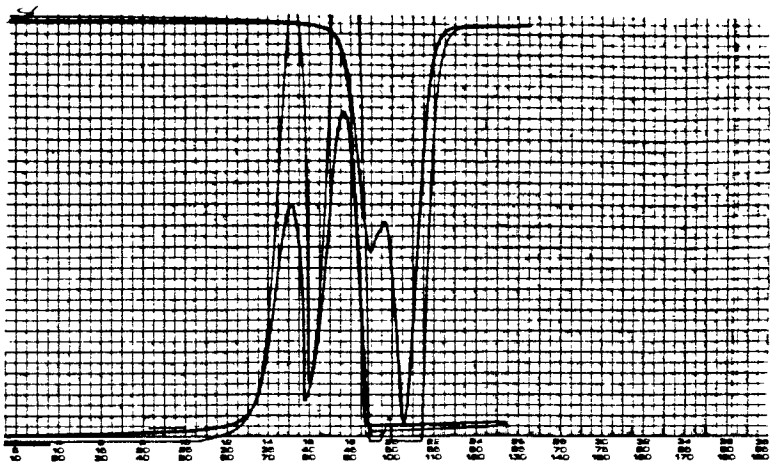

First Cycle

Heating °C
44.9 (0.9)*
49.1 (0.6)

Cooling °C
48.6 (0.8)
41.5 (0.6)

Sample: Hexadecanol, L2475
Weight: 6.37 mg
Heating Rate: 5°C/min
Range (y): 5, 10 mV/cm X axis: 2.5°C

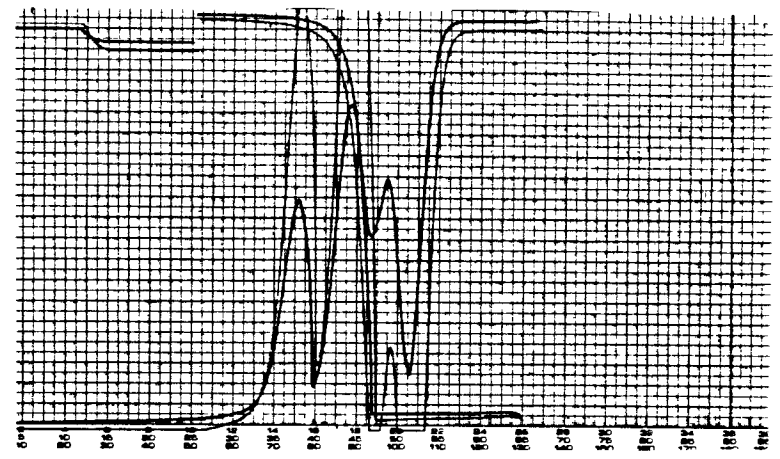

Second Cycle

Heating °C
44.6 (0.6)
48.7 (0.7)

Cooling °C
48.2 (0.5)
40.8 (0.6)

* n = 5, (std. dev.)

Figure 28 - Thermal Profiles for Octadecanol, High Purity

Endo.

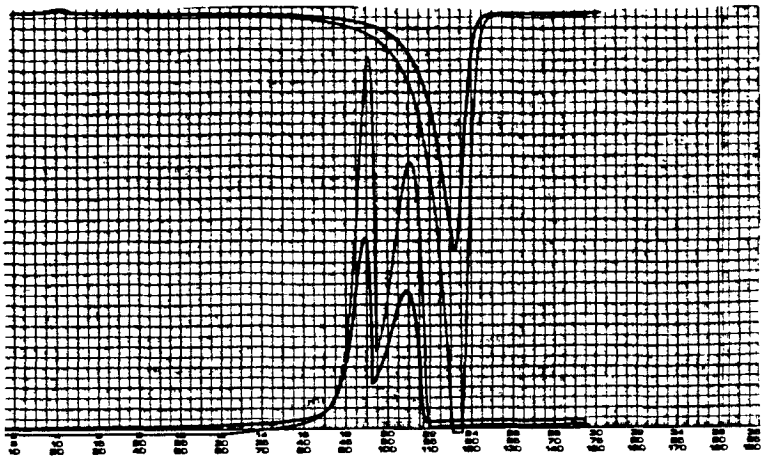

Exo.

First Cycle

Heating °C
57.5 (0.4)*

Cooling °C
56.3 (0.2)
51.1 (0.5)

Sample: Octadecanol, LO20A
Weight: 3.28 mg
Heating Rate: 5°C/min
Range (y): 5, 10 mV/cm X axis 2.5°C/cm

Endo.

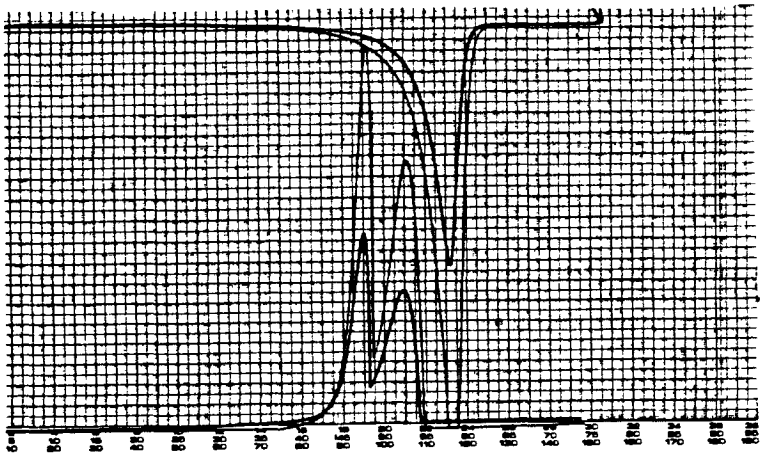

Exo.

Second cycle

Heating °C
56.8 (0.5)

Cooling °C
56.1 (0.3)
51.4 (0.3)

* n = 5, (std. dev.)

Figure 29 - Thermal Profiles for Octadecanol, Commercial Purity

Endo.

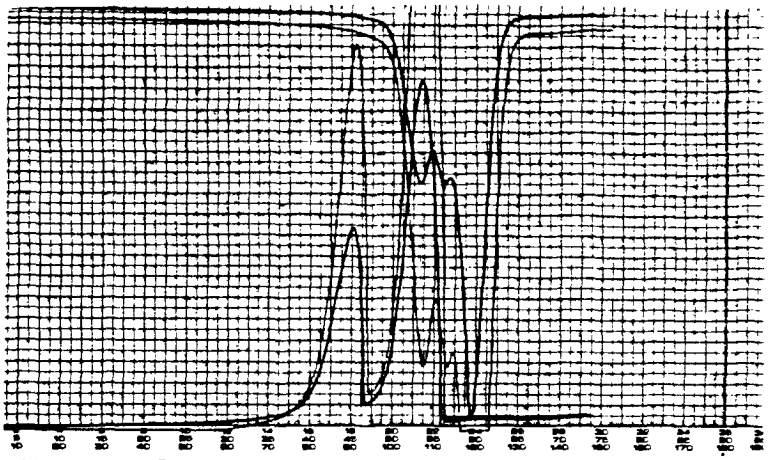

Exo.

First Cycle

Heating °C
51.3 (0.3)*
52.6 (0.5)
58.5 (0.4)

Cooling °C
57.3 (0.4)
47.6 (0.4)

Sample: Octadecanol, 000140
Weight: 6.11 mg
Heating Rate: 5°C/min
Range (y): .5, 10 mV/cm X axis: 2.5°C/cm

Endo.

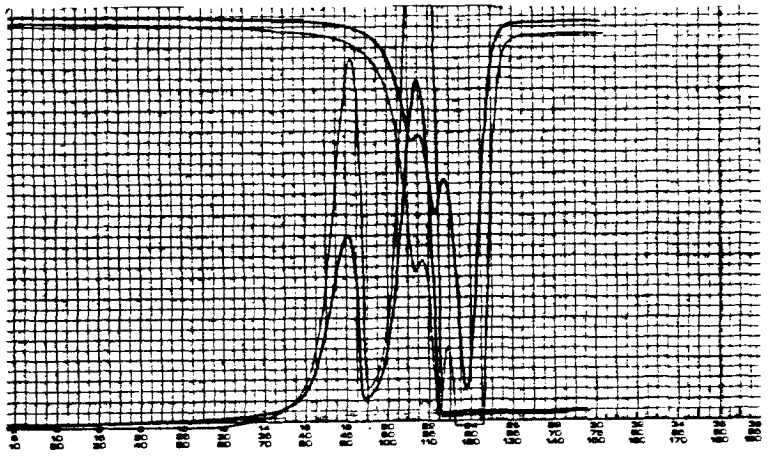

Exo.

Second Cycle

Heating °C
49.6 (0.5)
52.5 (0.4)
57.3 (0.6)

Cooling °C
56.5 (0.4)
47.4 (0.7)

n = 5 std dev

* n = 5, (std. dev.)

Figure 30 - Thermal Profiles for Octadecanol, Commercial Purity

Endo.

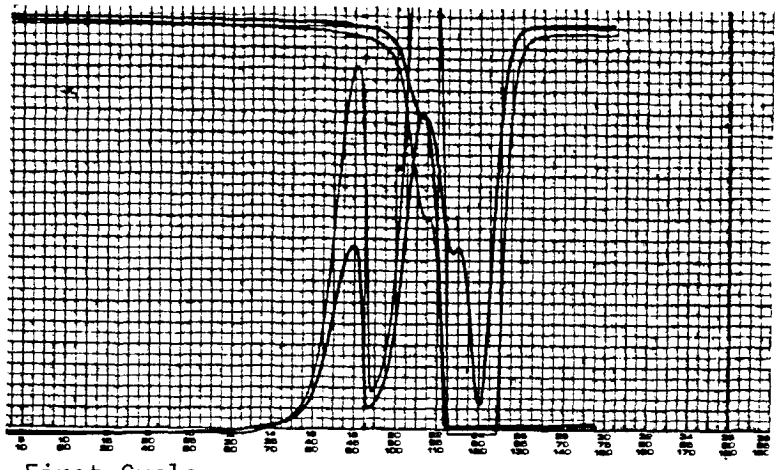

Exo.

First Cycle

Heating °C
51.0 (0.4)*
54.8 (0.2)
57.8 (0.4)

Cooling °C
56.5 (0.4)
47.4 (0.3)

Sample: Octadecanol, M488
Weight: 6.56 mg
Heating Rate: 5°C/min
Range (y): 5, 10 mV/cm X axis: 2.5°C/cm

Endo.

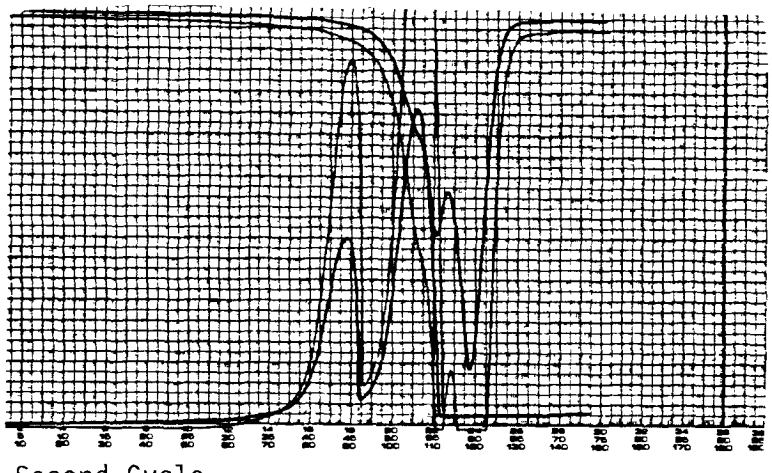

Exo.

Second Cycle

Heating °C
48.5 (0.5)
52.5 (0.3)
56.3 (0.2)

Cooling °C
56.1 (0.3)
47.2 (0.4)

* n = 5, (std. dev.)

Figure 31 - Phase Diagram of Hexadecanol and Octadecanol[a]

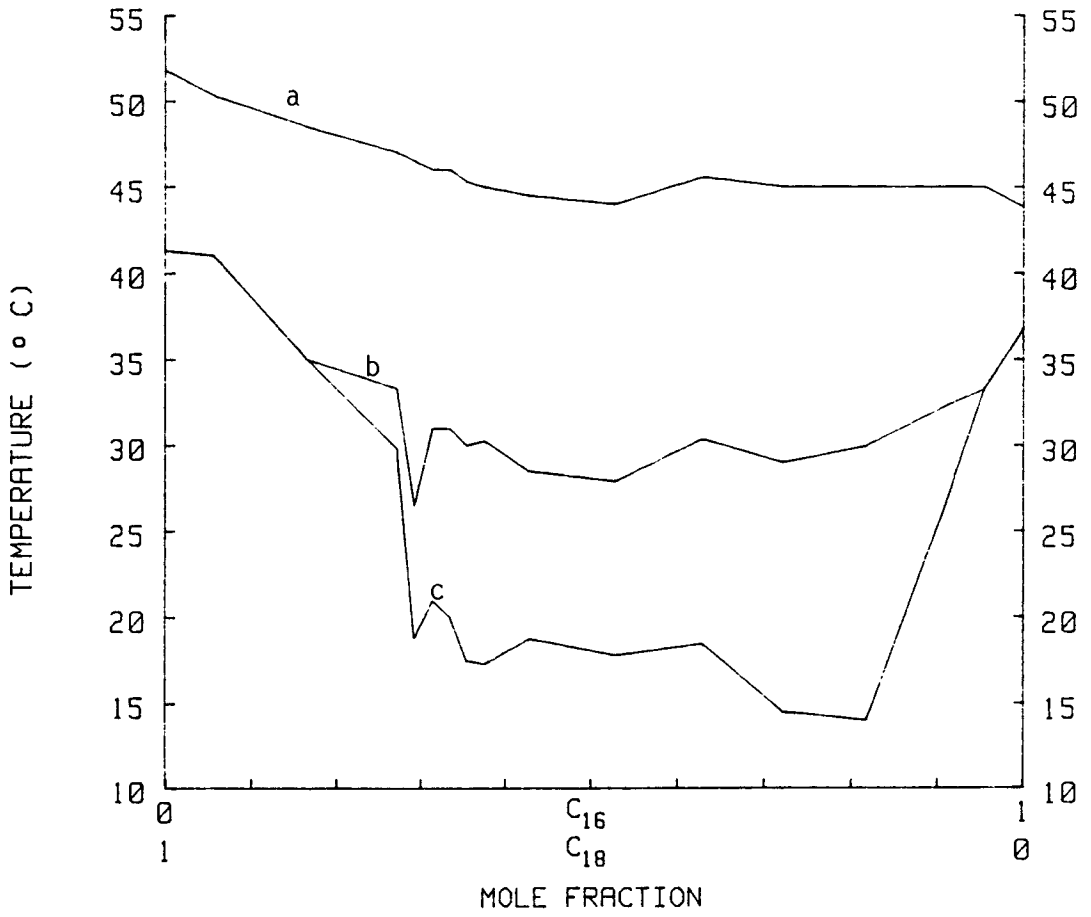

[a] Line a represents the freezing points and b and c indicate solid transition points.

Figure 32 - Energy of Freezing (ΔH_1) as a Function of Compact Strength

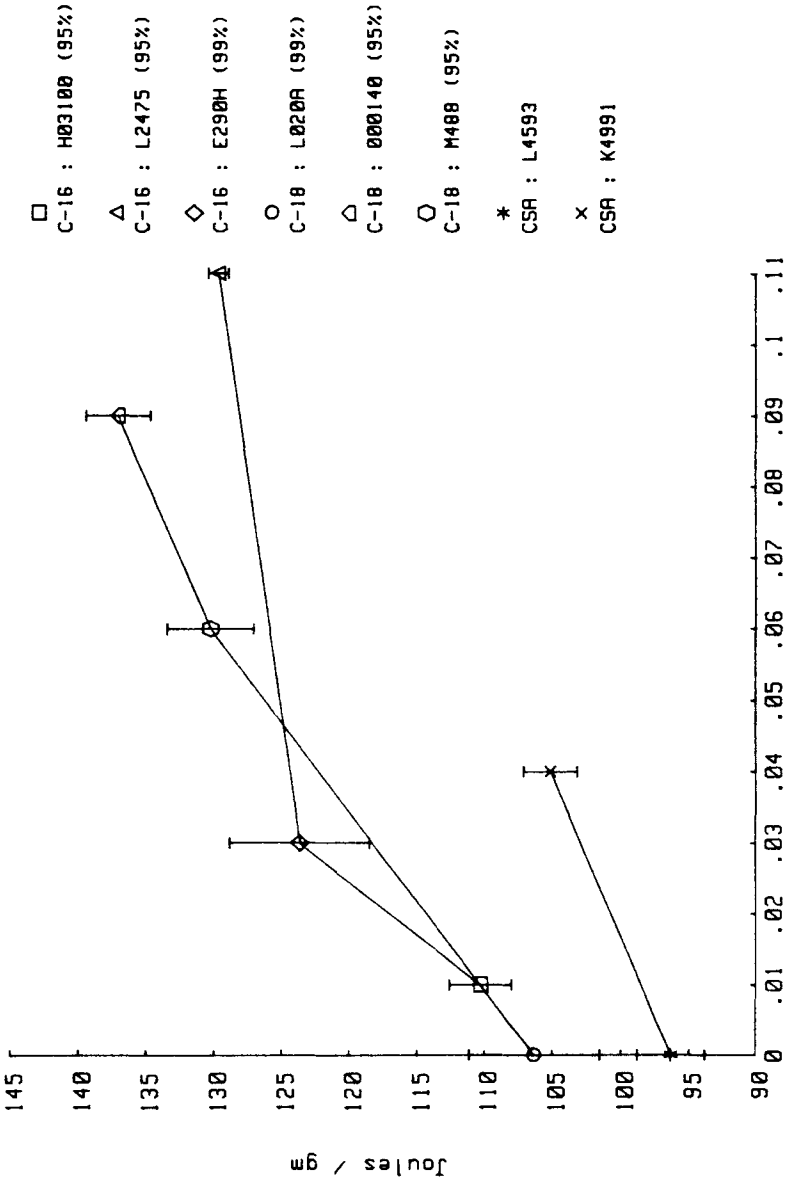

Page

230

is missing

Figure 34 - Aging Effects on Thermal Properties of Cetostearyl Alcohol, Lot L4593

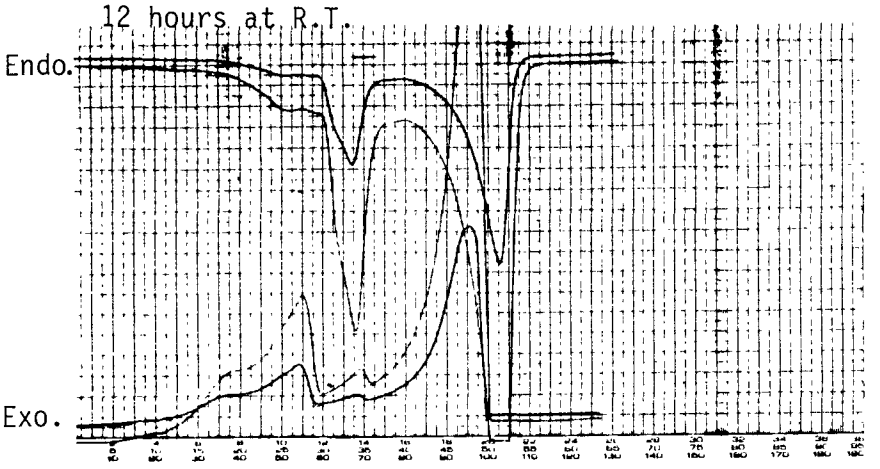

Sample: Cetostearyl Alcohol, L4593
Weight: 2.97 mg
Heating Rate: 5°C/min
Range (y): 5, 10 mV/cm X axis: 2.5°C/cm

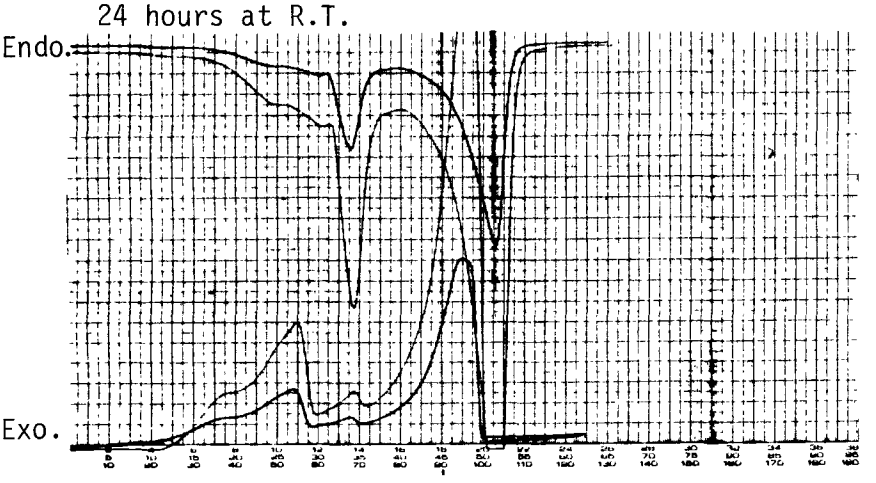

Figure 35 - Aging Effects on Thermal Properties of Cetostearyl Alcohol, Lot L4593

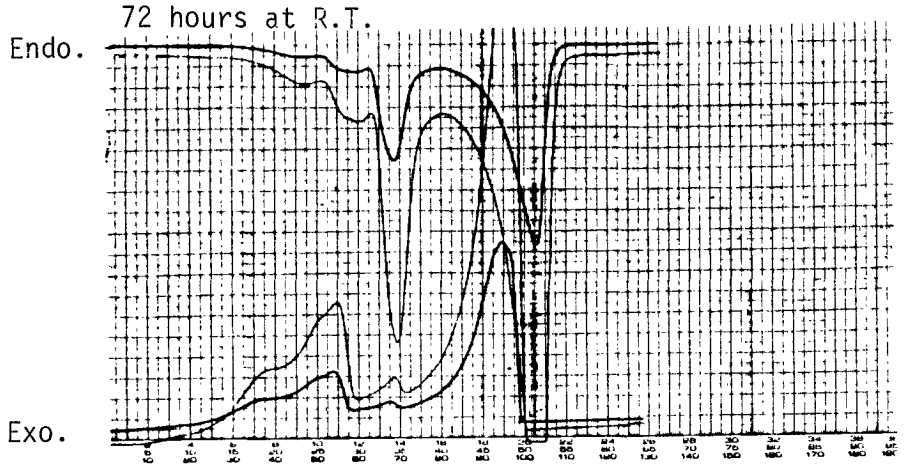

Sample: Cetostearyl Alcohol, L4593
Weight: 2.97 mg
Heating Rate: 5°C/min
Range (y): 5, 10 mV/cm X axis: 2.5°C/cm

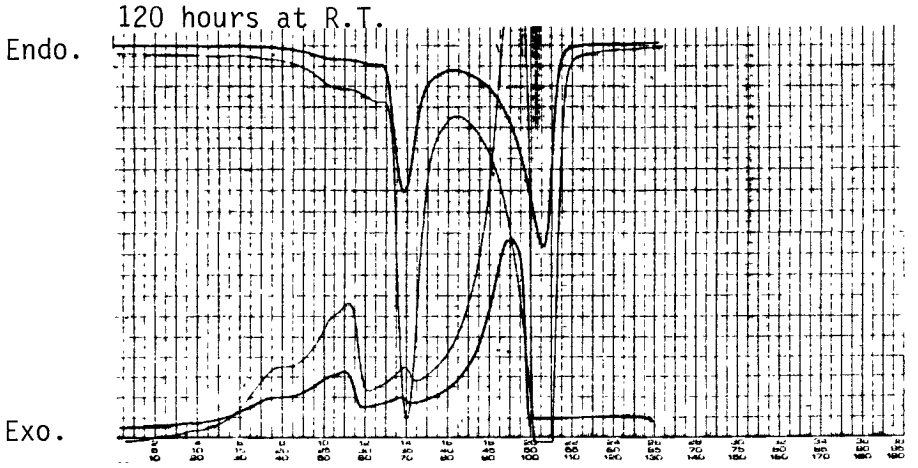

Figure 36 - Aging Effects on Thermal Properties of Cetostearyl Alcohol, Lot K4991

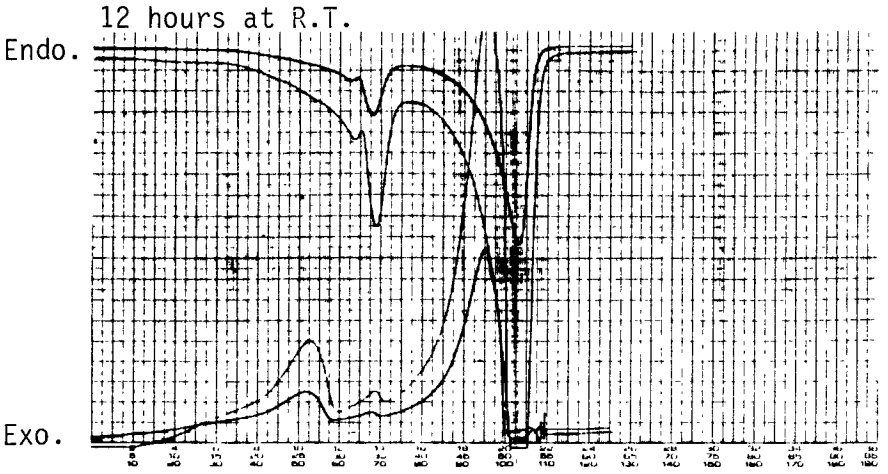

Sample: Cetostearyl Alcohol, K4991
Weight: 2.79 mg
Heating Rate: 5°C/min
Range (y): 5, 10 mV/cm X axis: 2.5°C/cm

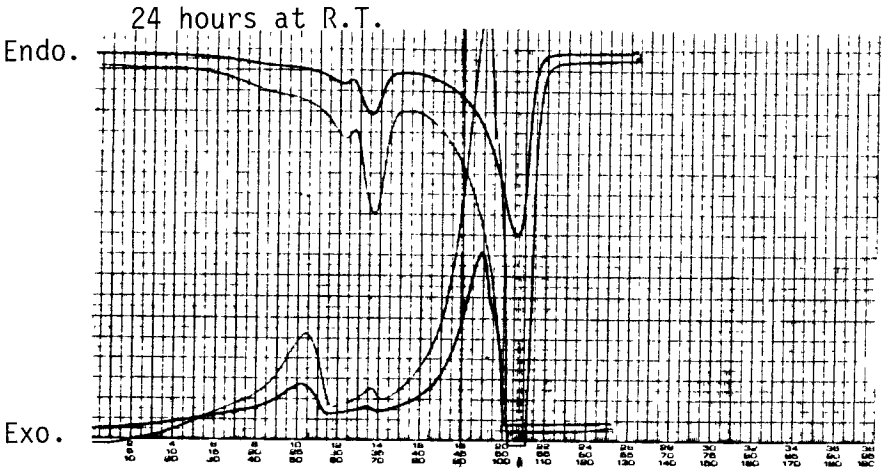

Figure 37 - Aging Effects on Thermal Properties of Cetostearyl Alcohol, Lot K4991

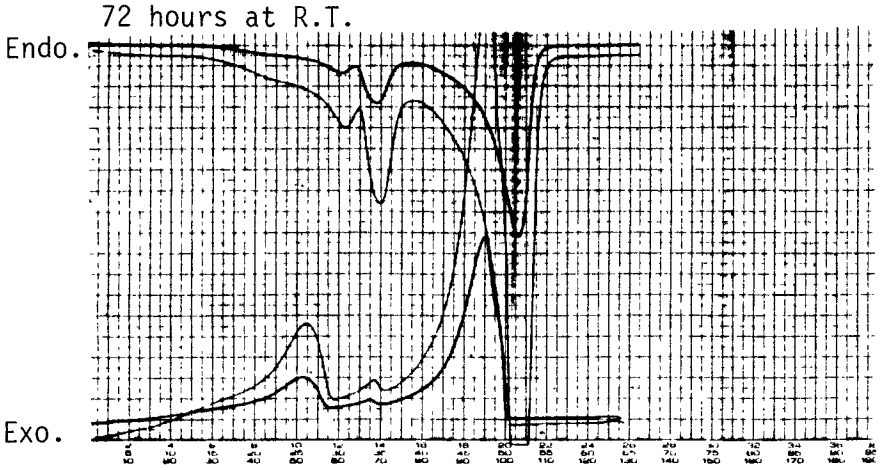

Sample: Cetostearyl Alcohol, K4991
Weight: 2.79 mg
Heating Rate: 5°C/min
Range (y): 5, 10 mV/cm X axis: 2.5°C/cm

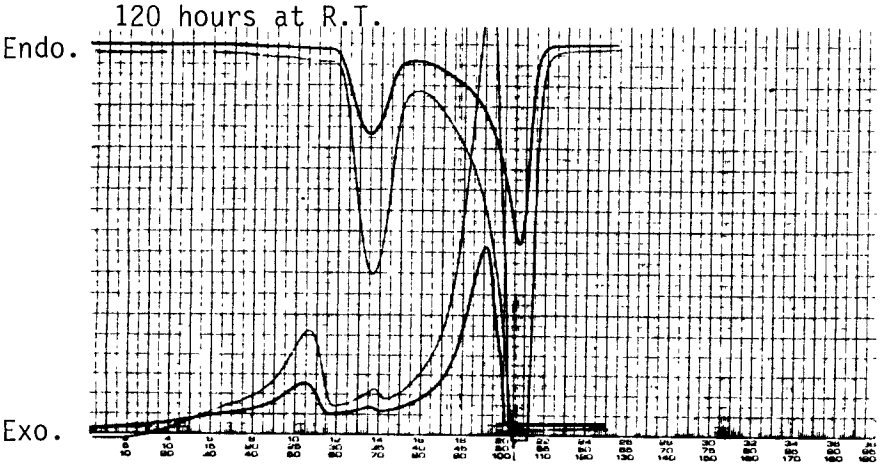

Figure 38 - Aging Effects on Thermal Properties of a Pure Sample Mixture C_{16}/C_{18}

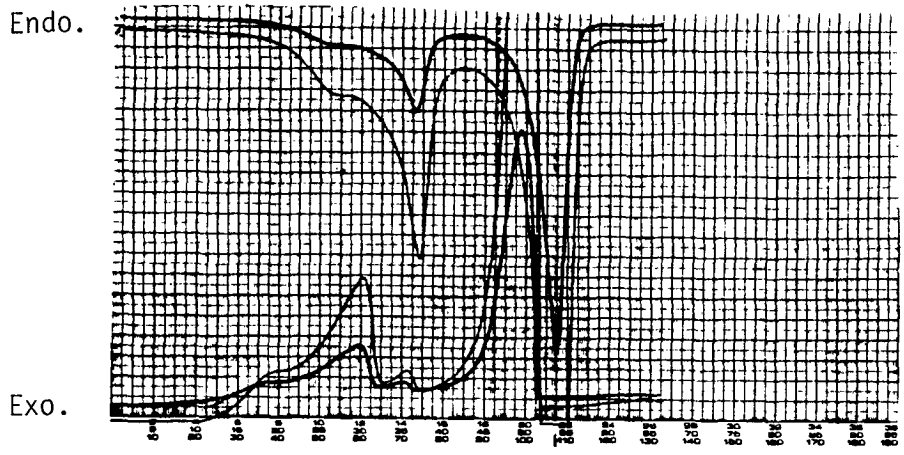

Sample:	Pure Sample, .687 C_{18}/.313 C_{16}
Weight:	3.23 mg
Heating Rate:	5°C/min
Range (y):	5, 10 mV/cm X axis: 2.5°C/cm

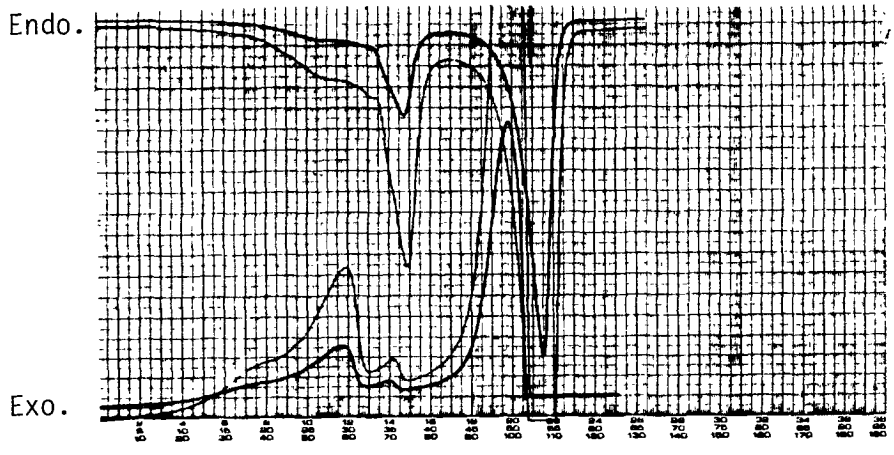

Figure 39 - Aging Effects on Thermal Properties of a Pure Sample Mixture C_{16}/C_{18}

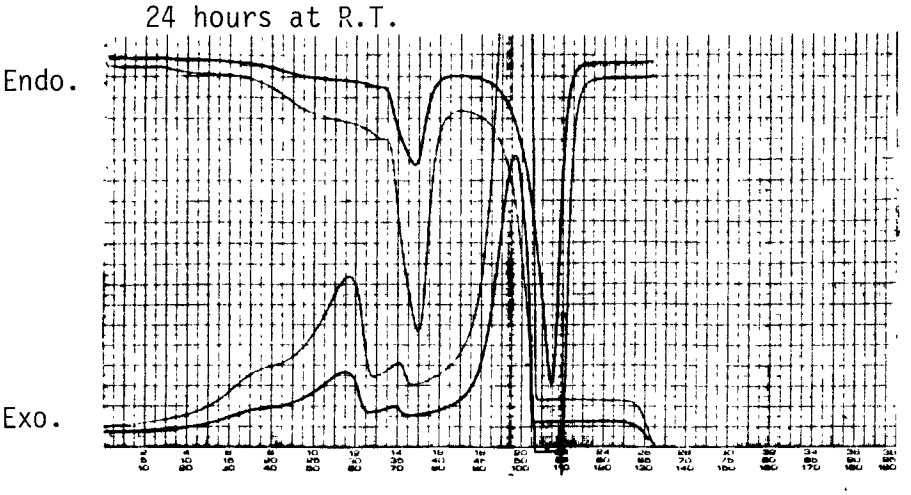

Sample: Pure Sample, .687 C_{18}/.313 C_{16}
Weight: 3.23 mg
Heating Rate: 5°C/min
Range (y): 5, 10 mV/cm X axis: 2.5°C/cm

Figure 40 - Drying Curve of Potassium Chloride, Lot 10195[a]

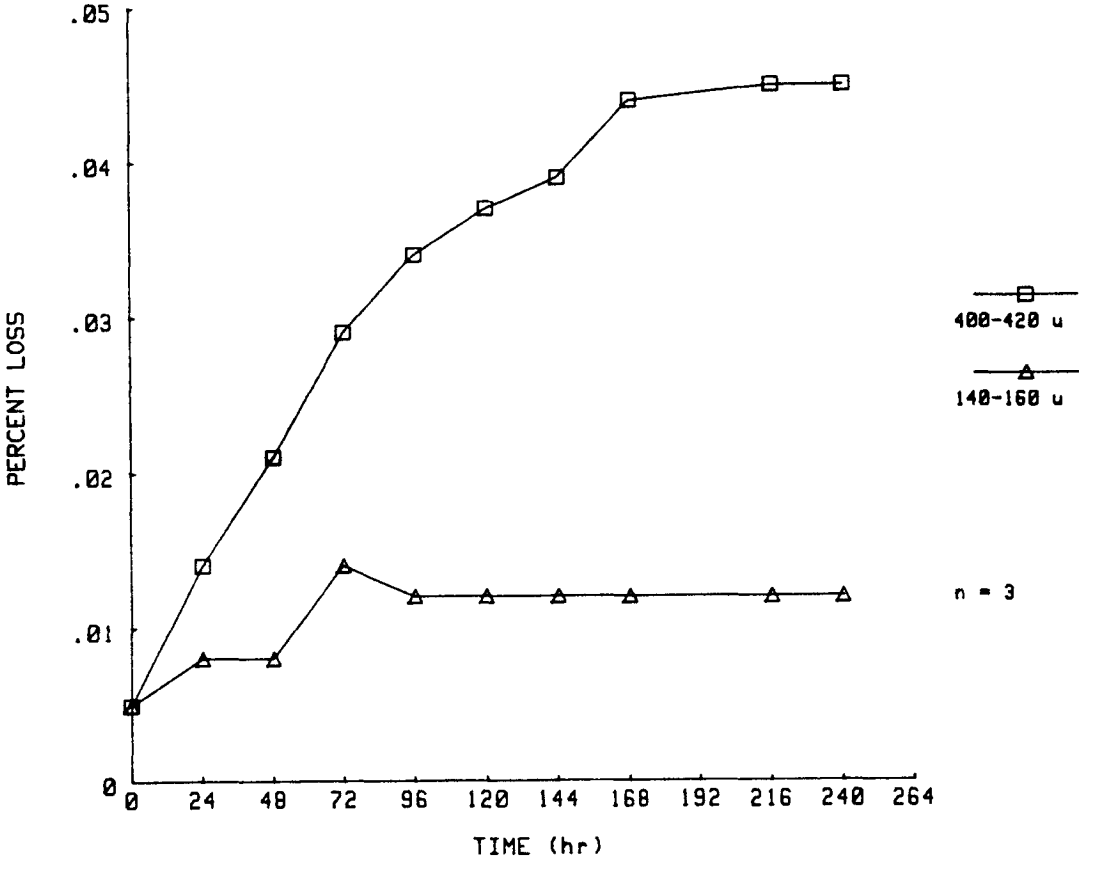

[a] All samples were pre-dried for 2 hours at 120°C, all drying was subsequently carried out at 170°C.

Figure 41 - Drying Curve of Potassium Chloride, Lot L7490[a]

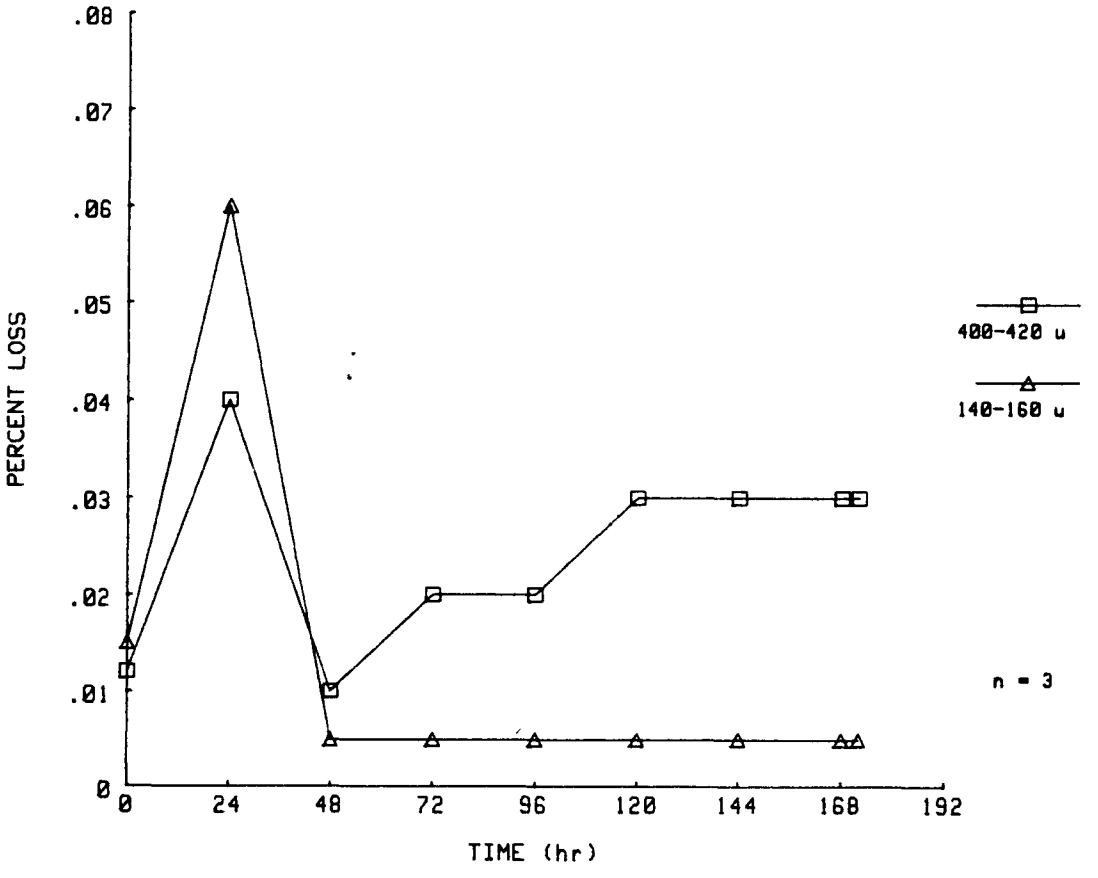

[a] All samples were pre-dried for 2 hours at 120°C, all drying was subsequently carried out at 170°C.

Figure 42 - Dark Field Microscopy, Potassium Chloride, Lot L7490

Potassium Chloride, Lot #L7490
140-160μ , 107X Magnification

Potassium Chloride, Lot #L7490
400-420μ , 107X Magnification

Figure 43 - Compact Tensile Strength, Potassium Chloride, Lot L7490, 140-160μ Particles[a]

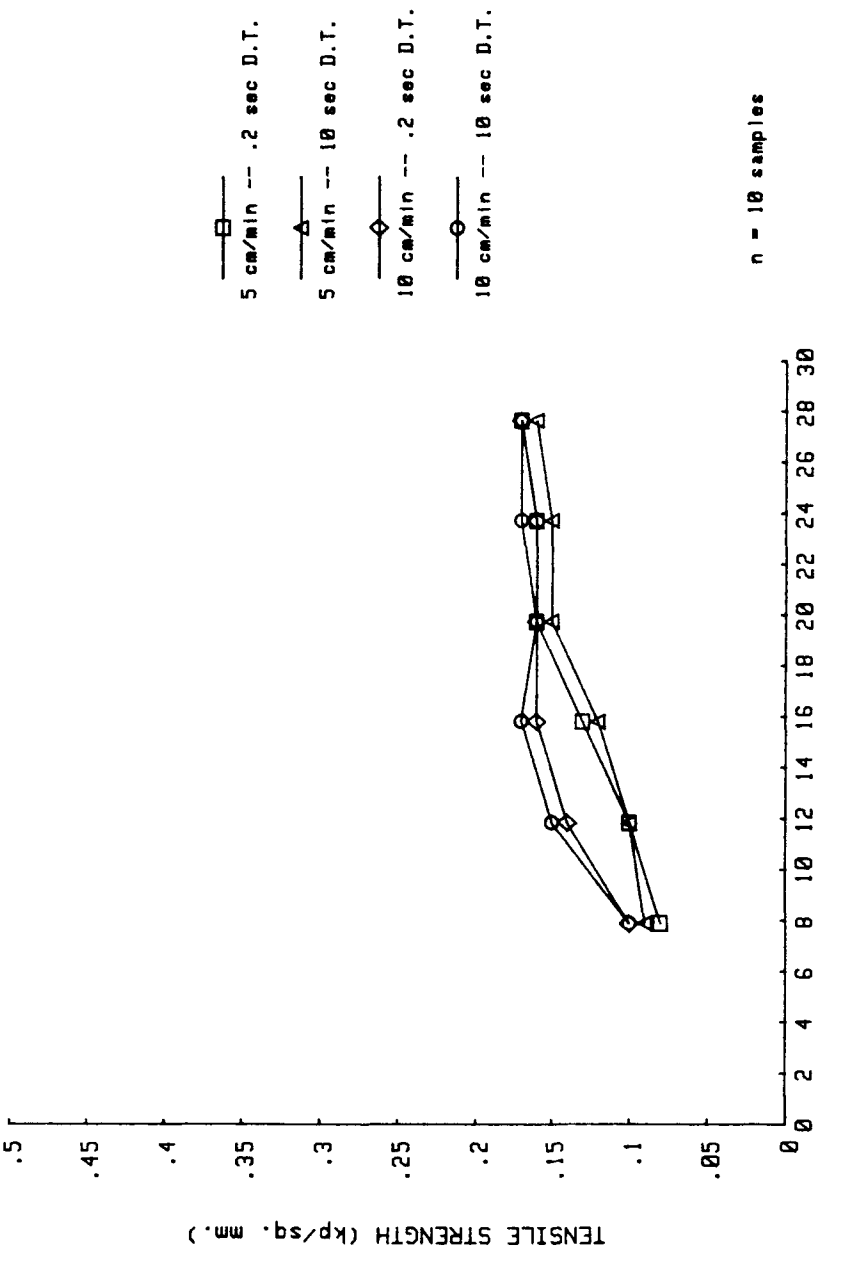

[a]Compacts processed at two dwell times and two strain rates.

Figure 44 - Compact Tensile Strength, Potassium Chloride, Lot 10195, 400-420μ Particles[a]

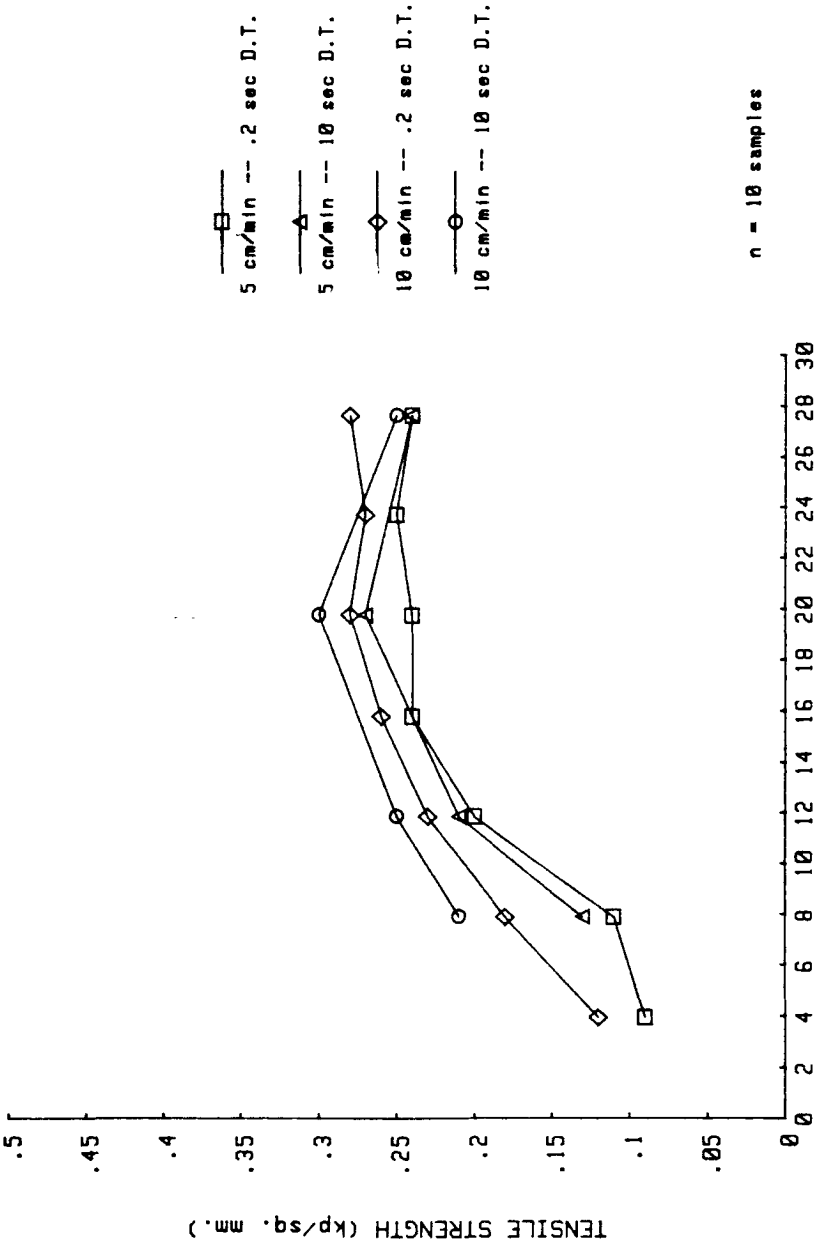

[a] Compacts processed at two dwell times and two strain rates.

Figure 45 - Compact Tensile Strength, Potassium Chloride, Lot 10195, 140-160μ Particles[a]

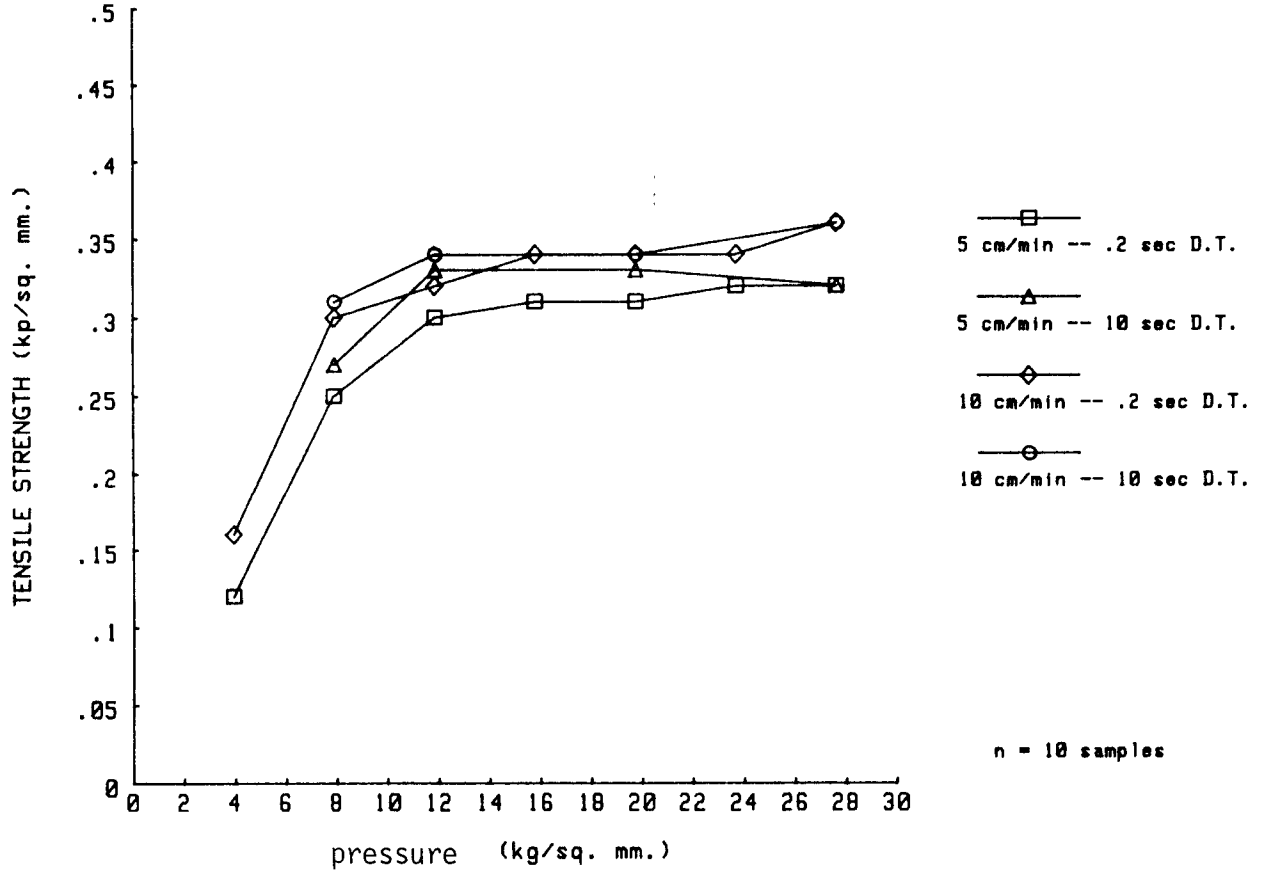

[a] Compacts processed at two dwell times and two strain rates.

Figure 46 - Compact Tensile Strength, Potassium Chloride, Lot 10195, Milled[a]

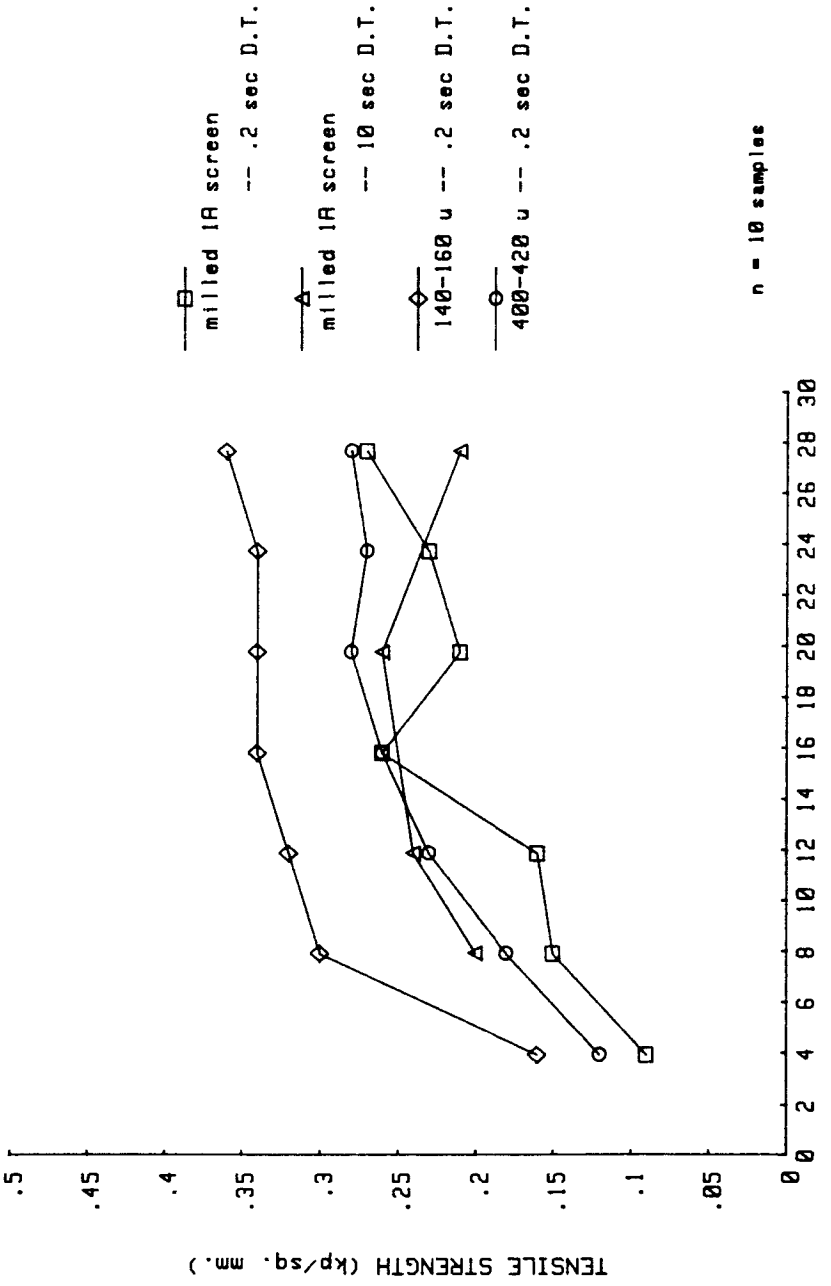

[a] Compares milled material without classification to classified samples. Two dwell times are used but only one strain rate (10 cm/min).

Case 4

U3C

~~244~~

BG SCHEME

~~Figure 47.~~ SEM, Potassium Chloride Compact, Lot 10195

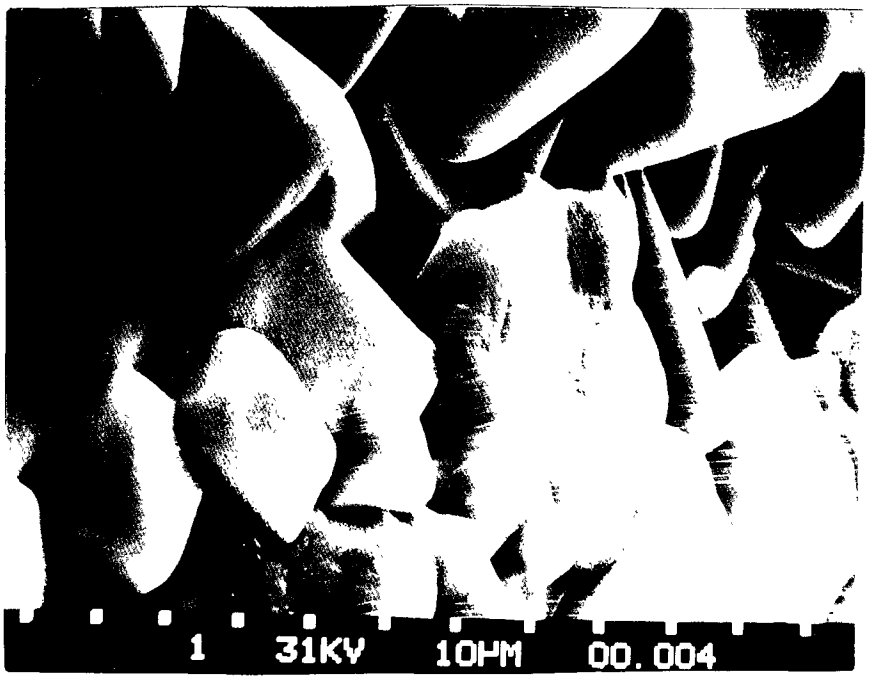

Potassium Chloride, Lot #10195
Milled 1A, 1000X Magnification

Figure 48 - Tensile Strength as a Function of Stress Decay

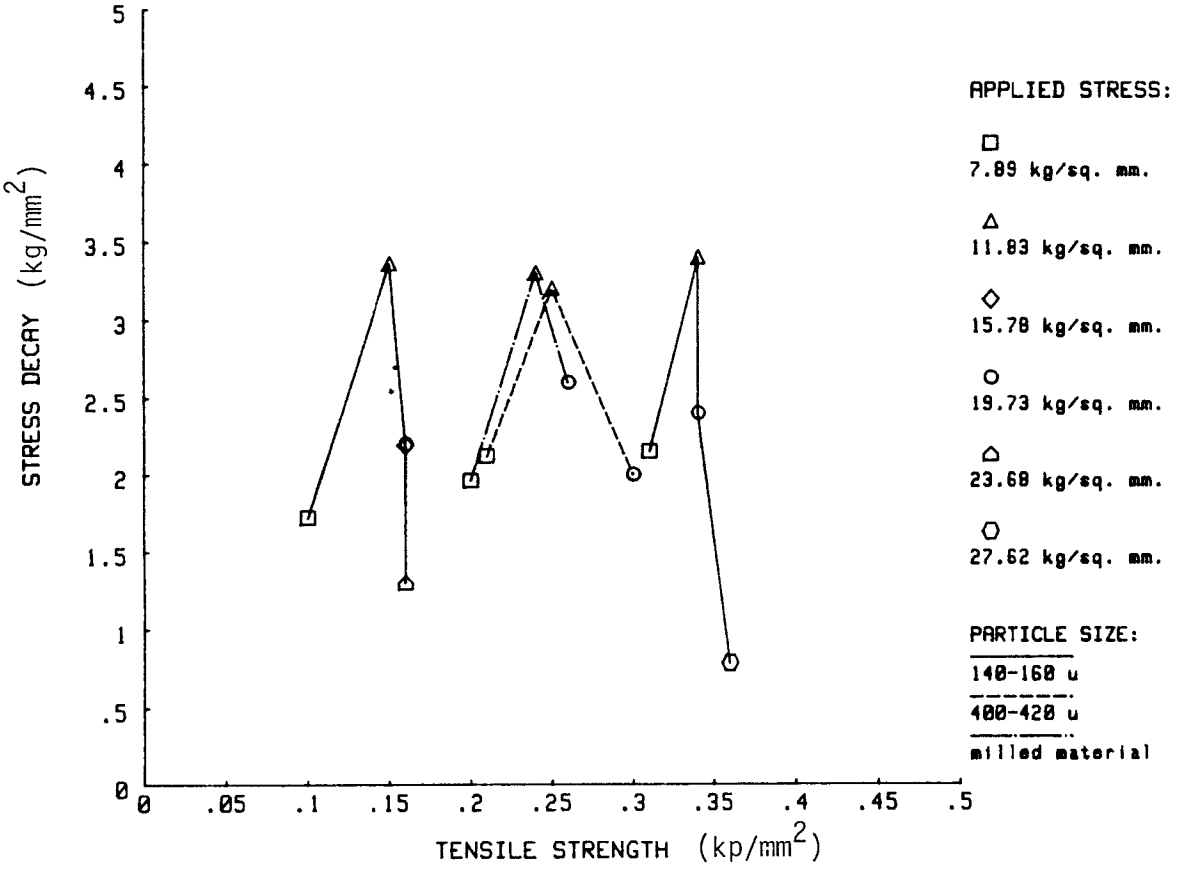

Figure 49 - SEM, Potassium Chloride Compact, Lot L7490, Dried/ Undried

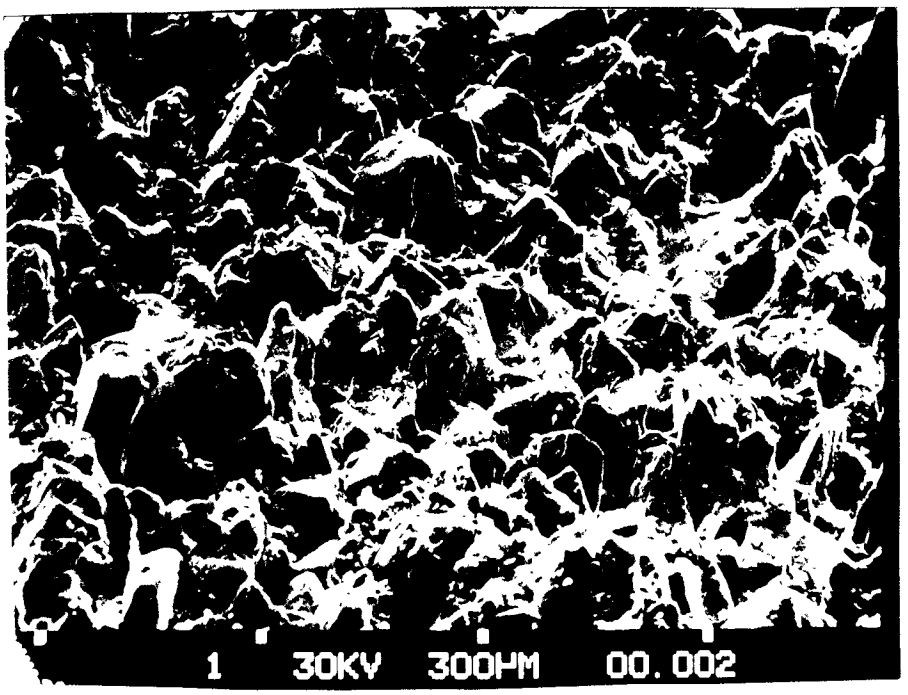

Potassium Chloride, Lot #L7490
140-160μ, undried, 100X Magnification

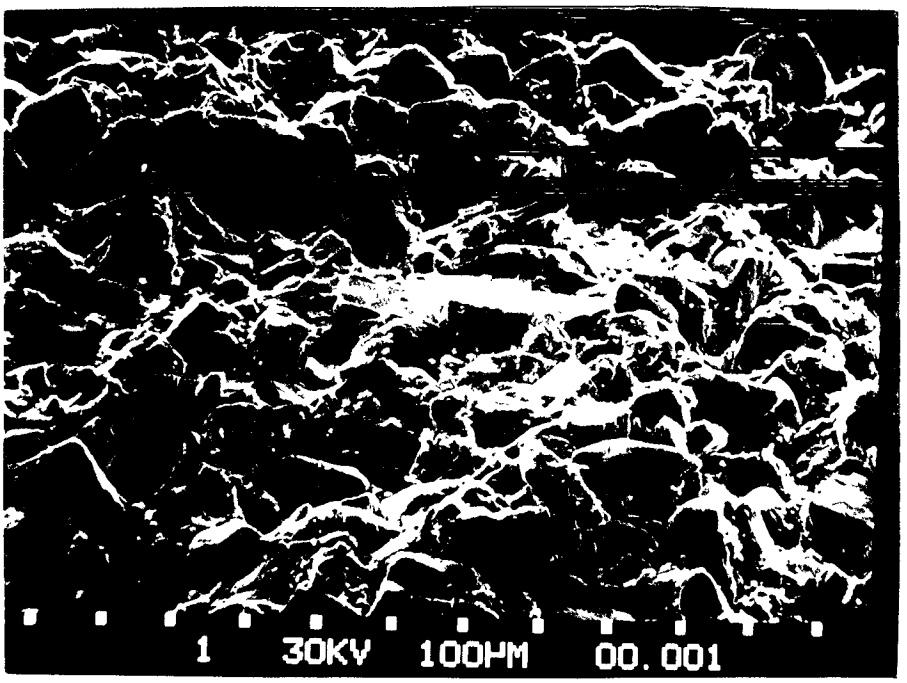

Potassium Chloride, Lot #L7490
140-160μ, dried, 100X Magnification

BG SCHEME

Case 4 43b

~~247~~

Figure 50 - SEM, Potassium Chloride Compact, Lot L7490, Dried/ Undried

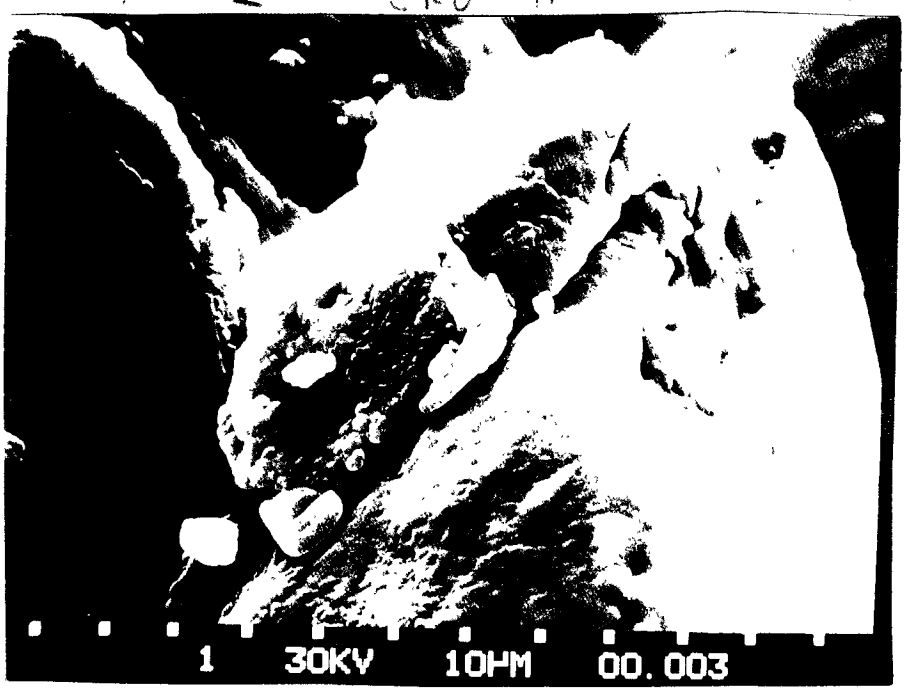

Potassium Chloride, Lot #L7490
140-160μ, undried, 1000X Magnification

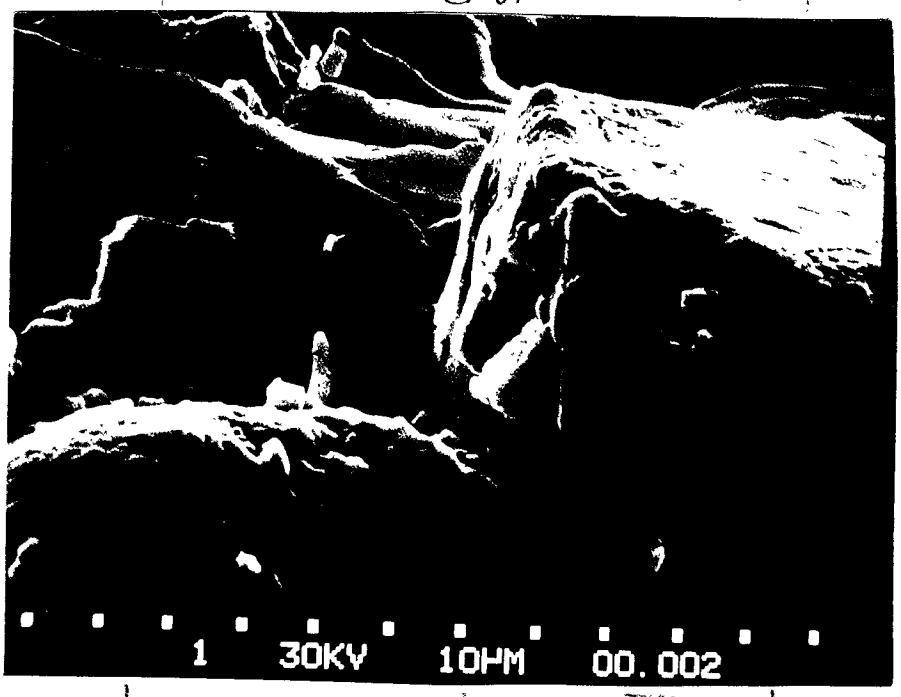

Potassium Chloride, Lot #L7490
140-160μ, dried, 1000X Magnification

Figure 51 - Heckel Plot, Potassium Chloride, Lot L7490

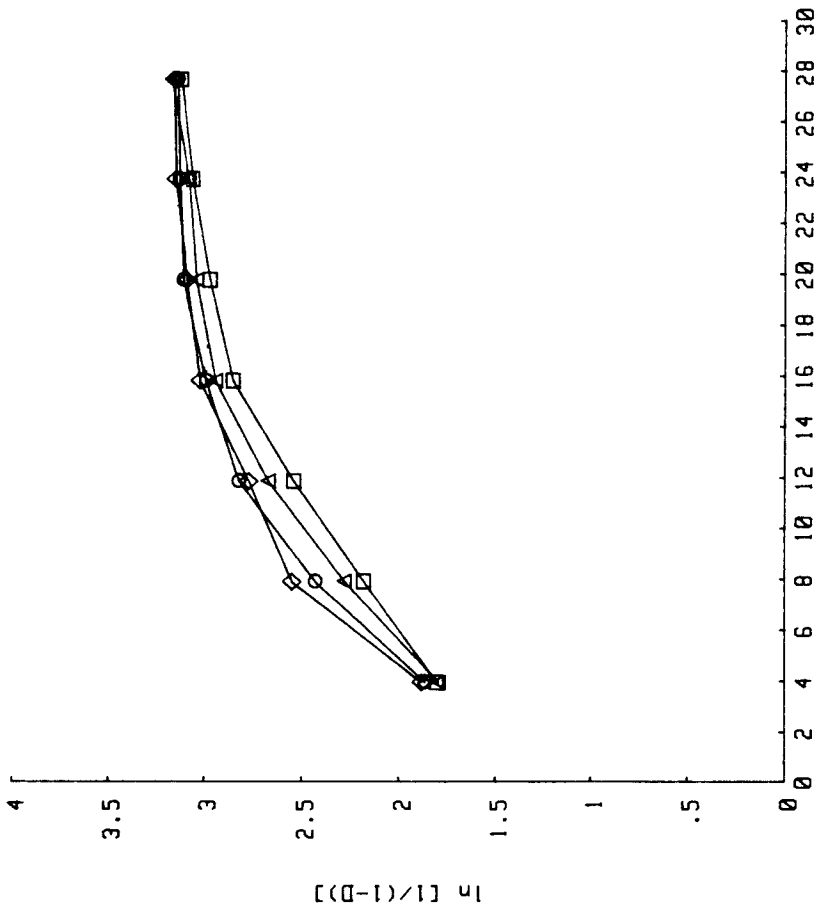

Figure 52 - Heckel Plot, Potassium Chloride, Lot 10195

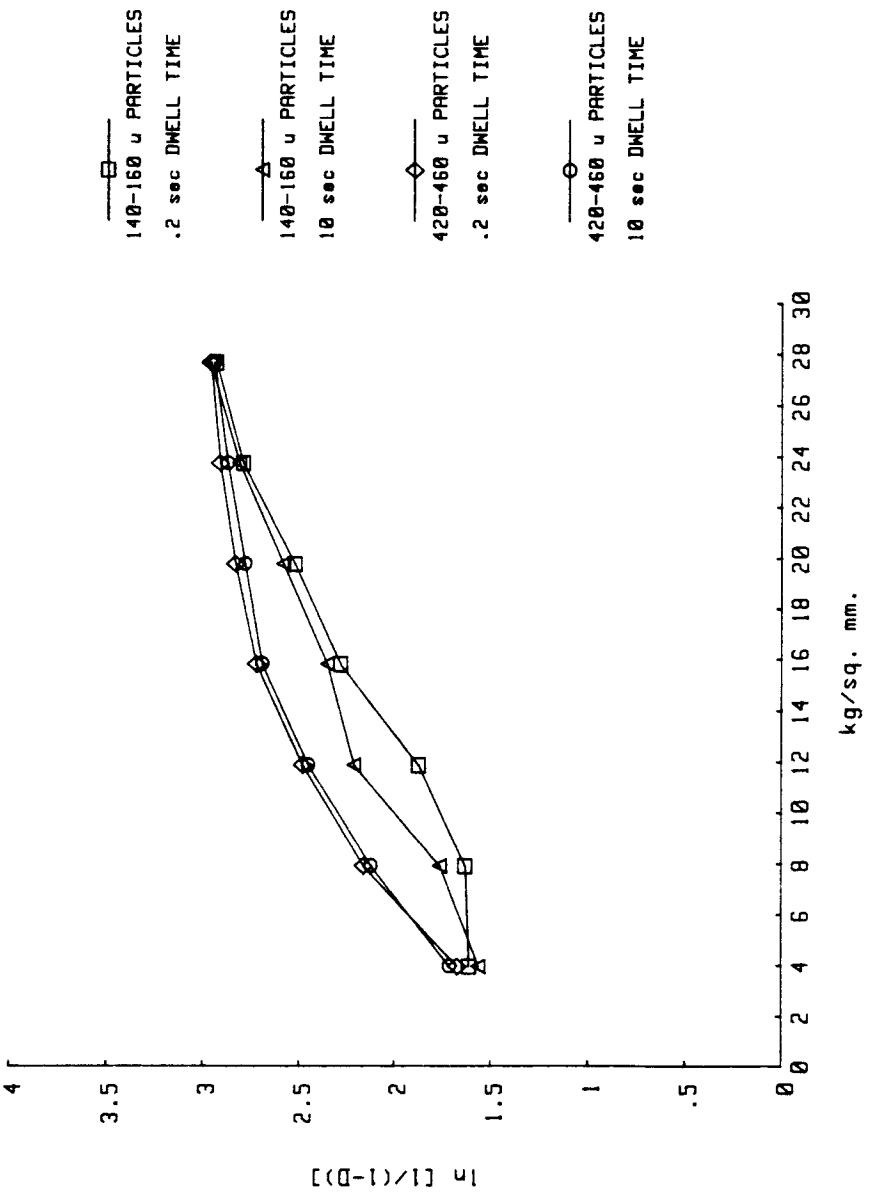

Figure 53 - Tensile Strength as a Function of Mean Yield Pressure (Py)

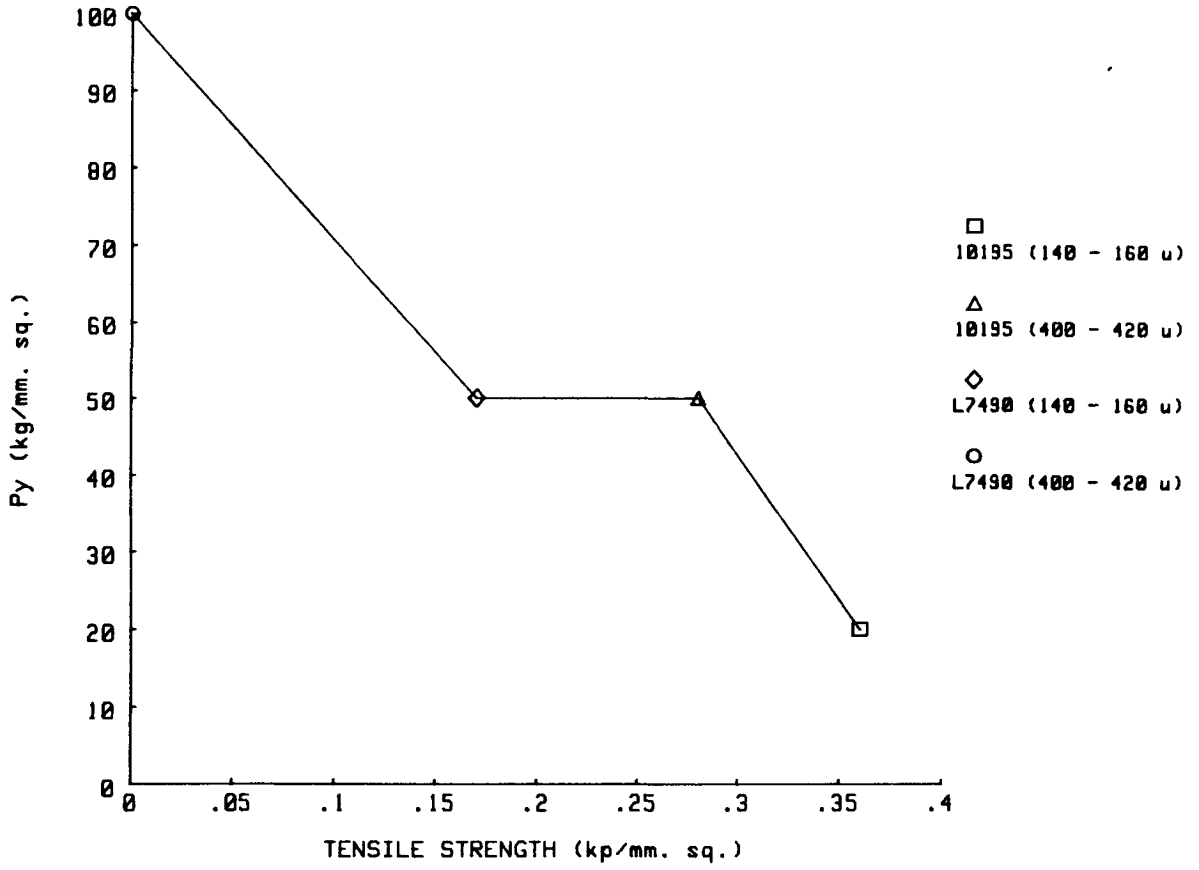

Figure 54 - SEM, Potassium Chloride and Cetostearyl Alcohol Mixture, Compact Fracture Edge

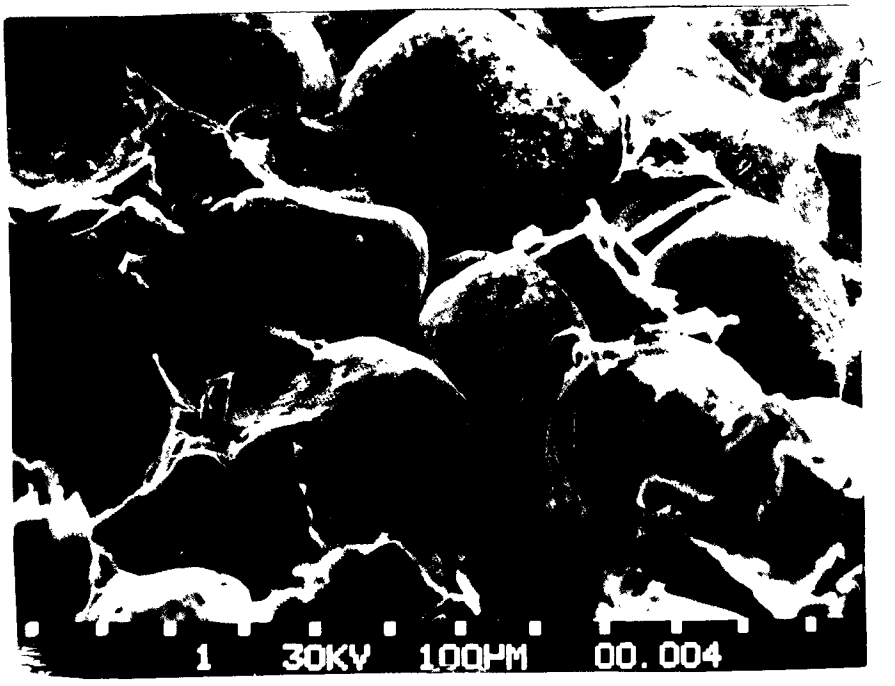

Potassium Chloride/Cetostearyl Alcohol
L7490/K4991 100X Magnification

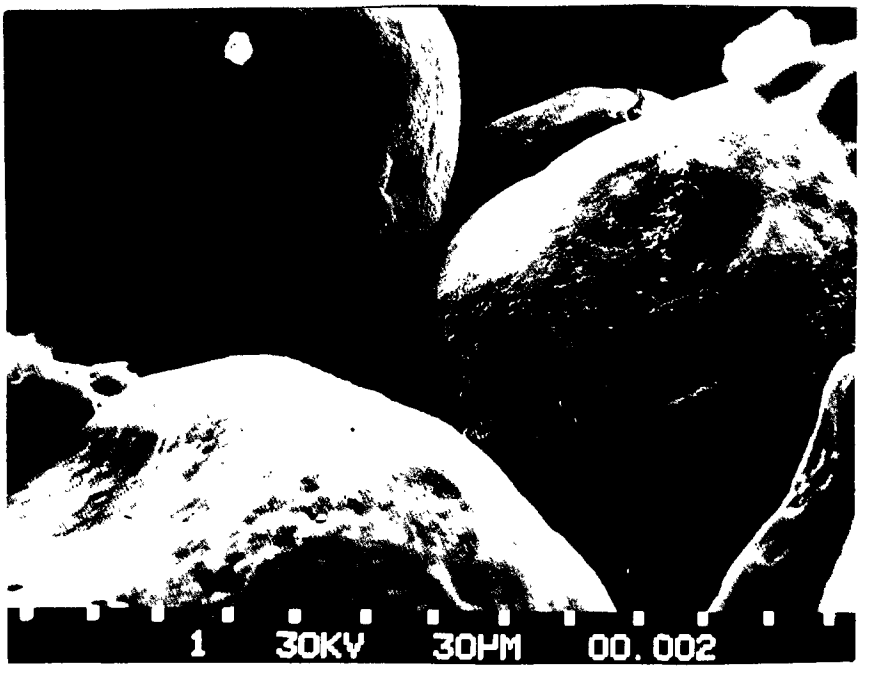

Potassium Chloride/Cetostearyl Alcohol
L7490/K4991 300X Magnification

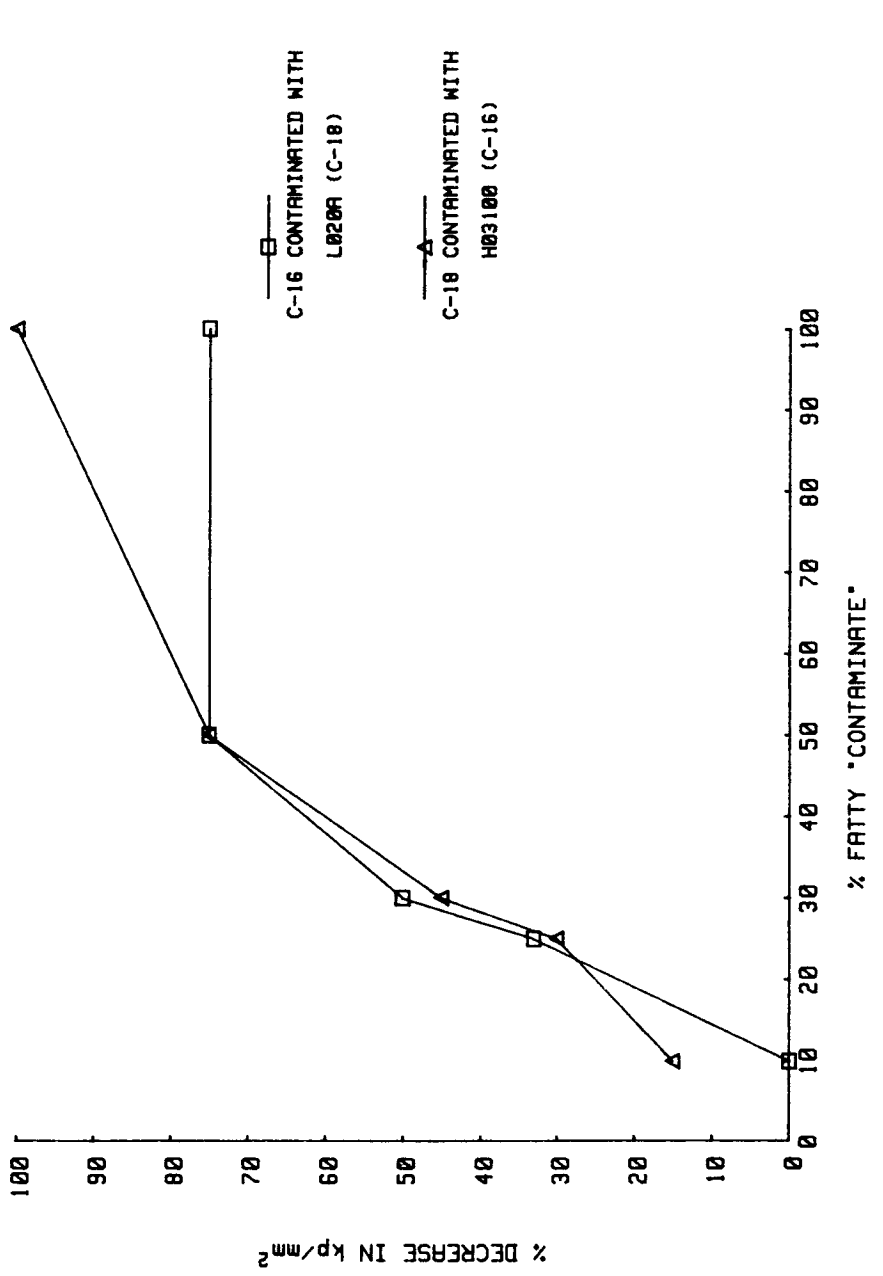

Figure 55 - Effect on Tensile Strength as a Result of Fatty Alcohol Contaminates

Figure 56 - Thermal Properties of Cetostearyl Alcohol and a Potassium Chloride Mixture

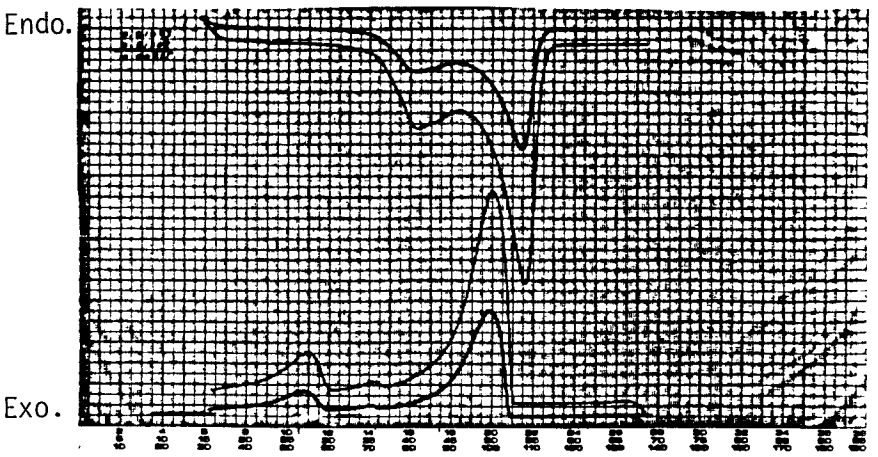

Sample: Cetostearyl Alcohol, K4991
Weight: 3.35 mg
Heating Rate: 5°C/min
Range (y): 5, 10 mV/cm X axis: 2.5°C/cm

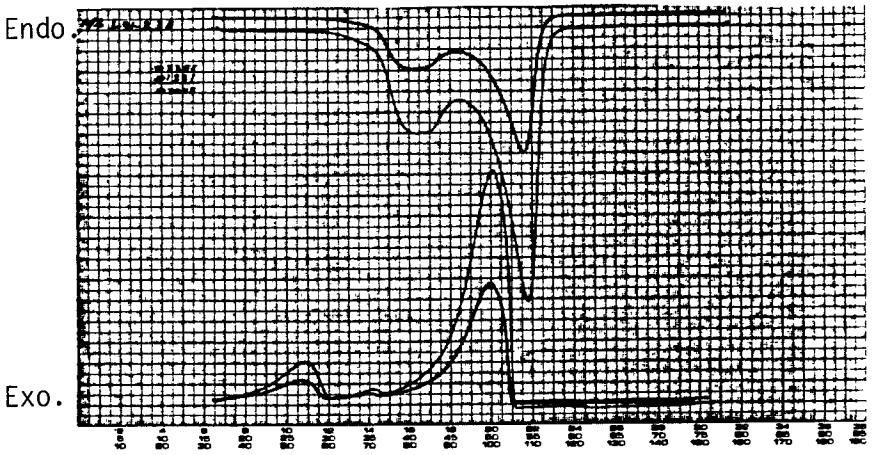

Sample: Cetostearyl Alcohol, K4991/
Potassium Chloride 10195
Weight: 20.24 mg
Heating Rate: 5°C/min
Range (y): 5, 10 mV/cm X axis: 2.5°C/cm

Figure 57 - Thermal Properties of Cetostearyl Alcohol, Lot K4991, and Potassium Chloride Mixture[a]

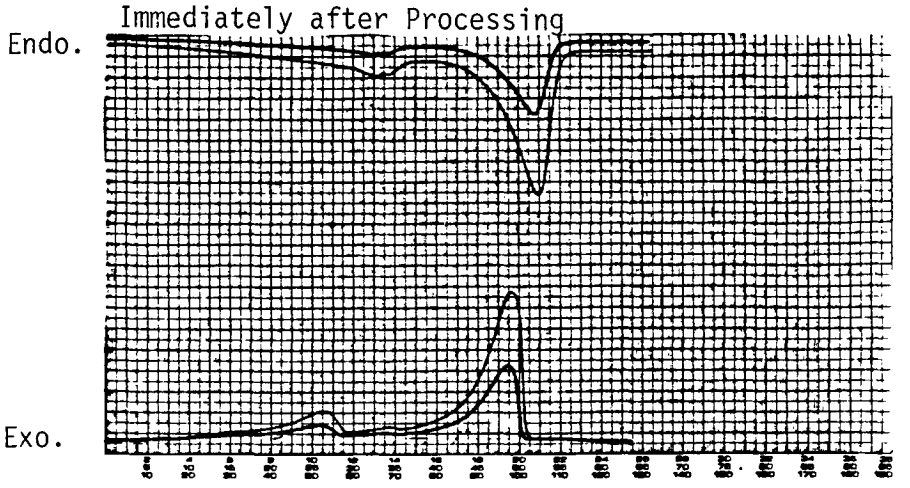

Sample:	Cetostearyl Alcohol, K4991/ Potassium Chloride, 10195
Weight:	19.53 mg
Heating Rate:	5°C/min
Range (y):	5, 10 mV/cm X axis: 2.5°C/cm

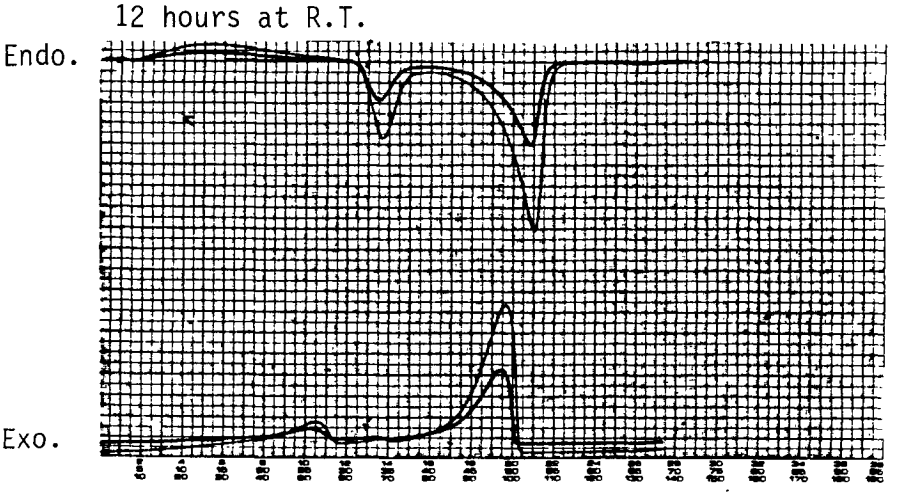

[a] Measured also as a function of aging at room temperature.

Figure 58 - Thermal Properties of Cetostearyl Alcohol, Lot L4593, and Potassium Chloride Mixture[a]

Immediately after Processing

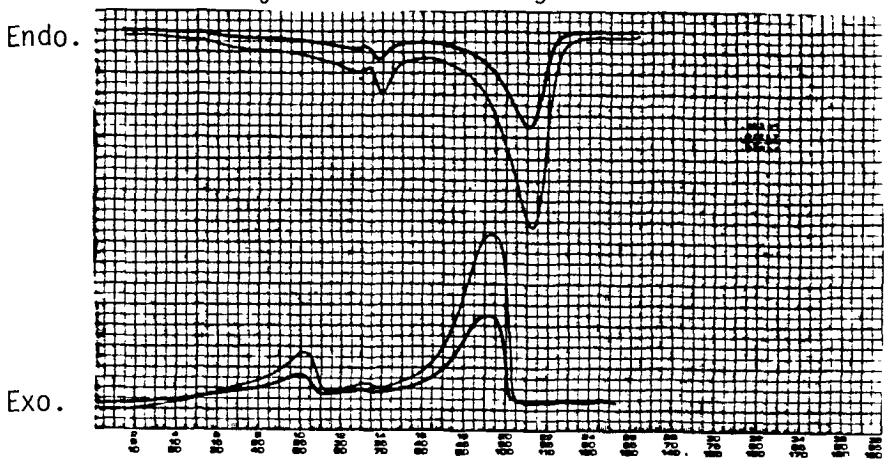

Sample:	Cetostearyl Alcohol, L4593/ Potassium Chloride, 10195
Weight:	33.10 mg
Heating Rate:	5°C/min
Range (y):	5, 10 mV/cm X axis: 2.5°C/cm

12 hours at R.T.

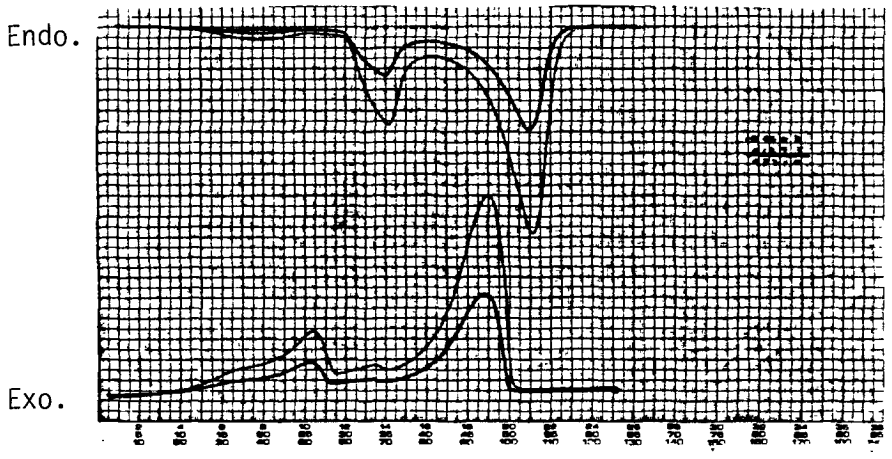

[a] Measured also as a function of aging at room temperature.

Figure 59 - Effects of Storage at 45°C on Thermal Properties of Cetostearyl Alcohol and Potassium Chloride

24 hours at 45°C

Endo.

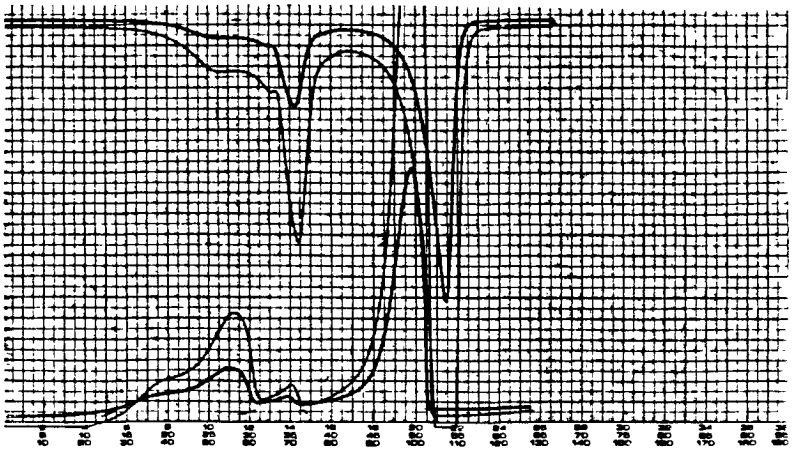

Exo.

Sample: Cetostearyl Alcohol, L4593/ Potassium Chloride, 10195
Weight: 25.20 mg
Heating Rate: 5°C/min
Range (y): 5, 10 mV/cm X axis: 2.5°C/cm

24 hours at 45°C

Endo.

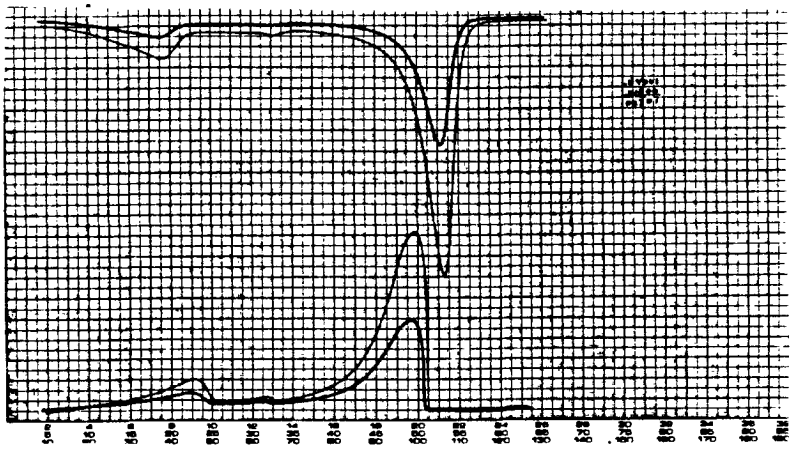

Exo.

Sample: Cetostearyl Alcohol, K4991/ Potassium Chloride, 10195
Weight: 27.30 mg
Heating Rate: 5°C/min
Range (y): 5, 10 mV/cm X axis: 2.5°C

Figure 60 - Compression Profiles, Potassium Chloride, Lot L7490, 140-160μ Particle Size[a]

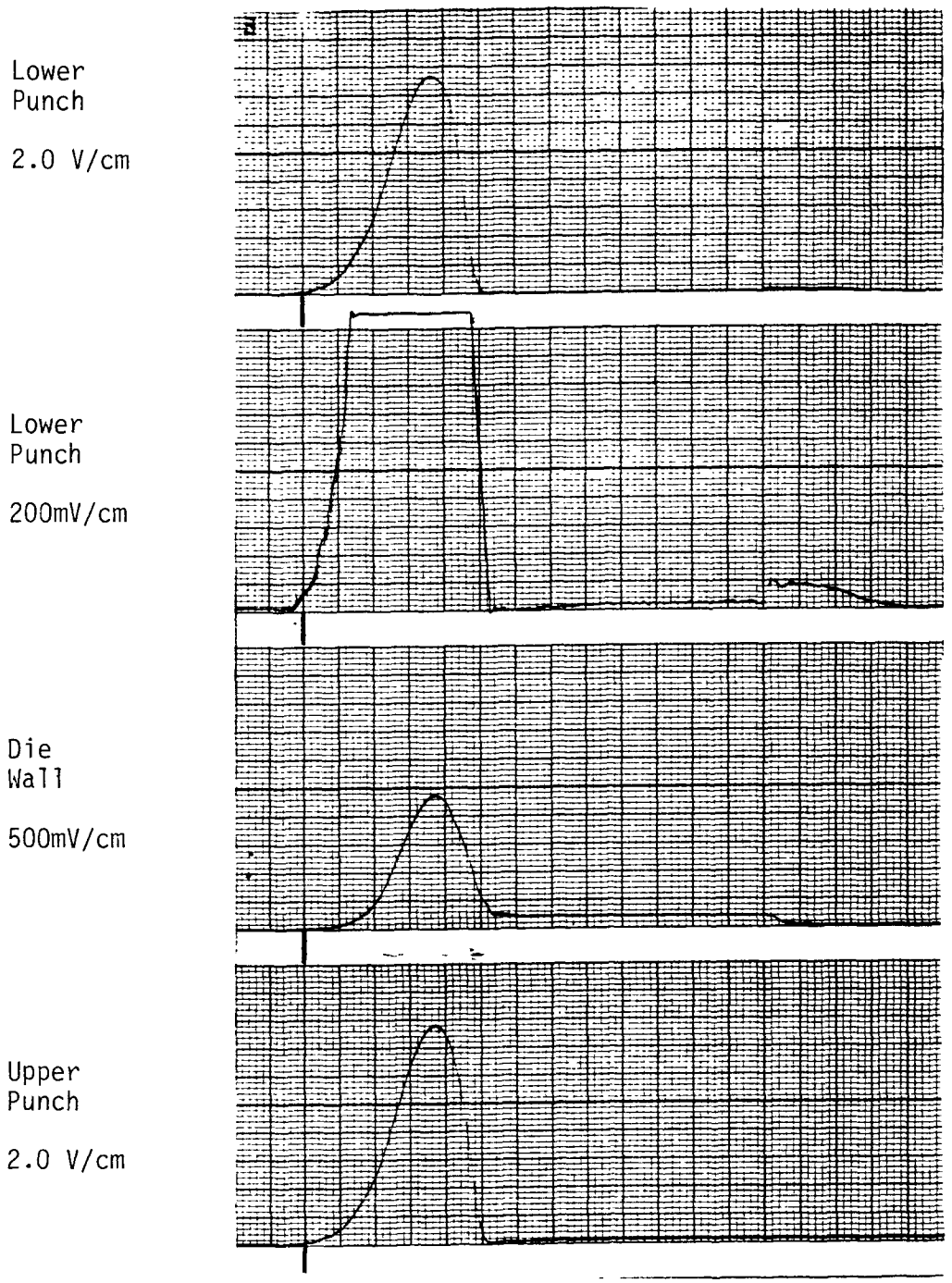

[a] All recordings were made using a high speed oscilligraphic recorder, amplification level (y axis) and chart speed (x axis) are noted for each location.

Figure 61 - Compression Profiles, Potassium Chloride, Lot L7490, 400-420μ Particle Size[a]

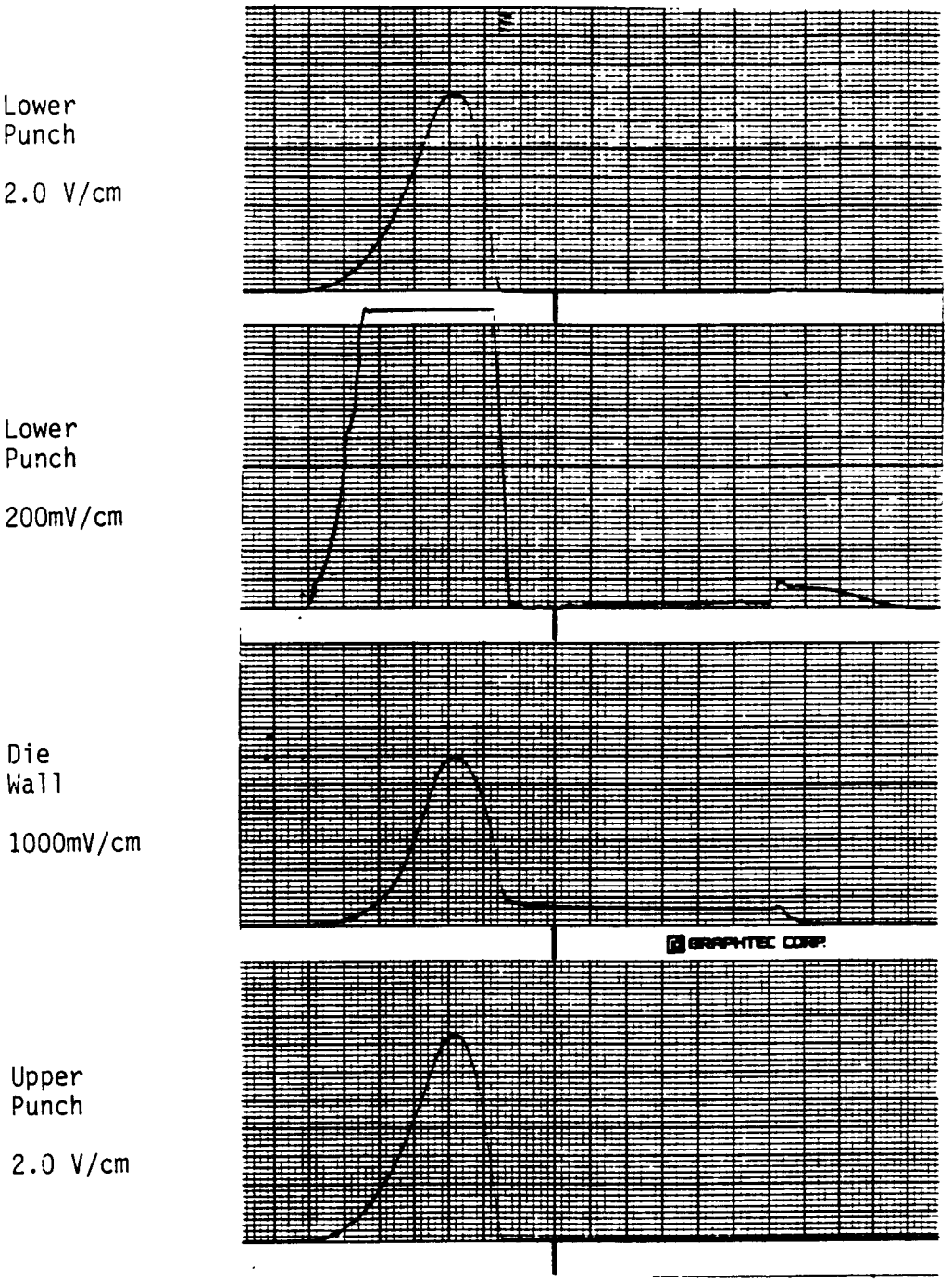

[a] Oscilligraphic recorder using amplification noted on y axis at each location, chart speed 250 mm/sec.

Figure 62 - Cycle Plot, Potassium Chloride, Lot L7490, 400-420μ

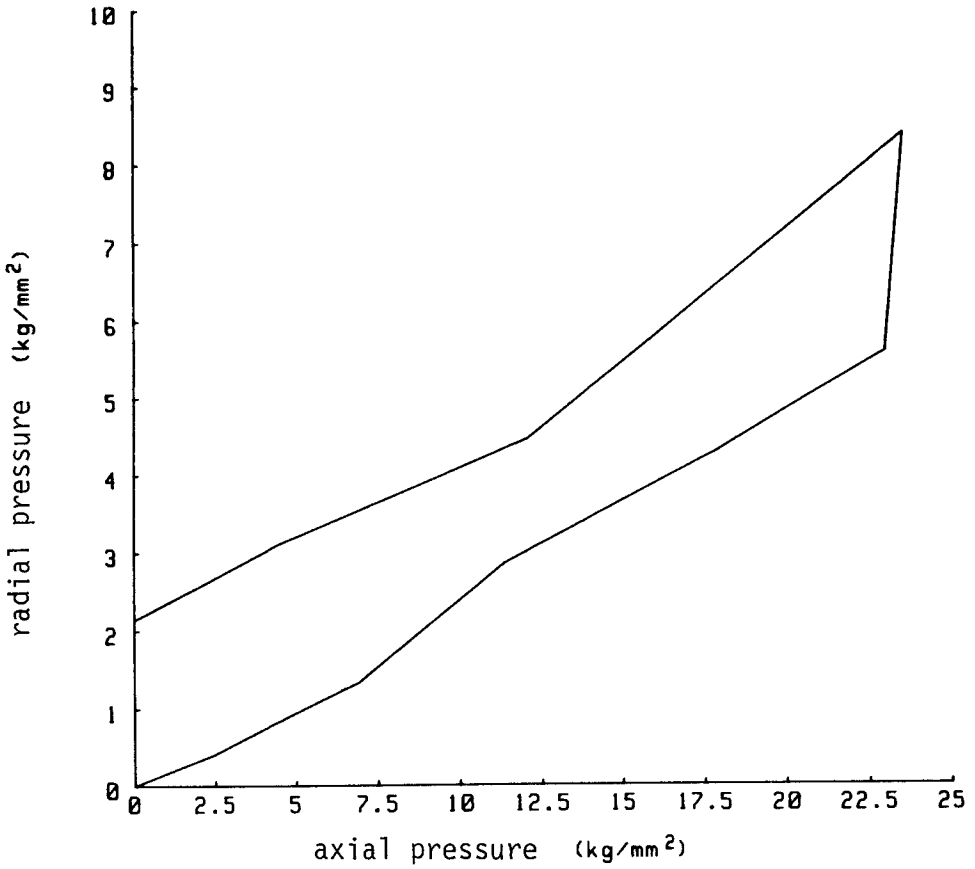

Figure 63 - Cycle Plot, Potassium Chloride, Lot L7490, 140-160μ

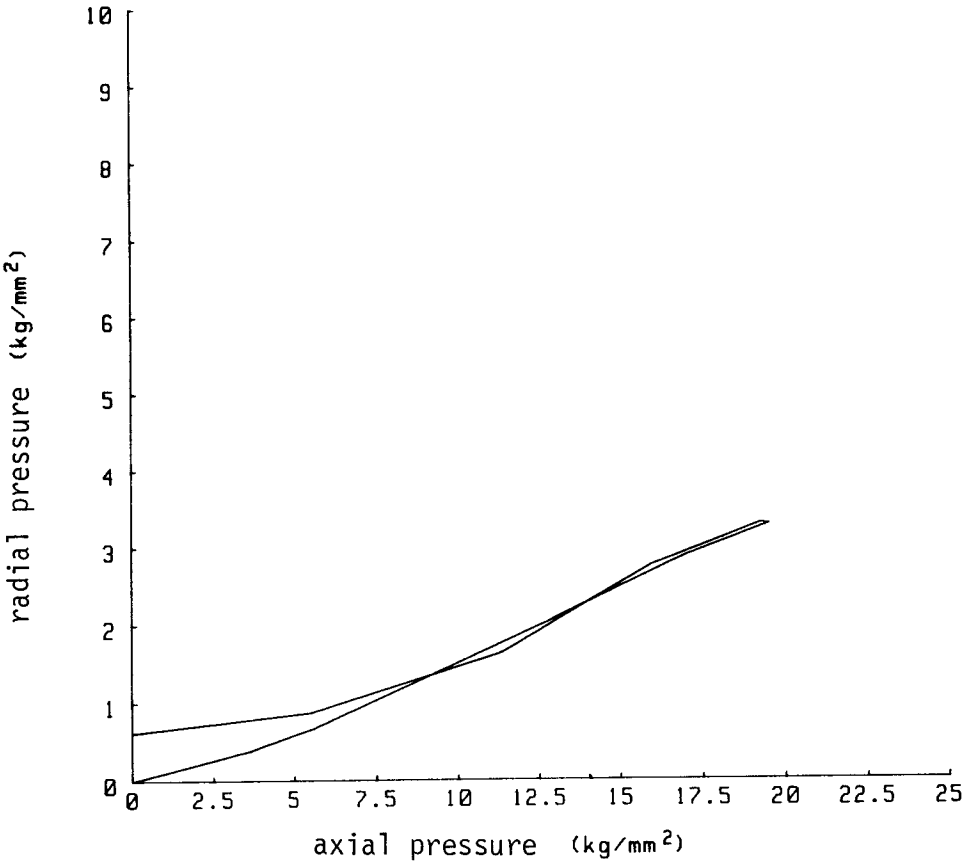

Figure 64 - Compression Profiles, Potassium Chloride, Lot 10195, 400-420μ Particle Size[a]

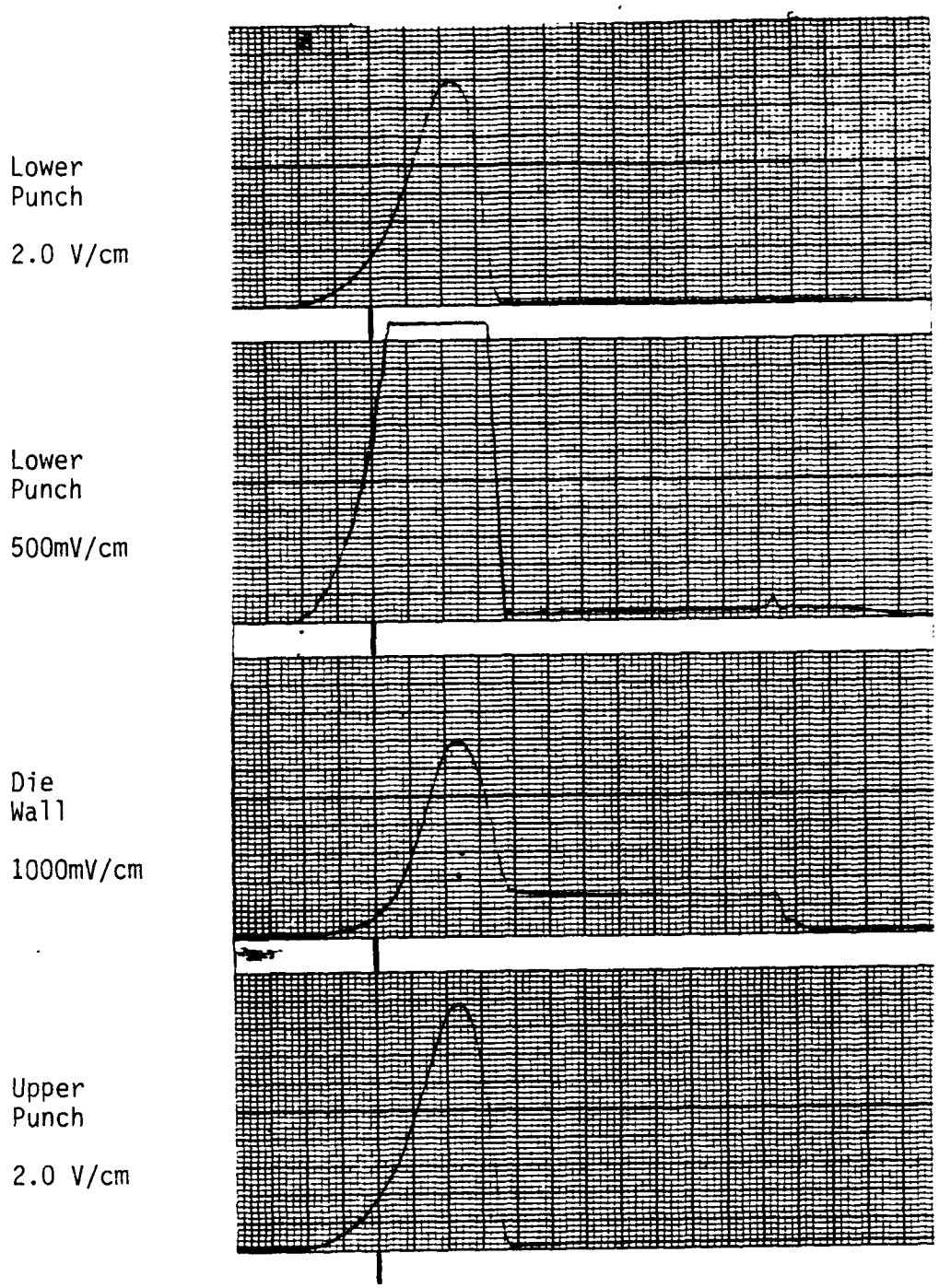

[a] Oscilligraphic recorder using amplification noted on y axis at each location, chart speed 250 mm/sec.

Figure 65 - Compression Profiles, Potassium Chloride, Lot 10195, 140-160μ Particle Size[a]

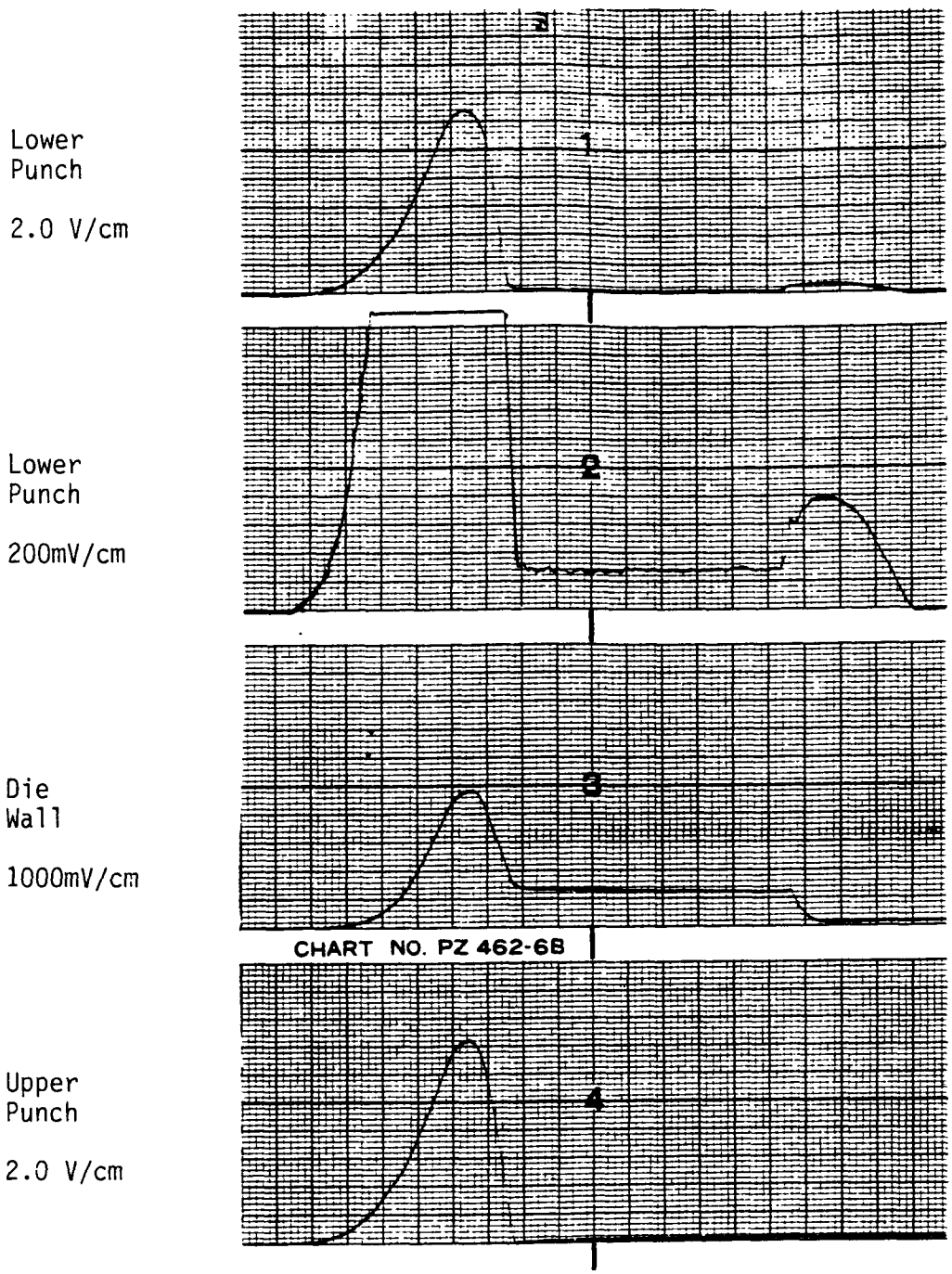

[a] Oscilligraphic recorder using amplification noted on y axis at each location, chart speed 250 mm/sec.

Figure 66 - Compression Profiles, Potassium Chloride, Lot 10195, 1A Milled[a]

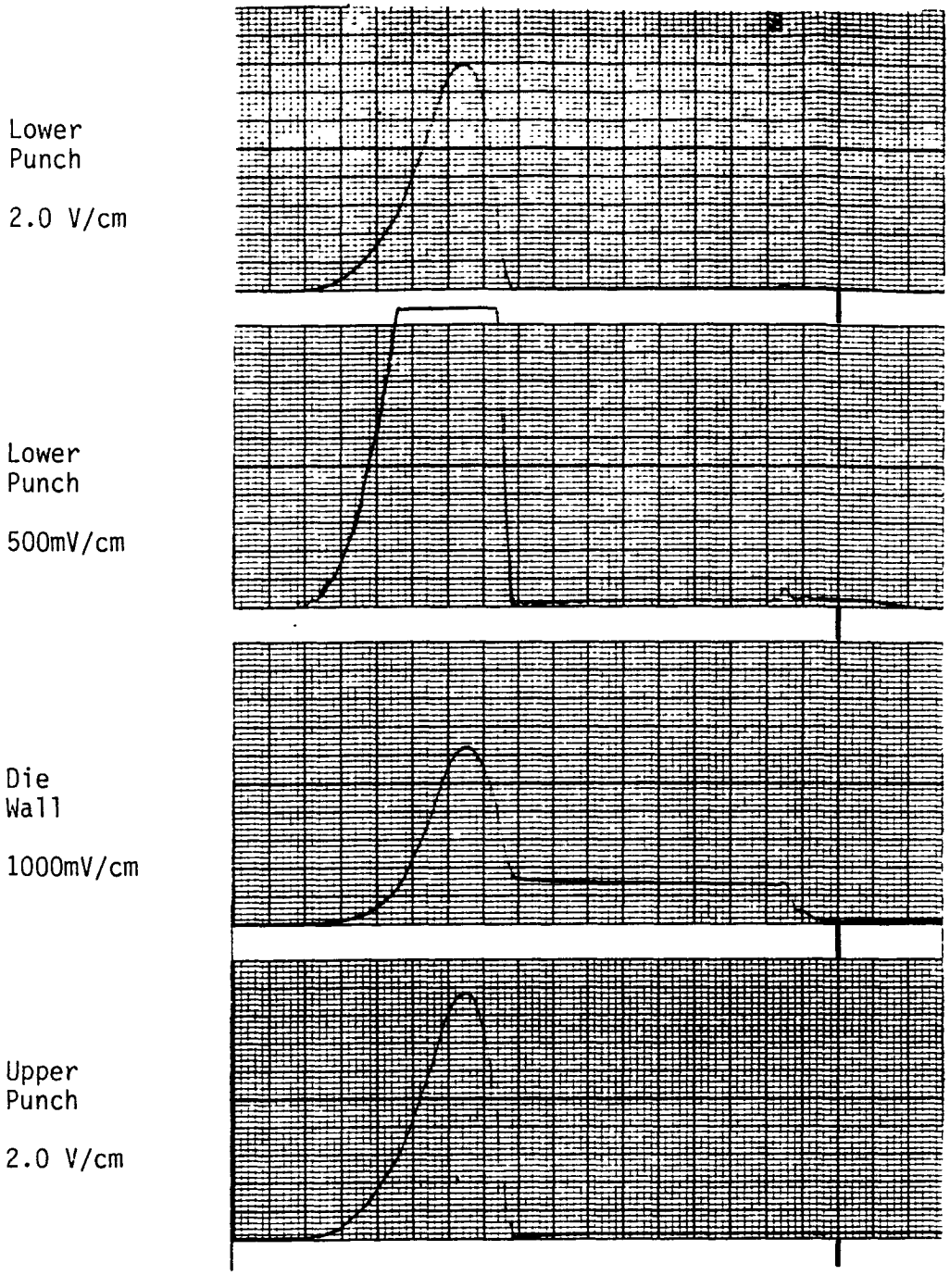

[a] Oscilligraphic recorder using amplification noted on y axis at each location, chart speed 250 mm/sec.

Figure 67 - Cycle Plot, Potassium Chloride, Lot 10195, 400-420μ

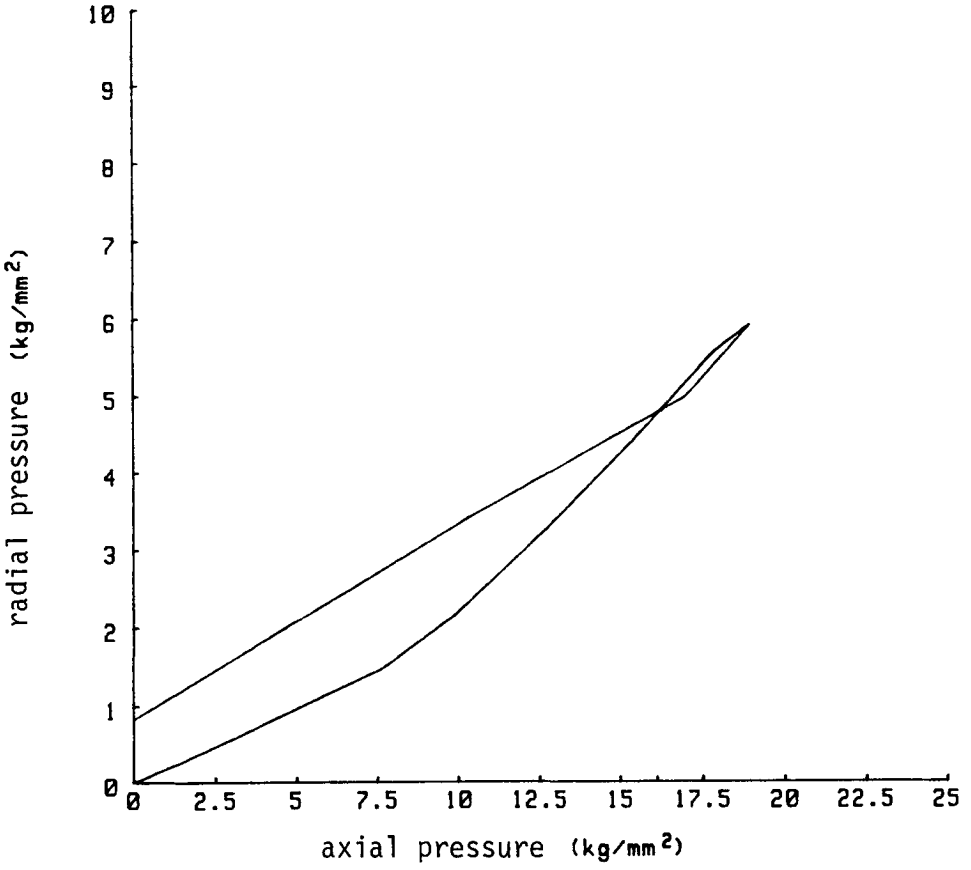

Figure 68 - Cycle Plot, Potassium Chloride, Lot 10195, 140-160μ

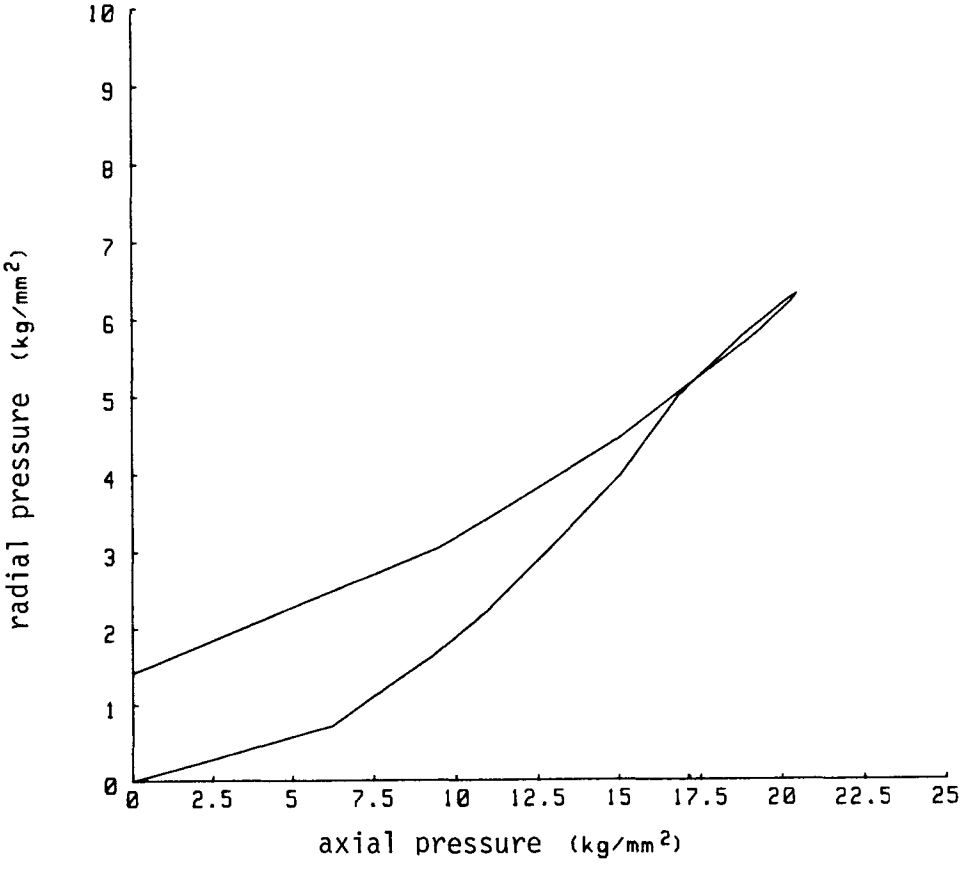

Figure 69 - Compression Profiles, Cetostearyl Alcohol and Potassium Chloride Mixture[a]

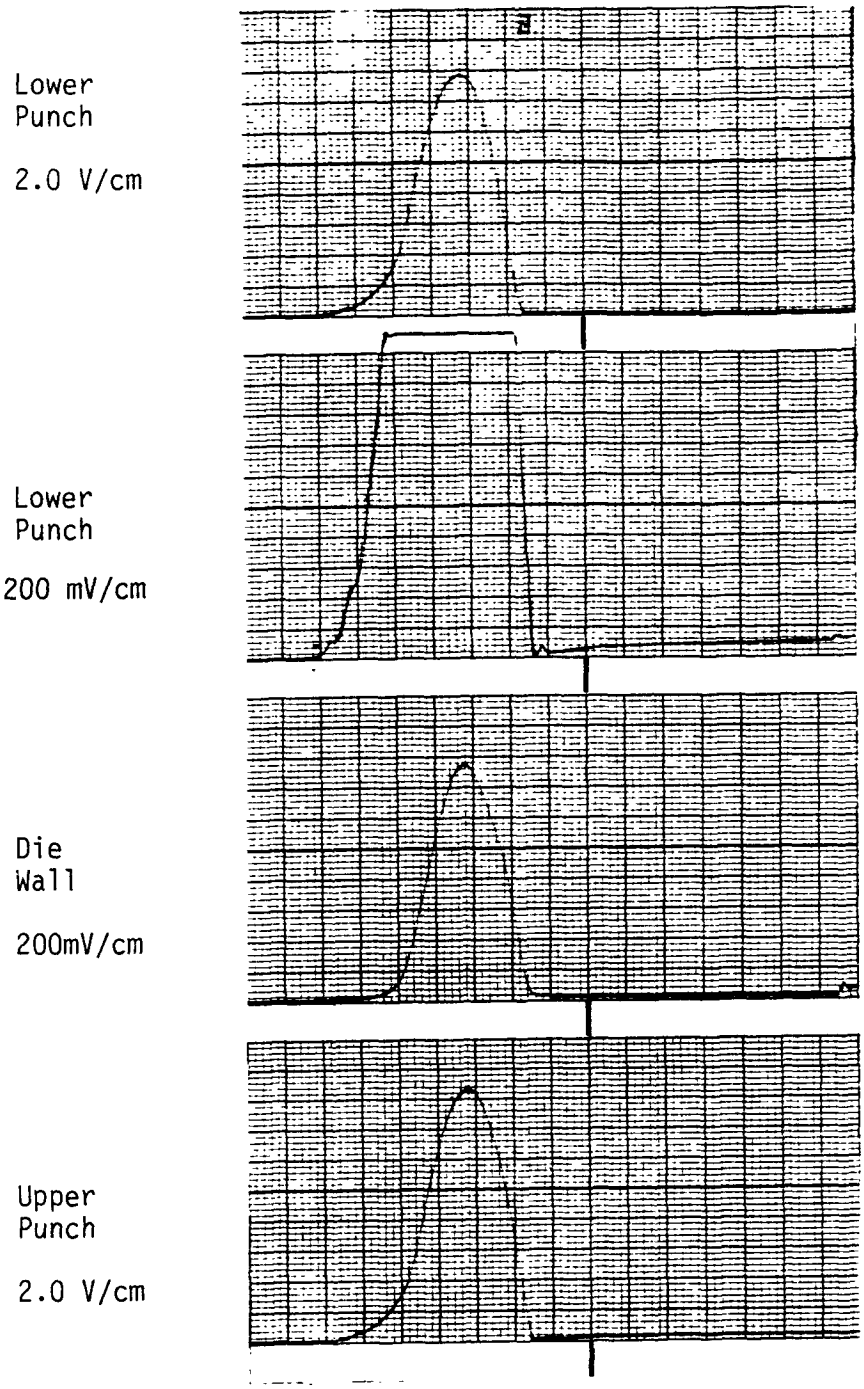

[a] CSA, Lot K4991, KCl, Lot L7490, 140-160μ, 1:7.5 ratio, recorder set at amplification noted on y axis at each location, chart speed 250 mm/sec.

Figure 70 - Compression Profiles, Increased Level of Cetostearyl Alcohol and Potassium Chloride Mixture[a]

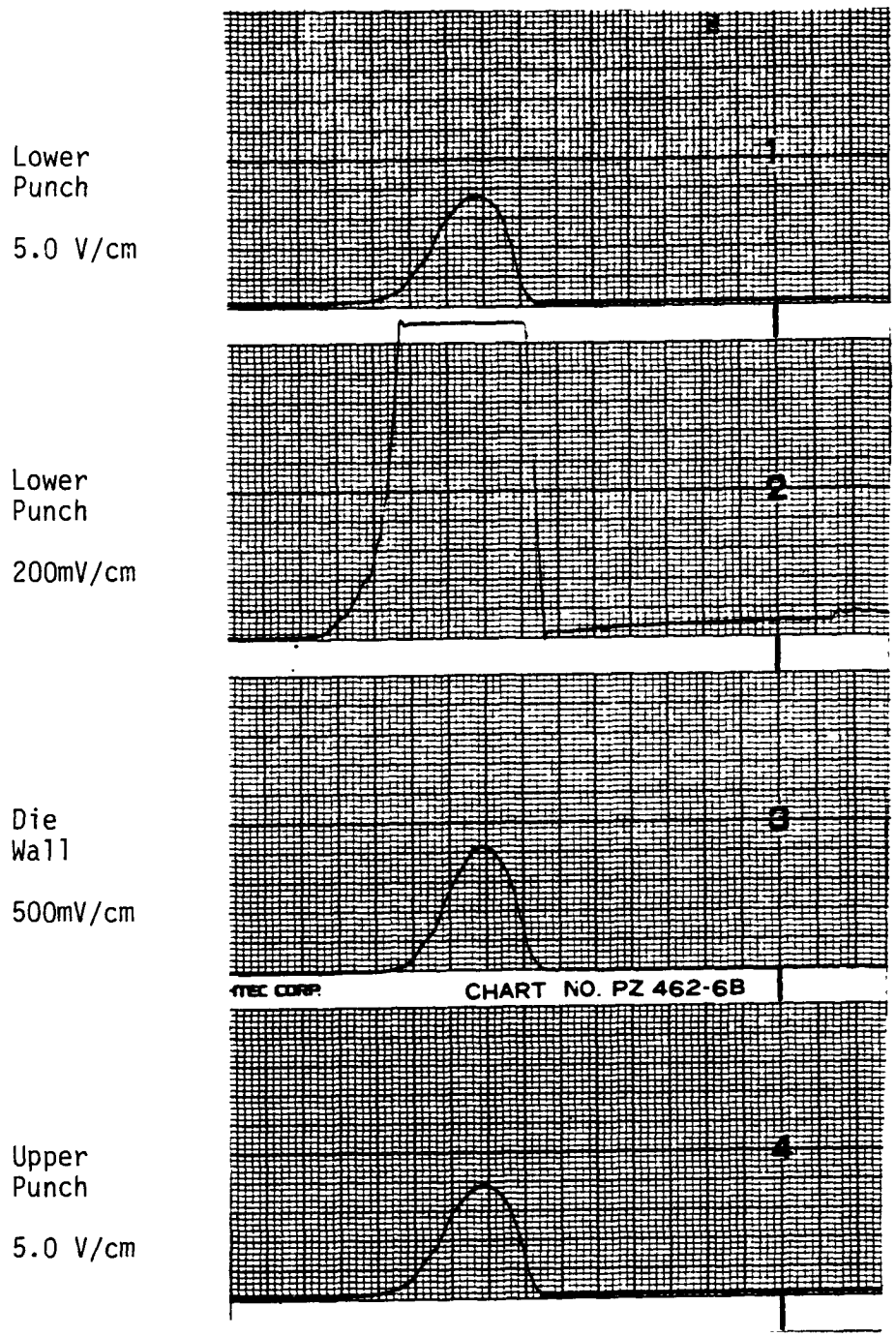

[a] CSA, Lot K4991, KCl, Lot L7490, 140-160μ, 1:7.5 ratio, recorder set at amplification noted on y axis at each location, chart speed 250 mm/sec.

Figure 71 - Cycle Plot, Cetostearyl Alcohol and Potassium Chloride[a]

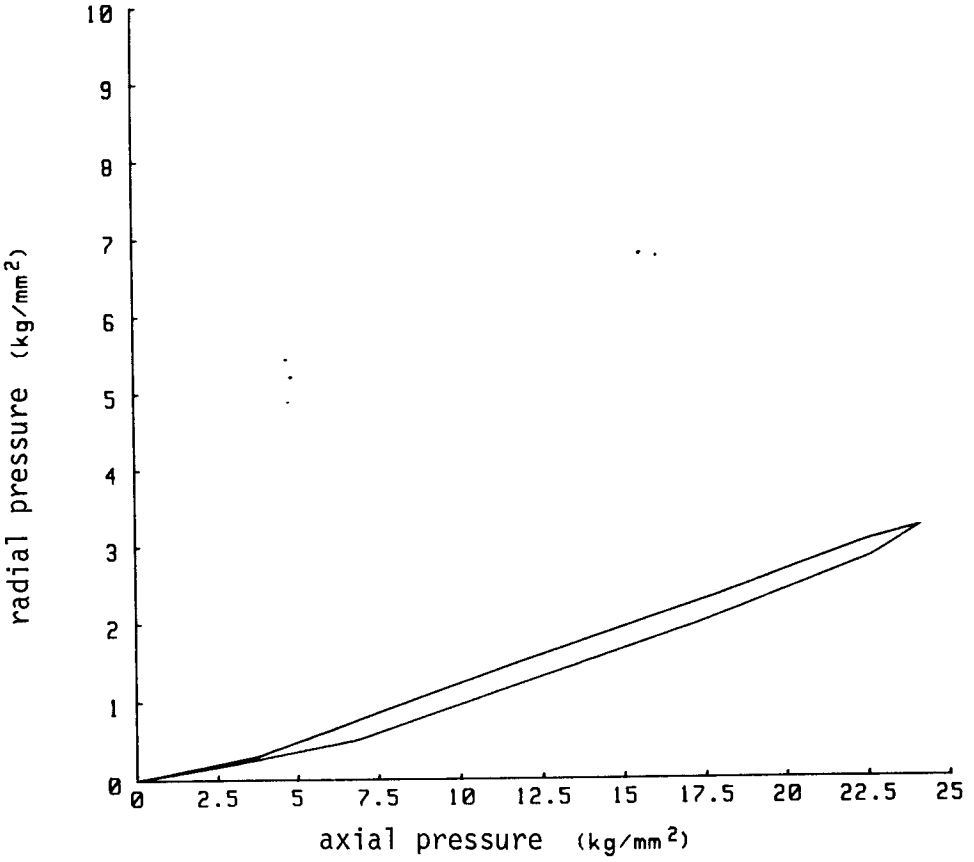

[a] Cetostearyl Alcohol, Lot K4991, Potassium Chloride, Lot L7490, 140-160 , 1:7.5 ratio.

VII. References

(1) G. S. Banker, C. T. Rhodes (Eds.) "Modern Pharmaceutics," Vol. 7, Chapter 10, K. Marshall, Marcel Dekker Inc., New York, N.Y., 1979, p. 359

(2) T. Higuchi, J. Pharm. Sci., 52, 1145 (1963)

(3) S. T. David and L. I. Augsberger, J. Pharm. Sci., 66, 155 (1977)

(4) E. Nurenburg and A. Hopp, Pharm. Tech., 9, 81 (1981)

(5) E. J. Hanus and L. D. King, J. Pharm. Sci., 57, 677 (1968)

(6) Z. T. Chowhan and L. Palagyi, J. Pharm. Sci., 67, 1385 (1978)

(7) S. T. Horhota, J. Burgio, L. Lonski and C. T. Rhodes, J. Pharm. Sci., 65, 1746 (1976)

(8) N. G. Lordi and P. Shiromani, Drug Dev. and Ind. Pharm., 8, 1399 (1983)

(9) R. T. Morrison and R. N. Boyd, "Organic Chemistry," Second Edition, Chapter 15, Allyn and Bacon Inc., Boston, Mass., 1969, p. 498

(10) D. Swern, (Ed.), "Bailey's Industrial Oil and Fat Products," Vol. 1, Fourth Edition, Chapter 9, E. Jungermann, John Wiley & Sons Inc., New York, N.Y., 1979, p. 617

(11) H. G. Schroeder, A. Dakkuri and P. O. DeLuca, J. Pharm. Sci., 67, 350 (1978)

(12) G. R. Wilson, J. Am. Oil Chem. Soc., 11, 564 (1954)

(13) F. O. Barrett, J. D. Fitzpatrick and R. G. Kadesch, Ind. and Eng. Chem., 5, 1114 (1953)

(14) E. F. Hill, G. R. Wilson and E. D. Steinle, Ind. and Eng. Chem., 9, 1917 (1954)

(15) H. F. Mark, J. J. McKetta, D. F. Othmer and A. Standen (Eds.), "Encyclopedia of Chemical Technology," Second Edition, Vol. 1, K. R. Ericson and H. D. VanWagenen, John Wiley & Sons, New York, N.Y., 1965, p. 542

(16) C. Mosselman, Arch. Pharm., 314, 279 (1981)

(17) J. Haleblian and W. McCrone, J. Pharm. Sci., 58, 911 (1969)

(18) M. Tasumi, T. Shimanouchi, A. Watanbe and R. Goto, Spectrochemica Acta, 20, 629 (1964)

(19) D. G. Kolp and E. S. Lutton, J. Amer. Chem. Soc., 73, 5593 (1951)

(20) K. Tanaka, T. Seto and T. Hayashida, Bull. Inst. Chem. Res., Kyoto Univ., 35, 123 (1957)

(21) S. Abrahamsson, G. Larsson and E. von Sydow, Acta Cryst., 13, 770 (1960)

(22) K. Tanaka, T. Seto and T. Hayashida, Bull. Inst. Chem. Res., Kyoto Univ., 37, 281 (1959)

(23) M. Davies and B. Kybett, Trans. Faraday Soc., 61, 2646 (1965)

(24) J. W. G. Phillips and S. A. Mumford, J. Chem. Soc., 1657 (1934)

(25) K. Asai, E. Yoda and S. Yamanaka, J. Phys. Soc. of Japan, 8, 634 (1955)

(26) C. Mosselman, J. Mourik and H. Dekker, J. Chem. Thermo dynamics, 6, 477 (1974)

(27) T. Malkin, J. Amer. Chem. Soc., 52, 3739 (1930)

(28) V. Vand and I. P. Bell, Acta Cryst., 4, 30 (1951)

(29) D. Precht, Fette Seifen Anstrichmittel, 4, 145 (1976)

(30) D. Precht, Fette Seifen Anstrichmittel, 5, 189 (1976)

(31) A. S. C. Lawrence and M. A. Al-Mamun, Trans. Faraday Soc., 63, 2789 (1967)

(32) R. G. Vines and R. J. Meakins, Aust. J. Appl. Sci., 105, 190 (1959)

(33) J. C. S. Smith, J. Chem. Soc., 737 (1932)

(34) S. D. Pradhan, S. S. Katti and S. B. Kulkarni, Indian J. of Chem., 8, 632 (1970)

(35) M. A. Al-Mamun, J. Amer. Oil Chemists Soc., 5, 234 (1974)

(36) Y. K. Kuchhal, R. N. Shukla and A. B. Biswas, Indian J. of Chem., 19A, 1165 (1980)

(37) S. Fukushima and M. Takahashi, J. Colloid and Interfacial Science, 2, 201 (1976)

(38) F. H. C. Stewart, Aust. J. Appl. Sci., 11, 157 (1960)

(39) Y. K. Kuchhal, R. N. Shukla and A. B. Biswas, Thermochimica Acta, 31, 61 (1979)

(40) M. Grayson, (Ed.), "Encyclopedia of Chemical Technology," Third Edition, Vol. 18, W. B. Dancy, John Wiley & Sons, New York, N.Y., 1982, p. 920

(41) E. Nelson, S. M. Naqvi, L. W. Busse and T. Higuchi, J. of Am. Ph. Assoc., Sci. Ed., 43, 596 (1954)

(42) C. L. Huffine, Ph.D. Thesis, Columbia Univ., New York, N.Y., 1953

(43) S. Shlanta and G. Milosovich, J. Pharm. Sci., 53, 562 (1964)

(44) J. Varsano and L. Lachman, J. Pharm. Sci., 55, 1128 (1966)

(45) J. Lazarus and L. Lachman, J. Pharm. Sci., 55, 1121 (1966)

(46) E. N. Hiestand and D. P. Smith, Powder Technology, 38, 145 (1984)

(47) J. E. Rees and J. A. Hersey, J. Pharm. Acta Helv., 47, 235 (1972)

(48) T. Eaves and T. M. Jones, J. Pharm. Sci., 61, 256 (1972)

(49) E. Y. Gutmanas, Powder Metallurgy Inst., 15, 129 (1983)

(50) J. T. Fell and J. M. Newton, J. Pharm. Sci., 60, 1866 (1971)

(51) A. McKenna and D. F. McCafferty, J. Pharm. Pharmacol., 34, 347 (1982)

(52) J. T. Fell and J. M. Newton, J. Pharm. Pharmacol., 22, 247 (1970)

(53) B. W. Mueller, Acta Pharm. Suec., 18, 74 (1981)

(54) A. H. DeBoer, G. K. Bolhuis and C. F. Lerk, Powder Tech., 20, 75 (1978)

(55) E. T. Cole, J. E. Rees and J. A. Hersey, Pharm. Acta Helv., 50, 28 (1975)

(56) J. T. Carstensen, "Solid Pharmaceutics: Mechanical Properties and Rate Phenomena," Academic Press, New York, N.Y., 1980, p. 187

(57) H. A. Lieberman, L. Lachman (Eds.), "Pharmaceutical Dosage Forms: Tablets," Vol. 2, Chapter 4, E. L. Parrott, Marcel Dekker, New York, N.Y., 1981, p. 153

(58) M. Reiner, "Deformation Strain and Flow," H. K. Lewis, London, 1960

(59) J. T. Carstensen and P. Toure, Powder Tech., 26, 199 (1980)

(60) P. Toure, F. Puisieux, D. Duchene and J. T. Carstensen, Powder Tech., 26, 213 (1980)

(61) T. Higuchi, A. Narismha Rao, L. W. Busse and J. V. Swintosky, J. Am. Pharm. Assoc. Sci. Ed., 42, 194 (1953)

(62) M. Peleg, J. Food Sci., 43, 1087 (1978)

(63) J. Skotnicky, Czech. J. Physics, 3, 225 (1953)

(64) A. S. Rankell and T. Higuchi, J. Pharm. Sci., 57, 574 (1968)

(65) A. H. Cottrell, "Dislocations and Plastic Flow in Crystals," Oxford Univ. Press, London, 1953

(66) C. G. Goetzel, "Treatise on Powder Metallurgy," Vol. 1 and 2, Interscience, New York, N.Y., 1949

(67) E. N. Heistand, "Physical Processes of Tableting," presented at the Powder Technology Conference, Basle, Switzerland, 1978

(68) E. N. Heistand, J. M. Bane, Jr., and E. P. Strzelinski, J. Pharm. Sci., 60, 758 (1971)

(69) P. R. Templin, Ind. and Eng. Chem., 48, 154 (1956)

(70) P. York and N. Pilpel, J. Pharm. Pharmacol., 25 Suppl., 1P (1973)

(71) P. York and N. Pilpel, J. Pharm. Pharmacol., 24 Suppl., 47P (1972)

(72) I. Krycer, D. Pope and J. A. Hersey, Drug Dev. and Ind. Pharm., 8, 307 (1982)

(73) J. T. Carstensen and Xin-Pu Hou, Powder Tech., 42, 153 (1985)

(74) L. F. Athy, Bull. Am. Assoc. Petrol. Geologist, 14, 1 (1930)

(75) R. W. Heckel, Trans. Metal. Soc. of AIME, 221, 671 (1961)

(76) R. W. Heckel, Trans. Metal. Soc. of AIME, 221, 1001 (1961)

(77) J. E. Rees and P. J. Rue, J. Pharm. Pharmacol., 30, 601 (1978)

(78) J. E. Rees and P. J. Rue, J. Pharm. Pharmacol., 30, 642 (1978)

(79) M. Sheikh-Salem and J. T. Fell, J. Pharm. Pharmacol., 33, 491 (1980)

(80) Y. T. Chowhan and Y. P. Chow, Int. J. of Pharm., 5, 139 (1980)

(81) P. Paronen and M. Juslin, Acta Pharm. Suec., 18, 93 (1981)

(82) S. Strizbos and P. J. Rankin, Powder Tech., 18, 187 (1977)

(83) B. A. Obiorah, Int. J. of Pharm., 1, 249 (1978)

(84) S. Leigh, J. E. Carless and B. W. Burt, J. Pharm. Sci., 64, 1213 (1975)

(85) R. N. Chicamkurti, C. T. Rhodes and J. B. Schwartz, Drug Dev. and Ind. Pharm., 8, 63 (1982)

(86) L. Lachman, H. A. Lieberman and J. L. Kanig (Eds.), "The Theory and Practice of Industrial Pharmacy," Second Edition, Chapter 10, E. Shotton, J. A. Hersey and P. E. Wray, Lea and Febiger, Philadelphia, Pa., 1976, p. 296

(87) B. Charlton and J. M. Newton, J. Pharm. Pharmacol., 36, 645 (1984)

(88) D. Train and J. A. Hersey, Powder Metallurgy, 6, 20 (1966)

(89) G. E. Amidon, D. P. Smith and E. N. Hiestand, J. Pharm. Sci., 70, 613 (1981)

(90) I. Krycer, D. G. Pope and J. A. Hersey, J. Pharm. Pharmacol., 34, 802 (1982)

(91) K. Ridgway, The Pharm. J., 205, 709 (1970)

(92) A. Rudnick, A. R. Hunter and F. C. Holden, Mat. Res. Stand., 3, 283 (1969)

(93) J. T. Fell and J. M. Newton, J. Pharm. Sci., 60, 1428 (1971)

(94) J. T. Fell and J. M. Newton, J. Pharm. Sci., 57, 657 (1968)

(95) J. T. Fell and J. M. Newton, J. Pharm. Sci., 59, 688 (1970)

(96) E. N. Hiestand and C. B. Poet, J. Pharm. Sci., 63, 605 (1974)

(97) P. J. Jarosz and E. L. Parrot, J. Pharm. Sci., 71, 71 (1982)

(98) S. T. David and L. Augsburger, J. Pharm. Sci., 63, 933 (1974)

(99) D. B. Brook and K. Marshall, J. Pharm. Sci., 57, 481 (1968)

(100) D. P. Shoemaker, C. W. Garland and J. L. Steinfeld, "Experiments in Physical Chemistry," Third Edition, Chapter 6, McGraw-Hill, New York, N.Y., 1974

(101) G. R. B. Down and J. N. McMullen, Powder Tech., 42, 169 (1985)

(102) P. J. Rue, R. M. R. Barkworth, et al, Int. J. Pharm. Tech. and Prod. Mfr., 1, 2 (1979)

(103) A. A. van Dooren and B. W. Muller, Int. J. of Pharm., 20, 217 (1984)

(104) "Instruction Manual 910 Differential Scanning Calorimeter System," Revision B, Du Pont Company, Anal. Instr. Div., Wilmington, Del, 1980, p. 3-4.

(105) "Application Brief #900B35," Du Pont Company, Anal. Instr. Div., Wilmington, Del. (1973)

(106) H. Kambe, K. Horie and T. Suzuki, J. Thermal Analysis, 4, 461 (1972)

(107) "Instruction Manual 910 Differential Scanning Calorimeter System," Revision B, Du Pont Company, Anal. Instr. Div., Wilmington, Del., 1980, p. 3-5

(108) H. Leuenberger and W. Jetzer, Powder Tech., 37, 209 (1984)

(109) T. Higuchi and E. Nelson, J. of Am. Ph. Assoc., Sci. Ed., 43, 344 (1954)

(110) B. A. Obiorah and E. Shotton, J. Pharm. Pharmacol., 28, 629 (1976)

(111) J. J. Williams, Pharm. Tech., 8, 26 (1984)

(112) R. W. Lally, "Technical Brief, Transduction," PCB Piezotronics, Depew, N.Y., 1967

(113) N. D. Change, "General Guide to ICP Instrumentation," PCB Piezotronics, Depew, N.Y., 1971

(114) K. Ridgway, J. Glasby and P. H. Rosser, J. Pharm. Pharmacol., 215, 245 (1969)

(115) J. J. Windheuser, J. Misra, S. P. Ericksen and T. Higuchi, J. Pharm. Sci., 52, 767 (1963)

(116) H. Junginger, C. Fuhrer, A. Beer and J. Ziegenmeyer, Pharm. Ind., 41, 380 (1979)

(117) J. D. Hoffman and C. P. Smyth, J. Amer. Chem. Soc., 71, 431 (1949)

(118) A. Watanabe, Bull. Chem. Soc. of Japan, 34, 1728 (1961)

(119) W. O. Baker and C. P. Smyth, J. Chem. Soc., 60, 1229 (1938)

(120) T. Eckert and J. Muller, Arch. Pharm., 311, 31 (1978)

(121) W. R. Wilcox, Chem. Reviews, 2, 187 (1964)

(122) D. P. Shoemaker, C. W. Garland and J. L. Steinfeld, "Experments in Physical Chemistry," Third Edition, Chapter 20, McGraw-Hill, New York, N.Y. (1974)

(123) K. Y. Chow, J. Go, Wang Zhongshan, M. Mehdizadeh and D. J. W. Grant, Int. J. Pharm., 25, 41 (1985)

(124) P. York and D. J. W. Grant, Int. J. Pharm., 25, 57 (1985)

(125) A. H. L. Chow, P. K. K. Chow, Wang Zhongshan and D. J. W. Grant, Int. J. Pharm., 24, 239 (1985)

(126) W. C. Duncan-Hewitt and D. J. W. Grant, Int. J. Pharm., 28, 75 (1986)

(127) K. Y. Chow, J. Go, M. Mehdizadeh and D. J. W. Grant, Int. J. Pharm., 20, 3 (1984)

(128) R. Huttenrauch, Acta Pharm. Technol., 6, 55 (1978)

(129) E. N. Heistand, J. Pharm. Sci., 74, 768 (1985)

(130) G. Alderborn and C. Nystrom, Acta Pharm. Suec., 18, 101 (1981)

(131) E. N. Hiestand, J. E. Wells, C. B. Peot and J. F. Ochs, J. Pharm. Sci., 66, 510 (1977)

(132) J. E. Rees and P. J. Rue, Drug Dev. and Ind. Pharm., 4, 131 (1978)

(133) R. L. Carr, British Chem. Eng., 12, 1541 (1970)

(134) S. Malamataris and N. Pilpel, Powder Tech., 26, 205 (1980)

(135) S. Malamataris and N. Pilpel, J. Pharm. Pharmacol., 34, 755 (1982)

(136) S. Malamataris and N. Pilpel, Powder Tech., 28, 35 (1981)

(137) M. E. Aulton, D. N. Travers and P. J. P. White, J. Pharm. Pharmacol., 25S, 79P (1973)

(138) P. Humbert-Droz, D. Mordier and E. Doelker, Acta Pharm. Tech., 29, 69 (1983)

Vita

1951	Born June 23 in Hoboken, New Jersey.
1969	Graduated from Holy Family High School, Union City, New Jersey.
1969-74	Attended Rutgers, The State University of New Jersey, College of Pharmacy, Piscataway, New Jersey.
1974	B.S., Rutgers, The State University of New Jersey.
1974-75	Project Engineer, Chase Chemical Company, Newark, New Jersey.
1975-Present	Senior Research Scientist, Pharmaceutics and Pharmaceutical Technology, CIBA-GEIGY Corporation, Summit, New Jersey.
1977-80	Graduate studies in Pharmaceutical Science, Rutgers, The State University of New Jersey, New Brunswick, New Jersey.
1980	M.S. in Pharmaceutical Science, Rutgers, The State University of New Jersey.
1980-87	Graduate work in Pharmaceutical Science, Rutgers, The State University of New Jersey, New Brunswick, New Jersey.
1987	Ph.D. in Pharmaceutical Science, Rutgers, The State University of New Jersey.